



**UNIVERSITY OF LEEDS**

**Carbonation of Composite Cement under Different Relative  
Humidity Conditions**

**PhD Thesis**

Suraj Adedamola Rahmon

Submitted in accordance with the requirements for the degree of PhD in Civil  
Engineering

Main Supervisor: Prof. Leon Black  
Co- Supervisor: Dr Sam Adu-Amankwah

The University of Leeds  
School of Civil Engineering  
Faculty of Engineering and Physical Sciences

October 2023

## Intellectual Property and Publication Statement

The candidate confirms that the work submitted is his own and that appropriate credit has been given where reference has been made to the work of others.

This copy has been supplied on the understanding that it is copyright material and that no quotation from the thesis may be published without proper acknowledgement.

Parts of the works reported in chapter 2, 4, 5 & 6 have been jointly published in Journals or proceeding of conferences as follows:

(I). Samuel Adu-Amankwah, Suraj Rahmon, and Leon Black, **From composition to the microstructure and durability of limestone ternary blended cements: A systematic review**. Advances in Cement Research 2022 34:5, 206-224.

(II). S. Rahmon, S. Adu-Amankwah, and L. Black, **Accelerated carbonation of slag-rich blends under different relative humidity conditions**: 4th International Conference on the Chemistry of Construction Materials-ICCM 2022. Karlsruhe Sept. 26-28<sup>th</sup> 2022

(III). Suraj A. Rahmon, Sam Adu-Amankwah and Leon Black, **Phase changes during carbonation of slag-limestone cements**: 41st Cement & Concrete Science Conference Leeds Sept. 12-13<sup>th</sup> 2022

(IV). Suraj Adedamola Rahmon, Leon Black and Sam Adu-Amankwah, **Understanding hydration progress during carbonation of slag-limestone binary and ternary systems** presented at the RILEM/ IITM PhD Symposium on Construction Materials Technologies for Low Carbon and Lean Construction conducted on 24th September 2021,

(V). Suraj Adedamola Rahmon, Leon Black and Sam Adu-Amankwah, **Influence of relative humidity on the hydration, microstructure, transport, and moisture properties of the ternary blended binder during carbonation**. Poster presentation at University of Leeds, School of Civil Engineering Postgraduate Research Conference April 2-3, 2019

The right of Suraj Adedamola Rahmon to be identified as Author of this work has been asserted by him in accordance with the Copyright, Designs and Patents Act 1988.

© 2023 The University of Leeds and Suraj Adedamola Rahmon.

## Acknowledgements

I would like to express my gratitude to Professor Leon Black, my supervisor, for his unwavering guidance, patience, and support throughout my PhD journey. I also extend my appreciation to Dr. Sam Adu-Amankwah, my co-supervisor, for his technical expertise and contributions to this project.

I am deeply grateful to the members of the Materials and Structures group, including Professor Susan Bernal-Lopez, postdoctoral researchers, and PhD students, for their immense support and contributions towards the successful completion of this project.

I would also like to acknowledge and appreciate the invaluable support and cooperation provided by the technical and laboratory staff in Civil Engineering/Materials.

Finally, I owe my heartfelt thanks to my extended family, dear wife Muinat and my boys, Imran, Al-Hassan, and Mohammed, for their unwavering support during this time. Although I could not give all of you the attention you deserved due to my study commitment, I promise to share the valuable lessons I have learned from my PhD journey with you all, especially Mohammed, who always stayed up late with me during thesis writing.

## Abstract

The development of composite binders can drastically lower the carbon footprint of the concrete industry, estimated to contribute about 8% of total global anthropogenic CO<sub>2</sub> emissions, coupled with the use of unaccounted raw materials. Long-term durability concerns of these binders pose the most significant challenge for their wider acceptability since they are always compared to Portland cement with no consideration to their chemical composition and complex microstructure, which can make them more susceptible to poor performance during accelerated carbonation testing. Understanding the underlying carbonation mechanisms of these materials is essential to develop strategies to improve their durability and performance. Consequently, this study focused on the carbonation behaviour of composite cement exposed to different relative humidity levels. The research provides valuable insights into hydration mechanisms, phase assemblages, microstructure durability performance, and mechanical strength during carbonation.

Mortar and paste samples were prepared at two w/b ratios using four binders, comprising CEM I 52,5R, clinker-GGBS, and clinker-GGBS-limestone (10% and 20%), and subjected to ambient and accelerated aging at 4% CO<sub>2</sub> at 55%, 75%, and 95% relative humidity.

The possibility of hydration during exposure was investigated using both TGA and SEM-IA. Phase assemblages were also investigated using TGA, FTIR, and XRD to quantify the carbonation products throughout the study.

Microstructural development was followed using SEM backscattered electron (BSE) image analysis and complemented with mercury intrusion porosimetry (MIP) to relate pore characteristics found in PC, binary, and ternary blended cement binders. The carbonation depths and compressive strengths of mortar samples were investigated to give insights into the durability and engineering properties of various binders under carbonation at different exposure conditions.

The relative humidity and CO<sub>2</sub> concentration affect carbonation, with differences depending on the binder composition. Composite binders showed no significant changes in the degree of hydration and slag reaction during carbonation, and

water released during carbonation does not further hydration in non-carbonated areas. Carbonation initially converts portlandite to calcium carbonate, followed by decalcification of C-S-H. Elevated CO<sub>2</sub> concentrations led to aggressive carbonation and densification of the microstructure in CEM I systems and pore coarsening in composite cements. Carbonation was minimal at 95% RH and more rapid at lower RH, disadvantaging composite cement under standard accelerated carbonation conditions. There were no significant differences in carbonation resistance and compressive strength between binary and 10% limestone addition binders, but significant changes were observed with 20% limestone addition. Relative humidity and water binder ratio significantly influence mortar carbonation depth, with carbonation being greatest at 55% RH.

## Contents

Acknowledgements .....	ii
<b>Abstract .....</b>	<b>iii</b>
Contents.....	v
List of Tables.....	xiv
List of Abbreviations.....	xv
<b>Chapter 1: Introduction.....</b>	<b>17</b>
1.1 Background.....	17
1.2 Significance of the research .....	18
1.3 Research objectives .....	19
1.4 Thesis outline .....	19
<b>Chapter 2: Literature review.....</b>	<b>21</b>
2.1 Portland cement .....	21
2.1.1 Cement compounds .....	21
2.1.2 Portland cement hydration mechanism .....	23
2.1.3 Pore structure of Portland cement.....	25
2.2 Ground granulated blast furnace slag .....	27
2.2.1 Hydration of GGBS .....	28
2.2.2 Microstructures development and pore structure of GGBS .....	28
2.2.3 Mechanical strength of GGBS blended cement .....	29
2.3 Limestone.....	29
2.3.1 Hydration of limestone blended cement .....	30
2.3.2 Microstructure and transport properties of limestone blended binder .....	31
2.3.3 Mechanical strength of limestone blended cement .....	32
2.4 Carbonation.....	33
2.4.1 Accelerated carbonation vs natural carbonation. ....	35
2.4.2 Factors influencing accelerated carbonation of cementitious materials.....	39
2.4.3 Carbonation coefficient.....	42
2.4.3 Methods of assessing carbonation depth and products .....	43
2.5 Influence of carbonation on blended binders .....	44
2.5.2 Influence of carbonation on microstructures & transport properties of blended binder. ....	47

2.5.3 Influence of carbonation on mechanical strength of blended cement.	49
2.6 Summary of the literature review	50
<b>Chapter 3: Materials and Methods</b>	<b>52</b>
3.1 Raw materials	52
3.1.1 Binders	52
3.1.1 Fine aggregate	55
3.1.2 Water	55
3.1.3 Saturated salt	55
3.2 Method	56
3.2.1 Binder blending	56
3.2.2 Sample preparation	56
3.2.2. Paste samples	56
3.2.2. Mortar sample	57
3.2.3 Preconditioning	57
3.2.4 Carbonation	57
3.2.5 Hydration stopping and extraction	58
3.3 Testing Techniques	59
3.3.1 Carbonation depth measurement	59
3.3.2 Mechanical strength	60
3.3.3 Simultaneous thermal analysis (STA)	60
3.3.4 X-ray powder diffraction (XRD)	63
3.3.5 Fourier transform infrared spectroscopy (FTIR)	63
3.3.6 Scanning electron microscopy (SEM-EDS)	63
3.3.7 Mercury intrusion porosimetry (MIP)	66
<b>Chapter 4: Carbonation under ambient conditions</b>	<b>68</b>
4.1 Hydration progress during ambient carbonation	68
4.1.1 Chemically bound water	68
4.1.2 Effect of RH on chemically bound water during ambient exposure.	70
4.1.3 Portlandite and calcium carbonate content	73
4.1.4 Effect of RH on portlandite evolution and calcium carbonate formed.	76
4.2 Phase Assemblages by Thermogravimetric Analysis (TGA)	79
4.2.1 AFt, C-S-H and AFm	79
4.2.2 Portlandite evolution by DTG	81

4.2.3 Calcium carbonate by DTG .....	83
4.3 Phase Assemblages by Fourier Transform infrared spectroscopy (FTIR).....	84
4.3.1 Portlandite content .....	85
4.3.2 Calcium carbonate and polymorphs .....	86
4.3.3 Calcium Silicates Hydrates (C-S-H). .....	90
4.4 Compressive strength development.....	90
4.5 Summary.....	94
<b>Chapter 5: Carbonation under accelerated conditions.....</b>	<b>96</b>
5.1 Hydration progress during accelerated carbonation.....	98
5.1.1 Chemical bound water, portlandite content, and calcium carbonates. ....	98
5.2 Phase assemblage due to accelerated carbonation.....	102
5.1.2 Portlandite Evolution .....	102
5.2.2 Calcium carbonate .....	105
5.3 Phase Assemblages by Fourier Transform infrared spectroscopy (FTIR) .....	106
5.3.1 Portlandite .....	106
5.3.2 Calcium carbonate and polymorphs formation. ....	108
5.3.3 Calcium Silicates Hydrates (C-S-H) .....	112
5.3.4 Other phases.....	113
5.4 Microstructure changes due to carbonation. ....	113
5.4.1 MIP .....	113
5.5 Carbonation Performance .....	116
5.5.1 Effect of water-binder ratio and relative humidity on carbonation depth.....	117
5.6 Compressive strength .....	121
5.7 Summary.....	126
<b>Chapter 6: Comparison between ambient and accelerated carbonation.....</b>	<b>128</b>
6.1 Hydration progress during carbonation .....	128
6.1.1 Chemical bound water measured by TGA.....	128
6.1.2 Portlandite measured by both TGA & QXRD .....	132
6.1.3 Degree of reaction of clinker/slag by SEM-IA.....	134
6.2 Phase evolution due to carbonation .....	136
6.2.1 Differential Thermogravimetry Analysis.....	136

6.2.2 Phases Changes by FTIR .....	141
6.2.3 Phases changes by XRD .....	146
6.3 Microstructure changes due to carbonation. ....	149
6.3.1 SEM-BSE .....	149
6.3.2 C-S-H composition by SEM-EDS .....	157
6.4 Compressive strength due to carbonation.....	160
6.5 Summary.....	163
<b>Chapter 7 Conclusions and further research. ....</b>	<b>166</b>
7.1 Conclusions.....	166
7.2 Further research.....	168
<b>References.....</b>	<b>170</b>
<b>Appendices.....</b>	<b>189</b>
A. Rietveld Refinement .....	189
B. Mass against DTG plots (CaCO <sub>3</sub> decomposition temperature).....	195
C. Post-Covid Experimental Chart .....	198
D. Pre-Covid Experimental Chart (Original Plan) .....	199
E. Raw TGA and QXRD data.....	200

## List of Figures

Figure 2.1: A brief summary of cement chemistry .....	21
Figure 2.2: Hydration of Portland cement.....	25
Figure 2.3 Comparison of the pore size distribution of limestone ternary blended cements from GGBS (a) and calcined clay (b) compared to Portland cement.....	31
Figure 2.4: Carbonation of cement paste: Active and Passive .....	33
Figure 2.5: Factors influencing accelerated carbonation test .....	40
Figure 2.6: Systematic representation of carbonation front.....	43
Figure 2.7: Carbonation coefficient in binary and ternary blends .....	46
Figure 2.8 Total porosity of blended binders .....	48
Figure 2.9: Threshold pore diameter of blended cements.....	49
Figure 3.1: Particle size distribution of as-received CEM I, slag and limestone.....	55
Figure 3.2: Experimental chart .....	56
Figure 3.3: Accelerated carbonation setup(Photo & schematic diagram).....	58
Figure 3.4: Extracted paste .....	59
Figure 3.5: Unconfined compression test.....	60
Figure 3.6: Thermogravimetric analysis highlighting temperature changes for various mass loss due to decomposition of hydrate phase. ....	62
Figure 3.7: Grey scale histogram for slag binder system showing different thresholds for binders and pores adapted from [34].....	65
Figure 3.8: Method for determining unreacted slag particles from a combination of BSE image and magnesium map by image analysis: (a) BSE grey image, (b) magnesium map, (c) combined image, and (d) separated unreacted slag particles. (Images taken (110) ). ....	66
Figure 4.1: Measured bound water from TGA during 55% RH ambient carbonation (a) 0.50w/b (b) 0.55w/b .....	69
Figure 4.2: Measured bound water from TGA during 75% RH ambient carbonation (a) 0.50w/b (b) 0.55w/b .....	70
Figure 4.3: Measured bound water from TGA during 95% RH ambient carbonation (a) 0.50w/b (b) 0.55w/b.....	70
Figure 4.4: Chemically bound water with the exposure relative humidity during ambient carbonation at 7days. ....	72
Figure 4.5: Chemically bound water with the exposure relative humidity during ambient carbonation at 28days. ....	73
Figure 4.6: Portlandite evolution with CaCO <sub>3</sub> formed at 55% RH ambient carbonation (a) 0.50w/b (b) 0.55w/b.....	74
Figure 4.7 Portlandite evolution with CaCO <sub>3</sub> formed at 75% RH ambient carbonation (a) 0.50w/b (b) 0.55w/b .....	75
Figure 4.8: Portlandite evolution with CaCO <sub>3</sub> formed at 95% RH ambient carbonation (a) 0.50w/b (b) 0.55w/b .....	76

Figure 4.9: Portlandite evolution at different RH for ambient carbonation after 28 days. ....	77
Figure 4.10: CaCO <sub>3</sub> formed at different RH for ambient carbonation after 28 days. ....	78
Figure 4.11: AFt, C-S-H & AFm at 55% RH (Top) 0.55w/b (Bottom) 0.50w/b	79
Figure 4.12 AFt, C-S-H & AFm at 75% RH (Top) 0.55w/b (Bottom) 0.50w/b	80
Figure 4.13: AFt, C-S-H & AFm at 95% RH (Top) 0.55w/b (Bottom) 0.50w/b	81
Figure 4.14: DTG during 55% RH ambient carbonation.....	82
Figure 4.15: DTG during 75% RH ambient carbonation.....	82
Figure 4.16: DTG during 95% RH ambient carbonation.....	83
Figure 4.17: Enlarged FTIR plot between 3700-3500cm <sup>-1</sup> for 55% RH ambient carbonation at 7 & 28 days (a) CEM I, (b) CS (c) CS1L (d) CS2L .....	85
Figure 4.18: Enlarged FTIR plot between 3700-3500cm <sup>-1</sup> for 75% RH ambient carbonation at 7 & 28 days (a) CEM I, (b) CS (c) CS1L (d) CS2L .....	86
Figure 4.19: Enlarged FTIR plot between 3700-3500cm <sup>-1</sup> for 95% RH ambient carbonation at 7 & 28 days (a) CEM I, (b) CS (c) CS1L (d) CS2L .....	86
Figure 4.20: FTIR normalised plot between 600-2000cm <sup>-1</sup> for 55% RH under ambient exposure at 7 & 28 days (a) CEM I, (b) CS (c) CS1L (d) CS2L.....	88
Figure 4.21: FTIR normalised plot between 600-1700cm <sup>-1</sup> for 75% RH under ambient exposure at 7 & 28 days (a) CEM I, (b) CS (c) CS1L (d) CS2L.....	89
Figure 4.22: FTIR normalised plot between 600-1700cm <sup>-1</sup> for 95% RH under ambient exposure at 7 & 28 days (a) CEM I, (b) CS (c) CS1L (d) CS2L.....	90
Figure 4.23: Compressive strength following ambient carbonation at 55% RH. ....	91
Figure 4.24: Compressive strength following ambient carbonation at 75% RH. ....	92
Figure 4.25: Compressive strength following ambient carbonation at 95% RH. ....	92
Figure 5.1: Accelerated carbonation of paste samples at 55%, 75% and 95% relative humidity for 28 days exposure.....	97
Figure 5.2: Measured chemically bound water (CBW), CH & CaCO <sub>3</sub> from TGA during 55% RH at 4% CO <sub>2</sub> accelerated carbonation. ....	99
Figure 5.3: Measured chemically bound water (CBW), CH & CaCO <sub>3</sub> from TGA during 75% RH at 4% CO <sub>2</sub> accelerated carbonation. ....	100
Figure 5.4: Measured chemically bound water (CBW), CH & CaCO <sub>3</sub> from TGA during 95% RH at 4% CO <sub>2</sub> accelerated carbonation. ....	101
Figure 5.5: DTG during 55% RH accelerated carbonation .....	103
Figure 5.6: DTG during 75% RH accelerated carbonation .....	104
Figure 5.7: DTG during 95% RH accelerated carbonation .....	105
Figure 5.8: Enlarged CH decomposition for 55% RH during accelerated carbonation obtained from FTIR. ....	107
Figure 5.9: Enlarged CH decomposition for 75% RH during accelerated carbonation obtained from FTIR. ....	107

Figure 5.10: Enlarged CH decomposition for 95% RH during accelerated carbonation obtained from FTIR. ....	108
Figure 5.11: Enlarged FTIR plot between 600-2000cm <sup>-1</sup> for 55% RH under accelerated carbonation at 7 & 28 days (a) CEM I, (b) CS (c) CS1L (d) CS2L .....	110
Figure 5.12: Enlarged FTIR plot between 600-2000cm <sup>-1</sup> for 75% RH under accelerated carbonation at 7 & 28 days (a) CEM I, (b) CS (c) CS1L (d) CS2L .....	111
Figure 5.13: Enlarged FTIR plot between 600-2000cm <sup>-1</sup> for 75% RH under accelerated carbonation at 7 & 28 days (a) CEM I, (b) CS (c) CS1L (d) CS2L .....	112
Figure 5.14: Pore size distribution of samples subjected to accelerated carbonation at both 55% & 75% RH for CEM I paste.....	114
Figure 5.15: Pore size distribution of samples subjected to accelerated carbonation at both 55% & 75% RH for CS paste.....	115
Figure 5.16: Pore size distribution of samples subjected to accelerated carbonation at both 55% & 75% RH for CS1L paste.....	115
Figure 5.17: Carbonation depth measurement at 4% CO <sub>2</sub> at 55%, 75% and 95% relative humidity (top) 0.50w/b (bottom) 0.55w/b. ....	118
Figure 5.18: Coefficient of carbonation at 55% RH accelerated carbonation. ....	120
Figure 5.19: Coefficient of carbonation at 75% RH accelerated carbonation. ....	120
Figure 5.20: Compressive strength evolution after carbonation at 55% relative humidity.....	122
Figure 5.21: Compressive strength evolution after carbonation at 75% relative humidity.....	124
Figure 5.22: Compressive strength evolution after carbonation at 95% relative humidity.....	125
130	
Figure 6.1: Measured chemically bound water (CBW), CH & CaCO <sub>3</sub> from TGA during ambient and accelerated carbonation for CEM I at all relative humidities.....	130
Figure 6.2: Measured chemically bound water (CBW), CH & CaCO <sub>3</sub> from TGA during ambient and accelerated carbonation for CS (Binary blend) at all relative humidities. ....	131
Figure 6.3: Measured chemically bound water (CBW), CH & CaCO <sub>3</sub> from TGA during ambient and accelerated carbonation for CS1L (Ternary blend) at all relative humidities. ....	132
Figure 6.4: DTG plot comparison of CEM I at 55, 75 & 95% relative humidity for both ambient (Amb) and accelerated carbonation (Acc).....	137
Figure 6.5: DTG plot comparison of CS (Clinker/Slag binary mix) at 55, 75 & 95% relative humidity .....	139

Figure 6.6: DTG plot comparison of CS1L (Clinker/Slag/Limestone ternary mix) at 55, 75 & 95% relative humidity.....	140
143	
Figure 6.7: FTIR spectra plot comparing CEM I at both ambient & accelerated carbonation at different humidity. ....	143
Figure 6.8 : FTIR spectra plot comparing CS (binary blends) at both ambient & accelerated carbonation at different humidity.....	145
146	
Figure 6.9: FTIR spectra plot comparing CS1L (Ternary blends) at both ambient & accelerated carbonation at different humidity.....	146
Figure 6.10: XRD pattern comparism for CEM I at both ambient & accelerated carbonation. ....	147
Figure 6.11: XRD pattern comparism for CS at both ambient & accelerated carbonation. ....	148
Figure 6.12: XRD pattern comparism for CS1L at both ambient & accelerated carbonation. ....	148
Figure 6.13: Micro-cracks developed during accelerated carbonation at 55% RH (a) CEM I (b) CS & (c) CS1L.....	150
Figure 6.14: Micro-cracks developed during accelerated carbonation at 75% RH (a) CEM I (b) CS & (c) CS1L.....	151
Figure 6.15: Micro-cracks developed during accelerated carbonation at 95% RH (a) CEM I (b) CS & (c) CS1L.....	151
Figure 6.16: SEM-BSE Images of CEM I paste samples following (a) ambient carbonation at 55% RH (b) accelerated carbonation at 55% RH core (c) accelerated carbonation at 55% RH edge (d) ambient carbonation at 75% RH (e) accelerated carbonation at 75% RH (f) ambient carbonation at 95% RH (g) accelerated carbonation at 95% RH. ....	153
Figure 6.17: SEM-BSE Images of CS (binary) paste samples at (a) ambient carbonation at 55% RH (b) accelerated carbonation at 55% RH (c) ambient carbonation at 75% RH (d) accelerated carbonation at 75% RH core (e) accelerated carbonation at 75% RH edge (f) ambient carbonation at 95% RH (g) accelerated carbonation at 95% RH. ....	155
Figure 6.8: SEM-BSE Images of CS1L (Ternary paste) samples at (a) ambient carbonation at 55% RH (b) accelerated carbonation at 55% RH (c) ambient carbonation at 75% RH (d) accelerated carbonation at 75% RH core (e) accelerated carbonation at 75% RH edge (f) ambient carbonation at 95% RH (g) accelerated carbonation at 95% RH. ....	156
Figure 6.20: SEM-EDS point analysis of CEM I (A), CS (B) & CS1L(C) at 55% relative humidity .....	158
Figure 6.22: EDS point analysis of CEM I (A), CS (B) & CS1L(C) at 95% relative humidity.....	160
6.23: Compressive strength comparison for mortars at 55%, 75% and 95% relative humidities in both accelerated and ambient carbonation.....	161

6.24: Carbonation depth against ambient & accelerated carbonation scatter  
diagram.....163

## List of Tables

Table 2-1: Major compound of cement and functions .....	22
Table 2-2: Pores classification (Taken from (26)).....	26
Table 2-3: Ranges of GGBS oxides composition. (Taken from (30)) .....	27
Table 2-4: Summary of selected European accelerated carbonation tests ....	37
Table 2-5: Summary of the stability of the cement phases according to pH...45	
Table 3-1: Binder configuration .....	52
Table 3-2:Oxide composition of the as-received raw materials. ....	53
Table 3-3: Blaine and fineness of the as-received cementitious materials. ....	53
Table 3-4: Phase composition of the raw materials. (As received).....	54
Table 5-1: Total porosity of samples subjected to carbonation at both 55% & 75% RH (a) CEM I (b) CS and (c) CS1L.....	116
Table 6-1: CH content measured with both TGA & XRD after 28 days ambient and accelerated carbonation.....	134
Table 6-2: Degree of clinker hydration/slag reaction measured by SEM-IA .	136
Table 6-3: Mass loss temperatues for CaCO <sub>3</sub> decomposition.....	141

## List of Abbreviations

### Cement Nomenclature

C = CaO    S = SiO<sub>2</sub>    A = Al<sub>2</sub>O<sub>3</sub>    S = SO<sub>3</sub>    M = MgO  
F = Fe<sub>2</sub>O<sub>3</sub>    C = CO<sub>3</sub>    N = Na<sub>2</sub>O    K = K<sub>2</sub>O    H = H<sub>2</sub>O

### Clinker Phases and Hydrates

Alite	3CaO.SiO <sub>2</sub>
Belite	2CaO.SiO <sub>2</sub>
Tricalcium aluminate	3CaO.Al <sub>2</sub> O <sub>3</sub>
Tetracalcium aluminoferrite	4CaO.Al <sub>2</sub> O <sub>3</sub> .Fe <sub>2</sub> O <sub>3</sub>
Calcium carbonate	CaCO <sub>3</sub>
Portlandite	Ca(OH) <sub>2</sub> / CH
Calcium silicate hydrate	CaO-SiO <sub>2</sub> -H <sub>2</sub> O
Calcium aluminate silicate hydrate	CaO-Al <sub>2</sub> O <sub>3</sub> -SiO <sub>2</sub> -H <sub>2</sub> O
Ettringite / AFt	3CaO.Al <sub>2</sub> O <sub>3</sub> .3CaSO <sub>4</sub> .32H <sub>2</sub> O
Monosulfate / Ms	3CaO.Al <sub>2</sub> O <sub>3</sub> .CaSO <sub>4</sub> .12H <sub>2</sub> O
Hemicarboaluminate / Hc	3CaO.Al <sub>2</sub> O <sub>3</sub> .0.5Ca(OH) <sub>2</sub> .0.5CaCO <sub>3</sub> .11.5H <sub>2</sub> O
Monocarboaluminate / Mc	3CaO.Al <sub>2</sub> O <sub>3</sub> .CaCO <sub>3</sub> .11H <sub>2</sub> O
Stratlingite	2CaO.Al <sub>2</sub> O <sub>3</sub> .SiO <sub>2</sub> .8H <sub>2</sub> O
Hydrotalcite / Ht	Mg <sub>6</sub> Al <sub>2</sub> (OH) <sub>16</sub> .CO <sub>3</sub> .4H <sub>2</sub> O

## **List of abbreviations and symbols**

CS	Clinker-GGBS
CS1L	Clinker-GGBS-10%Limestone
CS2L	Clinker-GGBS-20%Limestone
DoH	Degree of hydration
GGBS	Ground granulated blast-furnace slag.
Ip	Inner product C-S-H
Op	Outer product C-S-H
PC	Portland cement
SCM	Supplementary cementitious material
w/b	water/binder ratio
w/c	water/cement ratio

## **Techniques**

BSE	Back Scattered Electron
DTG	Differential Thermogravimetric Analysis
EDX	Energy Dispersive X-ray
FTIR	Fourier Transform Infrared Spectroscopy
MIP	Mercury Intrusion Porosimetry
SEM	Scanning Electron Microscopy
SEM-IA	Scanning Electron Microscopy – Image Analysis
STA	Simultaneous Thermal Analysis
TGA	Thermogravimetric Analysis
XRD	X-ray Diffraction

# Chapter 1: Introduction

## 1.1 Background

Cement is the most critical component of concrete, which is the most widely used man-made material in the world [1]. The abundance of the raw materials in the earth's crust required for cement production allows cement's production in almost every continent of the world except Antarctica and enhances its popularity in the construction industry. In practical terms our infrastructural, and social-economic development are hinged on cement usage. However, with embodied CO<sub>2</sub> estimated at 830kgCO<sub>2</sub>/tonne [2], the widespread and extensive use of Portland cement has a profound environmental impact [2]. The cement and concrete industry contribute 5-10% of the total global anthropogenic CO<sub>2</sub> emissions [3], plus the use of unaccounted tonnes of raw materials. It is challenging to both the cement and construction industries to find a definite solution to reduce the emissions associated with the manufacture of one of the most important commodities on earth, while keeping in line with the 2015 Paris Agreement and other protocols, to reduce greenhouse gas emissions and thereby limit global temperature rise to 1.5° Celsius above pre-industrial levels.

One of the most viable recommendations proposed for reducing emissions is clinker substitution [4]. Supplementary cementitious materials (SCMs) from industrial by-products, agricultural wastes and raw materials are being processed to partially replace cement clinker, showing promising results with high replacement levels of clinker already available in the market with CEM II, III & V. Among the most used SCMs are ground granulated blast-furnace, usually shortened to GGBS or slag, kiln bypass dust, silica fume, metakaolin and PFA. A major advantage of SCMs, is the low CO<sub>2</sub> emissions associated with their production compared with cement, since they are usually industrial by-products, and as such, convention dictates that emissions are allocated to primary products, not by-products. They have also traditionally been relatively cheap and have the advantage of improving concrete properties such as mechanical strength and fresh properties i.e., workability, setting time etc. [5-7]. However, declining production and supply concerns for major industrial SCMs may threaten what seems to be a promising breakthrough toward de-carbonization. Furthermore, slag production is only 5-10% of cement production, due to increased steel recycling limiting fresh production [8]. One viable option in achieving sustainable

low carbon binders and managing declining supply concerns is combinations of Portland cement, slag, and limestone powder in a composite system in which all components complement each other to achieve a suitable low-carbon binder. Furtherance to this proposition, there have been many studies into the properties of these blends, including microstructure evolution, mechanical strength, hydration kinetics and durability [9-11]. These appear to show that 50% clinker reduction can be achieved with these blends [9]. However, long term durability concerns pose a greater threat to wider acceptance of these composite cements, especially regarding carbonation. This is compounded by assessment using accelerated ageing tests designed for CEM I, where the use of a constant (and relatively low by meteorological standards) relative humidity disadvantages materials with refined pore structures such as composite cements.

## 1.2 Significance of the research

Despite enormous benefits that can be derived from low-carbon composite binders, long term durability is still uncertain. Carbonation is a well-known durability problem that lowers binder pH, thereby reducing the alkalinity around reinforcement and causing corrosion. Natural carbonation is slow and will not help in short-term assessments of durability performance of new blends. However, the common method to determine the resistance of cement-based materials to carbonation, i.e., an accelerated aging test, shows far better performance of Portland cement compared to composite cements [12, 13]. This is due to several factors such as testing parameters, different microstructural profiles, ongoing hydration, and products formed. Hydration is slow in composite cements due to the reactivity of SCM's and this could lead to undeveloped microstructure upon testing, while mature composite cements will have relatively fine pore structures through the formation of additional C-S-H that will lead to a denser microstructure thus lowering the rate of diffusion of CO<sub>2</sub> [15] and hindering carbonation. Furthermore, as well as uncertainty over carbonation, there is also a question over the role of water. Carbonation reactions release water and there is lack of understanding as to whether this water will cause further hydration, especially in composite cements, which has already been established as hydrating slower than Portland cement. It is particularly important to ascertain the role of water released during carbonation on phase assemblages, microstructure evolution and strength performance of composite cement under different environmental testing conditions.

This will contribute immensely to further understanding of carbonation of composite cements.

### 1.3 Research objectives

The main goal of this thesis is to understand the effects of accelerated carbonation at different relative humidity on hydration, phase changes, microstructure, and mechanical properties of binary and ternary slag blends. This should contribute immensely to the field of composite cement durability performance and enhance the understanding of SCMs during accelerated aging tests. The specific objectives are to evaluate the effects of varying relative humidity and water binder ratio on binary and ternary blended binders during accelerated and ambient exposure as specific below:

- I. Hydration characteristics observed in both full, partial, and ambient during accelerated aging of both binary and ternary blends.
- II. Phase assemblages during exposure to both accelerated and ambient carbonation.
- III. Microstructural characterization and changes upon exposure to ambient and accelerated carbonation conditions.
- IV. Determine of the carbonation depth of both binary and ternary blends at different relative humidities.
- V. Study the effect of carbonation on compressive strength of both ternary and binary mixes at different relative humidities and water-binder ratios.

### 1.4 Thesis outline

This thesis is presented in 7 chapters.

Chapter 1 provides background for the research and problem statement with the main goal and objectives of the research.

Chapter 2 presents a review of existing literature, showing the current understanding of the hydration of Portland cement, slag, and limestone cements. The current knowledge on carbonation and various parameters affecting carbonation of SCMs and its effect on the phase assemblage, microstructure, and mechanical properties of blended cement is also presented.

Chapter 3 describes materials, methods and techniques used in the research.

Chapter 4 presents the results and discussion of ambient carbonation at two water-binder ratios, examining ongoing hydration, phase changes and durability performance.

Chapter 5 focuses on accelerated carbonation at two water-binder ratios, examining ongoing hydration, phase changes and durability performance.

Chapter 6 focuses on the broader comparison of hydration, phase changes microstructural characterization and mechanical strength under both accelerated and ambient carbonation conditions.

Chapter 7 summarises the findings, presents the main conclusions obtained from the research and perspectives for further studies.

## Chapter 2: Literature review

### 2.1 Portland cement

Cement is manufactured by heating a mixture of raw materials containing calcium oxide and silicates. The calcium oxide is usually sourced from limestone or other raw deposits of chalk, shell, and calcareous mud while the silicates are from clays or other sources such as silts and other argillaceous rocks. The raw material is heated under controlled conditions in a kiln to a temperature between 1400 to 1600 °C. The main elements in the raw materials are Ca, Si, Al, Fe and other minor impurities which are heated in the kiln to form clinker. The clinker is cooled rapidly and ground together with a small amount of gypsum, to regulate the setting of the cement paste and contribute to its strength development.

CaO, SiO<sub>2</sub>, Al<sub>2</sub>O<sub>3</sub>, and Fe<sub>2</sub>O<sub>3</sub>, are the major oxides of Portland cement and comprise of 61-67%, 19-23%, 2.5-6% and 0-6% of the total clinker mass respectively [14]. Figure 2.1 shows the Portland cement chemistry flow chart.

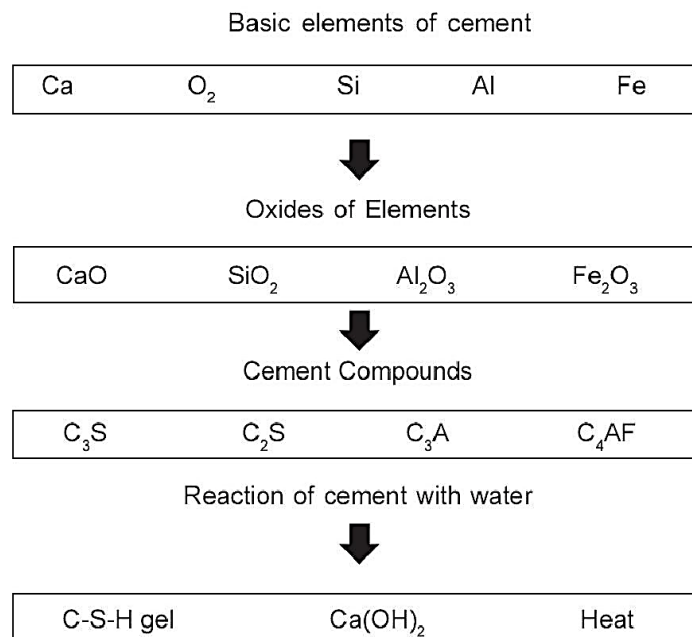


Figure 2.1: A brief summary of cement chemistry.

#### 2.1.1 Cement compounds

The four major phases of Portland cement, identified as tricalcium silicate (Ca<sub>3</sub>SiO<sub>5</sub>, C<sub>3</sub>S), dicalcium silicate (2CaO.SiO<sub>2</sub>, C<sub>2</sub>S), tricalcium aluminate (3CaO.Al<sub>2</sub>O<sub>3</sub>, C<sub>3</sub>A) and tetracalcium aluminoferrite (4CaO.Al<sub>2</sub>O<sub>3</sub>Fe<sub>2</sub>O<sub>3</sub>, C<sub>4</sub>AF), are the major contributors

to the mechanical strength, setting and durability properties of Portland cement. Table 2.1 shows these major compounds, with their percentage mass, mineral name, and functions in the cement paste. Being derived from natural raw materials, there are also trace elements that are usually present in Portland cement sufficient to form separate phases, notably Na<sub>2</sub>O, K<sub>2</sub>O and SO<sub>3</sub> which form alkali sulphates, and MgO which forms periclase [15].

Table 2-1: Major compound of cement and functions.

Chemical Name	Chemical Formula	Cement Notation	% Mass in Portland Cement	Mineral Name	Function in OPC paste
Tricalcium Silicate	Ca <sub>3</sub> SiO <sub>5</sub>	C <sub>3</sub> S	50-70	Alite	Responsible for early strength gain
Dicalcium Silicate	Ca <sub>2</sub> SiO <sub>4</sub>	C <sub>2</sub> S	15-30	Belite	Responsible for slow strength gain after 7 days
Tricalcium Aluminate	Ca <sub>3</sub> Al <sub>2</sub> O <sub>6</sub>	C <sub>3</sub> A	5-10	Aluminate	Contributes to early hydration and responsible for setting time.
Tetracalcium Aluminoferrite	Ca <sub>2</sub> Al <sub>2</sub> FeO <sub>5</sub>	C <sub>4</sub> AF	5-15	Ferrite	Contributes little to strength gain and influences majorly the grey colour of OPC.

The approximate content of each of the major clinker phases can be calculated based on Bogue calculations [16]:

If A/F = > 0.64

$$\%C_3S = 4.07(\text{CaO}) - 7.60(\text{SiO}_2) - 6.72(\text{Al}_2\text{O}_3) - 1.43(\text{Fe}_2\text{O}_3) - 2.85(\text{SO}_3) \quad 2.1$$

$$\%C_2S = 2.87\text{SiO}_2 - 0.75(3\text{CaO} \cdot \text{SiO}_2) \quad 2.2$$

$$\%C_3A = 2.65(\text{Al}_2\text{O}_3) - 1.69(\text{Fe}_2\text{O}_3) \quad 2.3$$

$$\%C_4A = 3.04(\text{Fe}_2\text{O}_3) \quad 2.4$$

If A/F = < 0.64

$$\%C_3S = 4.071 \text{ CaO} - (7.602 \text{ SiO}_2 + 4.479 \text{ Al}_2\text{O}_3 + 2.859 \text{ Fe}_2\text{O}_3) \quad 2.5$$

$$\%C_2S = 2.867 \text{ SiO}_2 - 0.7544 \text{ C}_3\text{S} \quad 2.6$$

$$\%C_3A = 0 \quad 2.7$$

$$\%C_4AF = 2.1 Al_2O_3 + 1.702(Fe_2O_3) \quad 2.8$$

Bogue calculations assume that all phases present in the clinker are in their purest form and heating in the cement kiln reaches about 1600°C for the reactions to reach thermodynamic equilibrium [17], and then properly cooled. In practice this is not common, especially with modern cement production that uses less heating and with clinker contaminated with some low fusing impurities [17, 18]. Moreover, Bogue calculations underestimate C<sub>3</sub>S and overestimate C<sub>2</sub>S, while some oxides replace CaO in C<sub>3</sub>S within the composition calculation [14].

Despite various anomalies associated with the aforementioned assumptions, the Bogue equations are a widely accepted means of calculating Portland cement phase composition. However, the anomalies observed in the calculations led to the development of Taylor's modified Bogue's calculation which considered the rapid cooling technique used in modern cement kilns and recognised minor components in cement clinker [19]. Determining the various compound composition of Portland cement can help in predicting the properties of the cement pastes and to manipulate the compound composition of Portland cement to modify cement properties to meet various applications in modern construction practices.

### 2.1.2 Portland cement hydration mechanism

Hydration of Portland cement is a series of chemical reactions that begins immediately water comes in contact with cement particles. Significant amount of dissolution and precipitation reactions are initiated, and the process continues with the formation of the cement microstructure, which directly determines the mechanical strength and the durability of the pastes or concrete [20]. Cement hydration is a continuous process where the clinker minerals are transformed through the aqueous reactions to a series of hydrates. The process usually continues until there is no cement component, moisture, and/or space within the matrix for the deposition of the formed hydrates. This may take months before such occurrence.

Hydration of Portland cement is exothermic, with generation of heat upon contact with water and with hardening of the cement paste. The most heat is released during the first few minutes of contact with water usually called pre-induction or dissolution stage. During this period, aluminates in the clinker and sulphates from the added gypsum

react. Without the addition of sulphates, aluminates would react rapidly with large heat evolution and cause flash setting [21, 22].

However, in the presence of sulphates, small amount of crystalline ettringite or AFt phase is formed at the surface of the mix, the heat release then decreases drastically as the cement paste slides into the dormant period, which can last up to about 3-6 hours [14].

The dormant or induction period is particularly important as it allows the concrete to be transported from the casting shop or premix yard and placed on the job site without any distortion due to plastic state of the cement during the period. Several hypotheses explaining the dormancy mechanism of the Portland cement have been proposed over the years. Among the hypotheses are the formation of protective metastable hydrate layers of grains on the surface which inhibit further hydration of the cement grains [23, 24], or SiO<sub>2</sub> pollution of the CH nuclei causing induction and ends when the level of super saturation is high enough to overcome the nuclei and CH products in the crystalline system [25]. The induction period ends when hydration of C-S-H starts to nucleate and grow. The last of the hypotheses is that the initial chemical reactions form a semi-permeable layer around the Portland cement grains which encloses an inner pore solution which is later destroyed by osmotic pressure [26]. All these hypotheses have been subjected to a lot of arguments over the years with recent experimental and numerical modelling evidence supporting the theory of geochemical dissolution, which gives a better understanding of the induction period [24].

Toward the end of the dormant stage the initial setting of the cement paste occurs, signifying the beginning of the acceleration stage, where a second evolution of heat occurs lasting for a few hours. This period is characterized by dissolution of belite, aluminate and primarily alite into solution, leading to the precipitation of C-S-H and CH, with ettringite also continuing its growth at this stage.

The deceleration stage follows the acceleration period, with slight heat peak observed as result of the renewed aluminate and ferrite hydration after consumption of the gypsum leading to conversion of ettringite to monosulphate (AFm phase). This usually lasts for about few hours. Alite hydration dominates at this stage with Portland cement paste gaining considerable strength. Subsequent belite hydration then provides progressive strength development.

After the deceleration period, the amount of unreacted material decreases and hydration becomes steady and determined by diffusion, with belite responsible majorly for the progressive strength development as long as water, anhydrous cement and pore spaces are present in the system. Figure 2.2 shows the diagrammatic representation of the hydration of Portland cement.

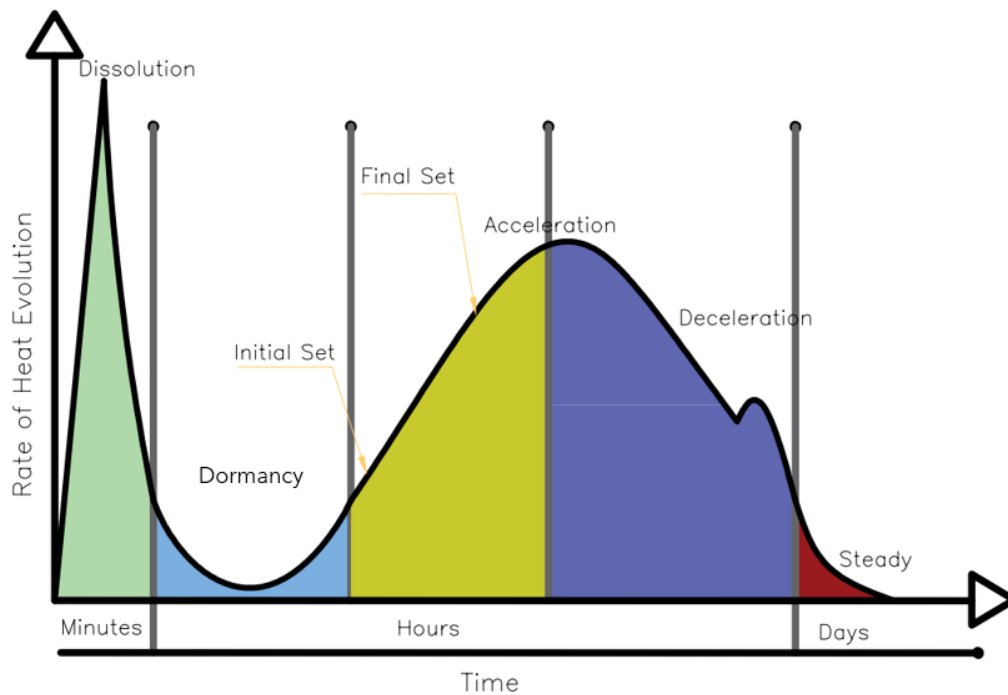


Figure 2.2: Hydration of Portland cement.

### 2.1.3 Pore structure of Portland cement

The hardening cement paste consists of CH, C-S-H (calcium silicate hydrate) gel, pores, entrapped air and unreacted cement [27]. Pores in hardening cement paste are classified according to their sizes, which range from large (from 10  $\mu\text{m}$  and above) to capillary pores (about 10000nm in diameter). The finest pores, ranging from approximately 10 nm to 0.5nm, are called gel pores [28] and constitute the internal porosity of the C-S-H gel phase. Pores of 0.5nm or smaller are formed by the interlayer spaces of C-S-H gel, where chemically bound water resides and leading to the refinement of the pore structure of the paste. Voids greater than capillary pores are usually entrapped air linked to the mixing procedure. Table 2-2 categorises different pores by size, the common technique of their measurement and paste properties affected.

Table 2-2: Pores classification (Taken from [26]).

Type of Pore	Description	Size	Water	Technique <sup>a</sup>	Properties
<i>Capillary Pores</i>	Large	10 $\mu\text{m}$ – 50 nm	Evaporable Bulk water	SEM, OM	Permeability, strength
	Medium	50 – 10 nm	Evaporable Moderate menisci	SEM	Permeability, strength, shrinkage (high RH)
<i>Gel Pores</i>	Small	10-2.5 nm	Evaporable Strong meniscus	Adsorption/ MIP/IS	Shrinkage (to 50% RH)
	Micropores	2.5-0.5 nm	Non-evaporable -No meniscus -Intermolecular interactions	Adsorption/ MIP/IS	Shrinkage, creep (35-11% RH)
<i>Interlayer Spaces</i>	Structural	< 0.5 nm	Non-evaporable -Ionic/covalent bond	Adsorption/ Thermal	Shrinkage, creep (< 11% RH)
<i>Other Features</i>	ITZ	20-50 $\mu\text{m}$	Bulk Water	SEM/OM	Permeability, strength
	Microcracks	50 - > 200 $\mu\text{m}$	Bulk Water	SEM/OM	Permeability, strength

<sup>a</sup> SEM: scanning electron microscopy; OM: optical microscopy; IS: impedance spectroscopy.

The mechanical properties of cement pastes or concrete are related to the capillary porosity of the mix, as porous mixes usually have poor mechanical strength [27]. Porous cement systems also allow transport of aggressive substances, which cause deterioration of the concrete or mortar. Although transport of aggressive substances is more affected by the interconnectivity of the pores than the total porosity in the system.

Different methods have been used to determine the pore system of cement paste (Total porosity, pore size distribution and specific surface area of the pores) from Mercury Intrusion Porosimetry (MIP), Nuclear Magnetic Resonance Spectroscopy (NMR), pycnometer, gas sorption, Scanning Electron Microscopy (SEM), to recently x-ray microtomography ( $\mu\text{CT}$ ). MIP is perhaps the most popular method to measure capillary pores, despite inconsistent results recorded due to sample preparation (drying) and large stress damages experienced during characterisation [29]. Other methods such as SEM analysis can be used to identify larger pores (>500nm) with BSE imaging also reported to measure total coarse porosity [30].

## 2.2 Ground granulated blast furnace slag

GGBS was first commercially produced in Germany in 1880 following discovery of its latent hydraulic nature in 1862 by Emil Langen [31]. Slag is a by-product of iron production, and mostly comes from floating molten liquid from newly produced iron from the blast furnace and rapidly cooling it to form granules. The granulated slag is then ground into a fine powder. It's used as a mineral addition in replacing clinker in blended cements as specified in BS EN 197-1:2011 [11]. The hydraulic activity of GGBS depends on its chemical composition, fineness, glass content (at least two third must contain glass as specify in BS EN 197-1:2011, alkalinity of the activating system and curing temperature [32].

GGBS has the most similar oxide content to Portland cement among the SCMs but differs in relative proportions [31]. It majorly comprises calcium, aluminium, magnesium, and silicon oxides as active ingredients, comprising around 95% of the total mass. The oxide composition varies slightly from different sources but is usually within the ranges as shown in Table 2.3. This variation is attributed to the raw materials available during production and the type of iron needed to be produced [33].

Table 2-3: Ranges of GGBS oxides composition (Taken from [30]).

Oxide composition	Percentage weight (%)
(CaO)	32.0-45.0
Silica (SiO <sub>2</sub> )	32.0-42.0
Alumina (Al <sub>2</sub> O <sub>3</sub> )	7.0-16.0
Magnesia (MgO)	5.0-15
Sulphur (S)	1.0-2.0
Iron Oxides (Fe <sub>2</sub> O <sub>3</sub> )	0.1-1.5
Manganese Oxide (MnO)	0.2-1.0

Apart from the latent hydraulic activity of GGBS, it is a widely used SCM in partial replacement of Portland cement due to its sustainability and low embodied CO<sub>2</sub> at 67kg/per tonne compared to CEM I at 830kg/per tonne [34]. GGBS utilization as partial replacement of Portland cement in concrete helps to improve the workability of fresh

concrete, resists harsh exposures such as chloride- and sulfate-rich environments, has a low heat of hydration (in turn reducing thermal cracking in large concrete structures), and improves the long-term mechanical strength of concrete.

### 2.2.1 Hydration of GGBS

The hydration reaction rate of GGBS when used alone is very slow, hence there is a need for activators. These are often alkalis, but sulphates can also be used, although they are less favoured due to requiring longer curing times. The alkalis may be added externally, but more commonly they are released upon Portland cement hydration in the form of portlandite. GGBS blended cement hydration is more complex than pure Portland cement hydration due to the interaction between cement clinker and GGBS [11, 35]. Slag-cement has low heat of hydration compared to Portland cement due to the slow hydraulicity and dilution property [11].

Studies have shown that composite GGBS cements hydrate to form similar hydration products to Portland cement paste [29] except the hydrotalcite like solids observed, due to the presence of MgO in the slag, and possibly stratlingite formed as AFm [36].

Cement clinker plays a significant role during hydration as CH is produced during the reaction. CH produced from the hydration reaction acts simultaneously both as activator and reactant [37]. Thus, the amount of portlandite in the slag -clinker system is reduced compared to neat OPC, while the formation of C-S-H with a lower Ca/Si ratio is observed and alumina from the GGBS is incorporated in the C-S-H to form the C-(A)-S-H [37].

### 2.2.2 Microstructures development and pore structure of GGBS

Blending GGBS with Portland cement plays significant role in concrete's microstructural development by refining the pore size, especially larger pores. This phenomenon can be attributed to the formation of more C-S-H gel which is much denser [37, 38] than that produced in neat Portland cement paste. At early ages, the total porosity is the same as for neat Portland cement paste while at later ages [37], the volume of capillary pores of slag-blended cement decreases. Also, Liu et al. [20], studied the total porosity of OPC and blended slag cement pastes using MIP and found minimal differences between OPC and blended cement containing 10-40% GGBS, but the slag cements had much finer microstructures after 90 days.

### 2.2.3 Mechanical strength of GGBS blended cement

Mechanical strength is the most important engineering property of any construction material, to ensure safety. Compressive and flexural strength tests are the indicators usually used in determining the mechanical strength of concrete and mortar, in accordance with the guideline of BS EN 196-1. The strength development of GGBS-blended cement is governed by GGBS replacement level, water-binder ratio and curing conditions [39, 40]. Shariq et al. [40] studied the optimization of the GGBS in both mortar and concrete samples using 20%, 40%, and 60% GGBS replacement for slag-cement blended binder. They found that 7-day strengths were lower for mortars at all replacement levels, but strengths were higher by 56 and 90 days for 20% and 40% replacement respectively. While at 60% replacement level strengths were lower at all ages but with the continued formation of C-S-H leading to pore filling and higher later-age strength. The optimal GGBS replacement level has been reported to be 55% [41] with further addition leading to lower strength gained over the course of testing.

### 2.3 Limestone

Limestone additions (blending or inter-grinding) in cement production has gained wide acceptance due to engineering and economic benefits derived from such additions.

The inclusion of ground limestone in Portland cement in the past was the subject of discussion with proponents claiming that it's an energy saving technique that has no effects on the quality of the cement, while opponents claimed that it was a clear adulteration of the original product [42]. Studies have shown limestone addition reduces CO<sub>2</sub> emissions when used as a clinker replacement, with ground limestone replacement also reducing demand for fossil fuels and mineral resources [43]. Apart from environmental and economic considerations, it has also been reported to help improve early age mechanical strength, porosity, and durability properties [6, 43] of cement-based material. Limestone blended cement did not gain wide acceptance in Europe and other developed countries until 1980's [7]. However, up to 10% inclusion of limestone was reported in Spanish cement production in 1960 rising to 35% in 1975 [44]. It was also attempted in Germany for speciality applications with 10% inclusion in 1965, adopted in France in 1979 and around 20% inclusion in Britain's standard in 1992 [44, 45]. Also, 5% inclusion was allowed in both Canada & USA in 1983 and 1974 respectively due to a shortage of oil in the 1970-80's [42, 44, 46]. BS EN 197-1 provides for up to 5% limestone addition as a minor constituent and two other types of

Portland limestone cement at 6-20% addition for types II/A-L, II/A-LL and 21-35% addition for types II/B-L, II/B-LL cement is available in the BS EN standard with a minimum 75% calcium carbonate content required from the limestone composition.

### 2.3.1 Hydration of limestone blended cement

In the past, limestone was believed to act as an inert filler in the limestone cement until research showed that it participates in the hydration reaction [44, 47]. There is a consensus among researchers that limestone reacts majorly with  $C_3A$  phases of the Portland cement and delays ettringite to form monosulfoaluminate [10, 46]. During hydration process, various carboaluminates are formed and the rates are dependent on limestone composition or content, reactivity or fineness and the amount of sulphate in the system [46]. Adu-Amankwah et al. [48] observed formation of ettringite in the first day of hydration of slag-blends containing limestone at 10, 20% and CEM I, while hemicarboaluminate was detected in all the mixes at 7 days.

Limestone addition provides nucleation sites for the hydrates, which aids C-S-H precipitation and so accelerates clinker hydration, aiding development of early age strength. However, limestone does not have pozzolanic or hydraulic properties and cannot add to C-S-H gel [44] but the amount of CH formed in limestone blended Portland cement was found to have been increased at early days due to the dilution and nucleation effects of limestone [49]. While Voglis et al. [10] concluded that 15% limestone addition did not have any effect on the amount of CH formed in the blended mix. Tsvivilis et al. [50] observed progressive increase in CH content from 2 days to 28 days measured with TGA and also higher bound water contents with 10% limestone addition in a cement paste, which further evidenced the participation of limestone in the reactivity and acceleration of C-S-H of the clinker. In ternary blended cement, limestone provides synergy to other SCMs such GGBS or PFA, which are known to have slow early hydration. This synergy with GGBS or PFA helps to hasten hydration at early days by providing nucleation sites for growth of C-S-H, which helps improve clinker hydration. Bentz et al. [51] showed nano-limestone reduces the setting time of PFA blends and accelerates early-age hydration of blended concrete. Similarly De Weerd et al. [46] reported 5% limestone inclusion in PFA ternary blended led to an increase in the volume of hydrates and subsequent increase in chemical shrinkage.

### 2.3.2 Microstructure and transport properties of limestone blended binder

Modification of hydration kinetics and phase assemblages in limestone ternary cements are reflected in the pore structure, so affecting transport properties. Additional hydration products densify the structure, reducing porosity over time. This however relies on hydration of the aluminosilicate. For example, greater capillary pore volume and larger critical diameters have been reported in limestone-PFA blends compared to CEM I, even after hydrating for 6 months [52]. Similar observations were made elsewhere [53] but the capillary pore volume reduced significantly after 90 days as more of the PFA reacted. Meanwhile, decreasing micro-capillary pores were reported, even after 7 days [54]. It is noteworthy that the latter study contained 80% clinker content as opposed to <60% in the preceding studies. In blends with more reactive SCMs e.g slag and calcined clay, refinement of capillary pores is observed at clinker contents of 50% and below in Figure 2.3. Lower critical pore sizes, and hence threshold radii, have been reported at 28 days in slag cements compared to CEM I [55, 56] whilst significant refinement was already evident after 3 days in LC3 systems [57]. However, one must recognize that this pore refinement does not necessarily lead to lower total porosity. Indeed, up to 10% increase in total porosity was determined in slag and LC3 blends with 50% clinker, for which the derivative plots are shown in Figure 2.3 below.

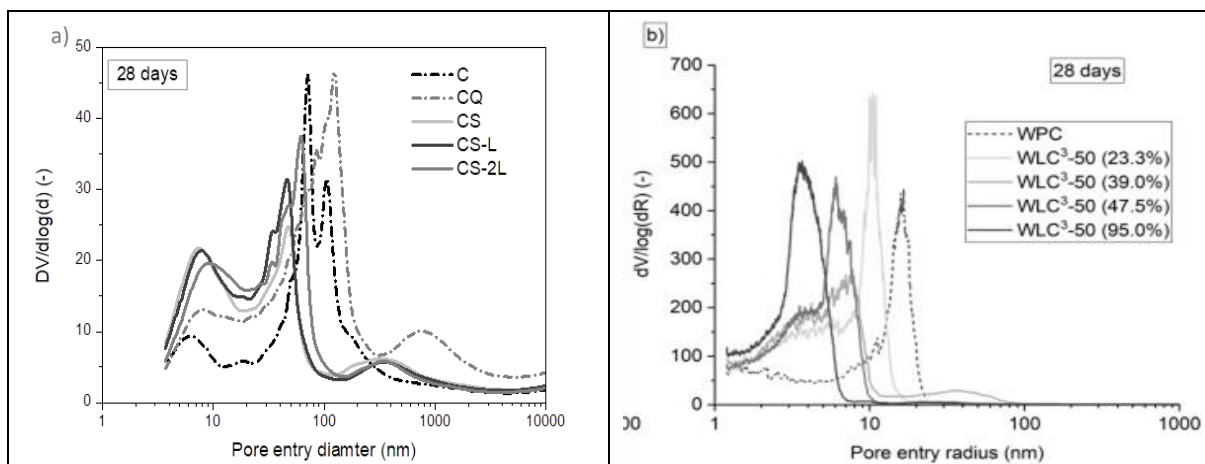


Figure 2.3 Comparison of the pore size distribution of limestone ternary blended cements from GGBS (a) and calcined clay (b) compared to Portland cement [56, 58, 59].

From a practical perspective, transport properties are defined by the pore size distribution and tortuosity more than the total porosity. Increasing gel porosity (i.e., <

10 nm) in ternary cements (Figure 2.3) arises from the additional hydrates formed from the reactive aluminosilicates. Moreover, these gel pores are mostly disconnected and hence don't impact on transport properties. Conversely, refinement of micro-capillary pores (50 – 1000 nm) reduces water, gas, and ion migration.

Lower sorptivity coefficients and ion conductivities were reported in limestone-natural pozzolan ternary blends in the RCPT test [60]. These were comparable to those observed for binary OPC-natural pozzolans but better than for OPC. Similar observations were made by Celik et al. who proposed ~50% clinker substitution threshold in limestone-aluminosilicate blends [61]. However, Elgalhud et al. [62] reviewed over 191 papers published from 1993 till 2006 to determine the effects of limestone additions on the porosity of pastes, mortars, and concretes. They found that the pore structure properties remain unchanged up till 25% limestone addition and with decrease in limestone content, it resulted to constant decrease in the porosity for all studies surveyed. One key property identified is fineness, which positively affects the porosity of the blended matrix thereby improving the microstructure. The carboaluminate hydrates formed by the reaction of limestone with  $C_3A$  reduces the porosity and is thereby a crucial factor in improving the mechanical strength of the mix [63].

### 2.3.3 Mechanical strength of limestone blended cement

The strength development of Portland limestone cement is attributed to the production methods (whether blending or inter-grinding with clinker), composition, quantity, fineness of both cement & limestone and the water-binder ratio [64]. Thongsanitgarn et al. [65] investigated the effect of including different limestone fineness at 5 $\mu$ m, 10 $\mu$ m and 20 $\mu$ m and different percentage increase in limestone content ranging from 5%-25% on the compressive strength of concrete. They observed an increase in the compressive strength with increasing limestone powder fineness and a decrease in the compressive strength at all ages as percentage of replacement increases, due to the dilution effect. Ramezaniapour [47] proposed that finer limestone can compensate adequately for the reduction of compressive strength at higher additions. On the contrary, 5% limestone addition has been reported to improve the early strength development due to effect of particle filling on the hydration, to produce a nucleation site for the promotion of calcium hydroxide [66]. In composite cement, replacing OPC with either PFA or GGBS can decrease the early mechanical

performance of cementitious materials at early ages. Longer curing times may be necessary to attain similar strength values to Portland cement concrete, but sometimes this is not practicable in construction due to time constraints. The introduction of limestone either as filler or inter-ground has been shown to enhance nucleation sites for portlandite crystals and participate actively in the formation of monocarboaluminate [55], which can also improve slag hydration and reduces the time to achieve the required strength. However, several studies [67-69] have shown that replacing more than 10-15% of PC with limestone is not recommended to prevent a dilution effect that may result in a loss of mechanical strength during advanced hydration ages [70].

## 2.4 Carbonation

Carbonation is a naturally occurring phenomenon which is one of the major causes of corrosion in reinforced concrete structure degradation [71, 72]. Also, an immensely helpful mechanism in the curing of un-reinforced concrete. According to [73], carbonation of cement paste can be divided into two parts, namely passive (deterioration) and active (utilization) as shown in Figure 2.4 below.

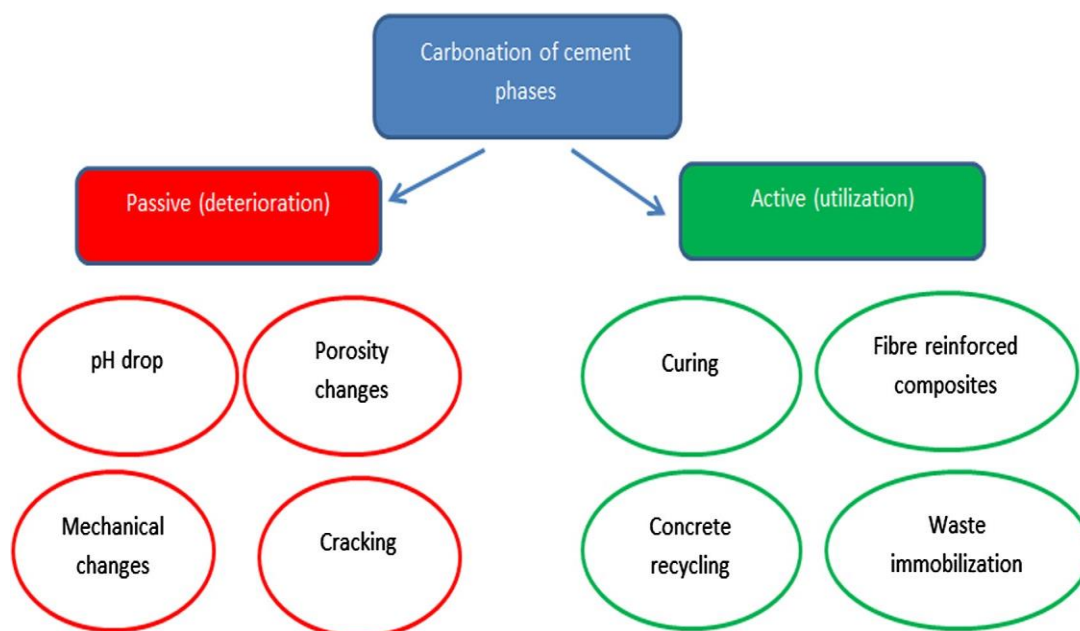


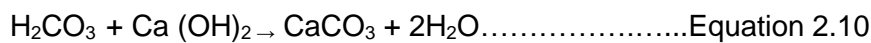
Figure 2.4: Carbonation of cement paste: Active and Passive (Taken from [62])

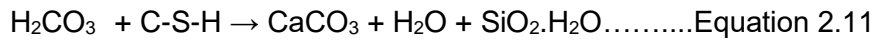
Carbonation curing in un-reinforced concrete is advantageous, especially in the early-stages of cement hydration, to improve the performance of the cement-based materials. Carbonation curing is an acceptable practice in the precast and fibre

reinforced composites industry and was reported to improve porosity, permeability, and the mechanical properties of the concrete [73, 74]. Carbonation in reinforced concrete has been a major concern since it can initiate corrosion [73]. Corrosion is well recognised problem causing degradation of reinforced concrete structures with estimated cost of corrosion worldwide around \$2.5 trillion in 2013 [75].

The carbonation mechanism in reinforced concrete structure involves the reaction of carbon dioxide from the atmosphere, water inside the pore structure and the calcium bearing hydrates in the cement paste. The interaction of these three, under favourable humid or moisture conditions will led to lowering of the highly alkaline state of cement paste around the reinforcement area from a pH more than 12 to around 9 or less [76]. The protective passive film of ferrous oxide on steel is attacked due to the reduction in alkalinity of the surrounding cement paste, initiating corrosion. While carbonation itself is not responsible for corrosion of steels in reinforced concrete, depletion of hydrated calcium bearing phases in the cement paste led to lowering of the highly alkaline pH of the cement paste in the system. The impact of steel corrosion will led to formation of cracks in and around the concrete [73]. Cracks are also considered as one of intrinsic attribute of corrosion [77] in reinforced concrete structures which later allows the ingress of water and other harmful chemicals into concrete core and reduced the service life of structures.

According to Taylor [29], carbonation proceeds with the dissolution of CO<sub>2</sub> in the interconnected pore structure of the cement matrix and reacts with the available water to form carbonic acid (H<sub>2</sub>CO<sub>3</sub>) as the first step in the chemical reaction. The carbonic acid formed then reacts with cement hydrates majorly Ca(OH)<sub>2</sub>, consuming the hydroxyl and other hydration product such as C-S-H and other calcium bearing phases including the aluminate and ferrite phases in the cement paste and converting it to CaCO<sub>3</sub> and water. CaCO<sub>3</sub> formed can exit in three crystal forms namely aragonite, vaterite and the most stable form calcite. Equations 2.1 - 2.4 represents the chemical reaction during the carbonation of cement paste.





Nine steps were identified in the entire reaction mechanism of the carbonation of cementitious material [29] namely:

- Diffusion of CO<sub>2</sub> in the atmosphere
- Permeation of CO<sub>2</sub> through the solid cementitious materials
- Solvation of CO<sub>2(g)</sub> to CO<sub>2(aq)</sub> in pore structure of the solids
- Hydration of CO<sub>2(aq)</sub> to H<sub>2</sub>CO<sub>3</sub>
- Ionisation of H<sub>2</sub>CO<sub>3</sub> to H<sup>+</sup>, HCO<sub>3</sub><sup>-</sup> & CO<sub>3</sub><sup>2-</sup>. (This lowers the pH from 12.5-13 to 9 or below).
- Nucleation of Ca(OH)<sub>2</sub> and C-S-H
- Dissolution of the hydration phases.
- Precipitation of solid phases and formation of CaCO<sub>3</sub>.
- C-S-H gel decalcification

#### 2.4.1 Accelerated carbonation vs natural carbonation.

Natural carbonation is slow, with CO<sub>2</sub> concentrations being around 0.04%. Therefore measurable changes are time-consuming despite being the most realistic means of examining the performance of the concrete [74]. Thus, accelerated testing regimes have been developed, which can be used to determine the carbonation resistance of cementitious materials in a manageably brief period. Viser [78] emphasised the discrepancies between the measured carbonation resistance during accelerated and natural carbonation is a major difficulty in implementing performance based concrete design for carbonation. Accelerated carbonation testing is when cement-based materials are subjected to severe conditions over short durations, to speed up the carbonation process. They are much more severe than the conditions which cement-based materials will experience under service conditions but help to predict the resistance of such materials to carbonation.

Table 2-4 summarises accelerated carbonation testing standards from various European countries and shows the various testing parameters considered and testing procedures adopted.

Table 2-4: Summary of selected European accelerated carbonation tests

Country	Preconditioning Regime	Specimen Type/size	Accelerated carbonation exposure conditions			Carbonation depth measurement method	Time of carbonation depth measurements
			CO <sub>2</sub> (% Vol.)	Temp. (°C)	RH (%)		
Belgium	Water cured for 8 weeks then transferred to 60°C room for 14 days or until constant mass	Concrete prism 150×50×600 mm	1	20	55	RILEM CPC-18 (RILEM, 1988)	3, 7, 14, 28, 35, 42, 56 days
Germany	7 days water then 21 days lab conditions (20-28° C, 65 ± 5%)	Concrete prism 100×100×500 mm	2	20	65	DIN EN 206	28 days
UK	28 days water then 14 days lab conditions (20-28°C, 65 ± 5%)	Concrete prism 100×100×500 mm	4.0±0.5	20 ± 2	55 ± 5	BS 1881-210:2013	Various ages up to 28 days
France	28 days or 90 days (water or RH 95%) vacuum saturation for 24 h followed by oven drying for (48± 2 hours) at 40± 5°C <sup>c</sup>	Concrete prism: 70×70×140 mm Concrete cylinder: 110 Ø x 70 mm	50±5	20 ± 2	65 ± 5	AFPC-AFREM (similar to RILEM CPC-18)	At least 7, 14 and 28 days
Italy	3 days water; 25 days in air (20°C, 50% RH)	Concrete cylinder Ø=80 mm, h=200 mm	50	20	55	UNI 9944	3, 6, 9, 12, 15 days
Nordic	Minimum of 4 weeks in atmosphere of 23 ± 2°C and 50 ± 5% RH	Mortar prism 40 × 40 × 160 mm	20±3	23±3	65 ± 10	NT Build 357	Exposed for 8 days, tested every 48 h

There have been several debates on whether results obtained from such accelerated testing can be relied upon to design or model the service life of concrete [79] and whether there is correlation between accelerated and natural carbonation to completely predict the carbonation resistance of cement-based materials. The major limitations of accelerated carbonation are repeatability and reproducibility of the test procedures, even in ordinary Portland cement specimens [79].

In the study conducted [80],  $\text{CaCO}_3$  polymorphs formed from the natural and accelerated carbonation using 100%  $\text{CO}_2$  exposure are different with calcite, vaterite and aragonite detected under natural carbonation testing and only calcite present in the accelerated test. The formation of only calcite was attributed to the high decalcification of the C-S-H gel due to high  $\text{CO}_2$  concentration applied in the accelerated carbonation [13, 81] and porosity was higher following accelerated carbonation than that obtained from natural carbonation of OPC with the same w/c.

Sanjuan et al. [82] tested concrete made from CEM I 42.5R and 52.5R with two different  $\text{C}_3\text{A}$  contents (3.6% and 11% respectively) at 5 and 100%  $\text{CO}_2$  for accelerated carbonation and natural exposure to ambient conditions. Accelerated carbonation changed the relative rankings of the concretes, and they concluded that comparison between accelerated and natural carbonation can only be made between concrete of the same raw materials, especially binders.

The accelerated carbonation testing standards in Table 2-4 above are more likely suitable for ordinary Portland cement concrete or mortars as various researchers have also challenged the use of some of the methods with supplementary blended binder and mineral additions in cement.

Younsi et al. [83] questioned the validity of the French accelerated carbonation standard applied to 50% PFA blended concrete compared to natural carbonation test by showing that accelerated carbonation is highly contingent on the reactions with hydration products of the binder and natural carbonation is dependent on the diffusion of  $\text{CO}_2$  in the atmosphere into the concrete. However, it's important to understand the carbonation mechanism of cement-based materials over brief periods, which brought about using accelerated carbonation test methods, the test results should be considered as a tool to understand the qualities of such material among its equals and not as a comparison tool or use to specifically evaluate the long-term exposure or

natural carbonation phenomenon. However, accelerated carbonation can be an important tool for laboratory studies of various cement-based materials, as far as its limitations are considered in interpreting test results [82]. This is due to changes in moisture distribution because of various seasonal periods on materials exposed to natural acceleration which in turn also have effects on the pore structure of the cement-based material as result of ageing [84].

#### 2.4.2 Factors influencing accelerated carbonation of cementitious materials.

Environmental conditions and binder properties have been clearly established as the two broad phenomena that influence accelerated carbonation tests [85]. Czarnecki et al. [86] categorises the factors affecting carbonation of concrete as external and internal, as shown in Figure 2.5 below. The external factors are further sub-divided into exploitation and technology factors. The exploitation factor comprises of various conditions that are based on the environmental exposure such as the concentration of CO<sub>2</sub>, relative humidity and temperature which are to simulate or represent the natural carbonation mechanism, while technology factors are curing and pre-conditioning effects that cementitious materials need to undergo to achieve sufficient hydration and moisture equilibrium or stabilisation of the internal relative humidity [82] before subjecting to accelerated carbonation.

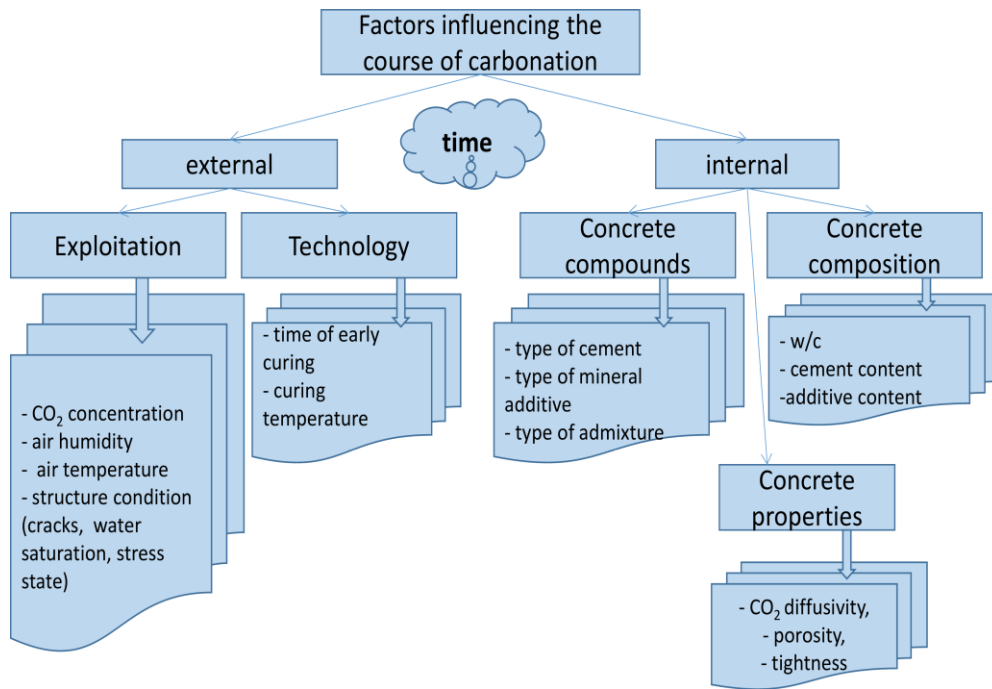


Figure 2.5: Factors influencing accelerated carbonation test (Taken from [66]).

The CO<sub>2</sub> concentration, relative humidity and temperature are the major factors that control the carbonation rate in both natural and accelerated testing and show variations across selected European standards for accelerated carbonation testing shown in Table 2-5. Curing techniques, pre-conditioning regimes and carbonation durations are also other concerns and the subject of discussion. However, the major concern with accelerated carbonation has been the exposure conditions, which has been the debatable over the years. The concentration of carbon dioxide in natural environment usually around 400ppm. However, CO<sub>2</sub> level in the atmosphere depends on types of human activities around the area where the reading is taken [87] and high in areas with industrial activities and congested transportation operation. The concentration of CO<sub>2</sub> used for accelerated carbonation tests in some of the European country's standard varies between 1-50% [79] and up to 20% in China [88].

Castellote et al. [89] researched the effect of different carbon dioxide concentrations, from natural to 3%, 10% and 100%, on the microstructural development and hydration products formed in ordinary Portland cement paste. They observed, using TGA, that uncarbonated portlandite remains following natural carbonation, but is absent following accelerated carbonation of samples at above 3% CO<sub>2</sub>. Also, there was a change in the Ca/Si ratio of the C-S-H during carbonation at natural, 0.03 and 3% compared to an unexposed sample, with Ca/Si falling to 1.87, 1.23 and 1.18

respectively, while no C-S-H was observed at 10 & 100% CO<sub>2</sub> exposure. They concluded that accelerated carbonation up to 3% is comparable to natural carbonation at a factor of up to 100 times and 3% CO<sub>2</sub> concentration will not significantly affect the microstructure of OPC paste with low aluminium and 5% limestone addition.

Harrison et al. [79] reviewed various accelerated carbonation testing standards across Europe, comparing various concentration of CO<sub>2</sub> used in accelerated testing and concluded that increasing or decreasing concentration of CO<sub>2</sub> from 4% did not change the ranking of the concrete mixes in the accelerated testing regime. This assertion was also collaborated by the study of Dhir et al. [90] that carbonation at 0.035% and 4% CO<sub>2</sub> concentration can be used to provide long-term indication for natural environment of concrete made from ordinary Portland cement and Portland limestone cement.

Relative humidity is the ratio of the partial pressure of water vapour to equilibrium vapour pressure of water at a specific temperature. Relative humidity affects the carbonation of cementitious materials and varies according to the ambient conditions [91]. While water is vital in the carbonation reactions, there is a counter effect due to interaction between drying and carbonation process [84]. Also, relative humidity effectively influences the degree of saturation in the system and affects the rate of accelerated carbonation [92]. When relative humidity is low (<50%), there is insufficient moisture to form carbonic acid in the pores thereby reducing the carbonation rate. At high relative humidity (>70%), the pores are saturated, and transport is minimal, which also slows down carbonation [93]. But at intermediate relative humidity (50-70%) [14], CO<sub>2</sub> diffusion and reaction kinetics are favoured, and carbonation proceeds faster. The carbonation rate is low upon field exposure due to cyclic wetting and drying conditions resulting in unstable internal saturation. The regular use of constant relative humidity in accelerated carbonation tests therefore disadvantages binders with finer pore structure e.g., GGBS composite cements. Binders with finer pore structures will have more water filled pores than binders with a coarse pore structure at the same relative humidity [93]. The filled finer pores will take longer to dry than coarse pore system, which will led to a different carbonation rate.

Other factors relating to cement composition and properties such as water-binder ratio, mineral additive type, curing age, fineness of the mineral additive and quantity of clinker are also significant parameters governing the carbonation resistance of

cement-based materials, especially in composite cement systems [12, 94]. The water-binder ratio contributes immensely to the structure of the paste and subsequently has major impact on the course of carbonation. It's common knowledge that low water-binder ratio concretes are less susceptible to carbonation [95]. Sulapha et al. [96] shows lower water/binder ratio and prolonged curing, up to 28 days in 30% slag replacement in a composite mix leads to slower carbonation rates in composite cements and resulted to densification and refinement of the pore structure.

#### 2.4.3 Carbonation coefficient

Carbonation in any concrete materials progresses with time and follows a square root of time law and carbonation depth is considered as proportional to the square root of exposure period and the carbonation constant, which is based on the binders' properties, and can be predicted using equation 2.14.

$$X_c = k\sqrt{t} \dots\dots\dots\text{Eq 2.14}$$

Where  $X_c$  = Carbonation constant or coefficient

$k$  = Depth of carbonation

$t$  = Time

The formula in equation 2.14 only applies to steady CO<sub>2</sub> concentrations and binder paste with uniform properties. Several other equations have been proposed to account for differences in CO<sub>2</sub> concentrations, relative humidity and various hydrates involved in the carbonation process. Papadakis [12] proposed a mathematical model to determine the carbonation coefficient of SCMs which captures the hydration products and relative humidity during carbonation process.

$$X_c = \sqrt{\frac{2D_eCO_2(CO_2/100)t}{0.33CH+0.214CSH}} \dots\dots\dots\text{Eq 2.15}$$

Where CO<sub>2</sub> is the % CO<sub>2</sub> content in the ambient air at the concrete surface and DeCO<sub>2</sub> is the effective diffusivity of CO<sub>2</sub> in carbonated concrete (m<sup>2</sup>/s). In an ambient relative humidity ( RH), the diffusivity is given by the following empirical equation 2.16.

$$DeCO_2 = A \left( \frac{\epsilon_c}{\frac{c}{P_c} + \frac{p}{P_p} + \frac{w}{P_w}} \right)^a \left[ 1 - \frac{Rh}{100} \right]^b \dots\dots\dots Eq 2.16$$

The parameters A, a, and b are  $1.64 \times 10^{-6}$ , 1.8, and 2.2, respectively, obtained from regression analysis of experimental data for  $0.5 < W/C < 0.8$ . C= kg cement/m<sup>3</sup>, P = kg SCM (SF, FL, or FH), W = kg water,  $\epsilon_c$ = m<sup>3</sup> of entrained or entrapped air/m<sup>3</sup>,  $P_c$  = cement density (kg/m<sup>3</sup>),  $P_p$  =SCM density (kg/m<sup>3</sup>)  $P_w$  = water density (kg/m<sup>3</sup>).

### 2.4.3 Methods of assessing carbonation depth and products

Different methods have been used or proposed to assess the depth of carbonation in cement-based material and to determine various products expected during carbonation. From the literature, there is a clear understanding of the carbonation process and the hydrates involved in the process, with the products that will be formed at the end of the process, especially with Portland cement binder. The traditional or most used method of determining the carbonation depth is the colorimetric method. Phenolphthalein and thymolphthalein are the two indicators used to determining the depth of carbonation, with phenolphthalein being most commonly used. The principle is based on colour change due to changes in pH on the surface of a freshly broken sample. With phenolphthalein, the carbonation depth is defined as the point where the pH indicator turns from fuchsia pink to colourless, and corresponds to a pH of 8.3 or less, as shown in Figure 2.6.

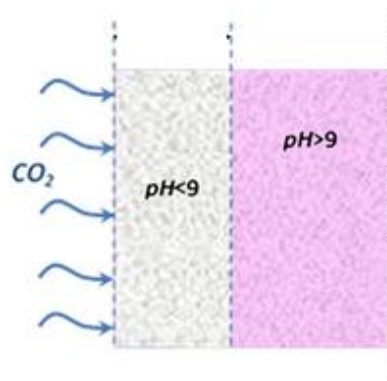


Figure 2.6: Systematic representation of carbonation front (Taken from [77]).

The major criticism of the colorimetric methods is non- identification of the partially carbonated areas as different studies have shown that carbonation is a diffusion process, and the front is not sharp but gradual [97, 98]. Also, the accuracy of the depth measurement depends on skill and knowledge of the individual who performs the test

[99]. TGA/DTA, XRD and FTIR techniques have also been widely reported in the literature in determining the carbonation hydrate product.

TGA has been used to quantify the amount of portlandite and calcium carbonate available in the sample during carbonation. XRD has been used to detect various crystalline phases in the carbonated sample while FTIR has been used to follow formation of various carbonate species. However, the characteristic peak of the C–O functional group in the wave number range of 1410–1510  $\text{cm}^{-1}$  would identify the carbonation reaction and products [97, 100]. Other techniques such SEM, grammadensimetry, chemical analysis, trimethylsilylation, neutron diffraction, ultrasonic phase velocity and electrochemical impedance spectroscopy (EIS) [98, 99, 101-104] have also been reported in the literature.

Cheng and Chang [97] studied and compared the carbonation depth of concrete using TGA, XRDA and FTIR techniques with the phenolphthalein indicator at 8 & 16 weeks at 20%  $\text{CO}_2$  and 70% RH with 28 days preconditioning at 23°C. They found out that TGA, XRDA and FTIR techniques gave comparable results while phenolphthalein indicator carbonation depth measurement was half that reported by the other techniques employed in the study. Also, Villain et al. [98] adopted the gammadensimetry technique, a non-destructive method based on the absorption of gamma-ray emitted by a radioactive substance Caesium  $\text{Cs}^{137}$  to determine the density variation due to ingress of  $\text{CO}_2$  combined with TGA and chemical analysis to study the carbonation profile of concrete. They concluded that all the techniques employed during the experiment agree with each other and are also complimentary to each other to predict the carbonation progression in concrete. While gammadensimetry makes it possible to determine the total penetrated  $\text{CO}_2$  without any specimen's preparation, TGA and XRD helps to accurately determine the portlandite in the concrete structure during carbonation.

## 2.5 Influence of carbonation on blended binders

### 2.5.1 Influence of carbonation on phase assemblage of blended cement.

The principal calcium-bearing phases involved in carbonation are portlandite (CH), calcium silicate hydrate (C-S-H) and ettringite. In all instances, calcite or its polymorphs form alongside alumina-silica gel or gypsum, depending on the carbonating phase [13, 77, 105] and the  $\text{CO}_2$  concentration to which the paste is

exposed [77]. From thermodynamic predictions, CH should carbonate first before C-S-H [106] but experimentally both CH and C-S-H carbonate simultaneously, although CH reacts faster than any other hydrates in CEM I. In composite cements, carbonation of CH and C-S-H are not simultaneous with decalcification of C-S-H occurring once no CH is available, especially in mixes containing PFA and GGBS [107]. This is in agreement with [76], and the stability of the phases is summarised in Table 2-5, showing carbonation stages of various phases according to the pH of the pore solution during accelerated carbonation.

Table 2-5: Summary of the stability of the cement phases according to pH.

Stages	pH	Stable Phases
<b>1 (non- carbonated)</b>	>12.6	Ca (OH) <sub>2</sub> , C-S-H (Ca/Si > 1.8 or at high common ion effect), Aft, AFm
<b>2</b>	11.6– 12.6	C-S-H (Ca/Si < 1.8), Aft, AFm
<b>3</b>	10.5– 11.6	C-S-H (Ca/Si < 1.05), Aft, Al (OH) <sub>3</sub>
<b>4</b>	10.0– 10.5	C-S-H (Ca/Si < 0.85), Fe (OH) <sub>3</sub> , Al (OH) <sub>3</sub>
<b>5 (fully carbonated)</b>	<10	SiO <sub>2</sub> with some CaO, Fe (OH) <sub>3</sub> , Al (OH)

The extent of carbonation is governed externally by the duration of exposure, the ambient relative humidity, and the CO<sub>2</sub> concentration [89, 108]. However, two intrinsic features of the binder also play a critical role in the extent of carbonation, namely: the pore structure governing CO<sub>2</sub> ingress into the matrix, and the CO<sub>2</sub> binding capacity of the hydrated cement paste [73, 109]. Both features are modified in limestone ternary cements. The higher the reactive CaO content of the cement, the greater the buffering capacity against carbonation [108]. With or without limestone additions, numerous studies have shown lower CO<sub>2</sub> binding capacities in blended cements than in OPC due to reduced portlandite availability. This, in-turn, reduces the carbonation resistance [105, 106, 110].

In accelerated carbonation studies of ternary limestone-slag and limestone-PFA blends, carbonation resistance was proportional to the clinker content [110, 111], with the limestone-slag mix slightly outperforming the corresponding limestone-PFA blend.

However, both performed less well than the reference OPC. This was attributed to clinker replacement in the blended mixes with more residual calcium hydroxide present in the slag-limestone mix than PFA-limestone mix [112] giving a greater CO<sub>2</sub> binding capacity. These findings have been corroborated elsewhere [106, 113]. Concrete formulated with binary (i.e., OPC with slag or fly ash) and LC3 ternary cement, showed an increased carbonation coefficient with decreasing clinker replacement as shown in Figure 2.7 [106, 114].

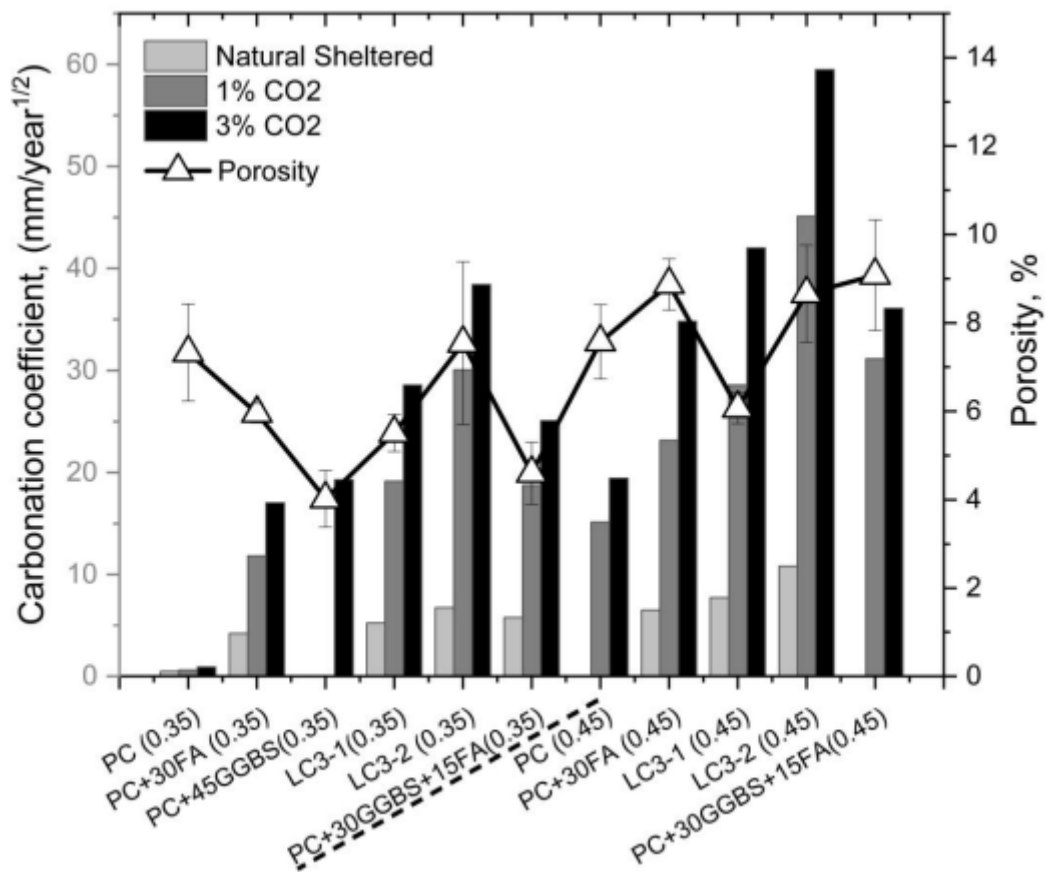


Figure 2.7: Carbonation coefficient in binary and ternary blends (Taken from [115]).

The blended cements were particularly sensitive to the high CO<sub>2</sub> concentrations used in accelerated tests. Similarly, while all mixes performed worse when the w/b ratio was raised from 0.3 to 0.45, at equivalent clinker content and w/b ratio, the LC3 blends carbonated more than binary OPC-slag and ternary OPC-Slag-PFA mixes.

### 2.5.2 Influence of carbonation on microstructures & transport properties of blended binder.

Carbonation of cement-based material is believed to lead to refined porosity and pore sizes while a decrease in the permeability and diffusivity is also observed [116, 117]. Borges et al. [117] observed an increase in porosity for slag-OPC blended paste at 9:1 under both accelerated and natural carbonation, attributed to carbonation of the C-S-H gel. In another study, Leemann et al. [93] studied the effects of various mineral additions such as limestone, microsilica, portlandite, slag-PC blender (CEM III/B) and CEM I in binary binder system on carbonation resistance and mix design in sheltered and unsheltered exposure conditions. They found that mixes with slag and microsilica underperformed under accelerated carbonation compared to other blends using 1 & 4% CO<sub>2</sub> at 57% relative humidity but showed higher carbonation resistance in field or natural conditions. This is due to their finer pore structures and slow drying behaviour exhibited during conditioning for oxygen diffusion. They concluded that the higher amount of water available in the pores of GGBS binder due to capillary condensation and pore fineness in GGBS blends led to slow drying in field conditions thus, improve the carbonation resistance and oxygen diffusion coefficient of the mix.

Pore refinement as seen with binary composite cements can reduce permeability [118] and capillary porosity is further refined in mature ternary blends. Furthermore, smaller pores remain saturated at lower relative humidity. Since the rate of CO<sub>2</sub> diffusion through water is many orders of magnitude less than through air, saturated pores significantly reduce the rate of carbonation [119]. However, not only does the initial pore structure influence carbonation, the process of carbonation itself alters the pore structure. Coarsening of pore structures and an increase in porosity due to carbonation of C-S-H as widely reported for blended binders [96, 109, 120]. Increase porosity was also reported upon natural carbonation of an OPC-slag-limestone ternary cement [119] explained by the higher C-S-H content from the pozzolanic reaction. Furthermore, the effect might be exacerbated by the slightly higher Ca/Si ratio of the C-S-H formed in the presence of limestone as discussed in [118]. C-S-H decalcification causes carbonation shrinkage, increasing porosity and coarsening the pores [73, 77, 117] in limestone blended cement. However, these observations should be treated with caution since coarsening of LC3 and other ternary cements was much more significant upon accelerated carbonation than under natural conditions [106].

The threshold pore diameter, defined as the inflexion point on the cumulative curve [121], above which the intruded volume sharply increases was coarsened in all samples after carbonation including the neat cement and limestone ternary blends in Figure 2.8 & 2.9 as reported elsewhere [109].

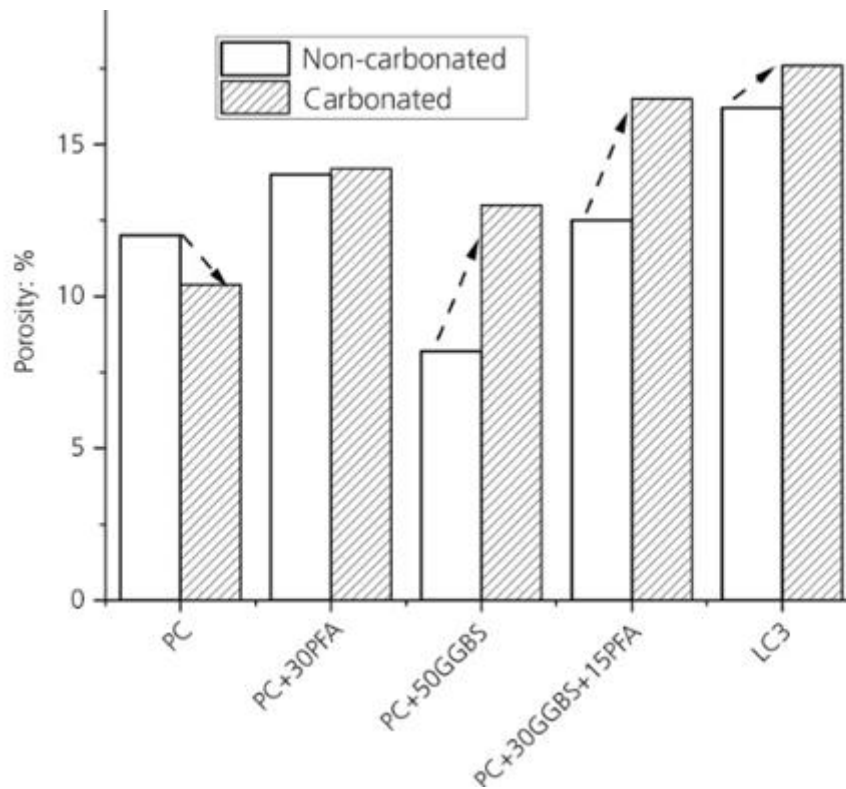


Figure 2.8 Total porosity of blended binders(Data extracted from [122]).

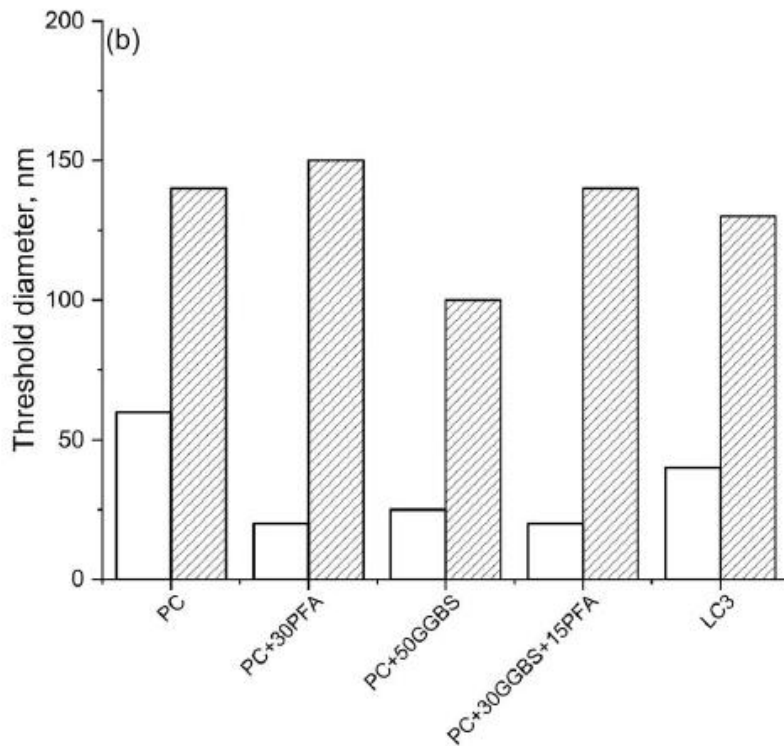


Figure 2.9: Threshold pore diameter of blended cements (Data extracted from [123]).

Figure 2.9 indicates that limestone ternary cements are much more susceptible to carbonation than OPC but only slightly more than corresponding binary cements. At equivalent clinker factor, blends containing PFA tend to carbonate more, with the carbonation depth increasing with the limestone content and w/c ratio due to a combination of matrix pH reduction and higher porosity. Lower gas permeability in these cements [124, 125] implies matrix pH is more critical and hence, the clinker factor must be optimized accordingly. More importantly, post carbonation performance of these cements' needs be assessed to evaluate the risk to carbonation-induced corrosion. This should consider the inherent pore refinement, CO<sub>2</sub> binding, and the role of the coarsened pores. Although portlandite and the C-S-H make the bulk of the phase assemblages in these cements with their carbonation mechanisms well reported [13, 109, 126]. However, stability of the additionally formed carboaluminate phases need examining.

### 2.5.3 Influence of carbonation on mechanical strength of blended cement

Mechanical strength tests are considered a measure of performance and quality of concrete over time as they measure resistance of concrete to loading. Increase in mechanical strength does not imply improved concrete durability under accelerated

aging, since once carbonation reaches the reinforcement and corrosion progresses, the concrete may fail. However, there is a strong relationship between hydration and compressive strength as well as how it affects carbonation. Carbonation of calcium bearing phases will be led to an increase in molar solid volume, estimated around 11-14% subject to the calcium carbonate polymorphs formed [13, 89, 117, 127]. Calcite produced during carbonation is expected to fill pores and led to decreased porosity, and thus is expected to increase concrete strength and this more prominent in PC system. Portland cement concrete shows a greater increase in compressive strength after carbonation than concrete containing supplementary cementitious materials when curing conditions and testing at equal age. This is clearly due to the amount clinker available for hydration compared to SCM concrete [81, 128-130]. Hren et al. [128] found an increase in compressive strength in CEM I after 105 days of accelerated carbonation however, both CEM III & CEM IV mortars with about 20% shows decrease in strength and no significant reduction with CEM II. They concluded that equivalent degree of hydration for different binders may have influenced the outcome. Consequently, it's well established in literatures that carbonation of portlandite is expansive and propagates well-ordered calcium carbonate, while C-S-H carbonation resulted in shrinkage, and with high SCM contents porosity can increase, and strength is lost. In contrast, limestone-blended concrete shows weaker strength during accelerated carbonation despite limestone providing nucleation sites for hydrates, filler effect and refinement of pore structure in blended cement [131, 132], although this is conflicting and need further understanding. Furthermore, concrete made from various SCMs subjected to accelerated carbonation shows an increase in compressive strength than non-carbonated samples as reported in [108, 128, 133] due to precipitation of calcium carbonate that densify the pore structure in comparison with natural environment.

## 2.6 Summary of the literature review

The current body of research regarding the carbonation of binders indicates that the accelerated testing available with different standards across the globe is applicable to Portland cements. This is because the buffering of CO<sub>2</sub> is based on the Ca(OH)<sub>2</sub> available in the binders. However, blended cements have less portlandite, which decreases their buffering capacity against carbonation despite the improved hydration and microstructural properties observed with composite cement mix.

The scientific gap in the field of carbonation of composite cement lies in the limited understanding of the intricate interactions between various constituents within these composites and the carbonation process. While many studies reviewed in this section has provided insights into the carbonation mechanisms of Portland cement, the complexities introduced by incorporating supplementary cementitious materials (SCMs) in novel binder systems as composite cement formulations especially with slag-limestone blended system have not been comprehensively addressed. Studying both accelerated and ambient carbonation conditions is essential for obtaining a comprehensive understanding of the long-term performance of composite binders. While accelerated testing allows for quicker assessment, it may not fully capture the intricacies of ambient exposure over extended periods, especially with composite binders and with different CO<sub>2</sub> level across various accelerated aging standards making it much more complicated. Studies under ambient conditions have reported slower but more realistic carbonation rates, phase assemblages, and microstructures. This emphasizes the necessity of considering both conditions for robust predictions of binder behaviour. The impact of carbonation-induced changes on the structural integrity and functional properties of these composite cement, particularly in the context of sustainable construction and infrastructure, presents a significant gap in current scientific understanding.

## Chapter 3: Materials and Methods

### 3.1 Raw materials

#### 3.1.1 Binders

Binders used for this study are CEM I 52.5R, clinker, slag, and limestone. Clinker, GGBS and limestone were blended as either binary or ternary mixes respectively with additional anhydrite included in all composite cements to maintain the sulphate concentration obtainable with commercially available cement. Clinker was preferred to CEM I with blended binders as modern cement contain certain percentage of limestone which is likely to increase percentage of CaO in the blended cement hence the use of clinker. The percentage composition of each binder mix is shown in Table 3-1 and with some properties such as hydration, freeze-thaw and mechanical strength previously study elsewhere [131].

Table 3-1: Binder configuration.

<b>Mix</b>	<b>CEM I (52.5R)</b>	<b>Clinker (%)</b>	<b>Slag (%)</b>	<b>Limestone (%)</b>	<b>Anhydrite (%)</b>
<b>CEM I</b>	100	-	-	-	-
<b>CS</b>		50.7	47.0	-	2.3
<b>CS1L</b>		51.1	38.0	8.6	2.3
<b>CS2L</b>		51.1	28.5	18.1	2.3

The elemental composition of raw materials as determined by XRF, the phase composition and particle size distribution, as provided by Heidelberg Cement, are presented in Tables 3-2 and 3-3 and Figure 3.1 respectively.

Table 3-2:Oxide composition of the as-received raw materials.

Oxide Composition (%)	CEM I 52.5R	Limestone	Clinker	GGBS
Loss of ignition %	1.52		0.33	
SiO <sub>2</sub>	20.29	3.12	21.44	35.312
Al <sub>2</sub> O <sub>3</sub>	5.29	0.79	5.43	10.99
TiO <sub>2</sub>	0.29	0.04	0.29	1.09
MnO	0.05	0.05	0.05	0.21
Fe <sub>2</sub> O <sub>3</sub>	2.38	0.4	2.44	0.28
CaO	63.22	52.74	65.87	41.58
MgO	1.58	0.57	1.55	5.92
K <sub>2</sub> O	0.77	0.12	0.81	0.56
Na <sub>2</sub> O	0.2	0.01	0.2	0.24
SO <sub>3</sub>	3.7	0.17	0.73	2.83
P <sub>2</sub> O <sub>5</sub>	0.14	0.02	0.13	0.01
<b>Total</b>	<b>99.43</b>		<b>99.27</b>	<b>99.03</b>

Table 3-3: Blaine and fineness of the as-received cementitious materials.

	CEM I 52.5R	Limestone	Clinker	GGBS
Blaine (cm <sup>2</sup> /g)	6120	3850	6400	5180
Density (g/cm <sup>3</sup> )	3.14	2.73	3.2	2.9

Table 3-4: Phase composition of the raw materials. (As received).

Phases	Chemical Formula	CEM I 52.5 R %	Limestone%	Clinker %	GBS%
<b>Alite, C<sub>3</sub>S</b>	Ca <sub>3</sub> SiO <sub>5</sub>	54.6		60.2	
<b>α-Belite, C<sub>2</sub>S</b>	Ca <sub>2</sub> SiO <sub>4</sub>	3.6		2.2	
<b>β-Belite, C<sub>2</sub>S</b>	Ca <sub>2</sub> SiO <sub>4</sub>	16.2		17.6	
<b>Σ Belite</b>		19.7		19.8	
<b>Aluminate (cub.), C<sub>3</sub>A</b>	Ca <sub>3</sub> Al <sub>2</sub> O <sub>6</sub>	6.5		6.9	
<b>Aluminate (or.), C<sub>3</sub>A</b>	Ca <sub>3</sub> Al <sub>2</sub> O <sub>6</sub>	2.5		3.6	
<b>Σ Aluminate</b>		9.0		10.5	
<b>Ferrite, C<sub>4</sub>AF</b>	Ca <sub>2</sub> (Al, Fe) <sub>2</sub> O <sub>5</sub>	7.6		7.5	
<b>Free lime, C</b>	CaO	0.1		0.7	
<b>Periclase</b>	MgO	0.2		0.2	
<b>Arcanite</b>	K <sub>2</sub> SO <sub>4</sub>	0.9		1.2	
<b>Anhydrite</b>	CaSO <sub>4</sub>	1.9			
<b>Bassanite</b>	CaSO <sub>4</sub> * 0.5 H <sub>2</sub> O	4.0			
<b>Quartz</b>	SiO <sub>2</sub>	0.4	2.2		0.1
<b>Calcite</b>	CaCO <sub>3</sub>	1.6	95.6		2.0
<b>Dolomite</b>	CaMg(CO <sub>3</sub> ) <sub>2</sub>		1.5		
<b>Muscovite<sup>+</sup></b>	KAl <sub>2</sub> [(OH, F) <sub>2</sub>  Si <sub>3</sub> AlO <sub>10</sub> ]		0.7		
<b>Amorphous content</b>					98.0

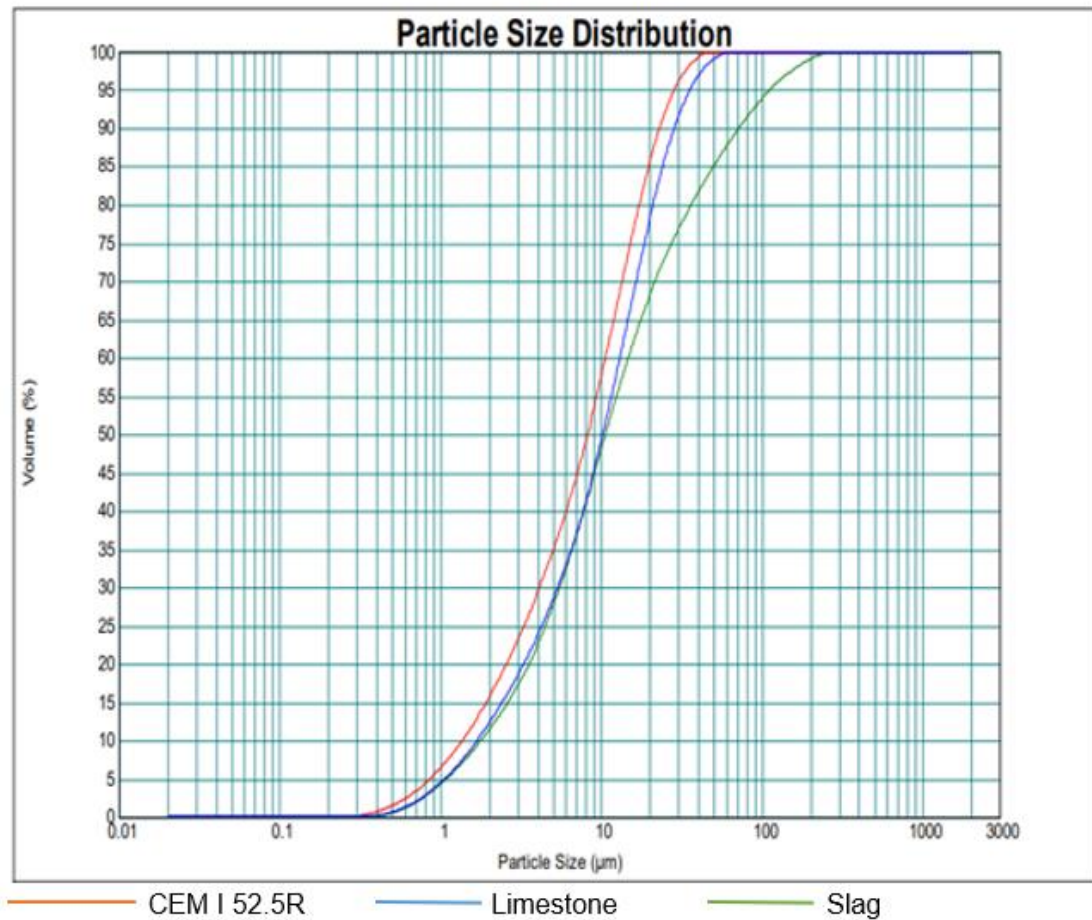


Figure 3.1: Particle size distribution of as-received CEM I, slag and limestone. (As received).

### 3.1.1 Fine aggregate

Sand used in preparation of mortar samples was sourced from a single batch of Travis Perkins sand delivered to the University of Leeds concrete casting shop. The particle sizes are between 0.75mm and 2.0mm. The sand was air-dry and sieved using 2mm sieve to remove unwanted larger particles.

### 3.1.2 Water

De-ionized water was used in casting both paste and mortar mixes.

### 3.1.3 Saturated salt

Saturated salts (sodium bromide, sodium chloride and potassium sulphate) were used for conditioning the accelerated carbonation chamber to achieve the desired relative

humidity. These were purchased from Fisher Scientific Ltd UK (United Kingdom) with 98% purity and the saturated salt solutions were subsequently prepared at the civil engineering materials laboratory.

### 3.2 Method

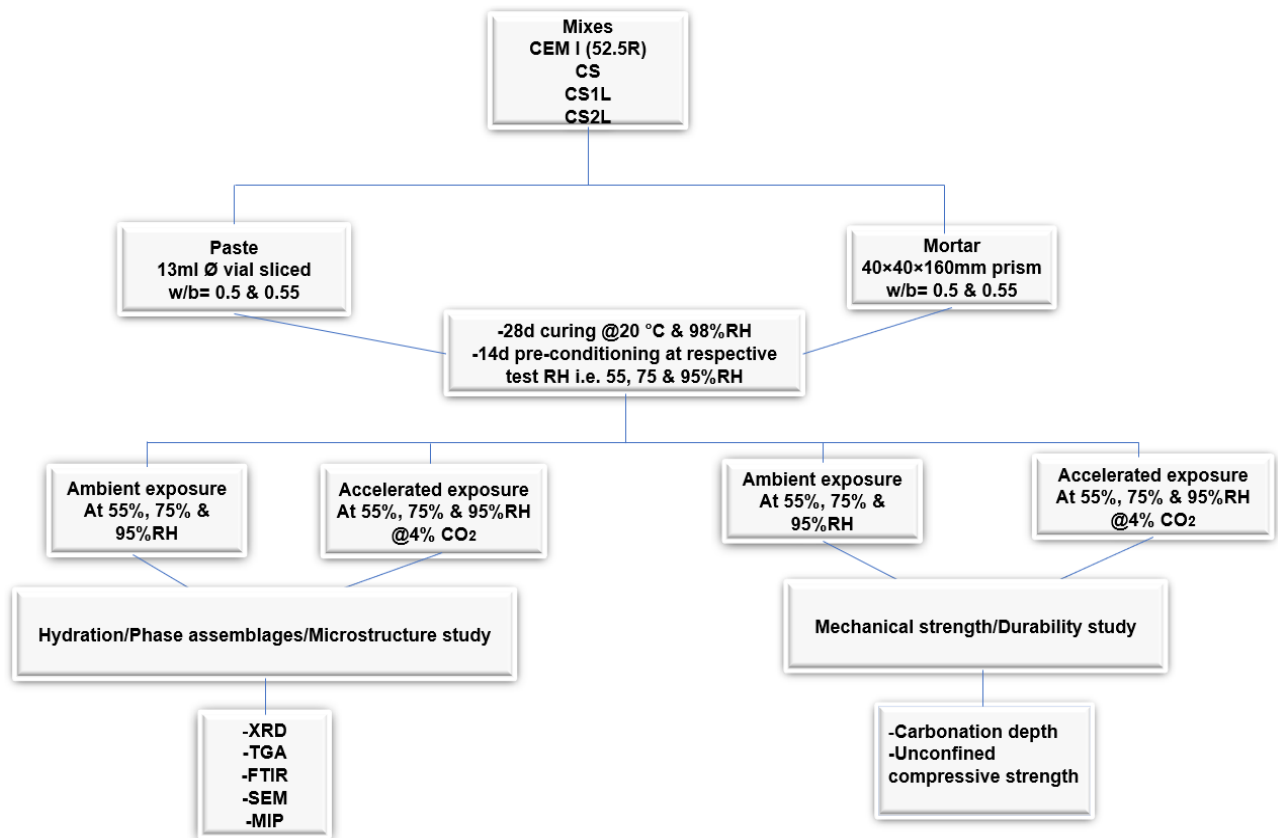


Figure 3.2: Experimental chart.

#### 3.2.1 Binder blending

Raw materials comprising clinker, slag, limestone, and anhydrite, in accordance with the mix ratios in Table 5, were blended in a 500ml Capco roller mill with graded polypropylene balls, for up to 2 hours with one-third mass filled. This was to eliminate binder segregation and achieve homogeneity of the blends.

#### 3.2.2 Sample preparation

##### 3.2.2.1. Paste samples.

Paste samples were hand mixed for 1-2 minutes in a plastic container and thoroughly stirred with the aid of spatula to achieve homogeneity. They were then filled into plastic sample vials ( $\phi 16 \times 50\text{mm}$ ) in three layers and vibrated at each layer to expel air pockets trapped in the mix. The samples were covered with plastics lids and wrapped

tightly with parafilm to prevent water leakage with samples rotated at 20rpm for 24 hours at room temperature to avoid segregation. Samples were then placed in large sample bag and vacuum sealed before being cured in a water bath set at ( $20^{\circ}\text{C} \pm 5^{\circ}\text{C}$ ) and 98% relative humidity for 28 days.

### 3.2.2. Mortar sample

Mortar samples were preferred to concrete as an increasing fraction of a more porous portlandite-rich interfacial transition zone will likely provide pathways for fast  $\text{CO}_2$  diffusion in concrete [134] and also the correlation of ( $R^2=0.96$ ) reported for both samples [135]. Mortars were prepared using an automatic mixer (Control Auto-Mix 65-L0006/AM) with pre-programmed procedure in accordance with BS EN 196-1:2005. 450g of binder and 1350g of sand were used to produce three 40mm×40mm×160mm prisms with w/b ratio corresponding to the one used in paste preparation. Prism moulds were removed after 24 hours before curing in a moist curing room at ( $20^{\circ}\text{C} \pm 5^{\circ}\text{C}$ ) and 98% relative humidity for 28 days.

### 3.2.3 Preconditioning

Samples subjected to either accelerated or ambient carbonation were preconditioned for 14 days to achieve hydric balance to aid diffusion of  $\text{CO}_2$  prior to exposure. This is recommended in all the carbonation standards. Both mortar and paste samples were preconditioned at predefined relative humidities corresponding the carbonation conditions adopted in the study i.e., 55%, 75% and 95% RH using a JTS environmental controlled chamber at ambient  $\text{CO}_2$  levels ( $\sim 400\text{ppm}$ ) and  $20^{\circ}\text{C}$ .

### 3.2.4 Carbonation

Accelerated carbonation was performed in air-tight chamber, as shown with setup in Figure 3.3, with relative humidity controlled by saturated salt solutions. These solutions (NaBr, NaCl and  $\text{K}_2\text{SO}_4$ ) were placed at the base of the chamber as shown in Figure 12. This gave relative humidities of  $55 \pm 5\%$ ,  $75 \pm 3\%$ , and  $95 \pm 5\%$  at  $20^{\circ}\text{C}$  respectively. 4%  $\text{CO}_2$  concentration was adopted to accelerate carbonation without any significant change in rankings for carbonation resistance [93, 129].

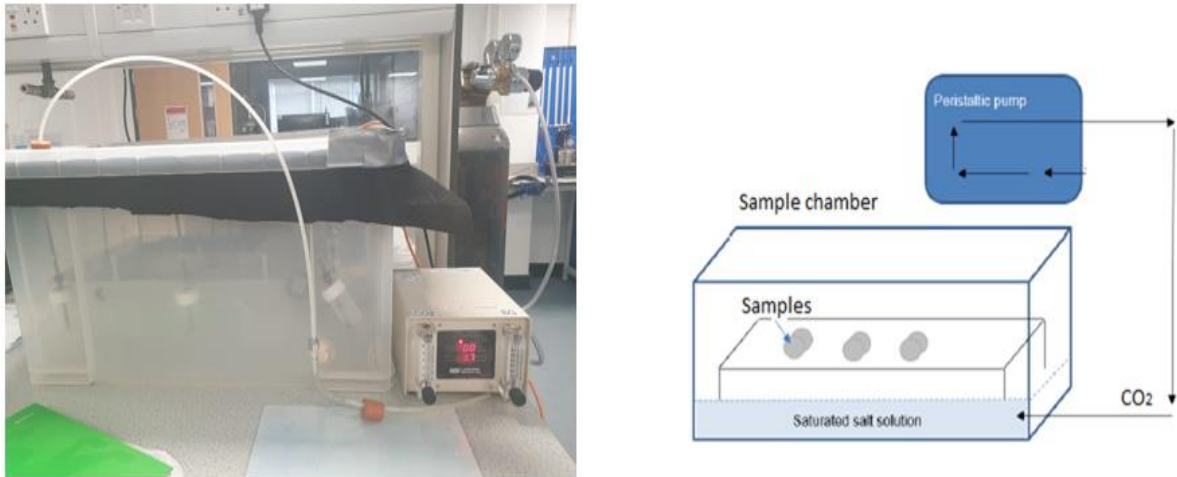


Figure 3.3: Accelerated carbonation setup (Photo & schematic diagram).

CO<sub>2</sub> was pumped into the chamber from the cylinder and peristaltic pump was used to circulate the CO<sub>2</sub> while Rotronic Hydrolog and Testo 535 CO<sub>2</sub> probes were used to monitor relative humidity and CO<sub>2</sub> concentration respectively to maintain the required levels.

For ambient carbonation, JTS environmental chambers with capability to regulate both humidity and temperature electronically were used to achieve the ambient condition with same relative humidity as accelerated carbonation. Periodic checks confirming CO<sub>2</sub> levels in the chamber at 350-400ppm were performed over the test period.

### 3.2.5 Hydration stopping and extraction.

Hydration was stopped in paste samples using double solvent exchange as described elsewhere [136, 137]. Pieces were extracted with the uncarbonated core and carbonated surface using tweezers. Carbonated & non-carbonated areas could be visually distinguished by using thymolphthalein indicator, as shown in Figure 3.4, to ensure sampling paste from both regions correctly. However, carbonation depth was not measured from the paste samples as it was reported to have less correlation compared to mortar or concrete due to differences in CO<sub>2</sub> diffusivity, degree of water saturation, variation in pore structure and the amounts of carbonation products expected to form [135]. Pastes were subsequently ground to fine powder using an agate mortar & pestle as soon as possible to avoid further carbonation, especially with samples placed in ambient conditions.

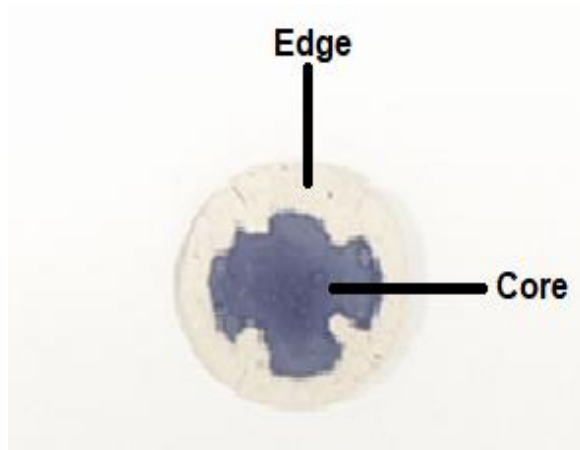


Figure 3.4: Extracted paste.

Samples were immersed in isopropanol (IPA) for 20mins and stirred several times during the process. The solution was then filtered using low grade filter paper and soaked in diethyl-ether for 10-15mins before vacuum drying. Hydration stopped powders were then stored in a vacuum dessicator with silica gel until testing. For other samples such as slices and pieces for SEM and MIP tests, paste samples were cut to 1-2mm thin slices and submerged in IPA for 48hrs and dried under vacuum before storing in dessicator under the same condition as powder samples. Hydration stopping using low vacuum pressure has been shown to preserve sample microstructure with minimal effect on phase composition [137, 138].

### 3.3 Testing Techniques

#### 3.3.1 Carbonation depth measurement

Carbonation depth measurements were taken on mortar prisms after carbonation (although there was no colour change observed for ambient samples). The use of mortars in measuring carbonation depth have been found to have no significant difference compared to concrete [139]. Samples were taken from prisms after unconfined compressive strength testing, splitting prisms with a hammer and chisel to expose the surface at 7, 14 and 28 days. Freshly prepared 1% thymolphthalein solution was sprayed on the exposed surfaces, left to dry and the carbonation depth measured using tape. The depth was defined as the distance from the sample edge to the colourless to blue colour change, representing a pH change from 9.5 to above 10. Five points were measured for each of the four prism faces using a Vernier calliper. Photographs were also taken for area measurement using image J. Both methods of depth measurement could then be compared.

### 3.3.2 Mechanical strength

Compressive strength test was determined at 7, 14 and 28 days exposure. 40mm x 40mm x 160mm mortar prism were cut using manual cutting with chisel to obtain three 40mm x 40mm cubes. These were in accordance with BS EN 1015-11:2019. Testing was then undertaken using an Instron 3300, 100KN capacity with a 2000N/min load rate. The average unconfined compressive strength was determined in line with Equation 3.1 on three specimens, with variation not more  $\pm 10$ MPa.



Figure 3.5: Unconfined compression test.

$$f_c = \frac{F}{1600} \quad 3.1$$

Where:

$f_c$  = compressive strength (MPa)

$F$  = maximum load at fracture (N)

1600 = area of the sample (40 mm x 40 mm)

### 3.3.3 Simultaneous thermal analysis (STA)

STA measures the changes when the sample is subjected to a controlled

temperature increase over time with various phase changes recorded. Samples are subjected to heating under controlled environment up to 1000°C to study decomposition patterns using mass loss at different temperature associated with each phase.

Analysis was undertaken in a 449 Jupiter NETZSCH STA with 30 mg of hydration-stopped powdered samples placed in an alumina crucible covered with a lid and heated from 30°C to 1000°C with a heating rate of 10°C/minute under nitrogen. The mass loss was plotted against temperature and the DTG curve also plotted showing various peaks associated with dehydration, dihydroxylation, and de-carbonation.

Mass loss (%) was calculated based on the tangent method [131, 137]. Bound water, portlandite and calcite contents could be quantified, as the peaks are clearly shown in both TG and DTA plots. The (BW) bound water was obtained from the mass loss from 50-550°C. The mass loss attributed to portlandite decomposition (CHw) was obtained at about 400°C to 550°C according to Equation 3.2 while calcite de-carbonation started immediately after portlandite decomposition as shown on both DTA & TG curve in Figure 3.6 and various weight losses were determined following equations 3.1-3.5.

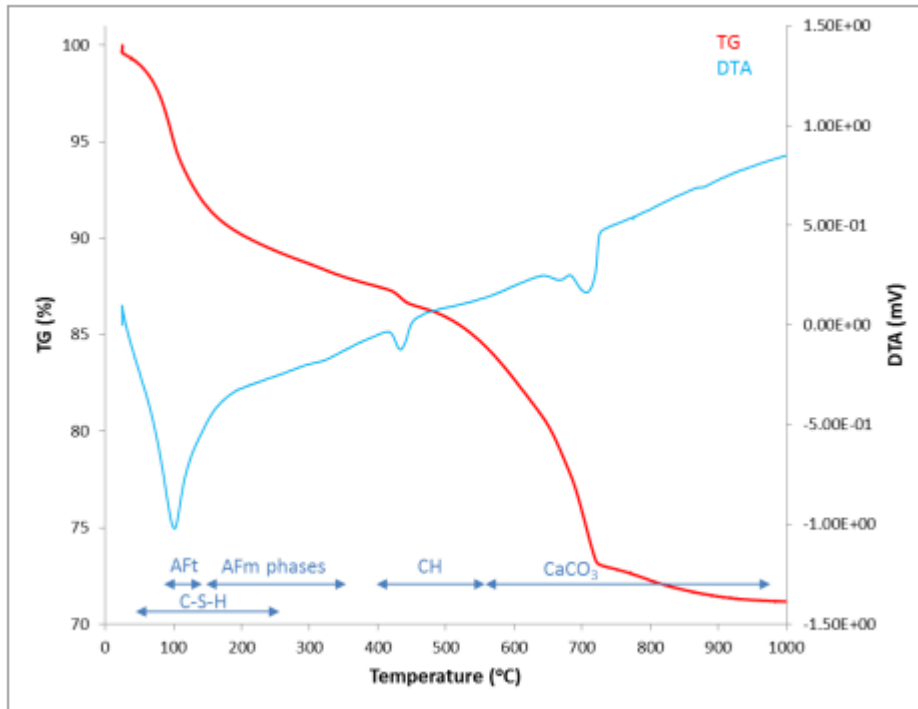


Figure 3.6: Thermogravimetric analysis highlighting temperature changes for various mass loss due to decomposition of hydrate phases (Taken from [140]).



$$\%CH = CH \times \frac{M_{CH}}{M_{H_2O}} \quad 3.4$$

$$\%CC = \text{CaCO}_3 \times \frac{M_{\text{CaCO}_3}}{M_{H_2O}} \quad 3.5$$

$$BW = \left( \frac{W_{50} - W_{550}}{W_{550}} \right) \times 100 \quad 3.6$$

%CH = mass loss due to carbonation of portlandite

(%) CC = mass loss due to decarbonation of calcite

$M_{CH}$  = molar mass of portlandite (i.e., 74g/mol)

$M_{H_2O}$  = molar mass of water (i.e., 18g/mol)

$M_{CaCO_3}$  = molar mass of calcite (i.e., 100g/mol)

$M_{CO_2}$  = molar mass of carbon dioxide (i.e., 44g/mol)

BW = bound water (%)

$W_{50}$  = residual mass at 50°C

$W_{550}$  = residual mass at 550°C

### 3.3.4 X-ray powder diffraction (XRD)

XRD together with Rietveld refinement was used to quantify the crystalline phases in the binder pastes. Selected samples exposed to both accelerated and ambient carbonation were investigated to follow the crystalline phases formed. Hydration stopped paste samples were crushed and ground using agate mortar and pestle to a fine powder passing through a 63 $\mu$ m sieve. Grinding was performed quickly to limit further carbonation. Panalytical Empyrean equipment operating at 60kV and 40mA were used and scanning was performed from 5-80 °2 $\theta$ , scanning stepwise in 0.334° increments. Each run lasted for around 30 minutes. Crystalline phases were quantified by Rietveld refinement using both X'Pert High Score Plus software with corundum as an external standard. Rietveld refinement detailed procedures used in this study were similar to the one developed elsewhere [115].

### 3.3.5 Fourier transform infrared spectroscopy (FTIR)

FTIR was used to understand the carbonation profile, carbonate speciation, portlandite content and C-S-H decalcification of the samples. Data were collected from a PerkinElmer ATR-FTIR at 400-4000cm<sup>-1</sup> wavelength with 4cm<sup>-1</sup> resolution. Hydration stopped fine powder samples were spread onto the diamond crystal component of the equipment and consistent force applied from the pressure arm having direct contact with sample through the flat shoe. Background spectra were collected before the start of the runs and after every run.

### 3.3.6 Scanning electron microscopy (SEM-EDS)

To follow the degree of clinker and SCM hydration, approximately 2mm slices were cut from the paste cylinders, hydration stopped as described above and impregnated with low viscosity epoxy resin. Cured resin impregnated samples were carefully

polished with silicon carbide papers using #600, #1200 and #2500 grit sizes on a Rotopol polisher while scratches were subsequently removed with diamond cloth from 6 $\mu$ m to 0.25 $\mu$ m to reveal the surface. Samples were carbon coated prior to analysis with a Carl Zeis EVO Ma 15 SEM with 150mm detector. 50 backscattered electron images (BSE) were randomly collected as suggested elsewhere [137] in carbonated and uncarbonated areas. Images were collected at 800x magnification, with a working distance of 8.0-9.0mm using 15KeV accelerating voltage.

To quantify unreacted slag grains in determining the degree of slag hydration, BSE images for composite blended paste were augmented with EDS Mg maps. The Mg map was used to aid the quantification of unreacted slag grains since Mg has very low mobility while its grey level overlaps with CH, as show in Figure 3.7. As a result, it was possible to apply a threshold to segregate the unreacted slags when the Mg map was overlaid by a matched BSE image using image J software as shown in Figure 3.7. EDS map data were obtained using an Oxford Instrument X-max SDD detector and AZTEC version 3.3 software with a process duration of 4 minutes each.

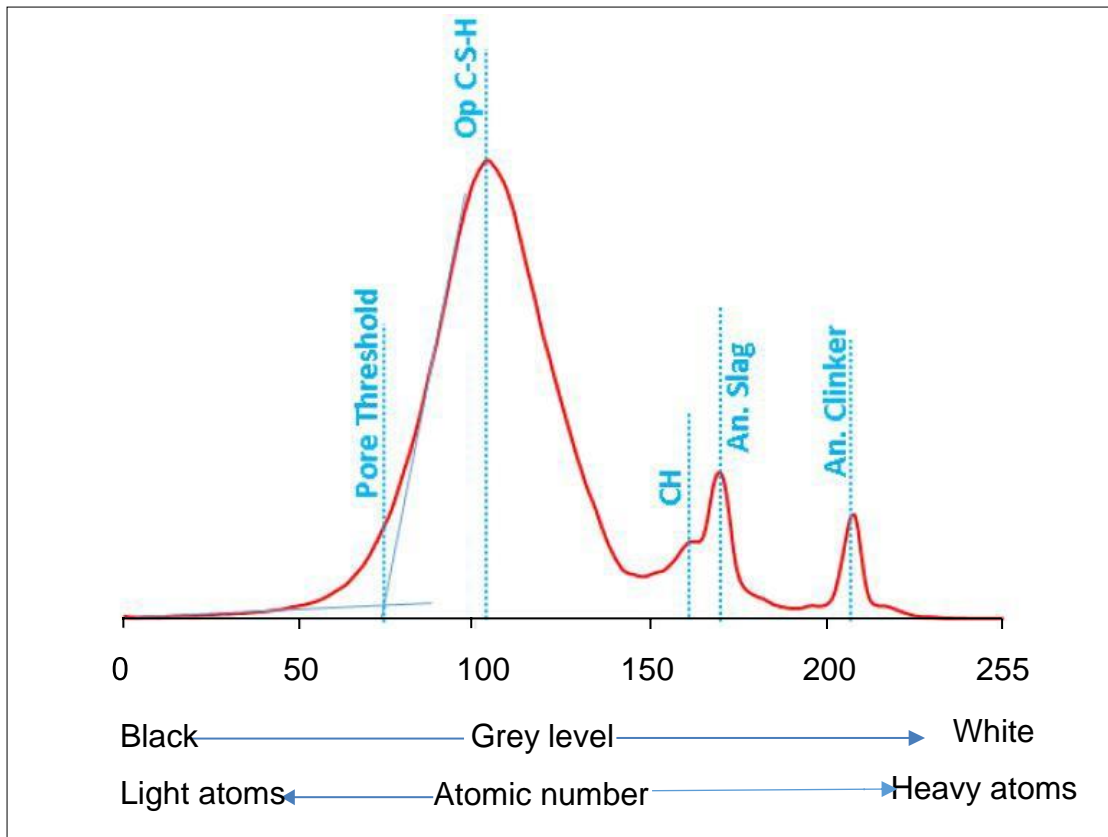


Figure 3.7: Grey scale histogram for slag binder system showing different thresholds for binders and pores adapted from [34].

To confirm whether slag particles were correlated to their magnesium contents, the unreacted slag threshold in the BSE image was inverted and superimposed on a matching magnesium map. The BSE image (a) was opened, processed, and a threshold applied for unreacted slag grains in Image J, as illustrated in Figure 3.8 followed by the Mg map (b). The BSE image was then inverted, and 40 percent opacity overlaid over the Mg map. The composite image (c) was flattened, and the unreacted slags were identified by their characteristic Mg concentrations. Then, a threshold was set to select the unreacted slag grains. The combined image was then transformed to greyscale before the last threshold was set to quantify the amount of anhydrous slag (d).

Also, changes in C-S-H composition were also investigated using EDS spot analysis on samples, which involved picking roughly 60-100 spots from both the inner and outer product C-S-H acquired from BSE images at 2000x magnification in as many points and analysed for atomic ratio changes.

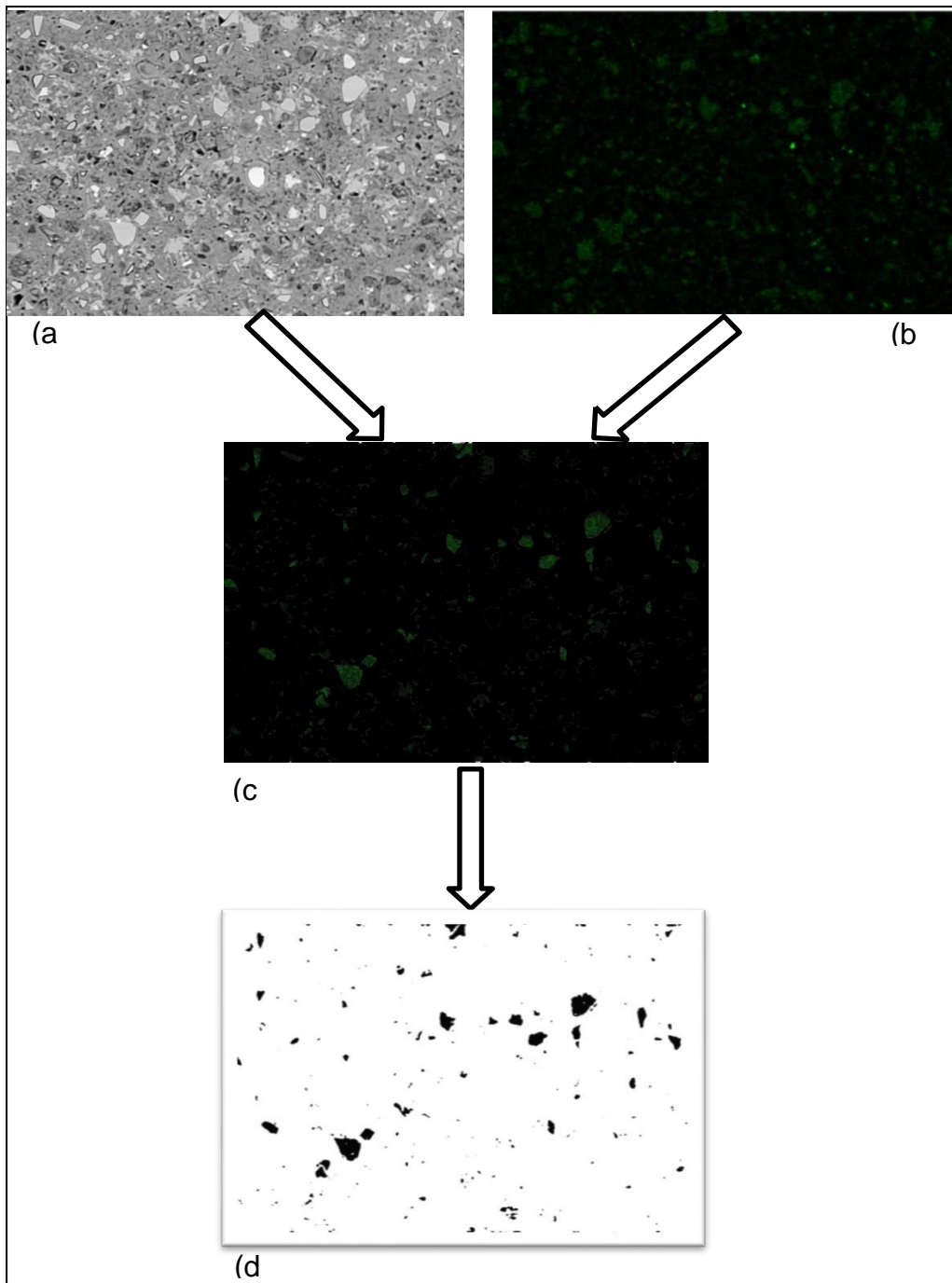


Figure 3.8: Method for determining unreacted slag particles from a combination of BSE image and magnesium map by image analysis: (a) BSE grey image, (b) magnesium map, (c) combined image, and (d) separated unreacted slag particles. (Images taken [110]).

### 3.3.7 Mercury intrusion porosimetry (MIP)

MIP is a technique used in measuring the porosity of cement-based material. Mercury is preferred liquid because it does not wet the binder surface [141]. Mercury intrusion

measurements were performed with Micrometrics Autopore IV porosimeter. The equipment can be used to determine pore size in range from 7nm-50 $\mu$ m. The samples were hydration stopped as described in 3.2.5 and about 1.5g slice were immersed in the mercury and pressure was gradually applied to force the mercury into the pores network of the samples up to maximum pressure of 414MPa. Data were collected and evaluation by the control module attached to the equipment.

## Chapter 4: Carbonation under ambient conditions

This chapter presents results and discussion on the continued hydration, phase assemblage and compressive strength of paste and mortar samples subjected to ambient carbonation. The samples were exposed to the same curing procedure as discussed in chapter three, prior to preconditioning and subsequent exposure to ambient (0.04-0.05%) CO<sub>2</sub> at controlled relative humidity (55%, 75% & 95%) and temperature (20°C) in an environmental chamber as shown in Figure 3.2 in chapter three. This methodology ensures disassociation of the drying to some extent from the carbonation process and serves as a reference for samples subjected to accelerated testing later in the following chapters.

Following 28 days of carbonation, none of the mortar samples showed any evidence of carbonation based on spraying with thymolphthalein. Similarly, paste samples used for subsequent characterisation showed no evidence of carbonation based on spraying with thymolphthalein. However, some carbonation may still have occurred since pH indicators may underestimate carbonation depths [142].

### 4.1 Hydration progress during ambient carbonation.

#### 4.1.1 Chemically bound water

The classical method for estimating the degree of reaction from chemically bound water is reported to be less reliable in blended cements because of the unknown stoichiometry of the reaction and changes in the C-S-H composition [143, 144]. However, this can still provide insights into hydration characteristics of the binder system [121, 145]. Figures 4.1-4.3 show the chemically bound water measured by TGA for samples subjected to ambient carbonation at 55%, 75%, and 95% RH at both water/binder ratios adopted in this study. The chemically bound water contents of the CEM I mixes (CEM I 50 and 55) at 55% RH, as shown in Figure 4.1a-b are similar except at 28 days' exposure that shows a slight drop, due to sample carbonation, because CBW was calculated at a mass loss of 50-550°C. Correcting the CBW for CH depletion due to carbonation could be done for the CEM I mixes and showed a slight increase in portlandite contents. But the calculation was complicated for the blends due to the presence of limestone in many of the mixes. That hydration beyond 7 days is almost stopped and consistent with [115, 121] findings that hydration does not continue at relative humidity below 80%. Both the binary (CS) and ternary binders

(CS1L) showed similar trends to CEM I at 55% RH; however, there was a slight decrease in CBW content for the CS2L mix compared with both CS and CS1L. This may be due to the carbonation as samples at this RH are likely susceptible to carbonation compared to other exposure conditions due to drying of the excess moisture out of the pores which are faster at lower RH [120, 122, 135] especially during the preconditioning stage which is designed for the drying out of the pores quickly to aid ingress of CO<sub>2</sub> into the binder system.

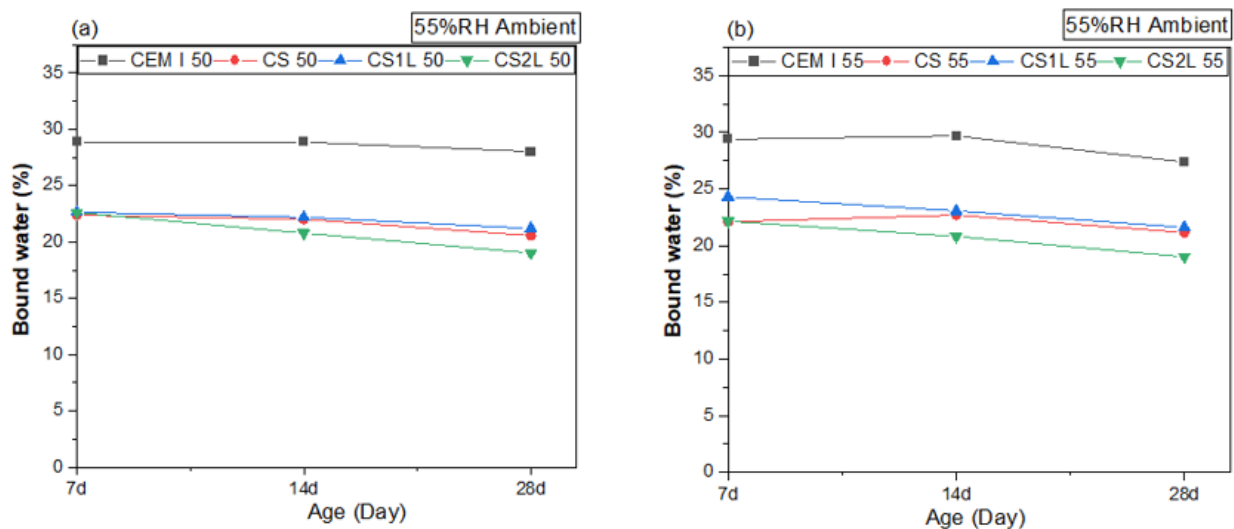


Figure 4.1: Measured bound water from TGA during 55% RH ambient carbonation  
(a) 0.50w/b (b) 0.55w/b.

Figures 4.2a-b present trends in the CBW at 75% RH. CEM I at both w/b ratios showed a significant increase of approximately 30% from 7 to 14 days and maintained a steady increase up to 28 days. This observation shows that hydration continues, despite the exposure conditions being below the threshold where hydration is supposed to cease, that is, 80% RH. The trends observed at both 55% and 75% RH were also similar to those following exposure at 95% RH, albeit with this latter situation showing a significant increase in CBW by 28 days of 33.65 and 33.42% for 0.5 & 0.55 w/b respectively, as shown in Figure 4.3a-b. The binary and ternary blends at 75% and 95% RH maintained steady CBW values between 7 and 28 days without any significant changes.

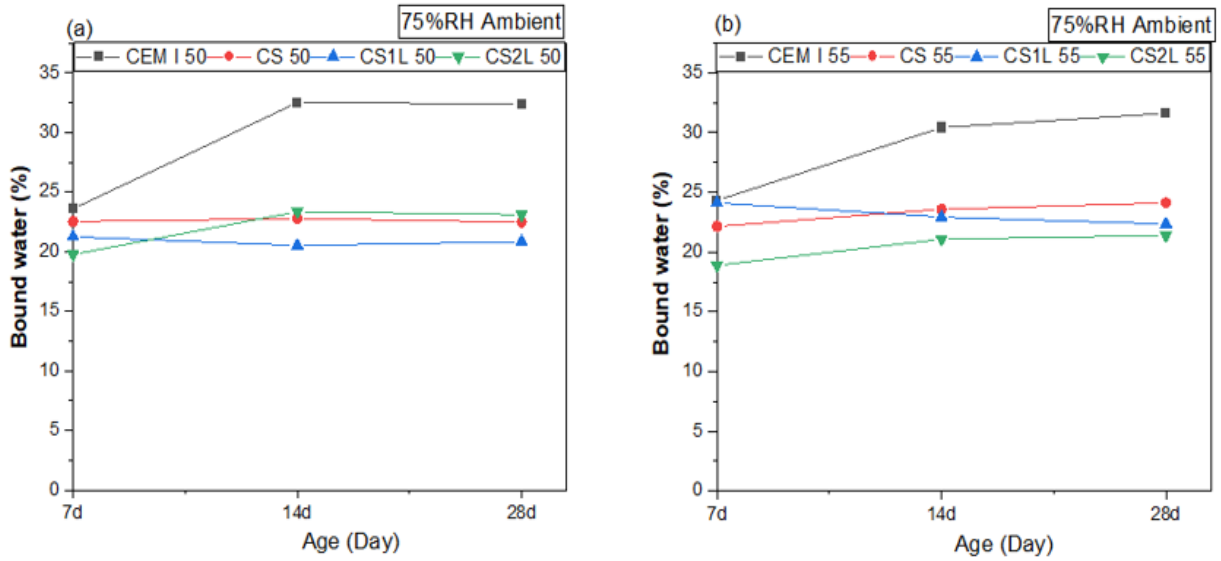


Figure 4.2: Measured bound water from TGA during 75% RH ambient carbonation  
(a) 0.50w/b (b) 0.55w/b.

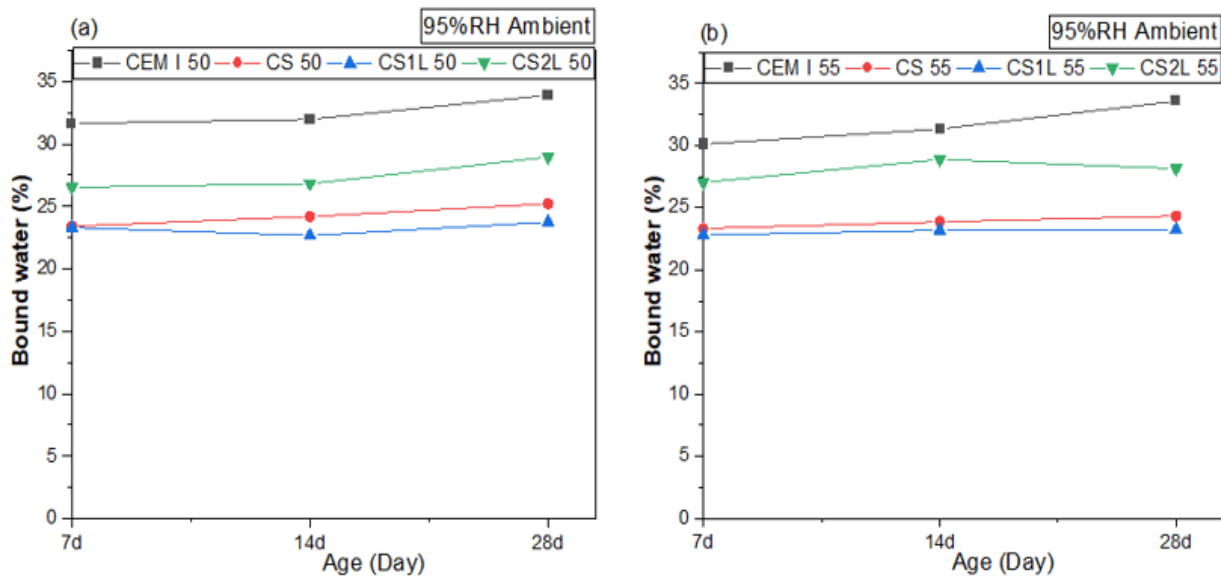


Figure 4.3: Measured bound water from TGA during 95% RH ambient carbonation  
(a) 0.50w/b (b) 0.55w/b.

#### 4.1.2 Effect of RH on chemically bound water during ambient exposure.

From Figures 4.4 and 4.5 below, a consistent trend emerges, demonstrating that CEM I binders (CEM I 0.55 & 0.50) exhibit higher CBW across all relative humidity levels i.e., 55, 75 & 95% when compared to other binders. which is due to high degrees of hydration during curing for 28 days before ambient exposure. Under such conditions, the degree of hydration is expected to achieve over 80% [146] for CEM I binders. At

95% RH, CEM I sample shows higher CBW compared to other RH i.e., 55 & 75%. The difference observed may be due variation in the vapour pressure in the capillary pores [147, 148] as degree of saturation falls below the 80% RH threshold, pores dried out quickly which affect hydration [149], however the effect was minimal for this study as samples were already cured over 28 days before exposure. The disparity observed between CEM I and composite binders are primarily attributed to the greater availability of clinker in the CEM I mix. Furthermore, CS2L binders also shows a higher CBW, particularly at a relative humidity of 95%. This phenomenon suggests that the nucleation sites provided by the inclusion of limestone may play a pivotal role in expediting clinker hydration, especially when the water-to-binder (w/b) ratio  $\geq 0.42$  [150]. However, this effect is not consistent across all relative humidity levels, as it does not hold true for 55% and 75% relative humidity. This trend of enhanced CBW at 95% relative humidity remains consistent for both the 7-day and 28-day periods, underscoring the effectiveness of maintaining stable hydration conditions over time. Conversely, the CBW for the CS1L mix is lower compared to CS2L, mainly due to reduced nucleation sites available for further clinker hydration [151, 152]. Bonnavetti et al. [150] indicates that only 5% of the 20% limestone replacement was involved in hydration process after 180 days of curing and in this case, a lower percentage likely with CS1L binder.

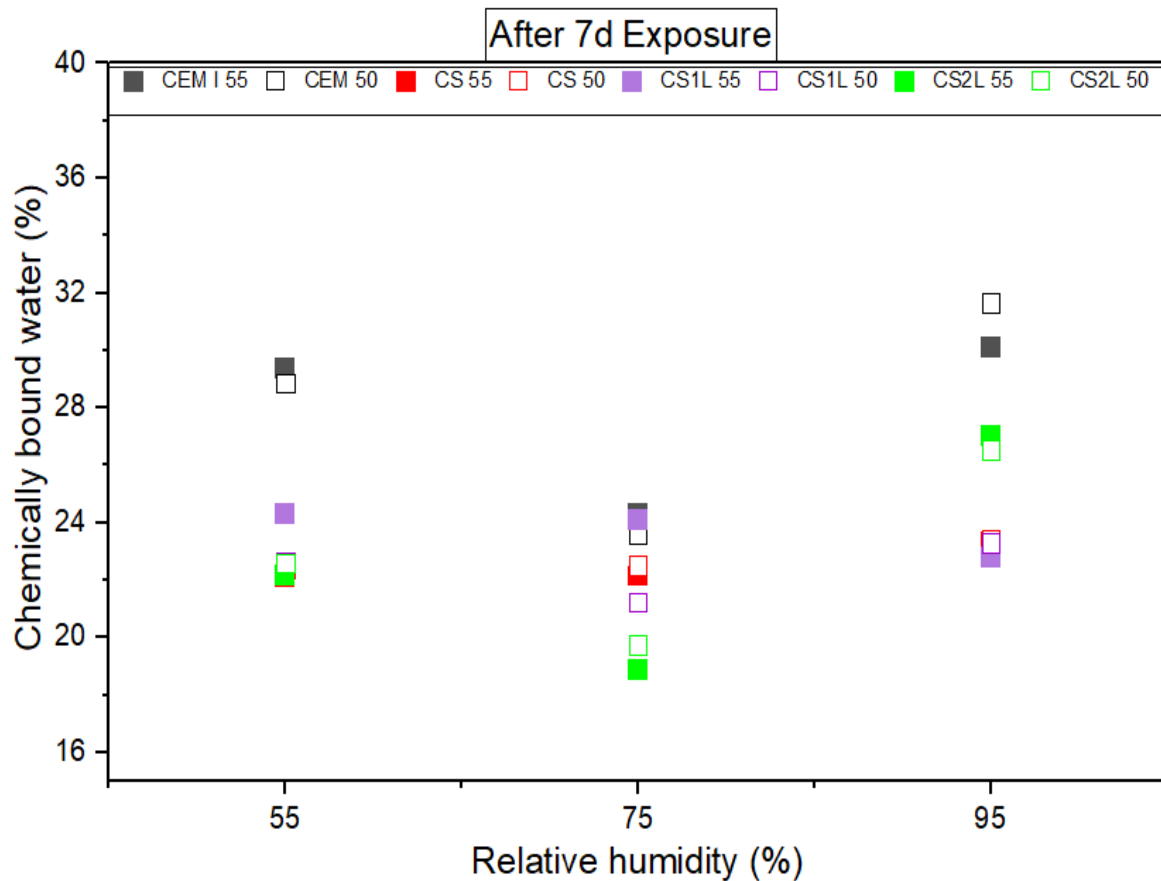


Figure 4.4: Chemically bound water with the exposure relative humidity during ambient carbonation at 7days.

The water-to-binder ratio did not appear to influence the measured CBW at any stage of exposure. This observation holds true across all relative humidity levels and binder types, with minimal differences observed between the two water-to-binder ratios employed in this study as seen in Figure 4.4-4.5. Nevertheless, no significant changes in measured CBW are evident not only with CEM I but also with composite binders (CS, CS1L & CS2L), at 55% relative humidity at the 28days when compared to the 7days CBW. CBW remains the same or slightly lower at 28d due to mass loss calculation measured up 550°C. This clearly suggests hydration already halted with no increase to CBW at 28d.

At 75% relative humidity, the preconditioning process appears to have a substantial impact on continuous hydration during the 7 days exposure period, as carbonation remains minimal. This impact is particularly noticeable as the samples progressively dry out and fail to maintain the initial curing relative humidity, i.e., 98% before the 14days preconditioning period. These changes may have affected hydration and led

to pore drying; however, there seems to be subsequent stabilization, potentially resulting in a slight increase in CBW at the 28 days mark, as depicted in Figure 4.5 below.

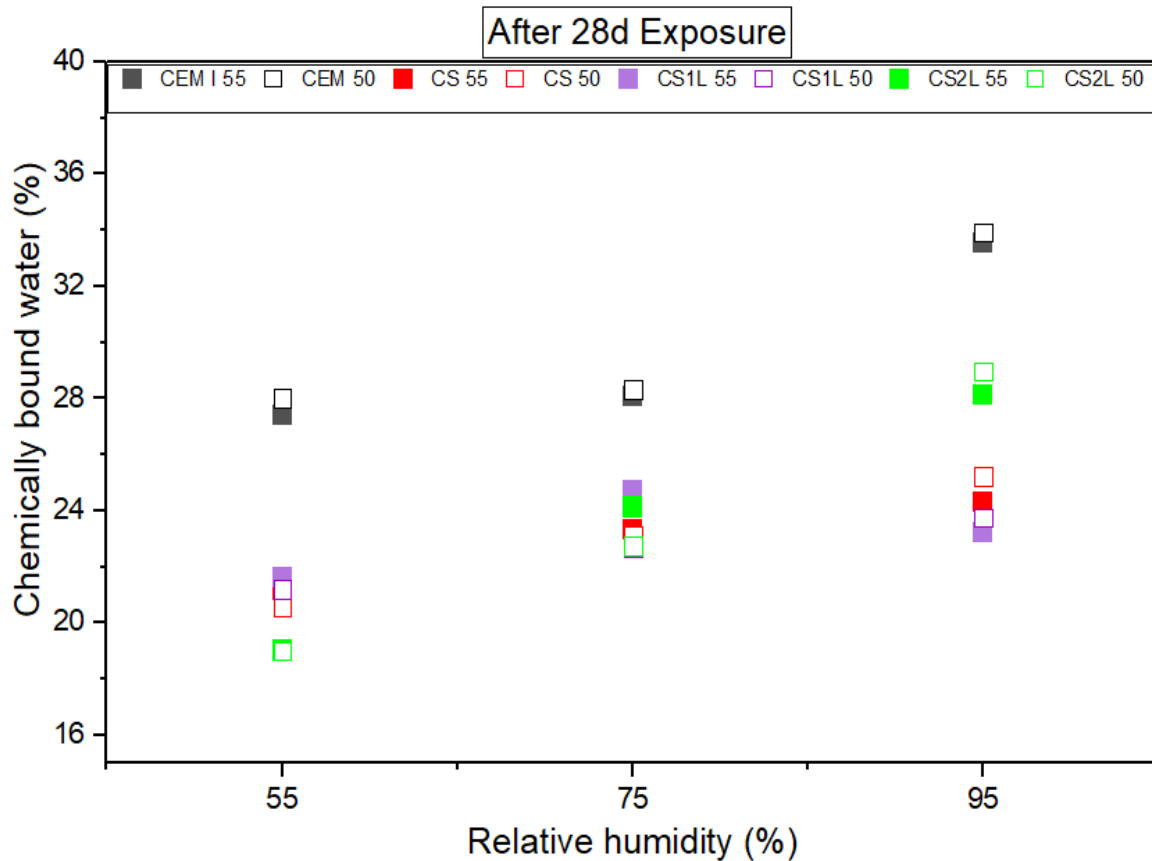


Figure 4.5: Chemically bound water with the exposure relative humidity during ambient carbonation at 28days.

Furthermore, at 95% relative humidity, there is no apparent distortion or decline in CBW for any of the binders. This finding indicates that all binders maintain a steady state at this humidity level. Although slight increases are observed compared to the 7 days exposure period, this suggests that hydration remains consistently active at 95% RH. Also, there is no significant impact of carbonation resulting from the shift from curing room conditions RH to preconditioning at 95% relative humidity.

#### 4.1.3 Portlandite and calcium carbonate content

Figures 4.6-4.8a-b present the evolution of portlandite, and calcium carbonate contents measured by TGA upon exposure to the three relative humidity levels. There is a general downward trend in the amount of portlandite measured upon carbonation at 55% RH for all samples, as shown in Figures 4.6a-b. The decreases were similar

and significant for both the binary and ternary blends. However, CEM I also showed a slight decrease in portlandite content. Carbonate contents showed a general increase for all mixes, from 7 days for CS2L and from 14 days for the other mixes. Carbonation is much favoured at relative humidities of 50-75% [122-124] as pores are not saturated and continued hydration is limited, as seen in the CBW results above and with calcium carbonate contents showing upward trends and CH decreasing, it's obviously CH and likely some minor phases are carbonating, and this explains the decrease of the measured CH at 55% RH.

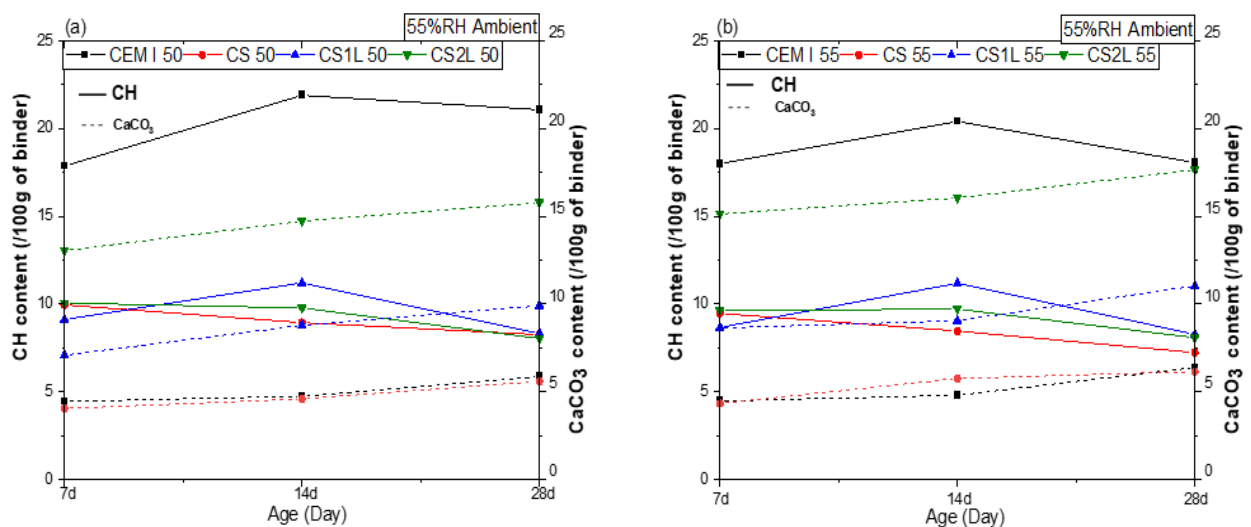


Figure 4.6: Portlandite evolution with CaCO<sub>3</sub> formed at 55% RH ambient carbonation (a) 0.50w/b (b) 0.55w/b.

Contrary to the observation at 55% RH for CEM I, Figures 4.7a-b show the results following ambient carbonation at 75% RH. There was a slight increase in CH contents at both w/b ratios up to 14 days of exposure and was steady thereafter, suggesting that clinker hydration is active as the internal moisture condition is relatively close to the 80% RH threshold reported for continuous hydration and corroborated with results obtained with measured CBW plotted in Figures 4.4-4.5 above. Slight carbonations were observed as about 4-6g of calcium carbonate was measured at 28 days exposure whereas it was nearly zero as 7 & 14 days. This may be due to exposure from handling and preparation, as well as carbonation of minor hydrates since CH not decreasing at this age. Both the binary and ternary blends showed no significant changes in CH content up to 28 days of exposure. An increase in CH may have suggested clinker hydration or a decrease may be due to either carbonation or slag

hydration; however, both cases cannot be established despite relative humidity conditions close to the hydration threshold. Interestingly, the calcium carbonate content increased despite the steady CH content. This suggests, as with the CBW data, that hydration was continuing during ambient carbonation.

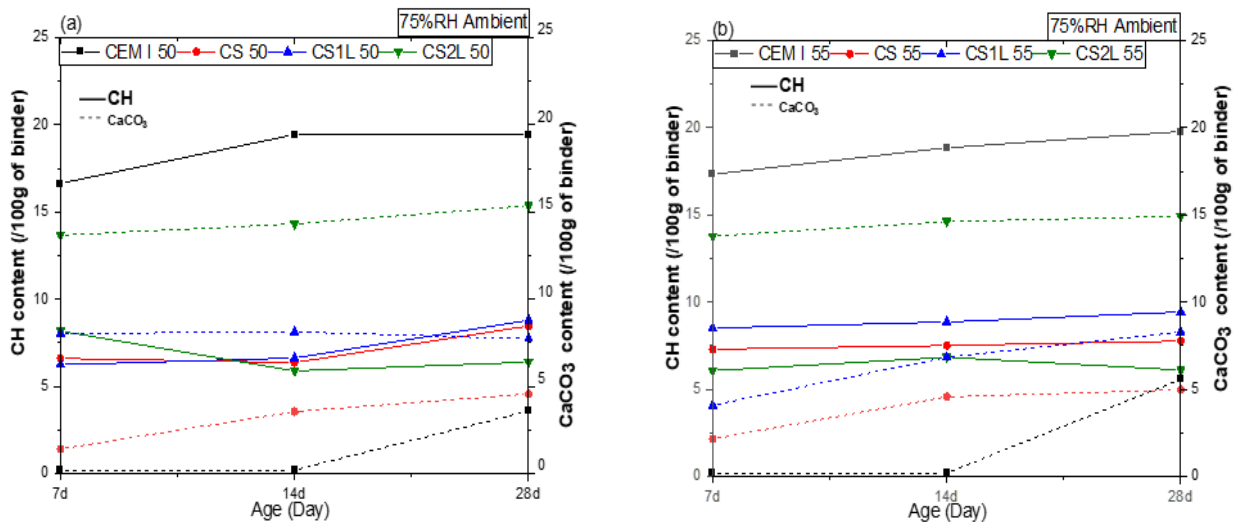


Figure 4.7 Portlandite evolution with CaCO<sub>3</sub> formed at 75% RH ambient carbonation  
(a) 0.50w/b (b) 0.55w/b.

Samples carbonated at 95% RH (Figure 4.8a-b) showed similar behaviour to those exposed at 75% RH, with steady CH contents measured up to 28 days. However, there was no notable change in carbonate content from 7 to 28 days carbonation was greatly slowed down due to water capillary condensation in the capillary pores, retarding the diffusion of CO<sub>2</sub> [19, 122, 125].

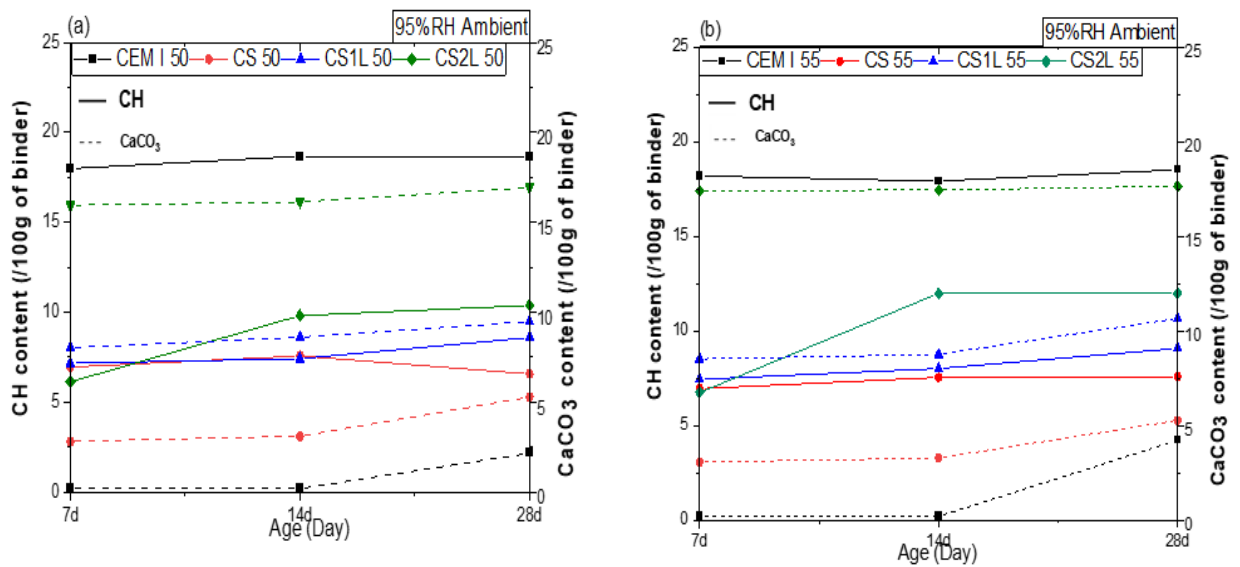


Figure 4.8: Portlandite evolution with  $\text{CaCO}_3$  formed at 95% RH ambient carbonation  
(a) 0.50w/b (b) 0.55w/b.

#### 4.1.4 Effect of RH on portlandite evolution and calcium carbonate formed.

When comparing the CH content at both water/binder ratios following ambient exposure for 28 days at different RH conditions, as depicted in Figure 4.9 below, there were slight differences between the binders following the same trend observed with measured CBW. CEM I, due to its much higher clinker content compared to composite binders contained more CH. However, samples exposed to 95% RH show the highest CH content among the three RH conditions, indicating continuous hydration and the absence of carbonation. As RH decreased, CH content decreased, likely due to carbonation. At lower RH, specifically 55%, binders are more susceptible to carbonation resulting from both handling and exposure due to extended drying during preconditioning, employed to facilitate  $\text{CO}_2$  ingress into the binder's pore structure. Composite binders generally mirror the behaviour of CEM I for this study in all RH, where CH decreases as RH decreases as result of carbonation, except for CS2L, which exhibits higher portlandite content at 95% RH compared to all composite binders at all RH levels. This divergence is attributed to limestone addition which provides more nucleation sites for further clinker hydration [153-155] and seems effective at 20% replacement similar to Adu-Amankwah findings [131].

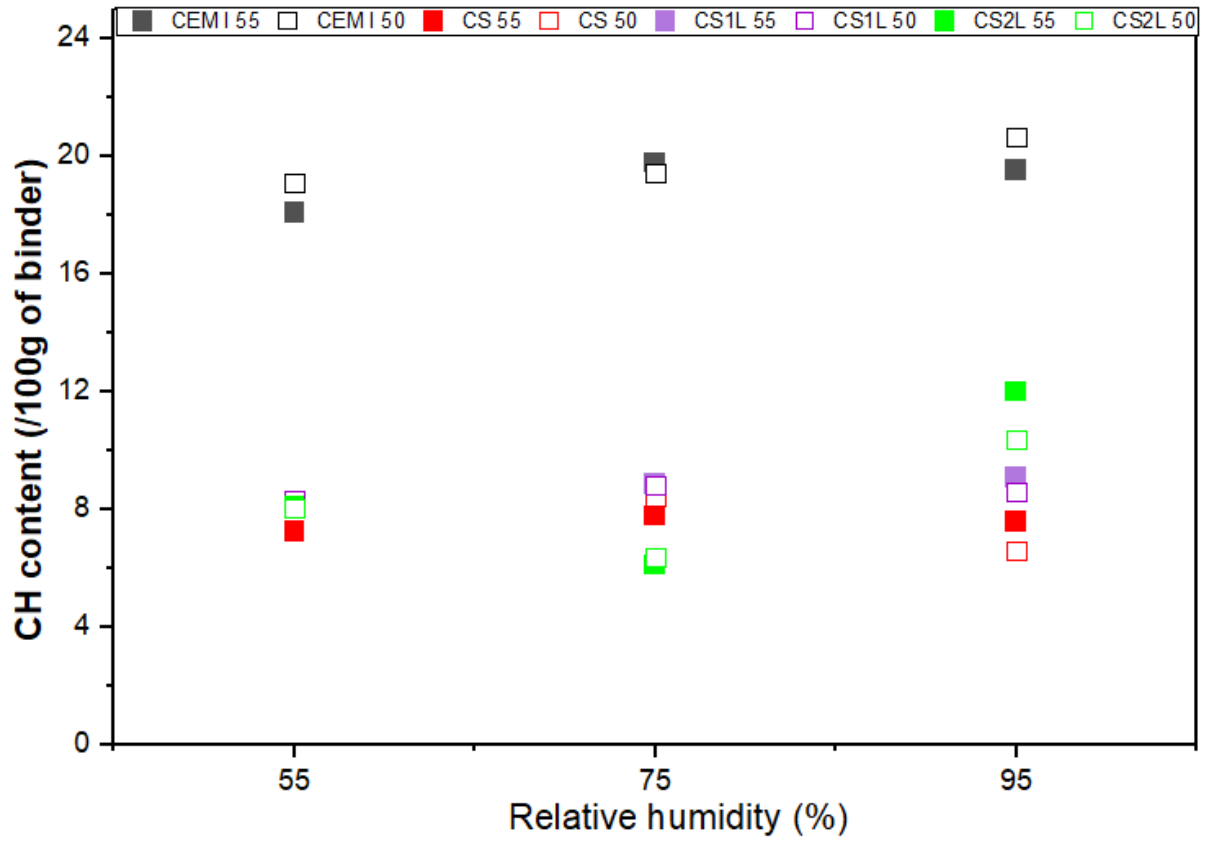


Figure 4.9: Portlandite evolution at different RH for ambient carbonation after 28 days.

Figure 4.10 below illustrates the formation of  $\text{CaCO}_3$  during ambient exposure, with the most significant changes occurring at 55% RH for all binders.

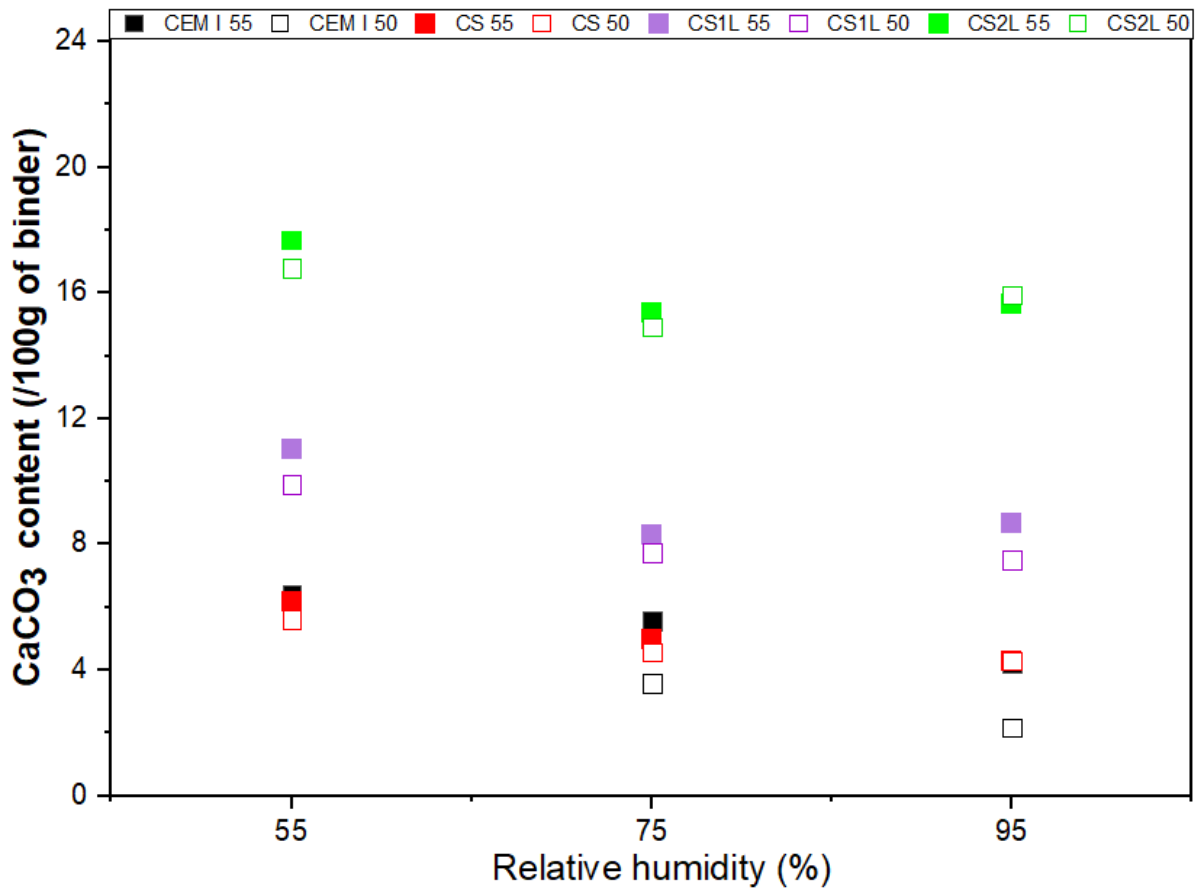


Figure 4.10: CaCO<sub>3</sub> formed at different RH for ambient carbonation after 28 days.

Notably in Figure 4.10, CS2L exhibit higher levels of CaCO<sub>3</sub> than other binders, owing to their higher limestone content in the mix. In contrast however, there was increase at 55% RH compared to other RH supporting earlier observation above that carbonation is active at lower RH. With all CEM I, it demonstrated minimal CaCO<sub>3</sub> formation, measuring less than 2g/100g of binder at 95% RH, but the levels slightly increase to over 6g/100g of binder at 55% RH, indicating ongoing carbonation of CH and other susceptible hydrates i.e AFm, at the lower RH level. This value, higher than that obtained at 95% RH, confirms the hypothesis, and aligns with the amount of CH available in the samples. For composite binders, a similar trend is observed as with CEM I, except there's a closer value measured at 75% RH and 95% RH, which is unexpected, as binders at 95% RH should have less CaCO<sub>3</sub>. However, the changes are insignificant to conclusively attribute them to carbonation exposure rather than superficial effects from handling and preparation.

## 4.2 Phase Assemblages by Thermogravimetric Analysis (TGA)

### 4.2.1 AFt, C-S-H and AFm

There was no significant transformation of either AFt or C-S-H upon exposure for all samples at all humidities, as shown by the DTG data at 110-130°C in Figure 4.11-4.13(a) & (b) for 0.55(Top) & 0.50(bottom) for PC and composite blends. However, there was a slight increase in the peak intensity at later exposures, i.e., 28 days, compared to 7 days. This may arise from the continuous hydration of both clinker and slag, producing more C-S-H, particularly at 75% and 95% relative humidity. This is consistent with the findings of Borges et al. [98], who found that C-S-H will not be at risk of decomposition when the permeability of the paste is too low to transport CO<sub>2</sub> in the pore structure, and also supported in Castello et al. [72]. AFt is expected to remain stable at low CO<sub>2</sub> concentrations for a longer duration [126].

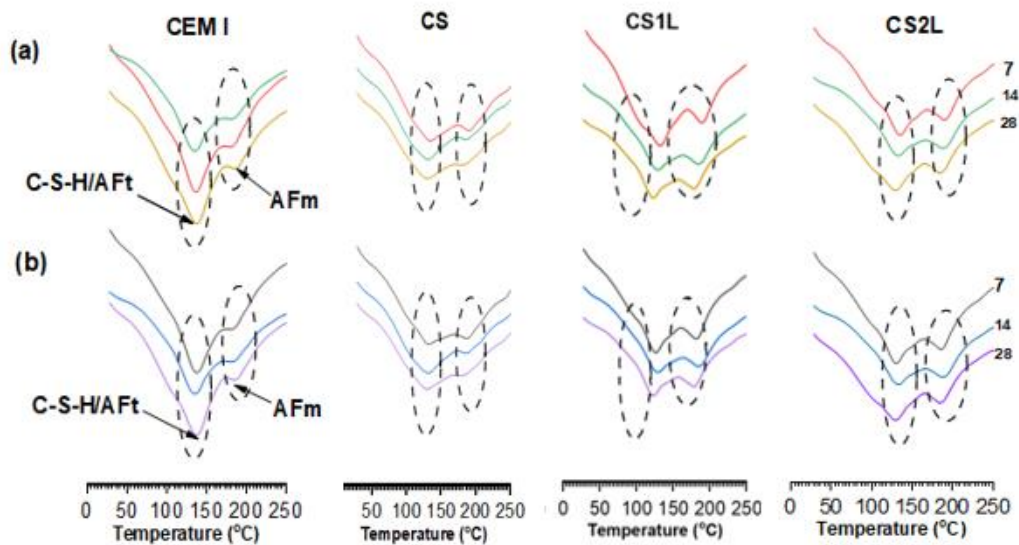


Figure 4.11: AFt, C-S-H & AFm at 55% RH (Top) 0.55w/b (Bottom) 0.50w/b.

The presence of peak at 150-170°C represents the AFm phase [89, 109], as shown in Figure 4.11-4.13 for w/b 0.5 (top) & 0.55 (bottom), respectively. There were no significant changes in this peak at all relative humidities from 7 to 28 d of exposure for the PC system, as shown in Figure 4.9 above, except after 28d of exposure at 55% RH for both w/b ratios. This is because limestone blends contain hemi- and monocarboaluminates, which are thermodynamically stable at low CO<sub>2</sub> concentrations, such as upon ambient exposure [72, 127]. However, a slight decrease

in the AFm for the binary binder (CS) at both w/b ratios from 7 to 28 days upon 55% RH exposure was observed, as shown in Figure 4.13, compared to other exposure conditions for the same system, indicating either transformation of AFm species or decalcification [131, 140]. No obvious decrease in peak intensity was observed under the other two conditions, i.e 75% and 95% RH. According to thermodynamic modelling [156] CO<sub>2</sub> volume concentration of approximately  $1.95 \times 10^{-15}$  will trigger AFm carbonation followed by carbonation of CH [157] and other hydrates at slightly higher concentrations. These findings show that AFm phases might be among the first phases to carbonate in composite binders if all other conditions, such as the water-binder ratio and pore saturation, are favourable.

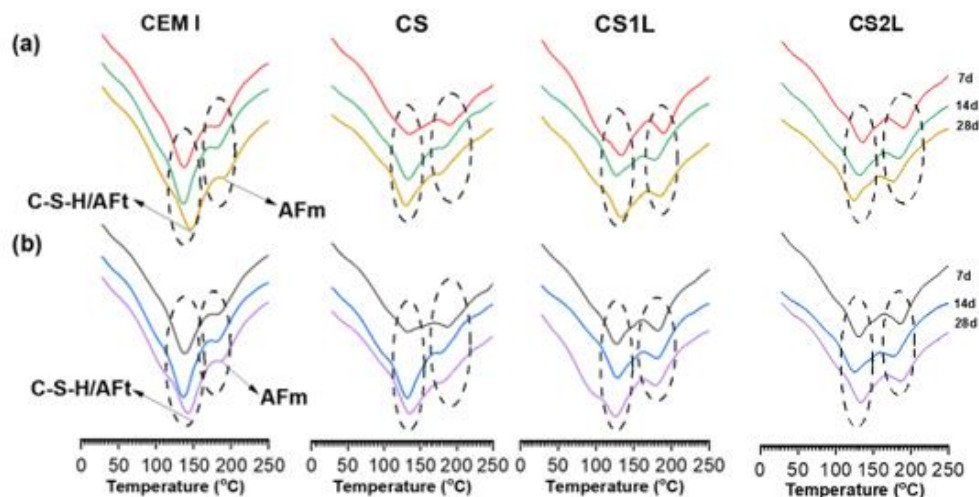


Figure 4.12 AFt, C-S-H & AFm at 75% RH (Top) 0.55w/b (Bottom) 0.50w/b.

Ternary binders showed no significant decrease of AFm peak intensity from 7 to 28 days' exposure at all conditions for both 75% & 95% RH. This is because the limestone blends contain hemi- and monocarboaluminate, which are thermodynamically stable at low CO<sub>2</sub> concentrations such that exist upon ambient exposure [89, 158].

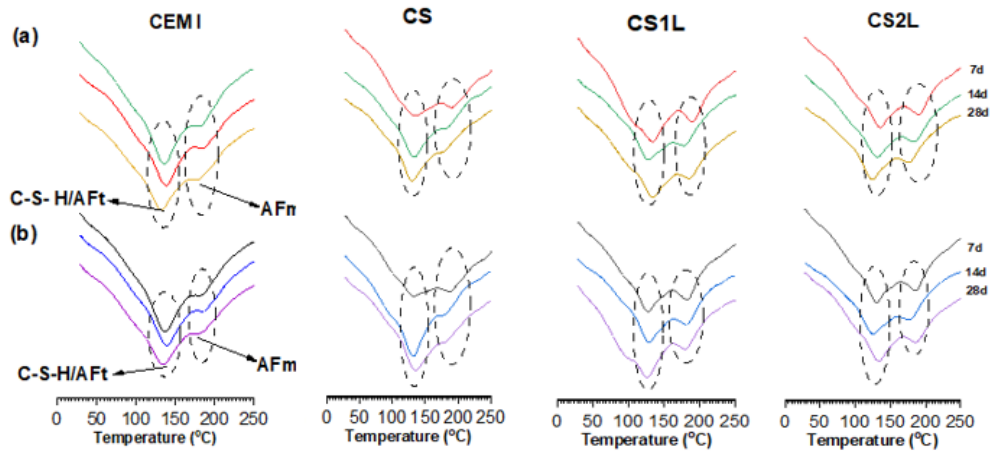


Figure 4.13: AFt, C-S-H & AFm at 95% RH (Top) 0.55w/b (Bottom) 0.50w/b.

#### 4.2.2 Portlandite evolution by DTG

Portlandite (CH) decomposition occurs at 450-500°C, which is consistent with Figure 4.14-4.16A-D. For each binder at 0.55 and 0.50 w/b ratio, there weren't any significant changes in peak intensity upon exposure from 7 to 28 days. Differences in peak intensity could be attributed to differences in clinker content between blends rather than changes due to ambient carbonation.

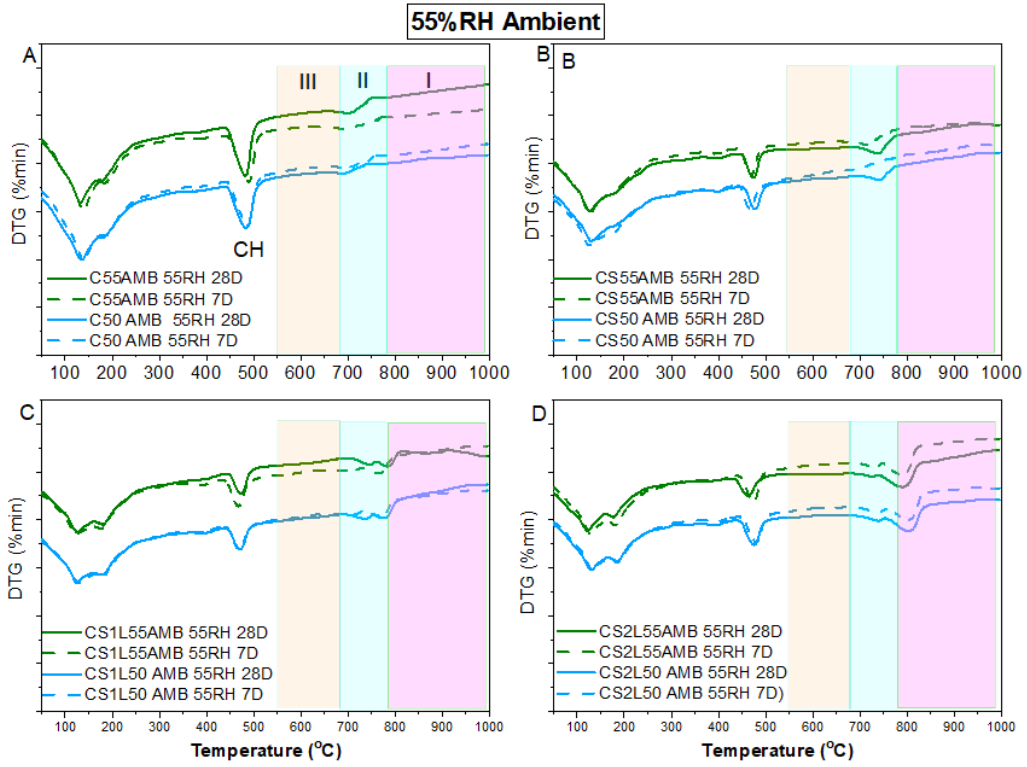


Figure 4.14: DTG during 55% RH ambient carbonation.

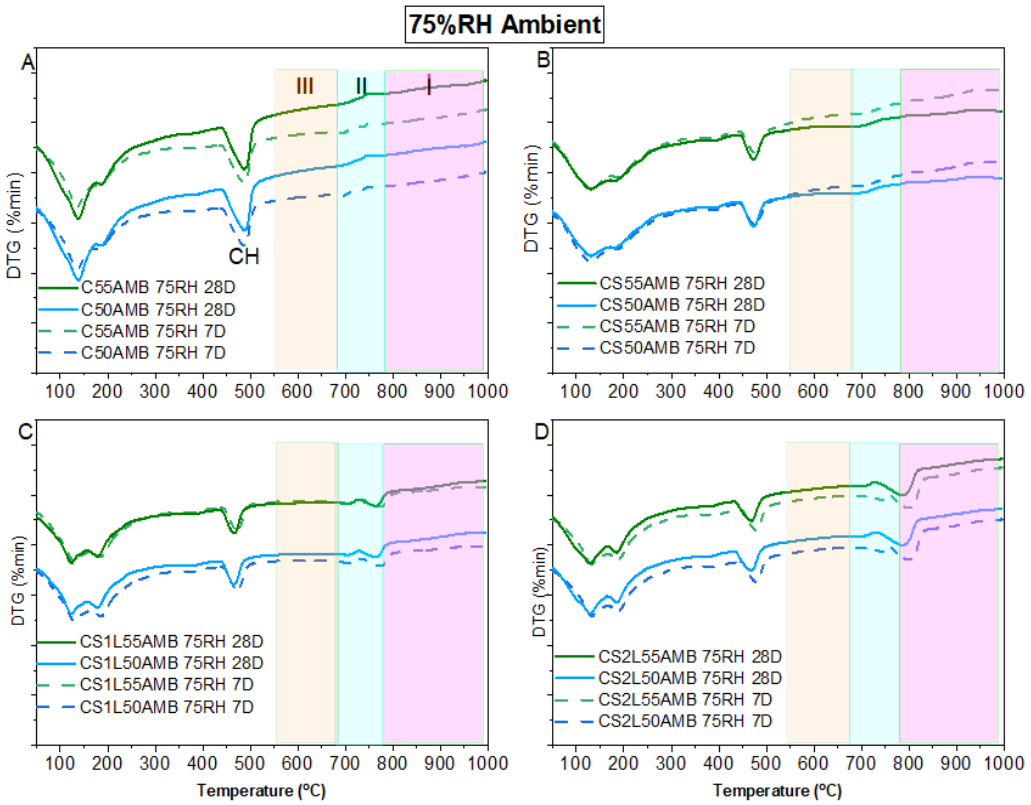


Figure 4.15: DTG during 75% RH ambient carbonation.

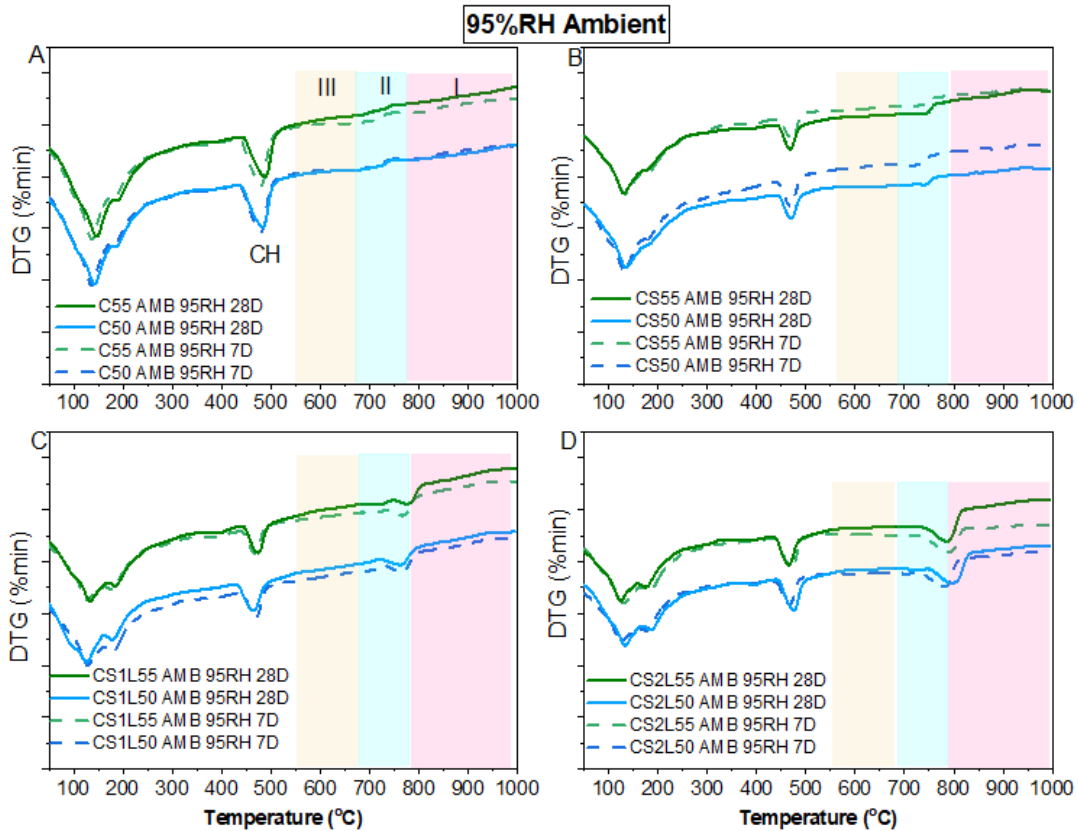


Figure 4.16: DTG during 95% RH ambient carbonation.

#### 4.2.3 Calcium carbonate by DTG

The DTG plots in Figure 4.14-4.16A-D above, show various decomposition temperature modes for calcium carbonates from 550-990°C representing both amorphous and crystalline  $\text{CaCO}_3$ , as already identified in many studies [89, 98, 140]. Obviously, samples containing limestone (CS1L & CS2L) shows a more intense peak at higher decomposition temperature, which is indicative of calcite from the limestone. The decomposition temperature modes are identified as I, II and III on the Figures. Mode I indicate decomposition of well-crystalline calcite at 780-990°C and is usually present following the carbonation of portlandite and calcium carbonate residues especially in limestone blended cement. Mode II & III are from calcium carbonate polymorphs, vaterite and aragonite at a decomposition temperature of 680-780°C or amorphous calcium carbonate at 550-680°C. Vaterite and aragonite have been reported to form from carbonation of C-S-H, aluminates and ettringite [126, 159-162]. Figure 4.14 above present data from the samples exposed to ambient carbonation at

55% RH. At both w/b ratios CEM I and composite binders showed a mass loss corresponding to all mode of decomposition temperature, albeit slightly intense mass loss at decomposition temperature corresponding to mode II & III. This observation suggest amorphous calcium carbonates seems formed due to carbonation of minor phases as collaborated with enlarged plot from Figure 4.16 above. The mass loss is more obvious and intense at 28 days especially with composite blends as carbonation progress despite low volume. Similarly, these temperature decomposition modes were also observed with both 75% and 95% RH ambient exposure from 7 days at both w/b ratios till 28 days exposure albeit slight changes which seems to have resulted from superficial carbonation during handling and consistent with decomposition temperature reported in [127] for CEM I under natural carbonation.

Generally, ternary blends (CS1L & CS2L) showed a similar trend to binary blends, albeit with a clear mode I decomposition arising from the limestone present within the blends, [131]. At 55% RH, CS2L peak shifted more to higher temperature (mode I) compared to CS1L although difference in limestone content at 20% might be the major factor contributing to this observation. However gradual shifts of decomposition temperature from mode II to mode I as relative humidities decreases were also noticed which implies portlandite carbonation cannot totally be neglected from these results especially with 55% RH exposure as it provides more ideal drying condition for ingress of CO<sub>2</sub> into the pore system. This is consistent with the findings of Herterich [107] that the presence of a better structured or crystalline CaCO<sub>3</sub> phase is as result of some modification in the carbonation mechanism of the paste system which is dependent on the relative humidity.

#### 4.3 Phase Assemblages by Fourier Transform infrared spectroscopy (FTIR)

The FT-IR spectra of samples subjected to ambient carbonation at different relative humidity, and w/b ratios are presented below. Both w/b ratios showed similar behaviour with the same reaction products. Hence results are presented here from only one w/b ratio and the remaining data are available in the appendix section of the thesis. The information obtained is important for a comprehensive understanding of phase changes, especially concerning C-S-H, CH, AFt and different carbonate species.

#### 4.3.1 Portlandite content

Figures 4.17-4.19 show the OH stretching band of portlandite at  $3640\text{ cm}^{-1}$  in the FTIR spectra of samples subjected to ambient carbonation at different RH conditions [140, 159]. The CEM I systems showed more intense peaks at all relative humidities compared to composite blends. This is due to more clinker availability, as confirmed by DTG above. At 55% RH, CH peaks decrease at 28 days' exposure compared to exposure for 7 days. This is due to partial carbonation of the portlandite. Generally, samples exposed at 75% RH showed a slight reduction in intensity, but there was no change following exposure at 95% RH. These results agree with TGA data, that lowering RH led to increased consumption of CH through carbonation. Composite blends also showed similar trends, but with complete consumption of the already depleted portlandite by 7 days at 55% RH, some portlandite present at 7 days but consumed by 28 days following exposure at 75% RH, but no consumption of portlandite at either age following exposure at 95% RH.

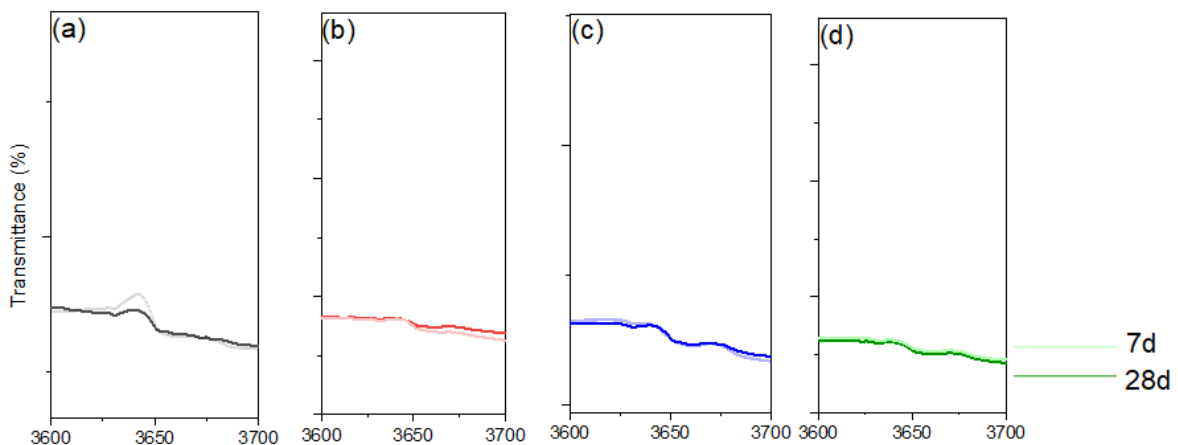


Figure 4.17: Enlarged FTIR plot between  $3700\text{-}3500\text{cm}^{-1}$  for 55% RH ambient carbonation at 7 & 28 days (a) CEM I, (b) CS (c) CS1L (d) CS2L.

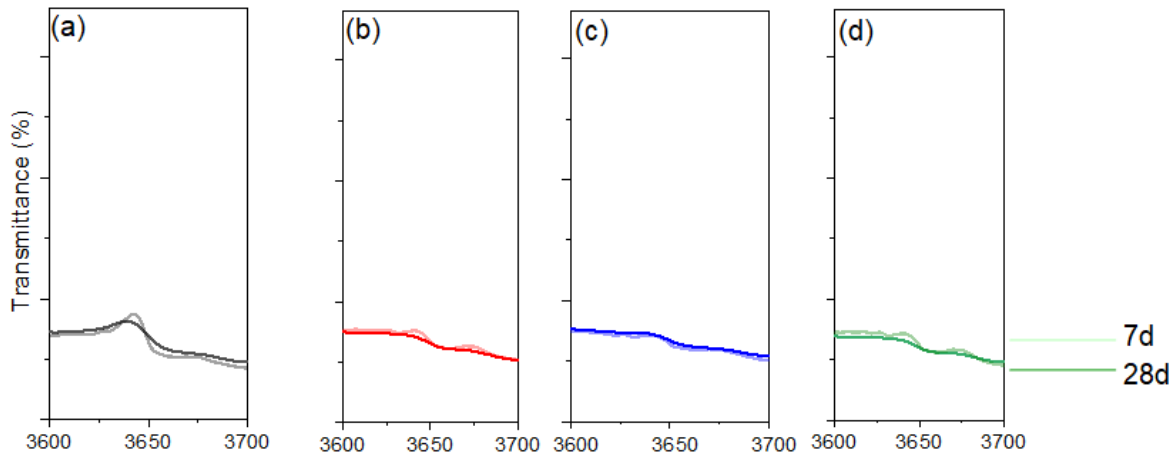


Figure 4.18: Enlarged FTIR plot between 3700-3500cm<sup>-1</sup> for 75% RH ambient carbonation at 7 & 28 days (a) CEM I, (b) CS (c) CS1L (d) CS2L.

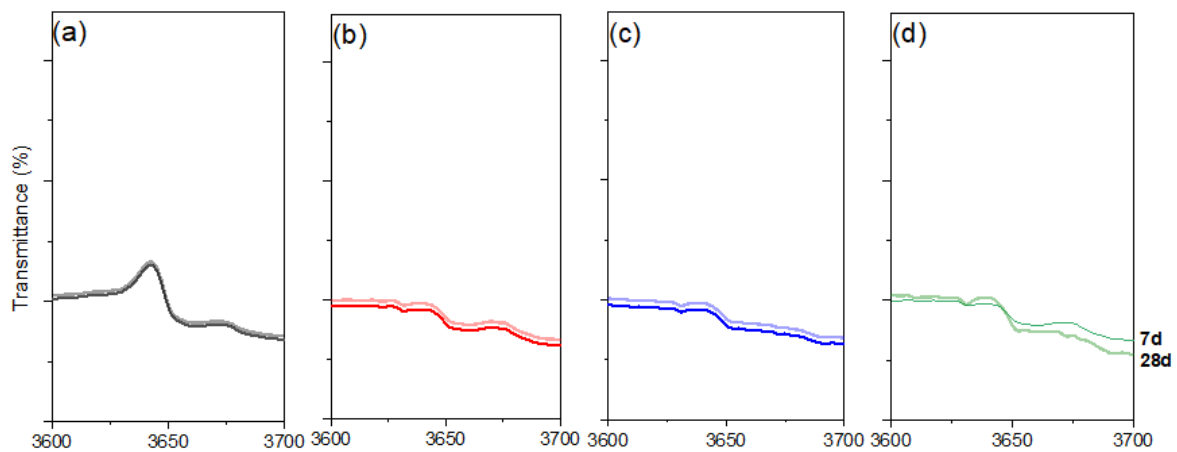


Figure 4.19: Enlarged FTIR plot between 3700-3500cm<sup>-1</sup> for 95% RH ambient carbonation at 7 & 28 days (a) CEM I, (b) CS (c) CS1L (d) CS2L.

#### 4.3.2 Calcium carbonate and polymorphs

Carbonate species give characteristic FTIR absorption bands namely: asymmetric C–O-stretching mode ( $\nu_3$ ) usually around 1400-1500 cm<sup>-1</sup>, symmetric C–O-stretching mode ( $\nu_1$ ) within 1067 cm<sup>-1</sup> to 1089 cm<sup>-1</sup>, CO<sub>3</sub><sup>2-</sup>-bending ( $\nu_2$ ) around 870 cm<sup>-1</sup>, and O–C–O-bending ( $\nu_4$ ) with spectra around 700 cm<sup>-1</sup> to 746 cm<sup>-1</sup>. Most of these identified absorbance bands are reported as characteristic bands of both amorphous and crystalline CaCO<sub>3</sub>, vaterite, aragonite, and calcite in the literature [163, 164].

The strong absorbance peaks at 1400-1500  $\text{cm}^{-1}$  (I) correspond to the asymmetric stretching vibration of ( $V_3$ ) C-O from the formation of both amorphous and crystalline  $\text{CaCO}_3$  phases [159], shows the intensity of calcium carbonate formed at different testing ages in Figure 4.20-4.22 below. At 55% RH, the intensity of 28 days is higher than 7 days samples suggesting an increase in calcium carbonates due to carbonation for all samples and collaborates TGA result from Figure 4.14-4.16 above. For samples exposed at 75 & 95% RH, there is no significant changes in peak intensity from 7 to 28 days suggesting minimal changes in carbonation behaviour during exposure Also, the narrow band at 870 $\text{cm}^{-1}$  (III) assigned to calcite shows similar characteristic with  $V_3$  band albeit reduced intensity at both 75% and 95% RH for all of the binders compared to 55% RH confirming calcite were predominant in all samples especially with 55% RH collaborated with the studies of [140, 164, 165].

In addition, the minor peak at 714  $\text{cm}^{-1}$  due to in-plane bending ( $V_4$ ) and assigned to calcite, or aragonite if a split band  $V_4$  exists between 713 $\text{cm}^{-1}$  and 700 $\text{cm}^{-1}$  [159, 163, 164] was observed in Figure 4.18-4.20. This can likely be assigned to calcite as they are more prominent when limestone is present within the CS1L and CS2L blend. This is also consistent with observations that aragonite is normally formed in young samples [166]. But, both SEM-EDS and XRD should be able to provide an insight into aragonite formation following ambient carbonation, as aragonite formation is also highly dependent on Ca/Si ratio of the samples [167, 168].

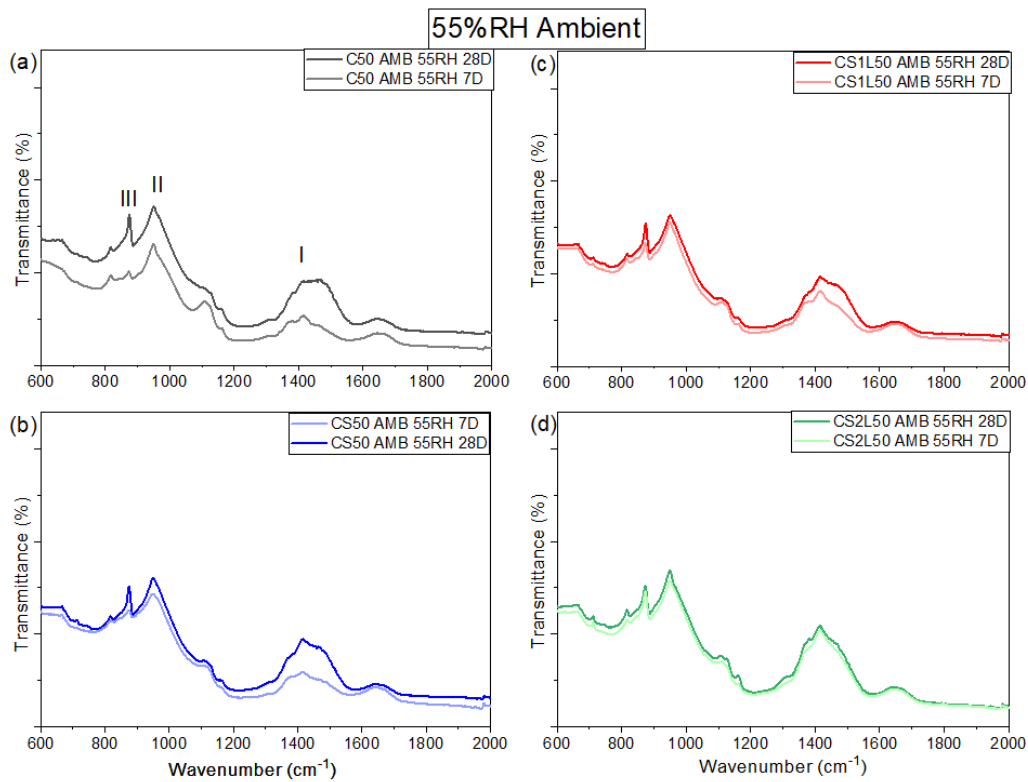


Figure 4.20: FTIR normalised plot between 600-2000 $\text{cm}^{-1}$  for 55% RH under ambient exposure at 7 & 28 days (a) CEM I, (b) CS (c) CS1L (d) CS2L.

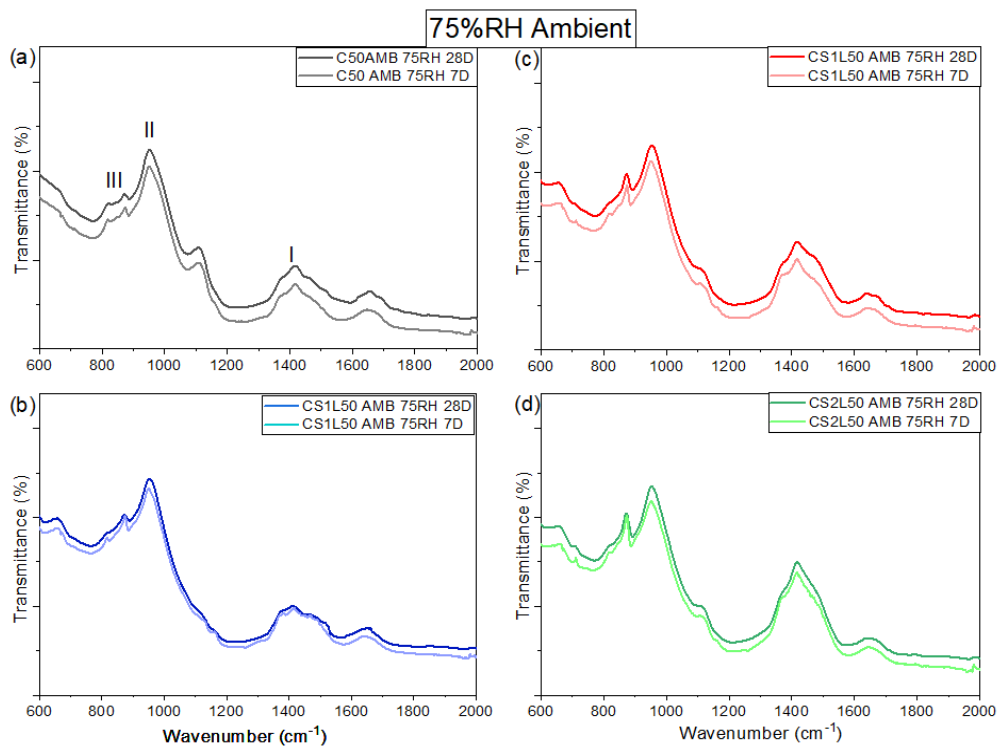


Figure 4.21: FTIR normalised plot between 600-1700cm<sup>-1</sup> for 75% RH under ambient exposure at 7 & 28 days (a) CEM I, (b) CS (c) CS1L (d) CS2L.

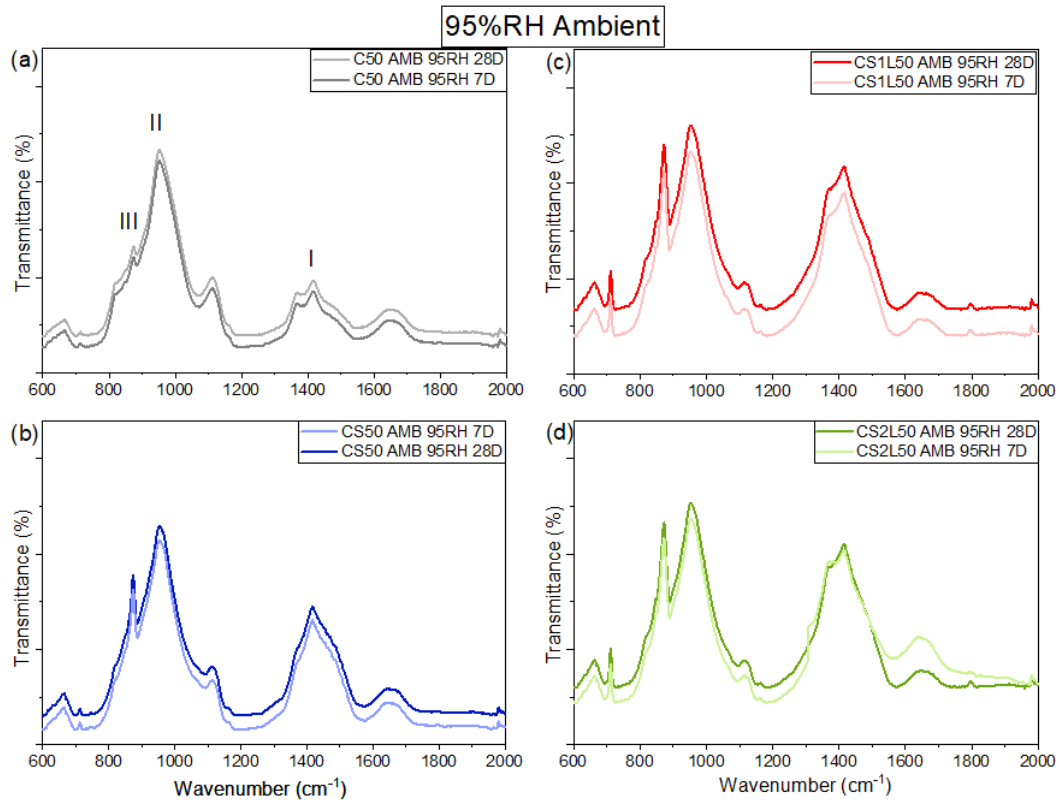


Figure 4.22: FTIR normalised plot between 600-1700cm<sup>-1</sup> for 95% RH under ambient exposure at 7 & 28 days (a) CEM I, (b) CS (c) CS1L (d) CS2L.

#### 4.3.3 Calcium Silicates Hydrates (C-S-H).

The primary absorption band for silicates is between 800 cm<sup>-1</sup> and 1200 cm<sup>-1</sup>, attributed to both asymmetric and symmetric stretching of the Si-O-Si band [169]. Here this is seen at band 970 cm<sup>-1</sup> labelled as (ii) on Figures 4.20-4.22 corresponding to C-S-H [170], with no peak shifts in this band following ambient carbonation at any RH. This suggests that C-S-H was unaffected by ambient carbonation exposure throughout the test in both CEM I and composite blends for all relative humidity levels.

#### 4.4 Compressive strength development

Figures 4.23-4.25 below present compressive strength results for mortar samples subjected to ambient carbonation at 55%, 75%, and 95% RH. Generally, there were marginal changes in compressive strength due to exposure conditions, binder composition i.e., limestone addition and water-binder ratio.

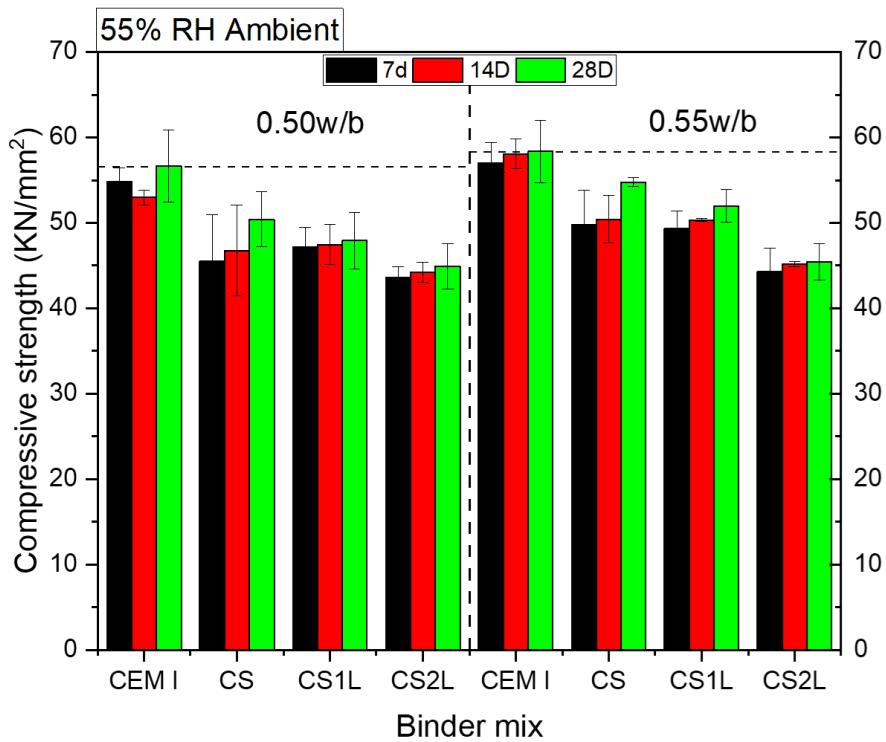


Figure 4.23: Compressive strength following ambient carbonation at 55% RH.

It would be expected that strength would be lower with a higher w/b ratio. However, this was not the case contrary to with mortar samples at 55% RH. The mortar samples at w/b 0.55 exposed at 55% RH showed higher strengths after exposure than the w/b 0.50 samples. Since the degree of carbonation was only slight, this cannot be explained by the precipitation of calcite within pore spaces. This is thus likely as a result of the degree of saturation [171] since it is known that dried samples (such as those exposed to 55% RH) show slightly higher strengths than samples that are fully saturated. The w/b 0.55 samples will have dried to a greater extent than the w/b 0.5 samples, thus increasing their apparent strengths, the extent of which diminished with increasing RH. However, Leemann et al. [108] concluded that water-binder ratio and cement-specific properties affect the ranking of concrete more than relative humidity in natural carbonation.

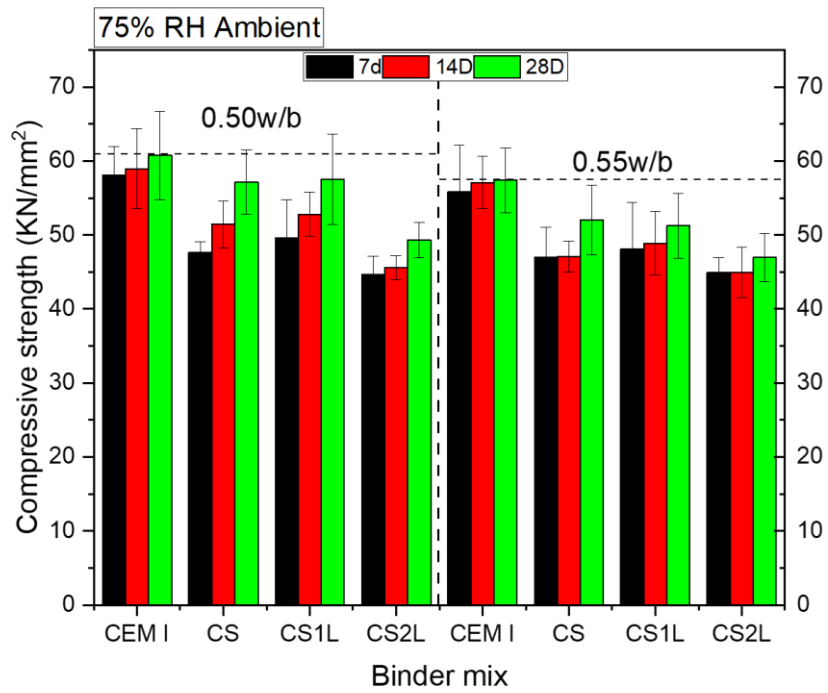


Figure 4.24: Compressive strength following ambient carbonation at 75% RH.

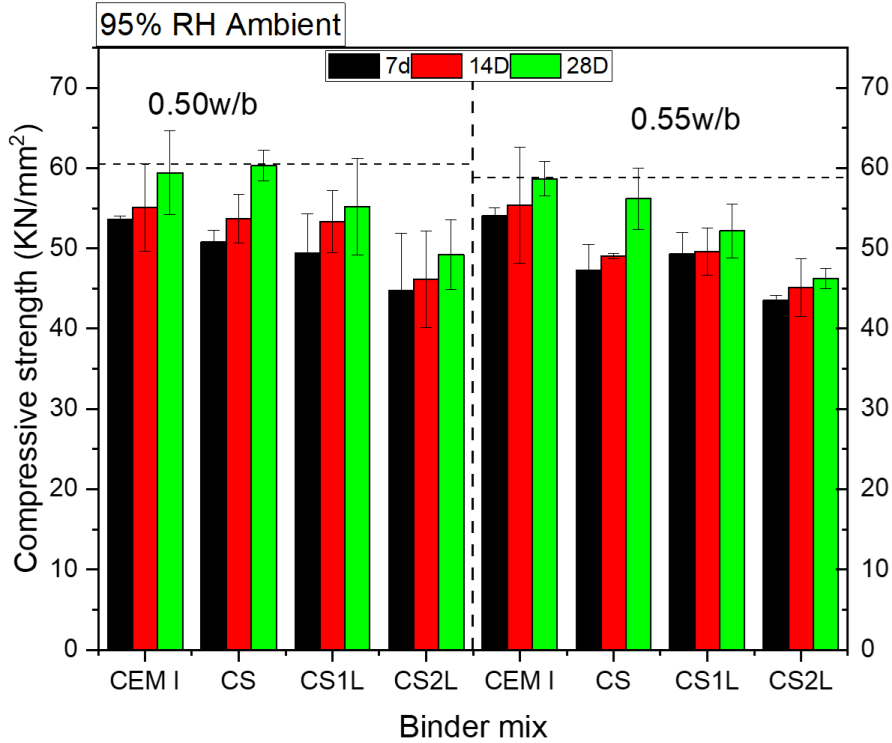


Figure 4.25: Compressive strength following ambient carbonation at 95% RH.

At 75% RH, the compressive strengths were comparable at the two w/b ratios with 0.5 w/b mortar samples slightly stronger than 0.55w/b samples for all mixes, while at 95% RH, the results were as expected, as it shows similar trends with 75% RH with the higher w/b ratio leading to a lower strength however, the difference in compressive strength (10-15kN/mm<sup>2</sup>) at both w/b ratio are marginal across the mix. CS mortar with w/b 0.5 at 95% RH shows higher compressive strength at 28 days than CEM I which suggest a late compressive strength gain emerged since both 7&14 days results did not support the trend as it recorded lower strength compared to CEM I at both ages. The late compressive strength gain suggest GGBS hydration are eminent and continuous at this age and may have influence increase in compressive strength as GGBS concrete or mortar are known to react at later age [172, 173] and with adequate curing at 95% RH, such occurrence is expected. Similar result was also reported Adu-Amankwah [131] study regarding late strength of slag mix at 90days curing.

In general, minimal carbonation was observed in all samples at various relative humidity (RH) levels, which suggests that changes in compressive strength were not likely due to carbonation. However, it's worth noting that higher water-to-binder (w/b) ratios resulted in higher strengths after exposure at 55% RH, possibly due to the drying of the samples. In contrast, at 75% and 95% RH, the trends aligned with expectations, with lower w/b ratios yielding higher strength.

Furthermore, there was a significant increase in strength in the CS samples after exposure to 95% RH for 28 days, indicating ongoing hydration under these conditions. It's important to mention that the samples had already been cured for 28 days before exposure, so this strength gain can be considered as the result of hydration over a period of more than 56 days.

When comparing the overall compressive strength at various relative humidity levels for mortar samples, CS mortar with a w/b ratio of 0.5 at 95% RH, after 28 days of exposure, exhibited the highest compressive strength at approximately 61 kN/mm<sup>2</sup> among all binders tested at different RH levels. In contrast, CS2L at 55% RH, after 7 days of exposure, achieved the lowest strength at around 43 kN/mm<sup>2</sup> among all the binders studied. It's worth noting that there is a slight difference observed after 28 days of exposure at all relative humidity levels, about 15 kN/mm<sup>2</sup>, which could be attributed

to the fact that the samples were initially moist cured at 98% RH before being exposed to different ambient carbonation conditions.

#### 4.5 Summary

- Exposure of both paste and mortar samples to ambient levels of CO<sub>2</sub> at 55, 75, and 95% RH did not lead to any evidence of carbonation, as determined through the absence of a visible colour change upon spraying with thymolphthalein after 28 days carbonation. This was true for all binders and both water-binder ratios. However, both TGA and FTIR suggested slight carbonation occurred, especially at 55% RH.
- Hydration ceased at 55% RH but continued at both 75 & 95% RH, evidenced by the amount of CH and CaCO<sub>3</sub> formed and supported by chemically bound water contents as measured by TGA. This was true for both w/b ratios.
- The CH content of the various binders depended primarily on the clinker content, with the CEM I systems showing the highest levels. This was particularly so for the samples exposed at 95% RH. CS2L exhibited a higher-than-expected CH content after exposure at 95% RH due to limestone providing additional nucleation sites, however this was not observed with exposure at lower RH levels suggesting appropriate RH can influence the CH formed.
- There was some evidence of carbonation following exposure at 55% RH. But there was minimal CaCO<sub>3</sub> formation at both 75% & 95% RH for all binders, suggesting carbonation were likely from handling and preparation instead of during ambient carbonation however, composite binders show higher CaCO<sub>3</sub> at 55% RH comparable to CEM I.
- Partial carbonation of AFm, C-S-H, and CH in pastes was observed at 55% RH ambient exposure confirmed with DTG, and further corroborated with FTIR. However, minimal or no carbonation is observed at both 75 & 95% RH.
- Calcite was the primary carbonation product, formed from the carbonation of portlandite while other calcium carbonates were identified with both TGA and FTIR. There was no evidence of C-S-H decalcification upon carbonation as determined with FTIR.
- Mortars showed similar compressive strength gains throughout the test conditions i.e w/b and relative humidity. Since there was no clearly evident carbonation, this could not have affected strength development. In these

cases, the degree of saturation and binder composition i.e., limestone addition at 20% are crucial factors affecting compressive strength during ambient exposure as observed in all mortar samples. Comparing CEM I mortar with

- composite binders showed a comparable strength at higher relative humidity i.e., 75 & 95% RH due to continuous hydration whereas drying may have prevented prolonged strength gain in composite cements at 55% RH.
- In the case of CS mortar with water-binder ratio of 0.5 at 95% RH, a higher compressive strength is evident in comparison to other samples. This can be attributed to late hydration of the GGBS, which could potentially result in further strength gain after over 56 days curing/exposure. However, it's important to note that this difference falls within the margin of error and is less than 5% when compared to the compressive strength of the other samples.

## Chapter 5: Carbonation under accelerated conditions

This chapter presents and discusses the study of the effect of accelerated carbonation at two water-binder ratios under different relative humidity (55%, 75%, and 95%) following the same preconditioning explained in chapter three. CO<sub>2</sub> exposure was at 4% aiming to achieve significant carbonation of the samples within a 28 days testing period. The effect of accelerated exposure on hydration, phase assemblages, carbonation depth, and compressive strength on both paste and mortar samples from composite binders were compared to CEM I.

Unlike for the samples subjected to ambient carbonation, where there were no visible colour changes upon spraying with thymolphthalein indicator. Both mortar and paste samples showed evidence of considerable carbonation as shown in Figure 5.1 below for paste samples. The samples showed a carbonation edge surrounding an uncarbonated core and this nomenclature is used from now on. Samples labelled as edge were from the carbonated and partially carbonated region, and those labelled as core were from the region remaining blue following spraying with thymolphthalein. On the occasions when the entire sample had carbonated, such samples are labelled as “whole”.

Due to time limitations, it was not possible to investigate all of the samples. Thus, it was decided that paste samples for accelerated carbonation would only be prepared with a w/b ratio of 0.5. This was justified because there were no demonstrable differences in the trends for different binders and different RH levels, with the higher w/b ratio just leading to more pronounced carbonation. Mortar samples for strength and carbonation depth measurements however were still prepared at both w/b ratios. Moreover, paste samples with a 0.50 water-binder ratio demonstrated a higher buffering capacity than those with a 0.55 water-binder ratio, as evidenced by the amount of calcium hydroxide (CH) remaining after carbonation during the 7 to 28-day exposure period. This is due to the lower porosity of these samples restricting the ingress of CO<sub>2</sub> and supports the decision to focus exclusively on one water-binder ratio in the subsequent discussion and presentation of results, as outlined in Figure 5.1. This Figure clearly illustrates complete carbonation in nearly all samples at a 0.55 water-binder ratio especially at 55% RH, which presents challenges in accurately distinguishing between fully carbonated and partially carbonated samples. This

distinction is crucial for achieving a comprehensive understanding of the required phase assemblage and microstructure characterization for this study.

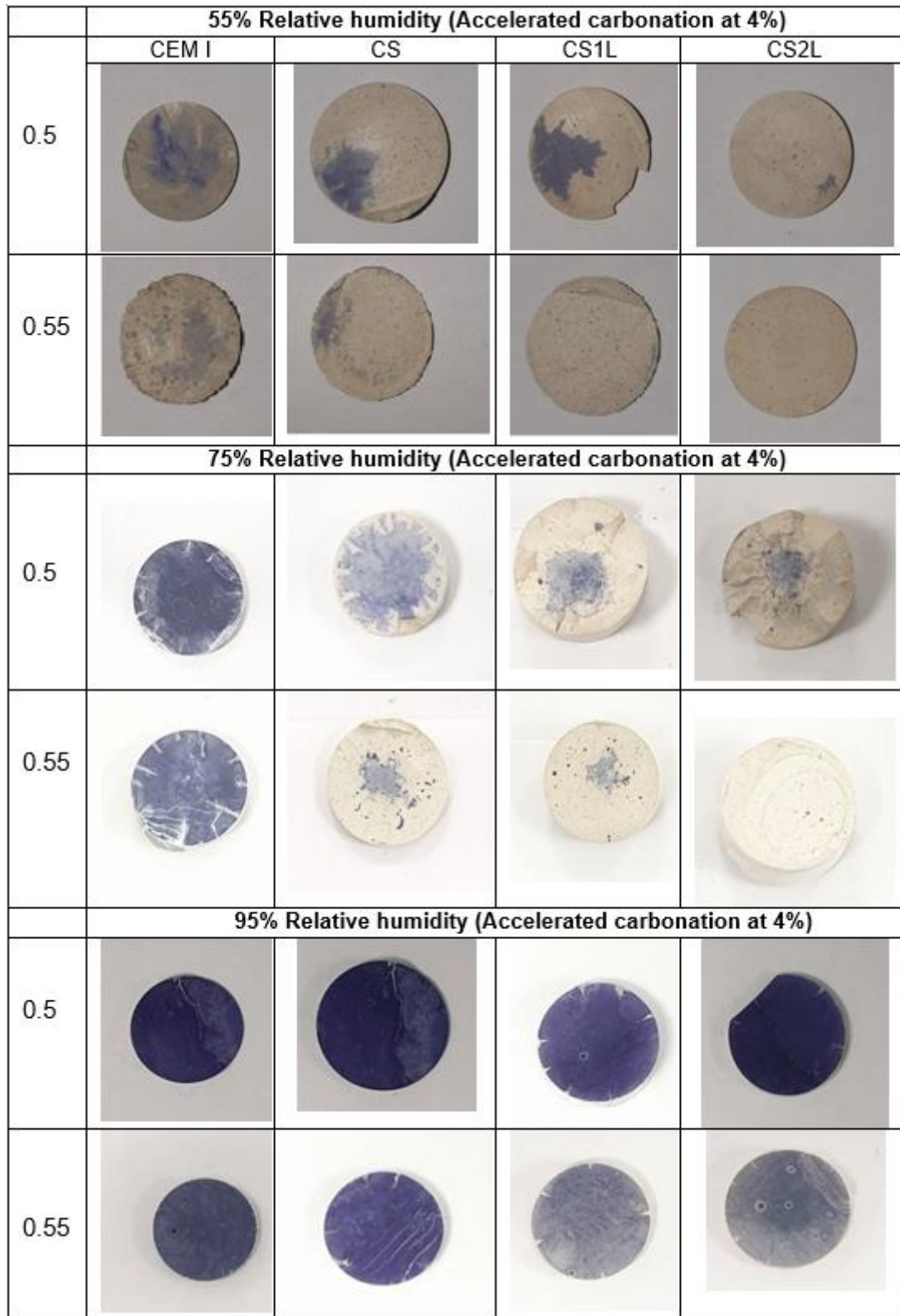


Figure 5.1: Accelerated carbonation of paste samples at 55%, 75% and 95% relative humidity for 28 days exposure.

## 5.1 Hydration progress during accelerated carbonation

### 5.1.1 Chemical bound water, portlandite content, and calcium carbonates.

Figures 5.2-5.4 present combined results of CBW, CH and CaCO<sub>3</sub> contents measured from pastes by TGA technique after exposure to accelerated carbonation at 55%, 75% and 95% RH.

CEM I samples consistently had the highest CBW irrespective of the exposure relative humidity during accelerated aging. However, there was a notable change in CBW following exposure, specifically between 7 and 28 days across all RH, as shown in Figure 5.2-5.4. At 55% RH, after exposure for 28 days CEM I displayed both fully carbonated (edge) and partially carbonated zones (core), each exhibiting different CBW. Furthermore, the CBW was higher at 7 days compared to 28 days. This may be due CBW calculation taken at mass loss between 50<sup>o</sup>-550<sup>o</sup>C which have included part of CH decomposing temperature and also carbonation of CH. This increases CaCO<sub>3</sub> formed especially with edge samples as seen in the Figures. This trend is generally observed with all other pastes i.e binary and ternary blends, as presented in Figure 5.2-5.4 below. An increase in CBW was anticipated, as this would typically signal ongoing hydration particularly within the core area of the sample that have less exposure to CO<sub>2</sub>. However, this expectation did not align with the findings of this study. Moreover, it was expected that the water produced at the carbonation front (edge) would find its way into the core part, participating in the hydration process. Nevertheless, this did not appear to lead to further hydration of the core area, as evidenced by the decrease in CBW measured at 28 days. Typically, an increase in CBW indicates the formation of new hydrates [137-139] and expectedly CH will also increase in CEM I due to clinker hydration albeit a decrease with composite binders due to slag hydration [138, 140,141]. In this instance, the CBW and CH were decreasing while CaCO<sub>3</sub> was increasing. This suggests carbonation may be controlling mechanism and hydration was halted considering the lower RH i.e 55% RH.

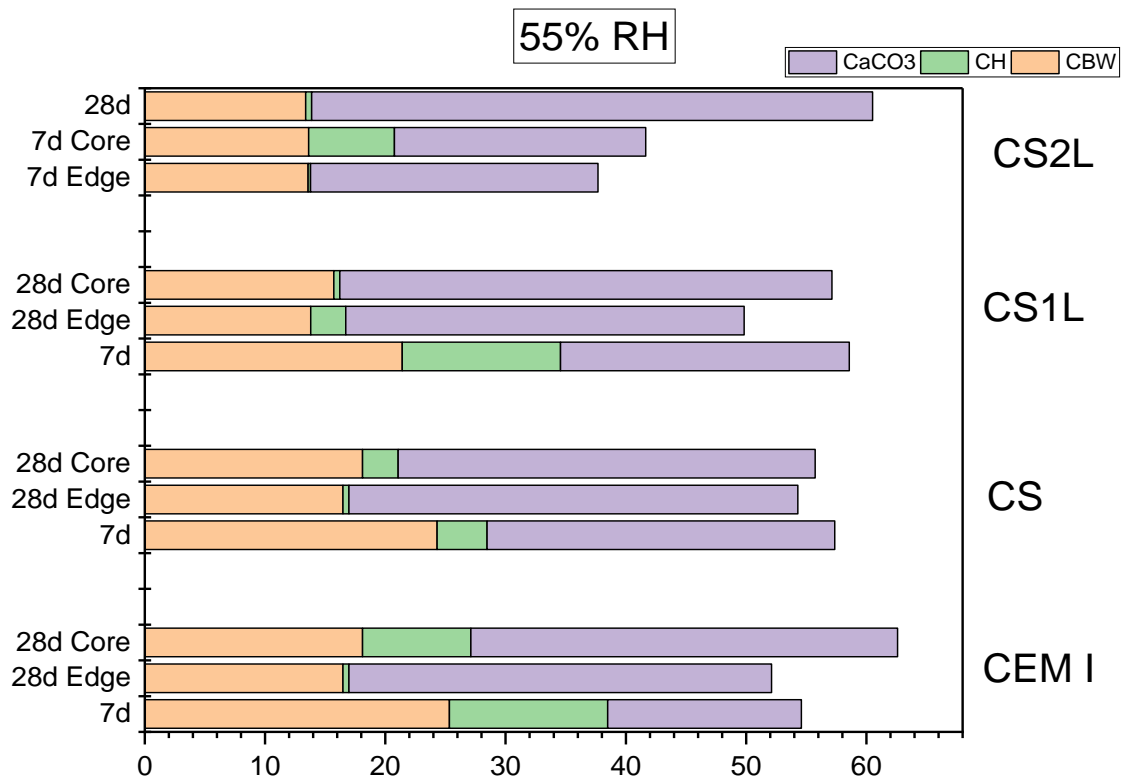


Figure 5.2: Measured chemically bound water (CBW), CH & CaCO<sub>3</sub> from TGA during 55% RH at 4% CO<sub>2</sub> accelerated carbonation.

Comparing composite paste i.e., CS, CS1L & CS2L exposed at 55% RH, the CBW didn't increase at 28 days, with only CS2L maintaining fairly stable CBW between 7-28days. However, changes were observed with both CS and CS1L are similar to trends observed with CEM I as both are partially carbonated at 28 days unlike CS2L that already fully carbonated at 28days and show partial carbonation at 7 days. This suggest CS2L have lesser hydrates that binder CO<sub>2</sub> over the duration in comparison to other two binder pastes as evident with conversion of CH to CaCO<sub>3</sub>.

For paste samples exposed at 75% RH, presented in Figure 5.3 below, the trends after exposure for 7 days were similar to those observed after exposure at 55% RH for CEM I. CEM I show insufficient colour change at 28days to extract paste needed to quantify CBW, CH and CaCO<sub>3</sub>. With exception of CEM I, which exhibits a higher CBW measurement at 7 days, all composite binders display nearly equal CBW values as measured by TGA at both 7 and 28 days. Furthermore, there is a decrease in CH and an increase in CaCO<sub>3</sub> content in all composite binder. Notably, in most cases, the edge samples showed the highest CaCO<sub>3</sub> content compared to either the core or non-

colour changed samples. This suggest carbonation was not intense to capture all sample areas for 75% RH compared to most samples exposed at 55% RH. Despite, continuous exposure up to 28days, the changes observed are less compared to 55% RH aligning with several studies [96, 174-176] reporting highest carbonation between 50-75% RH.

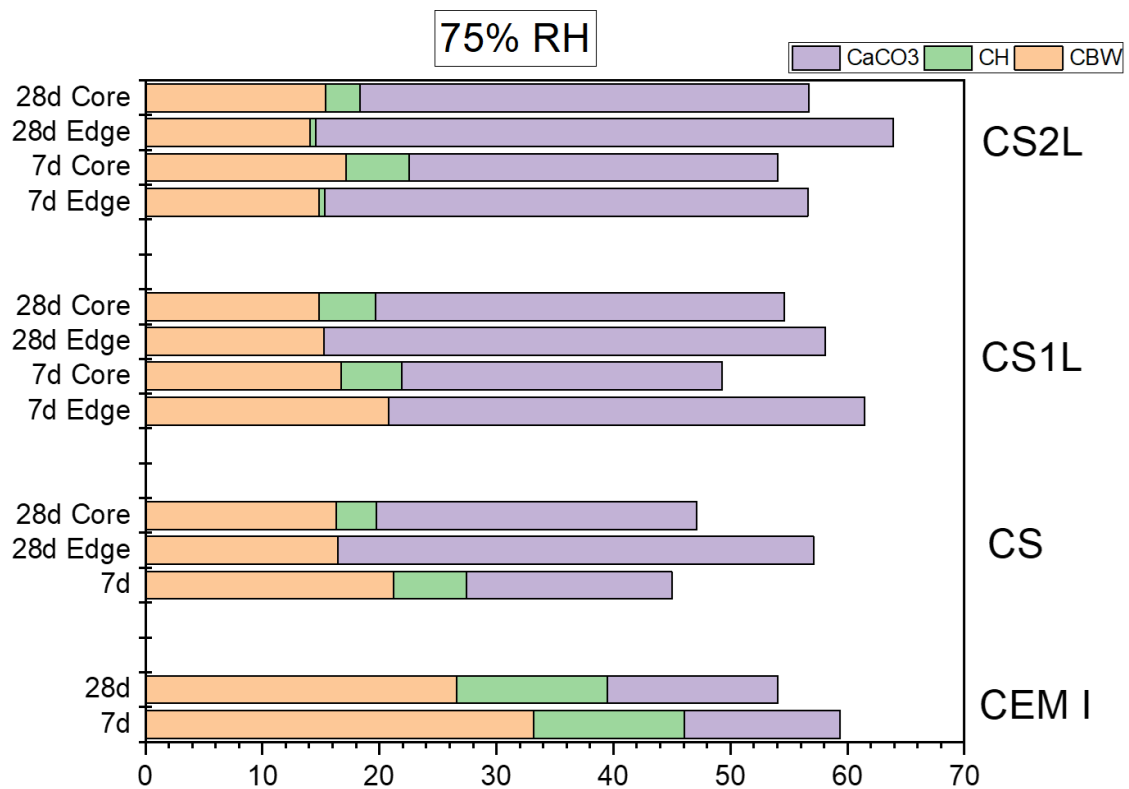


Figure 5.3: Measured chemically bound water (CBW), CH & CaCO<sub>3</sub> from TGA during 75% RH at 4% CO<sub>2</sub> accelerated carbonation.

Figure 5.4 presents the results from accelerated carbonation at 95%. In the case of CEM I, as well as a composite binder, minimal changes were observed with CBW. This trend also aligned with CH measured after exposure for both 7 and 28 days respectively, albeit with slightly more CaCO<sub>3</sub> formed at 28 days. This suggests that carbonation is active. But, CH may not be the hydrate carbonating as other phases are likely to carbonating due to their susceptibility to carbonation [73, 177]. Additionally, the continuous hydration of the clinker may be producing new portlandite at a rate that matches its consumption through carbonation.

Contrary to the observed trends seen at 55% and 75% RH for all composite binders, there was an increase in CH content in all composite cement at 95% RH, despite  $\text{CaCO}_3$  being formed at both 7 and 28 days. This suggest clinker hydration is continuous in this system however, slag hydration cannot be confirmed as it's expected to consume CH to form C-S-H thereby reducing the CH content available however this is not observed in this study.

A gradual decrease of CH may have suggested its carbonating or hydration of slag however, calcium carbonate was formed despite no colour change from thymolphthalein indicator, as seen in Figure 5.1. Several studies have suggested that indicators might not fully capture changes in the boundary between partially and fully carbonated samples due to pH changes [142, 178, 179].

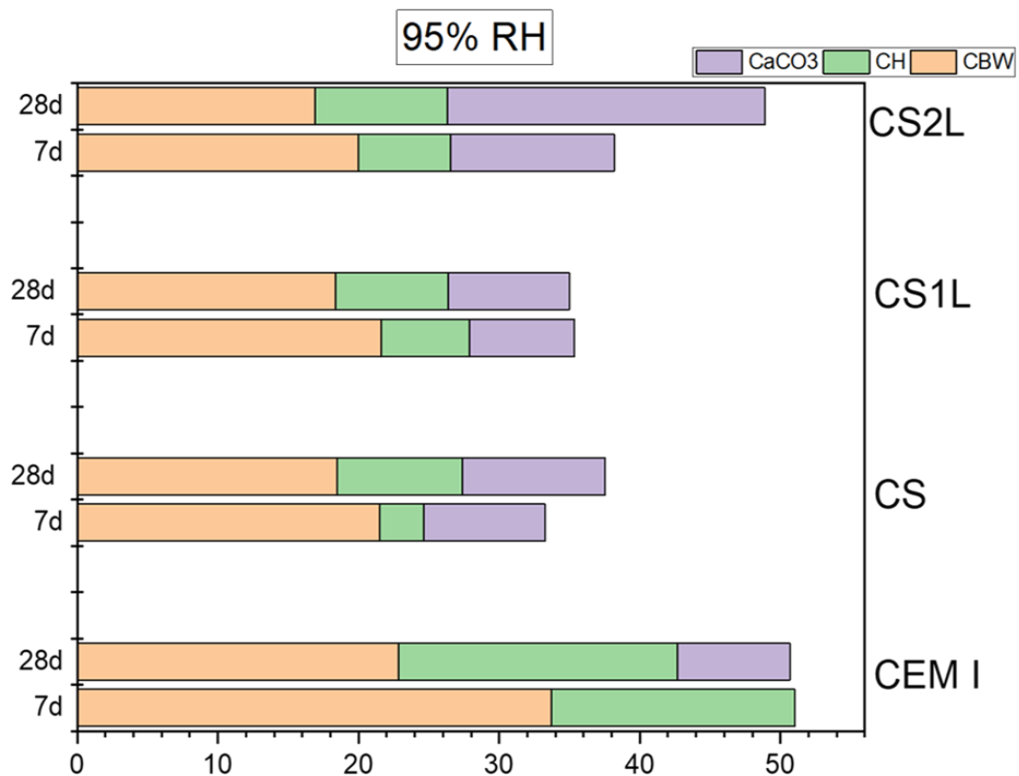


Figure 5.4: Measured chemically bound water (CBW), CH &  $\text{CaCO}_3$  from TGA during 95% RH at 4%  $\text{CO}_2$  accelerated carbonation.

Generally, the trends observed with CBW, CH and  $\text{CaCO}_3$  in Figure 5.2-5.3 above did not show convincing trends to suggest further hydration at 55% and 75% RH and this seems to also relate to findings from studies [148, 180] that hydration is halted below

80% RH. However, at 95% RH, the observed trends were slightly different. CBW was slightly higher compared to the other RH levels, and there was no depletion of CH as shown on Figure 5.4. Due to the test duration and RH, point of colour change on the samples to distinguish between the core and edge (carbonation front) for further examination of changes in CBW wasn't reached. Nevertheless, it's important to note that concurrent hydration and carbonation cannot be ruled out upon exposure at 95% RH, especially after 28 days. This is because hydration would still be ongoing due to the higher degree of saturation, and there is evidence of CO<sub>2</sub> slightly penetrating the pore structure, albeit low as indicated by the presence of CaCO<sub>3</sub> measured by TGA.

## 5.2 Phase assemblage due to accelerated carbonation.

### 5.1.2 Portlandite Evolution

Portlandite (CH) decomposition occurs at 450-550°C, as presented in Figure 5.5-5.7 for all relative humidities, consistent with earlier observations upon ambient carbonation. For each of the binders subjected to accelerated carbonation, portlandite content decreased irrespective of the relative humidity, with a significant decrease observed at the edge of the sample exposed for 28 days at 55% RH, i.e., carbonation front. CEM I showed the greatest portlandite content, with CS2L showing the lowest contents, even being absent at the carbonation front. The differences in CH content are attributed to differences in clinker content between blends and consistent with the literature [181-183]. Ultimately, accelerated carbonation at 4% CO<sub>2</sub> led to significant CH depletion at sample edges for 55% and 75% RH, as shown in Figure 5.5 & 5.6. When compared to the core area for 7 to 28 days., nearly all sample edge is not showing or decreasing CH peak. This was observed with samples expose at both 55% and 75% RH. Portlandite availability in these systems is majorly controlled by the rate of CO<sub>2</sub> diffusion rather than pore saturation however samples exposed at 95% RH (5.7) showed a slight decrease in CH content between 7 & 28 days despite no colour changes from the thymolphthalein indicator as presented in Figure 5.1. Although this contradicts the observation of [107] describing availability of portlandite been primarily controlled with CO<sub>2</sub> accelerated carbonation.

### 55%RH Accelerated

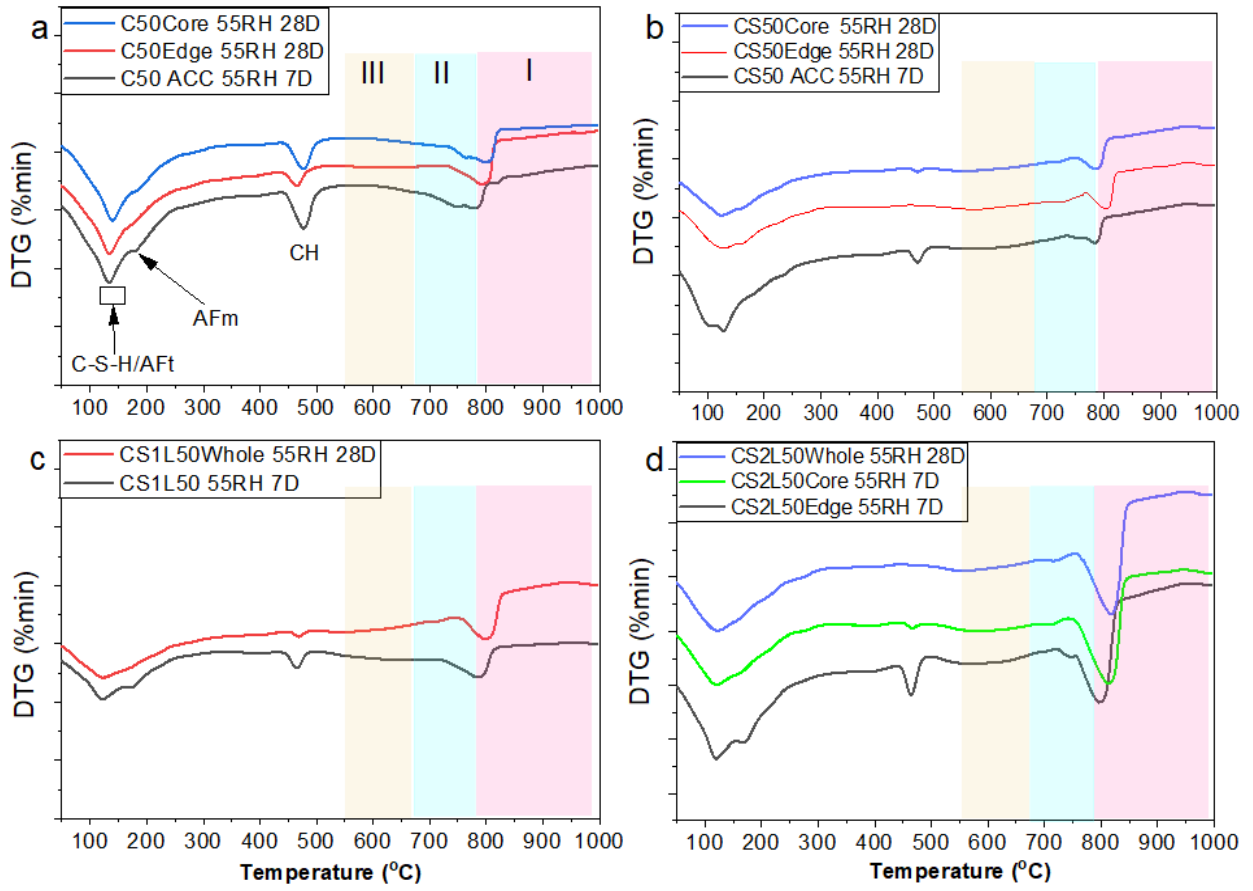


Figure 5.5: DTG during 55% RH accelerated carbonation.

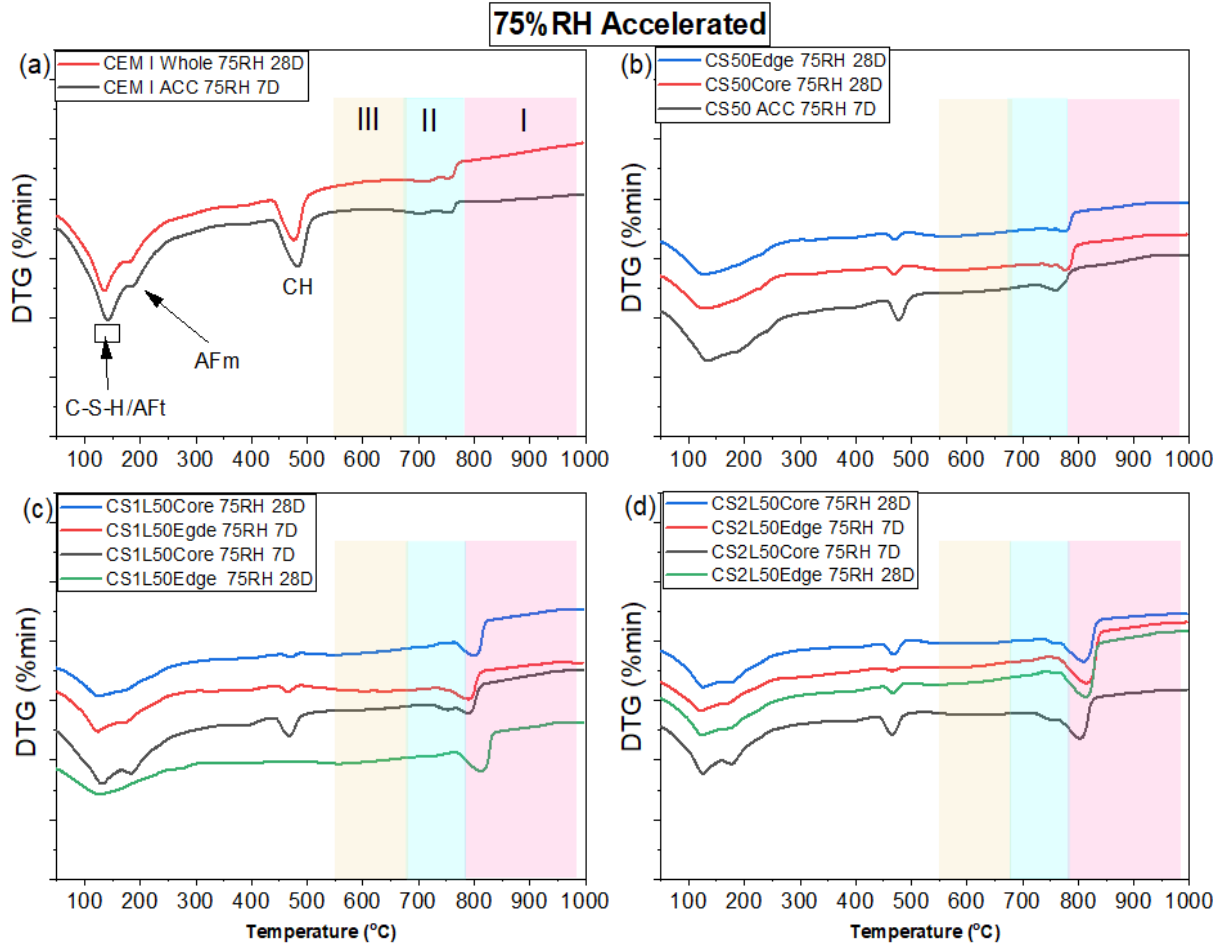


Figure 5.6: DTG during 75% RH accelerated carbonation .

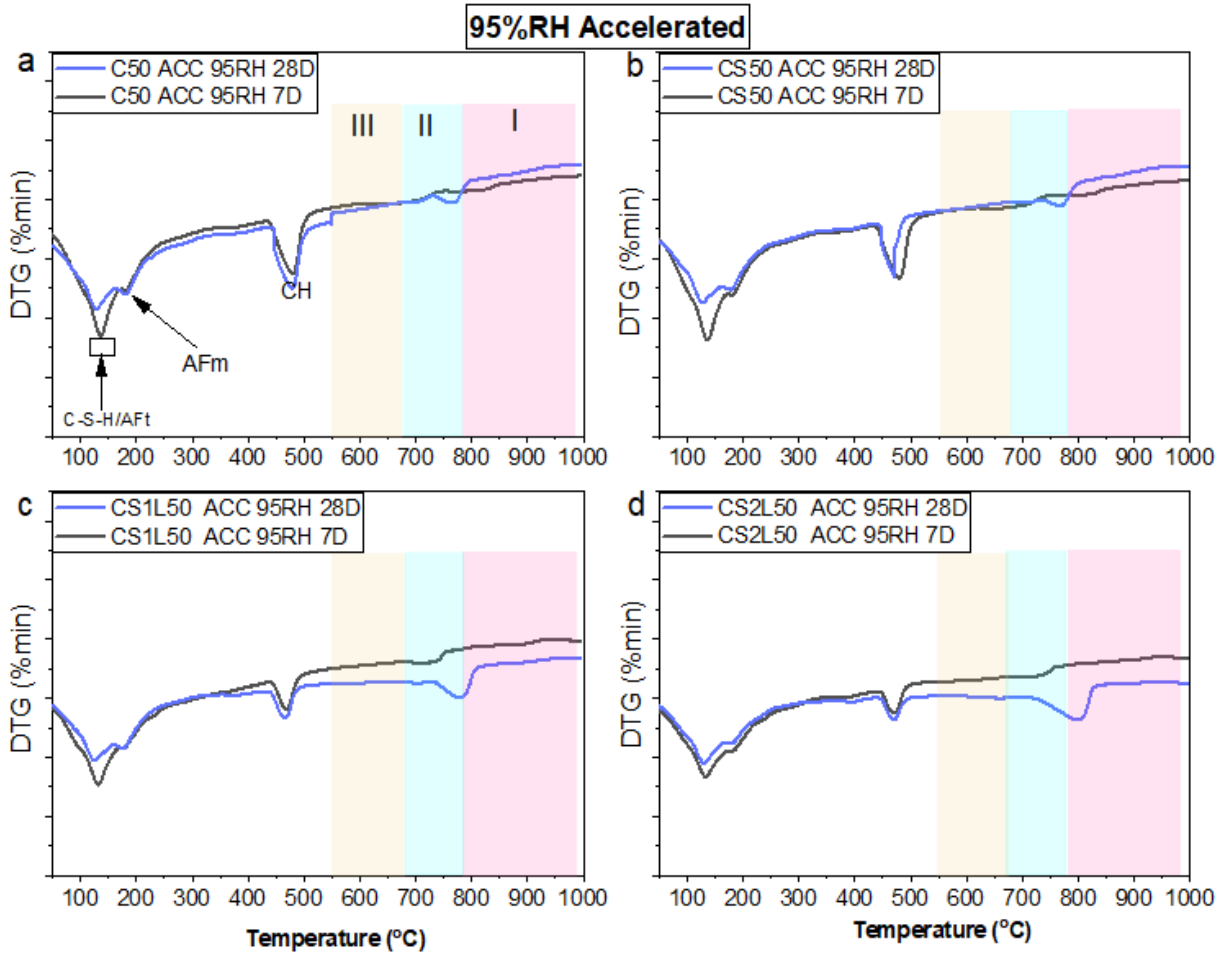


Figure 5.7: DTG during 95% RH accelerated carbonation.

### 5.2.2 Calcium carbonate

The main difference observed with accelerated carbonation samples is the extent of decomposition of various phases i.e., minor, and major phases and precipitation of calcium carbonates. Generally, all temperature range modes of calcium carbonate decomposition were observed, regardless of the degree of carbonation and relative humidity. CEMI showed the lowest calcium carbonate mass loss at 550-950°C irrespective of relative humidity. This is due to higher clinker contents in CEM I compared to all composite binders at 50% replacement.

Figure 5.5-5.7 presented above for samples exposed to accelerated carbonation at 55%, 75%, and 95% RH. Both CEM I and composite binders show calcium carbonate as a carbonation product with mass loss corresponding to all modes of decomposition temperatures attributed to the formation of calcium carbonate and its polymorph as identified in the literature [13, 81, 87, 115]. This suggests both amorphous calcium

carbonates and calcite are present during accelerated carbonation [61]. Moreover, there were significant mass losses at temperatures associated with AFm, AFt, and C-S-H for some samples, especially composite binders, after carbonation at 55% and 75% RH for 28 days, with the gradual shift of both mode III and II to mode I corresponding to further mass loss for the CH peak. This suggests further carbonation led to calcite which dominates portlandite phase changes as well as the conversion of amorphous calcium carbonates to calcite after continuous carbonation, especially within the carbonation front (edge). Samples exposed at 95% RH show minimal mass loss associated with CSH/AFt and portlandite when comparing 7-day exposure to 28 days, despite a higher degree of saturation which will have hindered diffusion and dissolution of CO<sub>2</sub> in the pore structure. However, the changes observed are similar with all binders which either suggest carbonation due to handling and preparation or surface carbonation from the carbonation front that can't be extracted for separate analysis.

### 5.3 Phase Assemblages by Fourier Transform infrared spectroscopy (FTIR)

#### 5.3.1 Portlandite

The OH stretching band due to portlandite, found at 3640 cm<sup>-1</sup> in the FTIR spectra of all samples subjected to accelerated carbonation at different RH conditions are plotted in Figure 5.8-5.10 below. The peak was more intense in the spectra from CEM I at 7 days at all relative humidities compared to composite blends, gradually depleting with increased exposure to 28 days. However, significant portlandite is still available after 28 days of accelerated exposure in 55% RH, especially the within the core for CEM I. This is due to the higher buffering capacity of CEM I due to availability of CH compared to blended cement [148, 183]. In the case of composite binders, portlandite depletion was significant with the peak nearly disappearing with C2SL at 55% RH after 7 days in both the core and edge area (Figure 5.8a-d) compared to CS & CS1L which offer higher buffering capacity at 7 days and only showed complete depletion after 28 days exposure.

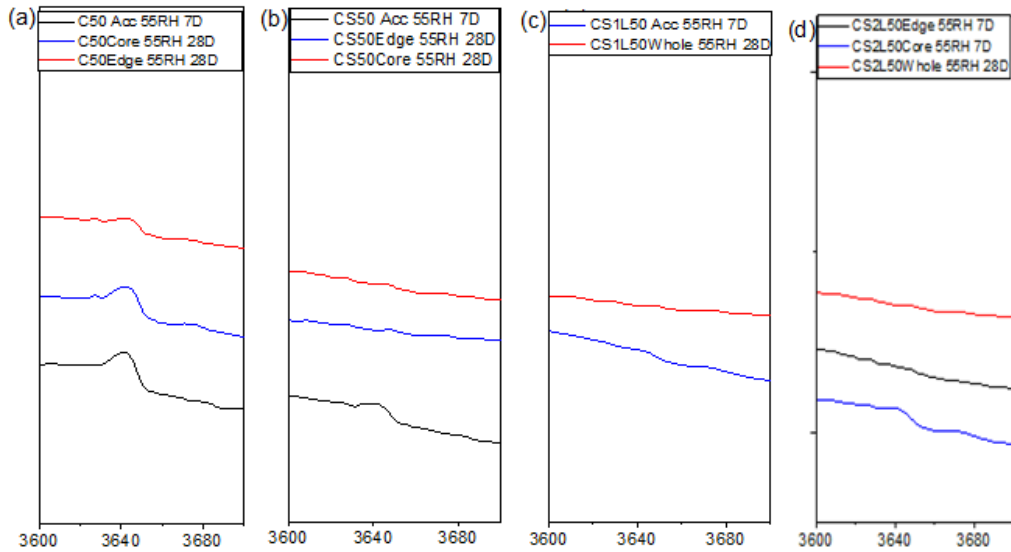


Figure 5.8: Enlarged CH decomposition for 55% RH during accelerated carbonation obtained from FTIR.

Generally, samples exposed at 75% and 95% RH as presented in Figure 5.8 & 5.9 below, showed a slight reduction in the intensity of the portlandite peak compared with exposure at 55% RH, but there were no significant changes following exposure at 95% RH due higher degree of saturation that hindered transport properties of the blends [183]. These results agree with TGA data on the depletion of portlandite and exposure conditions.

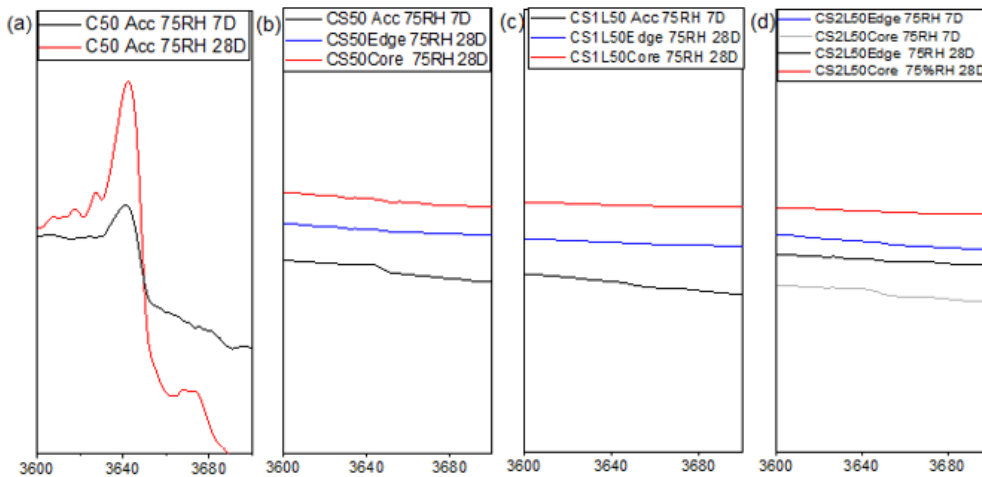


Figure 5.9: Enlarged CH decomposition for 75% RH during accelerated carbonation obtained from FTIR.

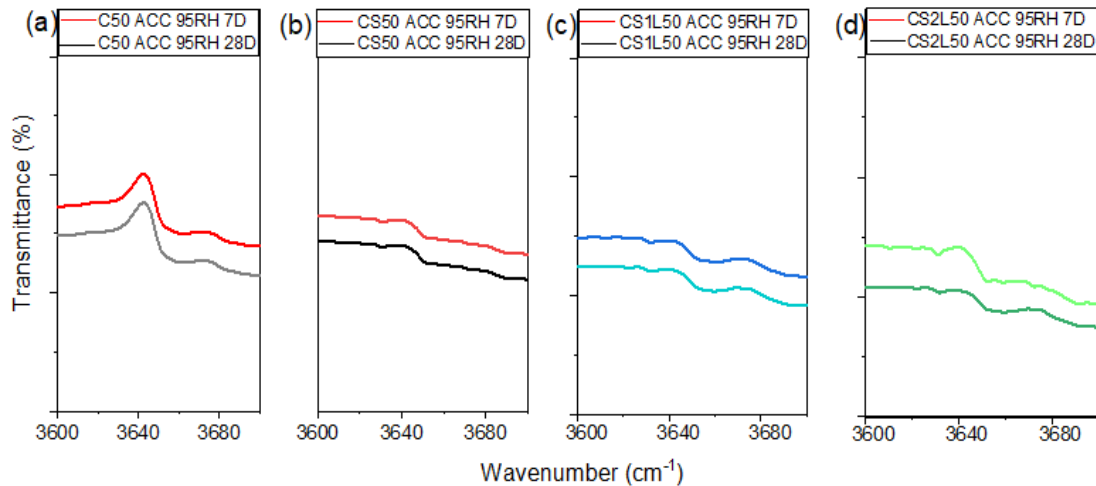


Figure 5.10: Enlarged CH decomposition for 95% RH during accelerated carbonation obtained from FTIR.

### 5.3.2 Calcium carbonate and polymorphs formation.

The strong peaks at 1400-1500  $\text{cm}^{-1}$  correspond to the carbonate asymmetric stretching vibration ( $V_3$ ) labelled as (I) in Figure 5.11-5.13. The figures show the intensity of the calcium carbonate bands formed for pastes subjected to accelerated carbonation. Samples exposed at 55% RH showed differences in peak intensity at 7 and 28 days, at either the core or carbonation front (edge). The peak intensity of the 28-day samples was greater than for the 7-day samples, especially at the carbonation front (edge), suggesting the significant transformation of hydrates to calcium carbonates due to severe carbonation for all samples and correlates with TGA results from the preceding section. Lo et al. [184] also reported similar findings with absorbance peaks for the surface of concrete during accelerated carbonation. This trend is also consistent with peak intensity at 870 $\text{cm}^{-1}$  (III) assigned to both calcite and vaterite [164] showing the same increasing intensity with prolonged exposure.

The precipitation of calcium carbonates and its polymorphs at 55% RH in all samples tested was also similarly found at both 75% and 95% RH, albeit a decrease in the intensity of the peak compared to 55% RH in all pastes. CEM I had the least peak intensity at both 1420 $\text{cm}^{-1}$  and 870 $\text{cm}^{-1}$  for all the conditions. Minor peaks formed at 714 $\text{cm}^{-1}$  assigned to calcite were found in all samples though split bands at 700  $\text{cm}^{-1}$  and 714  $\text{cm}^{-1}$  were found with both CS1L & CS2L at all relative humidities, which suggests possible traces of aragonite might be present. The study from Vegenas et al. [100] showed aragonite present for ternary blended pure synthetic powder.

However Black et al. [167] showed the presence of aragonite only after short periods of carbonation and where the C-S-H had a low Ca/Si ratio.

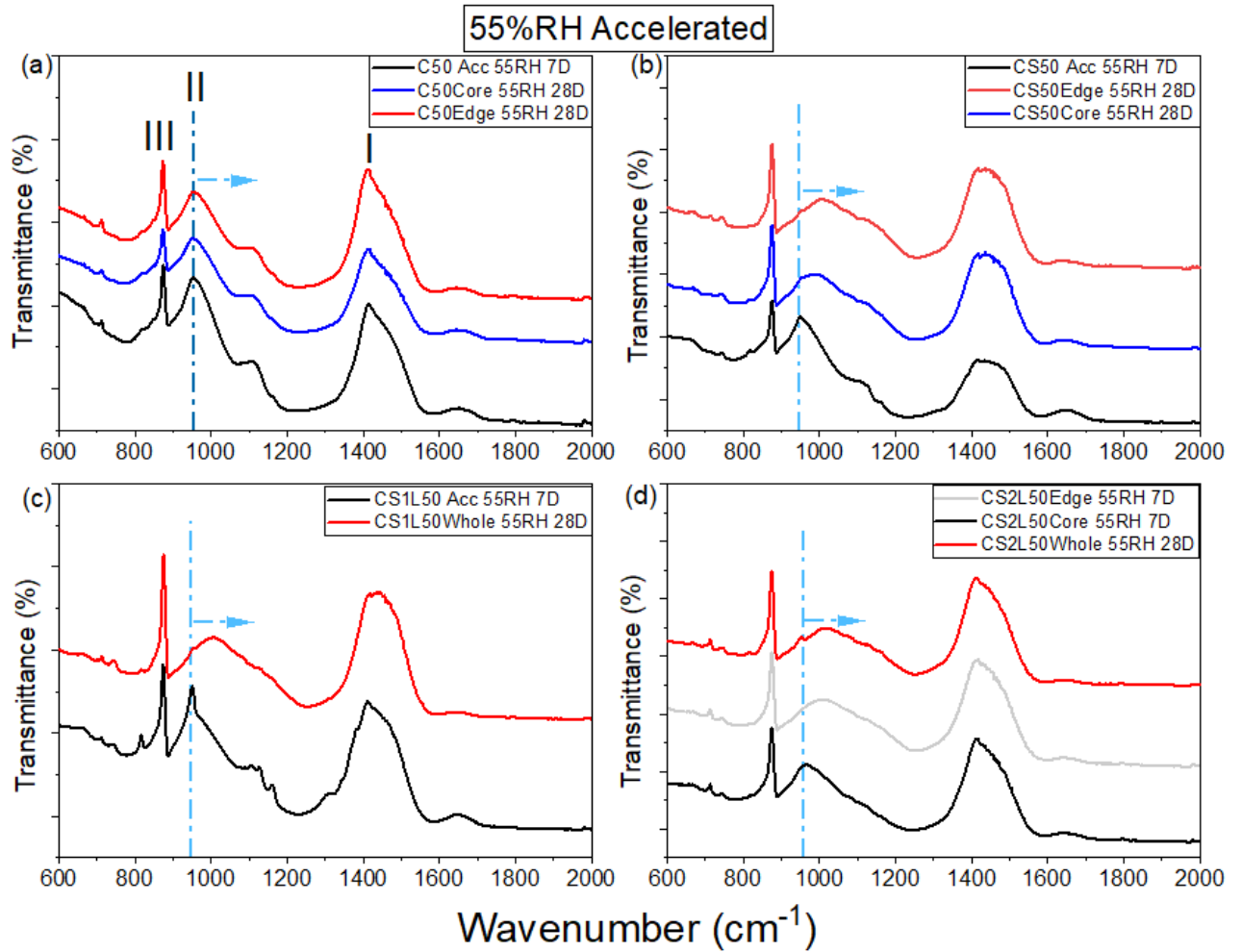


Figure 5.11: Enlarged FTIR plot between 600-2000 $\text{cm}^{-1}$  for 55% RH under accelerated carbonation at 7 & 28 days (a) CEM I, (b) CS (c) CS1L (d) CS2L.

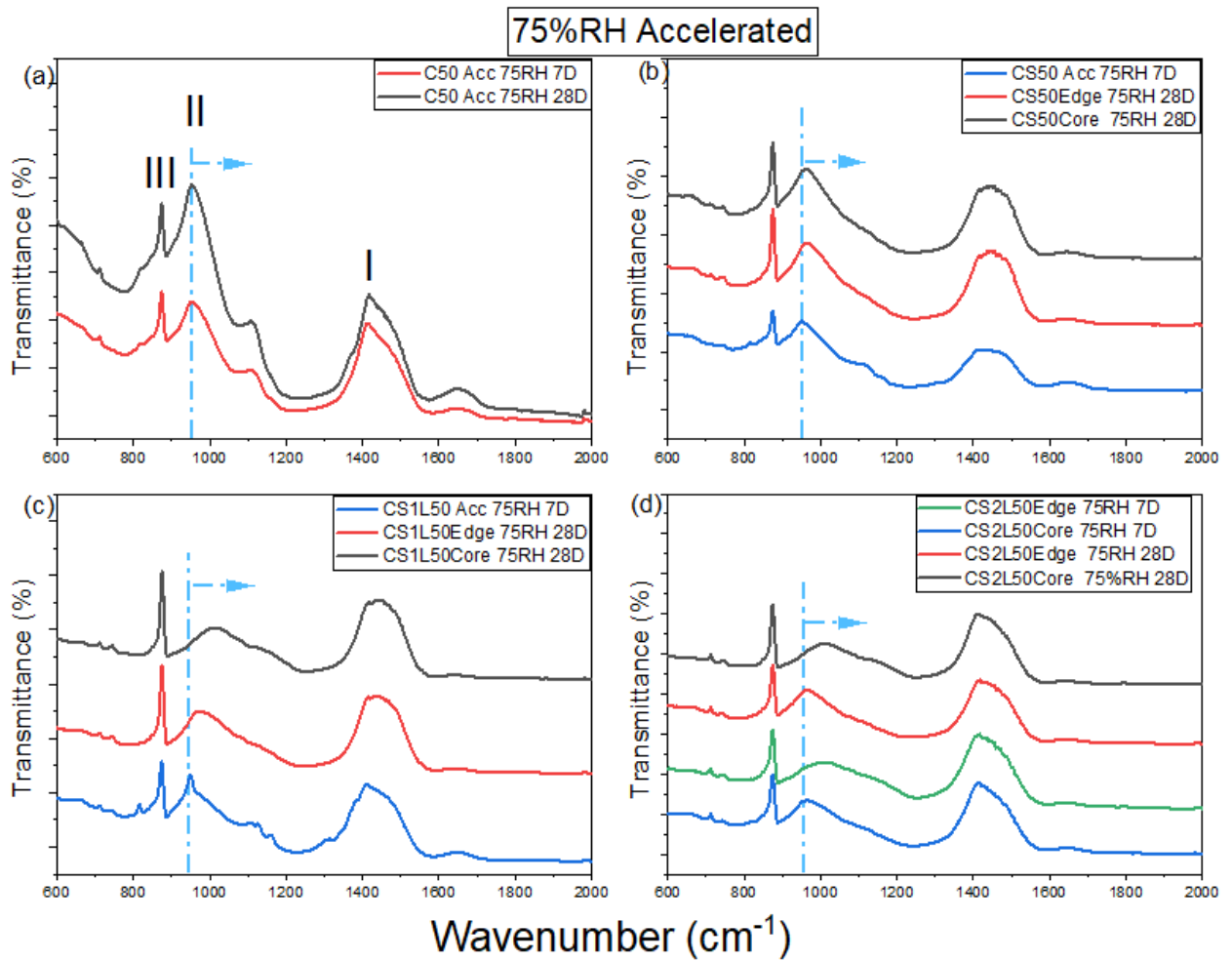


Figure 5.12: Enlarged FTIR plot between 600-2000cm-1 for 75% RH under accelerated carbonation at 7 & 28 days (a) CEM I, (b) CS (c) CS1L (d) CS2L.

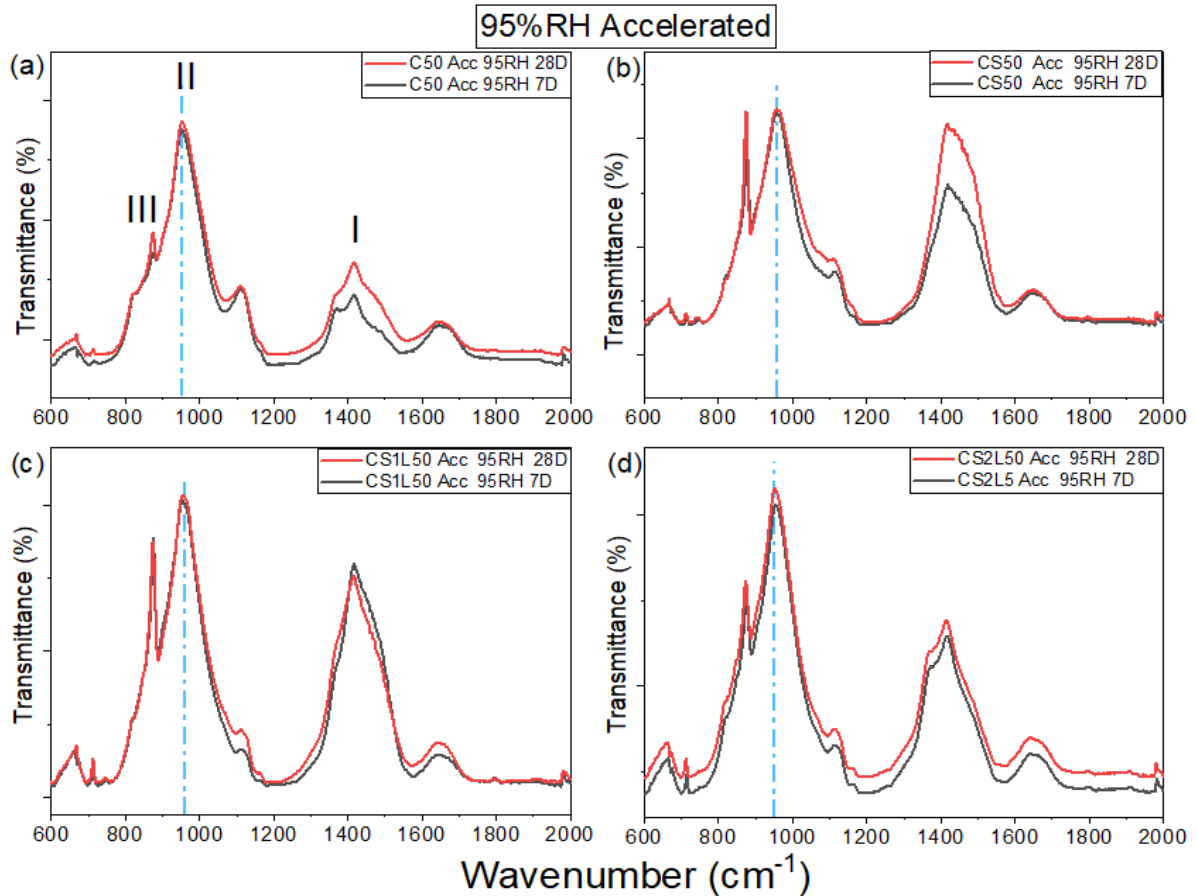


Figure 5.13: Enlarged FTIR plot between 600-2000 $\text{cm}^{-1}$  for 75% RH under accelerated carbonation at 7 & 28 days (a) CEM I, (b) CS (c) CS1L (d) CS2L.

### 5.3.3 Calcium Silicates Hydrates (C-S-H)

The absorption bands at 950 $\text{cm}^{-1}$  assigned to C-S-H labelled as (II) in Figure 5.11-5.13 above were identified in all samples. However, a pronounced shift toward higher wavelength was observed with all composite samples at 28 days following exposure at 55% and 75% RH, and a few samples at 7 days exposure, as observed in Figures 5.7 & 5.9 above. The shift toward higher wavelength suggests decalcification of C-S-H due to accelerated carbonation of the composite binders, consistent with [144] during carbonation of slag blended cement above 3%. Furthermore, Vanoutrive et al. [135] found a similar shift in the absorbance band from 950 $\text{cm}^{-1}$  to a higher wavelength, albeit no hump at 1065 $\text{cm}^{-1}$  to confirm the formation of amorphous silica gel in GGBS mixes due to the intensity of  $\text{CO}_2$  used in the study at 2% over 28 days exposure. However, they found that further exposure up to 90 days led to broadening of a band at 1000-1065 $\text{cm}^{-1}$  associated with decreasing Ca/Si ratio. This shift to higher wavelength in some of the samples suggests accelerated exposure seems to cause

significant decalcification of the C-S-H and with favourable moisture condition for accelerated carbonation as obtainable with 55% RH, amorphous silica gel is formed, as this also corresponds with the gradual decomposition of portlandite as seen in Figure 5.7 above collaborating the carbonation of both C-S-H and CH occur simultaneously however, significant changes in C-S-H were not noticed until after complete decomposition of CH. No significant shift of the assigned C-S-H band was observed with 95% RH from Figure 5.13(II), as no effect of CO<sub>2</sub> exposure was not noticed with the majority of hydrates with this RH.

#### 5.3.4 Other phases

AFt peak assigned at 1120cm<sup>-1</sup> were visible in all samples after 7 days of accelerated exposure, except for CS2L exposed at 55% and 75% RH (Figure 5.11-5.13) above. CS2L blends at both RH are susceptible to carbonation more than the rest of the samples and consistent with TGA results presented in 5.11. All samples exposed at 95% RH showed no changes in ettringite peak from 7 days to 28 days. But extending the exposure period to 28 days showed that nearly all AFt had carbonated in all composite samples at 55% and 75% RH except CEM I. This suggests the decomposition of ettringite after significant loss of portlandite or no CH as observed with the carbonation front; however, the sample from the core area of the sample also shows similar behaviour with the edge (carbonation front). This contradicts Soja et al. [185] findings that the dissolution of ettringite will occur after the complete depletion of portlandite.

### 5.4 Microstructure changes due to carbonation.

#### 5.4.1 MIP

The ingress of CO<sub>2</sub> into the pore structure can alter porosity, which is crucial in understanding the resistance of binders to carbonation. Therefore, it is essential to consider factors such as pore volume, distribution, and precipitation of dominant hydrate phases (CH, C-S-H/C-A-S-H, and others) during accelerated carbonation to explain microstructural changes observed due to carbonation. In order to understand the effect of accelerated carbonation on pore structures, selected mixes were subjected to MIP and SEM-BSE techniques, as explained in the methodology section of chapter three. Samples carbonated for 28 days at 55%, and 75% RH under accelerated CO<sub>2</sub> conditions were characterized. The changes in pore size distribution are presented in Figure 5.14-5.16, and the total porosity is shown in Table 5-1 below.

Pore refinement is expected due to slag/limestone finesses in binary and ternary blended binders, as reported elsewhere [100, 118], with similar mixes as used in this study. This suggests the closing of the microstructure due to hydration over long periods. However, accelerated carbonation plays a significant role in pore distribution. Edge samples carbonated at all relative humidities showed a further decrease in gel porosity and a subsequent increase in the large capillary pores over a more extensive range (between 100nm-10000nm). This suggests coarsening of the larger capillary pores, as already established in many studies [150-154], resulting from C-S-H carbonation and formation of metastable calcium carbonates and silica gel, plus ettringite carbonation. This was supported by TGA and FTIR results presented in the previous section and is consistent with other findings [106, 120, 167, 186, 187]. Carbonation is expected to lead to release of free water which will also contribute to porosity [186]. Coarsening of the pore structure seems to be caused by significant carbonation of C-S-H and resultant silica gel formation [120] and coincides with complete depletion of CH, as shown in TGA and FTIR results. This observation agrees with thermodynamic modelling predictions elsewhere [188]. However, significant coarsening of the pore structure does not occur when there is only partial depletion of CH, as observed with core or partially carbonated areas in Figure 5.14 below.

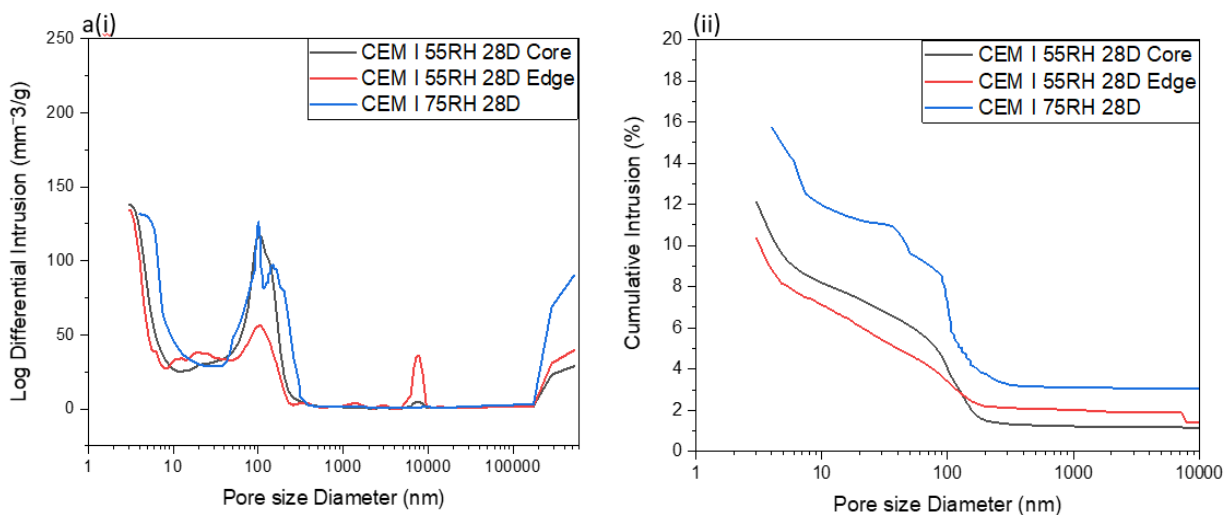


Figure 5.14: Pore size distribution of samples subjected to accelerated carbonation at both 55% & 75% RH for CEM I paste.

Here, the large capillary pores coarsening was only observed at the edge areas, as shown in Figures 5.14 & 5.15 (CS & CS1L) presented below. This again corresponds to when there is minimal or no CH available.

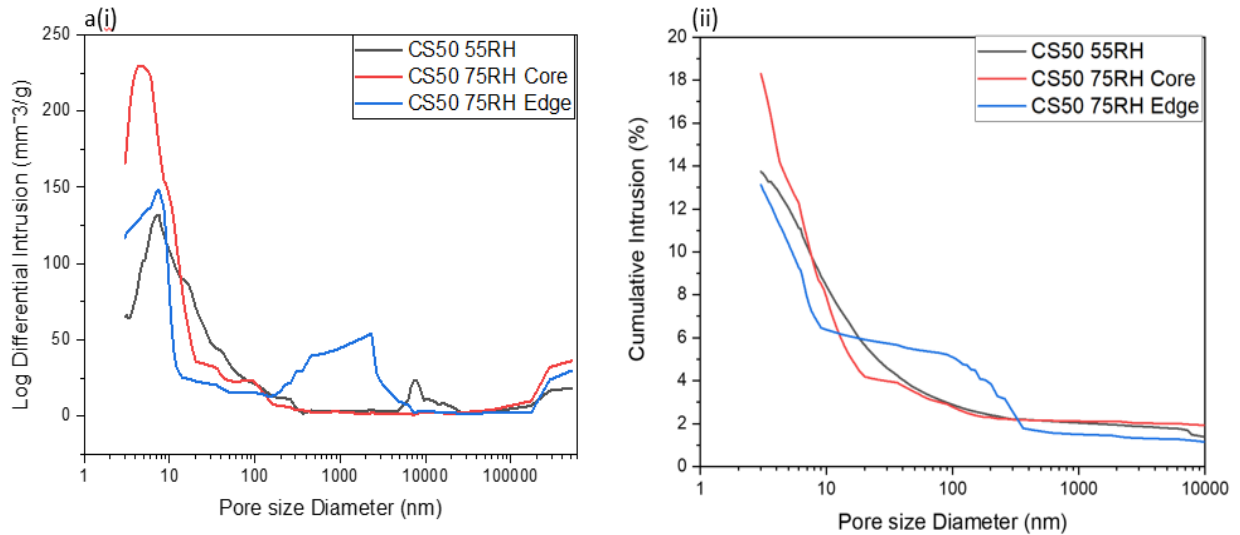


Figure 5.15: Pore size distribution of samples subjected to accelerated carbonation at both 55% & 75% RH for CS paste.

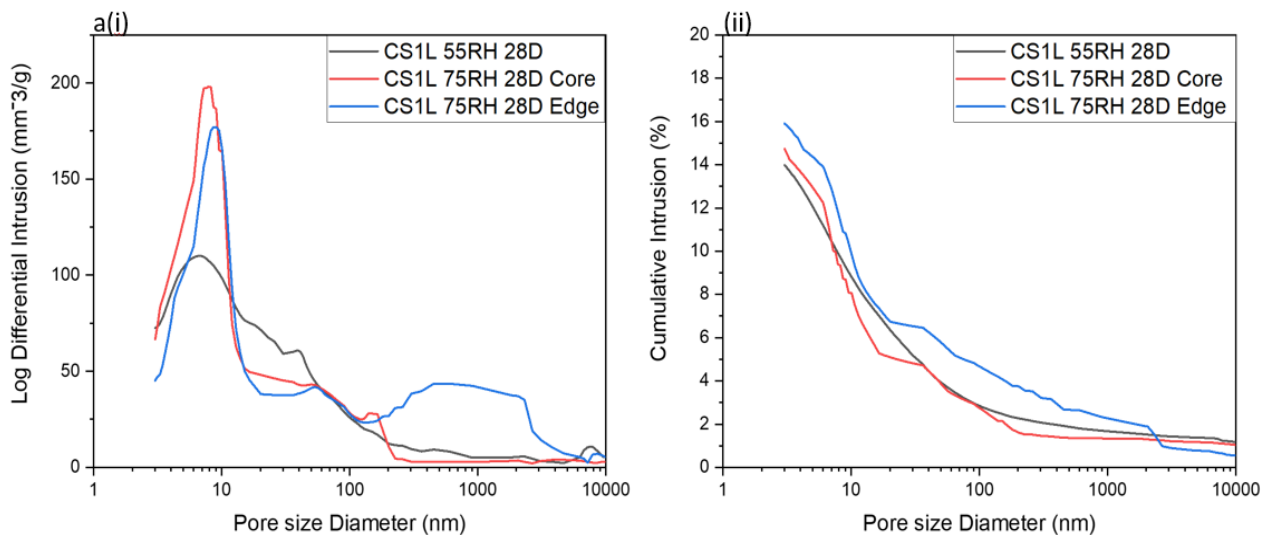


Figure 5.16: Pore size distribution of samples subjected to accelerated carbonation at both 55% & 75% RH for CS1L paste.

The total porosity derived from MIP are shown in Table 5-1 for CEM I, binary & ternary binders with variations in total porosity consistent with results from the pore size distribution. CEM I showed the lowest total porosity at the edge and in the core for 55% RH at 18.43% and 21.15%, respectively, while at 75% RH, the value of total

porosity was 25.7% (whole), as pH indicator did not show significant boundary to differentiate between both core and edge area. Both binary and ternary blends, i.e., CS & CS1L, followed the same trends observed elsewhere [131] following 180 days of hydration. The result suggests that carbonation of CH dominates CEM I, leading to the precipitation of well-ordered calcite [182, 189] as opposed to abundant C-S-H phases present for both binary and ternary blends that carbonate into metastable calcium carbonate (amorphous calcium carbonate, vaterite and calcite). With clinker replacement at 50% for both binary & ternary blends, C-S-H is crucial for results obtained for both mixes as it has higher molar volumes [93, 190] than CH, which has a significant influence on total porosity as obtained elsewhere [191, 192].

Binary and ternary blends showed no significant difference in total porosity for 55% RH, at 24.43% & 24.58%, respectively, although carbonation depth measurements also showed similar results, as discussed previously. Irrespective of relative humidity during accelerated carbonation considered in this study, the total porosity of samples from edge areas is lower than other areas (core & whole), and fewer pores in CEM I samples than in both binary & ternary blends.

Table 5-1: Total porosity of samples subjected to carbonation at both 55% & 75% RH (a) CEM I (b) CS and (c) CS1L.

	55% RH			75% RH		
	Edge	Core	Whole	Edge	Core	Whole
<b>CEM I</b> Total Porosity (%)	18.43	21.15	-	-	-	25.27
<b>CS</b> Total Porosity (%)	-	-	24.43	28.08	30.24	-
<b>CS1L</b> Total Porosity (%)	-	-	24.58	26.76	27.21	-

### 5.5 Carbonation Performance

The carbonation resistance of concrete is influenced by various factors such as water-binder ratio, CO<sub>2</sub> exposure, curing duration, relative humidity, temperature, concrete properties, etc. [90, 146,147]. It is well understood that the water-binder ratio and relative humidity could be a significant factor representing both the external and

internal factors that can influence the carbonation resistance of concrete [148]. Carbonation is a complicated physiochemical process involving diffusion-dissolution of the CO<sub>2</sub> [149] into the pore structure; several of these identified factors play a significant role in the resistance of mortars to carbonation and are examined in this section.

#### 5.5.1 Effect of water-binder ratio and relative humidity on carbonation depth

Generally, increasing water- binder ratio slightly from 0.50 to 0.55 led to increasing carbonation depth for all mortar samples across all relative humidities, except at 95% RH where the pH indicator did not show any significant colour change to distinguish carbonation boundaries at 28 days exposure (Figure 5.17). This agrees with [129, 193-195] findings that lower carbonation degree resulted from a higher water-cement ratio due to an increase in capillary porosity.

CEM I mortar samples had the lowest carbonation depth at both water-binder ratios and relative humidity conditions due to the amount of portlandite available to buffer CO<sub>2</sub>. This is consistent with studies from [76, 140, 185]. Papadakis et al. [196] and Leemann et al. [93] established that the resistance of concrete to carbonation is subjected to the amount of calcium oxide available within the system and is a clearly key factor affecting carbonation resistance. From Figure 5.17 below, carbonation depth was highest for CEM I at 55% RH exposure, with values at 2.55mm and 6.95mm for w/c 0.5 and 0.55, respectively.

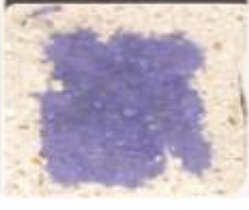
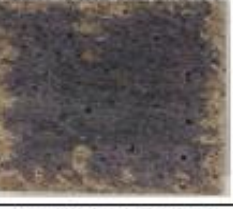
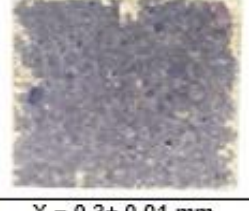
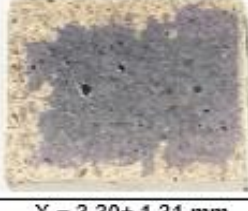
w/c	55% Relative humidity (Accelerated carbonation at 4%)			
	CEM I	CS	CS1L	CS2L
0.5				
	X = 2.55 ± 0.21 mm	X = 11.5 ± 0.12 mm	X = 13.77 ± 0.17 mm	X = 15.0 ± 0.13 mm
0.55				
	X = 6.95 ± 0.11 mm	X = 11.8 ± 0.21 mm	X = 16.0 ± 0.25 mm	X = 17.63 ± 0.14 mm
	75% Relative humidity (Accelerated carbonation at 4%)			
0.5				
	X = 0 mm	X = 2.8 ± 0.15 mm	X = 2.90 ± 0.07 mm	X = 4.90 ± 0.14 mm
0.55				
	X = 0.3 ± 0.01 mm	X = 3.30 ± 1.31 mm	X = 4.50 ± 0.16 mm	X = 6.30 ± 0.38 mm
	95% Relative humidity (Accelerated carbonation at 4%)			
0.5				
	X = 0 mm	X = 0 mm	X = 0.16 ± 0.01 mm	X = 0.17 ± 0.01 mm
0.55				
	X = 0 mm	X = 0 mm	X = 0.18 ± 0.01 mm	X = 0.22 ± 0.02 mm

Figure 5.17: Carbonation depth measurement at 4% CO<sub>2</sub> at 55%, 75%, and 95% relative humidity (top) 0.50w/b (bottom) 0.55w/b.

The carbonation depth was greatest after exposure at 55% RH, with very little carbonation measured at the other relative humidity conditions. This is consistent with

[108, 197, 198] that carbonation is greatest at 50-70% relative humidity. However, the effect of increasing the water-cement ratio from 0.5 to 0.55 led to about 33% greater carbonation depth at 28 days. The increasing water-cement ratio increases the porosity and permeability of concrete [93, 96, 199-201] and, in turn, speeds up the rate of CO<sub>2</sub> transport into the concrete pore structure. This is the primary reason for the difference in carbonation depth between the two water-binder ratios.

Slag blended mortars follow the same trend as CEM I at all relative humidities, with greatest carbonation depth at 55% RH, slightly less at 75% RH and no significant colour change at 95% relative humidity for CS mixes at both water-cement ratios. The increase in carbonation depth compared to CEM I might be due to the lower clinker content resulting in lower alkaline buffer potential of the pore solution [96, 202], despite refined pore structure. This is consistent with [203, 204] comparing composite cements to PC. Furthermore, the alkaline reserve of slag blended mortar is further consumed during hydration to produce C-S-H gel which explains its low alkalinity apart from clinker dilution. Interestingly, carbonation depth for CS mortars was similar for both water-binder ratios, at less than 1mm, and the trends observable for both 55% and 75% RH which suggests not only the amount of portlandite available in the mortar but also porosity is an essential factor since they have similar finer particles and pore size distribution despite differences in w/b.

CS and CS1L mortars show similar carbonation depth in 55% and 75% RH, and this is consistent with a coefficient of carbonation obtained from regression fitted line in Figures 5.18 & 5.19 presented below.

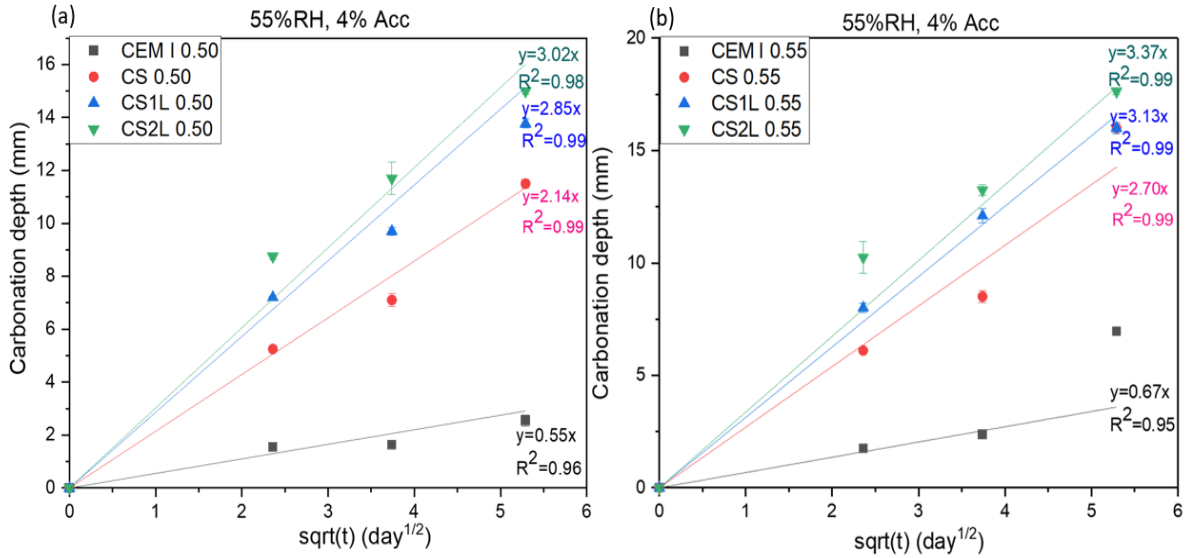


Figure 5.18: Coefficient of carbonation at 55% RH accelerated carbonation.

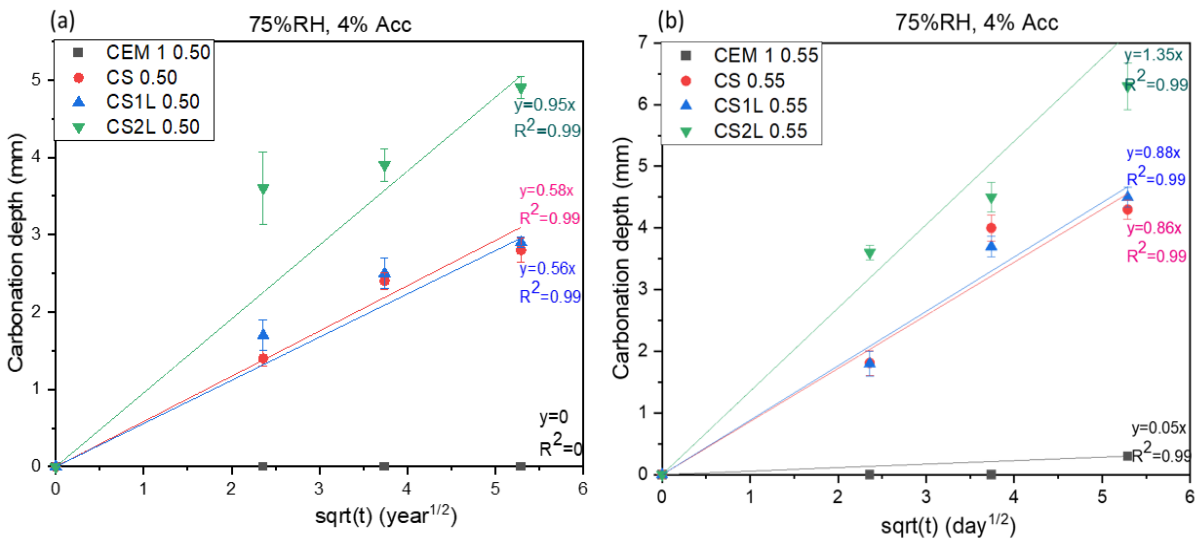


Figure 5.19: Coefficient of carbonation at 75% RH accelerated carbonation.

With 10% limestone addition for the ternary blend and subsequent reduction of slag content does not have any significant effect on the carbonation resistance of the mortar. This may be due to limestone providing nucleation sites for the growth of hydrates and also the finer texture of limestone that may block ingress of CO<sub>2</sub> into the system.

The mix with 20% limestone replacement (CS2L) showed the greatest carbonation depth of all mixes, suggesting further dilution had a significant effect on carbonation up to about 20% and 30% increase compared to CS1L for both 55% and 75% relative humidity, respectively. Since both binary and ternary mortars have 50% clinker

replacement, their porosity and particle size are likely the determining factor of carbonation resistance. From Figure 5.17 above, while the carbonation depths for CEM I and binary blends shows insignificant carbonation depth at 95% relative humidity after 28 days, irrespective of changes in the w/b ratio. However, both ternary blends show slight carbonation, of between 0.6-0.22mm for CS1L and CS2L. The absence of carbonation in CEM I and binary cement following exposure at 95% relative humidity was due to high moisture presence in the pores, which is one of many crucial factors that affect the rate of carbonation. Carbonation reaction is slow when the pores are fully saturated, such as obtainable for 95% RH since CO<sub>2</sub> transportation is slow with such relative humidity.

### 5.6 Compressive strength

The compressive strengths for different mortars at 7, 14, and 28 days of accelerated carbonation at different relative humidity are presented in Figure 5.20-5.22.

Generally, the compressive strength of mortar at water-binder ratio of 0.5 was slightly higher than at 0.55 water-binder in all cases, in line with carbonation depth measurements and the discussion presented in 5.5 above. This is consistent with the [183] study that a linear relationship exists between carbonation depth and compressive strength, with an increase in compressive strength leading to a decrease in carbonation depth and also corroborated with [205] findings that such existed in all concrete with or without SCMs replacement. Han-Seung and Wang [206] also showed similar results, with the compressive strength of slag mixes at a lower water-to-binder ratio of 0.5 having more excellent value than the one at a higher water-to-binder ratio after accelerated carbonation.

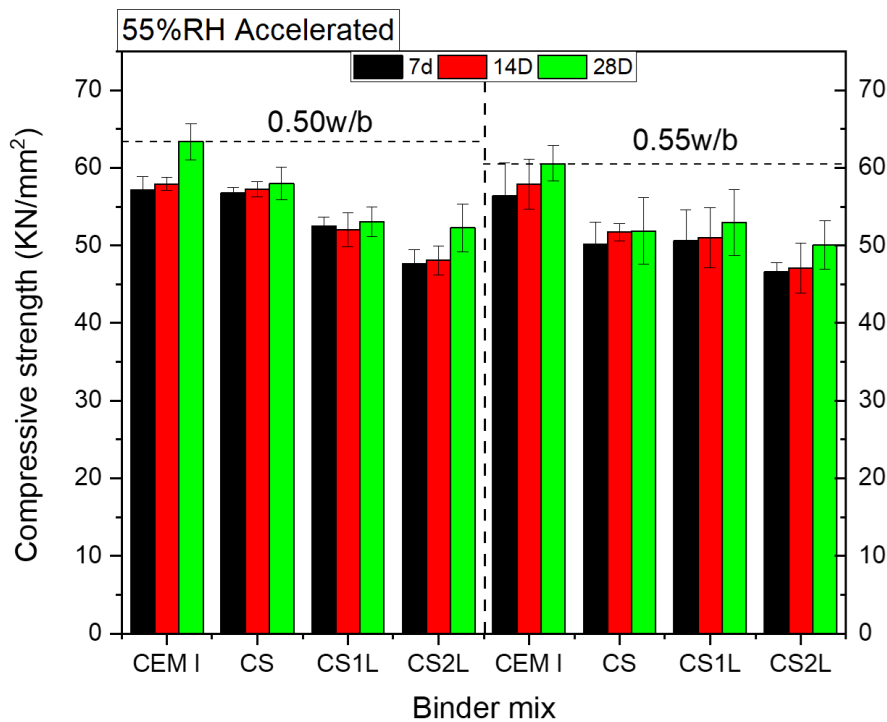


Figure 5.20: Compressive strength evolution after carbonation at 55% relative humidity.

In Figure 5.20 presented above, CEM I mortar samples exhibited the highest compressive strength after carbonation at relative humidity of 55% compared to binary and ternary blended mortar. This is likely due to the greater availability of CaO, which produces CH which then carbonates for form CaCO<sub>3</sub> which is expected to fill the pore structure and provide the needed impetus for compressive strength development [207, 208]. This is despite the relative humidity conditions at 55% not being conducive to continued hydration, as previously noted. The faster hydration of CEM I may have resulted in a substantial level of strength being reached before exposure to preconditioning and accelerated carbonation, with over 80% strength gained reported [41, 209] for CEM I after 28 days curing, in contrast to composite binders, which have a slower rate of reaction that may have distorted the hydration progress and have substantial strength gain at a later age. Furthermore, incomplete hydration hinders microstructure development, a crucial component for the strength development of cement-based materials. This finding is corroborated by the findings of Pacheco et al. [210] on the influence of the type and amount of binder on the compressive strength of mortars under various carbonation conditions. They found that CEM I mortar had

higher compressive strength than binary and ternary blended mortars due to the faster hydration rate and better microstructure development. Tapa et al. [211] also reported similar results for high slag-content concrete under 2% CO<sub>2</sub> and 50% relative humidity. They attributed the lower compressive strength of the binary mix to CEM I to increased porosity caused by carbonation shrinkage.

The compressive strength of CS and CS1L blended mortars at 55% RH accelerated carbonation shows similar trends to results obtained with carbonation depth. The differences in the volume of slag replacement in both CS & CS1L do not affect compressive strength development. There are marginal differences, and they can be classified as insignificant at less than 5% compared to CS2L, with clearer differences with limestone when increased to 20%. This is consistent with [67] study, showing increase over 10% led to decrease in mechanical properties. Generally, limestone addition is expected to provide nucleation space for the growth of hydrates which in turn should improve porosity and enhance compressive strength development, however higher replacement may be detrimental to concrete properties [67, 212] as observed in this study.

The compressive strength of binary blends (CS) mortar at 75% RH accelerated carbonation exposure is comparable to CEM I mortars during the same exposure, as shown in Figure 5.21 below.

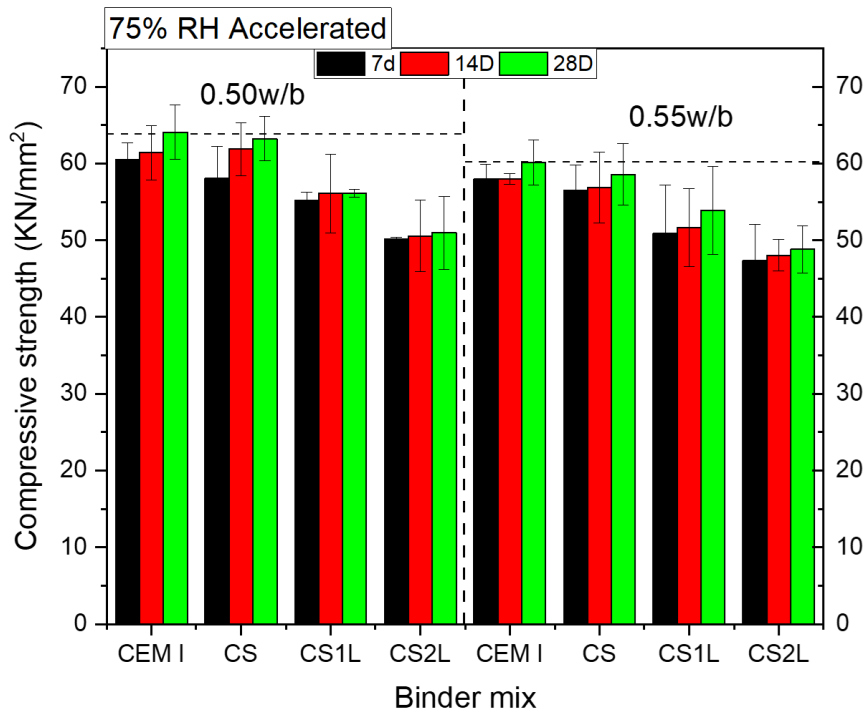


Figure 5.21: Compressive strength evolution after carbonation at 75% relative humidity.

Interestingly, CS mortar shows a significant increase in compressive strength from 7 days of exposure, with the trend continuing until 28 days. The increase in compressive strength is believed to be due to the continuous hydration of slag at a later age that will lead to the formation of calcium silicate hydrate (C-S-H) gel and other phases that fill the pores and thus increase the density of the blend coupled with a more favourable RH condition for achieving optimum hydration than obtainable at 55% RH above. Understandably, slag particles exhibit slower hydration at early ages, as often reported [144-146] and are expected to affect strength development when not sufficiently cured [115, 136]. Apart from closer to favourable RH condition >80% for hydration during accelerated carbonation at 75% RH condition, competition for C-S-H and other hydrates species is less with CO<sub>2</sub>, which may have reduced the effects of precipitation of amorphous carbon carbonate polymorph susceptible to coarsening of the pore.

Ternary blend CS1L at 10% limestone content also showed a similar trend to binary mortar (CS), and this suggests that the hydration of slag may be responsible for the increase in strength observed in both blends coupled with limestone acting as filler

and also providing nucleation sites for the growth of hydrates for the CS1L mortar. However, increasing the limestone to 20% with a subsequent decrease in slag shows a diminishing impact on CS2L mortar, suggesting that hydration of slag may play a more crucial role in the strength development than the filler effect provided from limestone during accelerated carbonation of mortars at 75% RH.

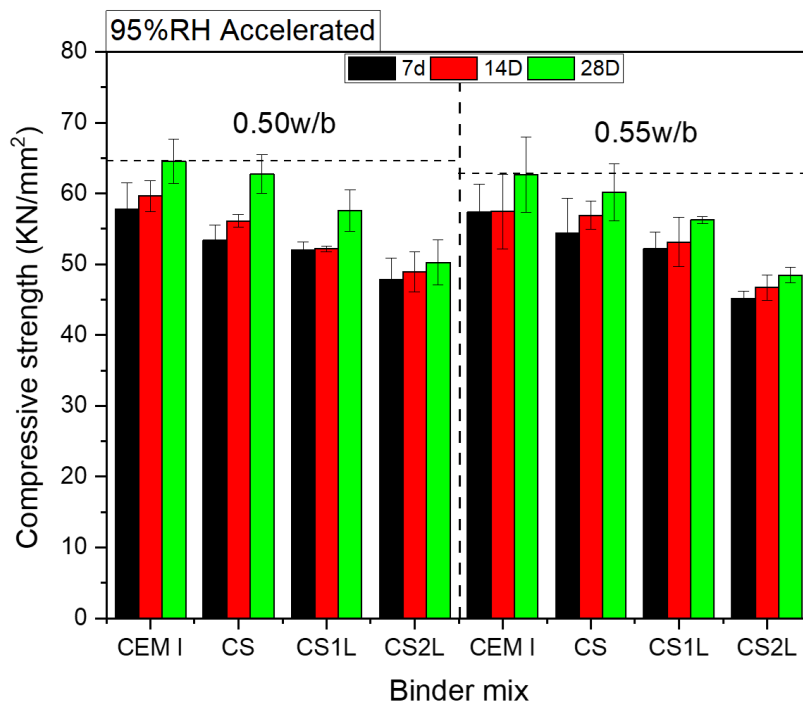


Figure 5.22: Compressive strength evolution after carbonation at 95% relative humidity.

Figure 5.22 above shows the evolution of compressive strength at 95% RH exposure under accelerated carbonation. Similar compressive strength development trends were observable with all mortars when compared with 75% RH with this result shown in Figure 5.15. This suggests that relative humidity's effects on the compressive strength after carbonation are not significant especially at higher RH i.e., >75% since the pores are fully saturated, and ingress of CO<sub>2</sub> are limited for this relative humidity condition especially for CEM I mortar. Consistent with other RH conditions, samples at 0.5w/b showed higher compressive strength in all mortars at all ages however CEM I mortar at 0.5w/b retained the slightly higher compressive strength than mortars made from composite binder.

Comparing the compressive strength after accelerated CO<sub>2</sub> exposure over the various relative humidities for all binders, CEM I mortar at w/b of 0.5 at 95% RH have highest compressive strength at about 65kN/mm<sup>2</sup> after 28 days exposure and with insignificant difference at 0.55 w/b of the same relative humidity. Binary mortar (CS) shows slightly comparable strength at both 75% and 95% RH with 63kN/mm<sup>2</sup> and 64kN/mm<sup>2</sup> respectively. For the ternary blended mortar, CS1L mortar have higher compressive than CS2L in all relative humidities. Generally, the ranking of the mortar subjected to accelerated carbonation over 55%, 75% and 95% RH are consistent with the depth of carbonation measurement presented in Figure 5.17 suggesting CO<sub>2</sub> ingress, binder mix, relative humidity and water/binder ratio play significant role in determining the compressive strength after accelerated carbonation exposure [93].

## 5.7 Summary

- Hydration halted during accelerated carbonation at 55% RH, and there seems to be no significant evidence to show water produced during carbonation is taken up for continuous hydration at both 55 and 75% RH as evidenced by no significant change or increase in the chemically bound water and portlandite formed or consumed in both CEM I and composite binders core area of the paste.
- Hydration and carbonation appear to coexist at 95% relative humidity, despite thymolphthalein indicator not showing any changes to suggest that carbonation is actively occurring. However, results from TGA show an increase in CH and the formation of CaCO<sub>3</sub> in all paste samples, indicating that clinker hydration is indeed taking place as well as carbonation of hydrates. It's possible that slag hydration may be active as this can't be certain at this time, along with the carbonation of other hydrates after 28 day accelerated exposure.
- Both TGA and FTIR show that both amorphous calcium carbonates and calcite are carbonation products formed in all binders; however, continuous carbonation led to calcite being the predominant product as other phases have converted to calcite throughout the exposure.
- FTIR shows evidence of decalcification of C-S-H, especially in 55% RH exposure for composite and all carbonation fronts with a shift of assigned band to higher wavelength.

- Elevated CO<sub>2</sub> concentrations up to 4% led to aggressive carbonation. In CEM I systems, this led to rapid carbonation of portlandite and densification of the microstructure at 55% RH, however, in composite cements this led to rapid decalcification of the C-S-H and coarsening of the pore structure.
- Relative humidity and water binder ratio significantly influence concrete carbonation depth. The carbonation depth increases with lower relative humidity exposure as discussed above and reaches the peak when the relative humidity is at 55% RH as seen in this study. Increasing the relative humidity i.e, to 75% and 95% respectively, it further slides down compared to 55% RH and with no significant effect at fully saturated condition, i.e., 95% RH. An increase in w/b also led to an increase in carbonation depth, irrespective of the binder type.
- There is no significant difference between binary binder (CS) and 10% limestone addition (CS1L) in carbonation resistance despite differences in the slag volume; however, there are significant changes in compressive strength and carbonation between CS, CS1L, and CS2L. Both CS and CS1L outperform CS2L in all relative humidity conditions.
- In general, the ranking of mortar samples subjected to accelerated carbonation at 55%, 75%, and 95% relative humidity aligns with the depth of carbonation measurements. This alignment suggests that factors such as CO<sub>2</sub> ingress, binder composition, relative humidity, and water/binder ratio all play significant roles in determining the compressive strength after exposure to accelerated carbonation.

## **Chapter 6: Comparison between ambient and accelerated carbonation.**

The previous chapters four & five demonstrated carbonation under ambient and accelerated conditions using two different water/binder ratios. The samples with a water/binder of 0.50 exhibited improved carbonation resistance and compressive strength under both exposure conditions adopted for this study. However, the phase assemblages are similar, except for the impact of accelerated carbonation. Therefore, this chapter further examines the hydration, phase changes, microstructure changes and compressive strength of selected mixes (CEM I, CS & CS1L) to understand better and compare CEM I, binary and ternary blends during ambient and accelerated carbonation. Techniques such as XRD and SEM-BSE were further introduced to evaluate the effect of carbonation during different RH conditions on the selected blends.

### **6.1 Hydration progress during carbonation**

Chemically bound water and portlandite contents provide insight into the hydration of any binder. Increasing chemically bound water signifies continued hydration in neat and composite systems, while portlandite formation in the PC system is due to the hydration of clinker phases. In contrast, portlandite in blended binders will be consumed in a pozzolanic reaction and serve as a calcium source for ettringite formation. However, carbonation also depletes portlandite to form calcite.

#### **6.1.1 Chemical bound water measured by TGA.**

Figure 6.1-6.3 below presents chemically bound water, portlandite contents, and calcium carbonate formed for selected samples CEM I, CS & CS1L under ambient and accelerated carbonation. Generally, the CBW is similar for CEM I samples for ambient exposure at 75% and 95% RH but was slightly lower at 55% RH as presented in Figure 6.1 below. This is due to the effect of preconditioning/drying on CBW and as reported elsewhere [135, 213] to have caused a lower degree of internal saturation below equilibrium for the reaction when compared to 75% and 95% RH conditions which are closer or above favourable 80% RH condition for continuous hydration. There were no significant changes in CBW levels observed at both 75% and 95% RH during ambient carbonation. However, at 55% RH, there was a decrease in CBW compared to the other RH levels, indicating that hydration had ceased, as shown in

Figure 6.1 below. It's worth noting that CBW were higher in ambient carbonation than those observed during accelerated carbonation for all CEM I samples, possibly due to the mass loss calculation being considered up from 50°C-55°C and CH will also be part of the measurement.

When comparing edge and core samples at 55% RH upon accelerated carbonation, both CBW measurements suggested that hydration had stopped. Additionally, it was observed that water released from the carbonation front (edge) did not seem to significantly contribute to further hydration in the core area. This lack of a substantial increase in CBW in the core area at 55% RH suggests that hydration would likely cease at lower RH levels than 80%. It's important to note that this observation could not be confirmed in other RH conditions, as explained earlier, due to the absence of significant colour changes that could distinguish between the two areas in the samples.

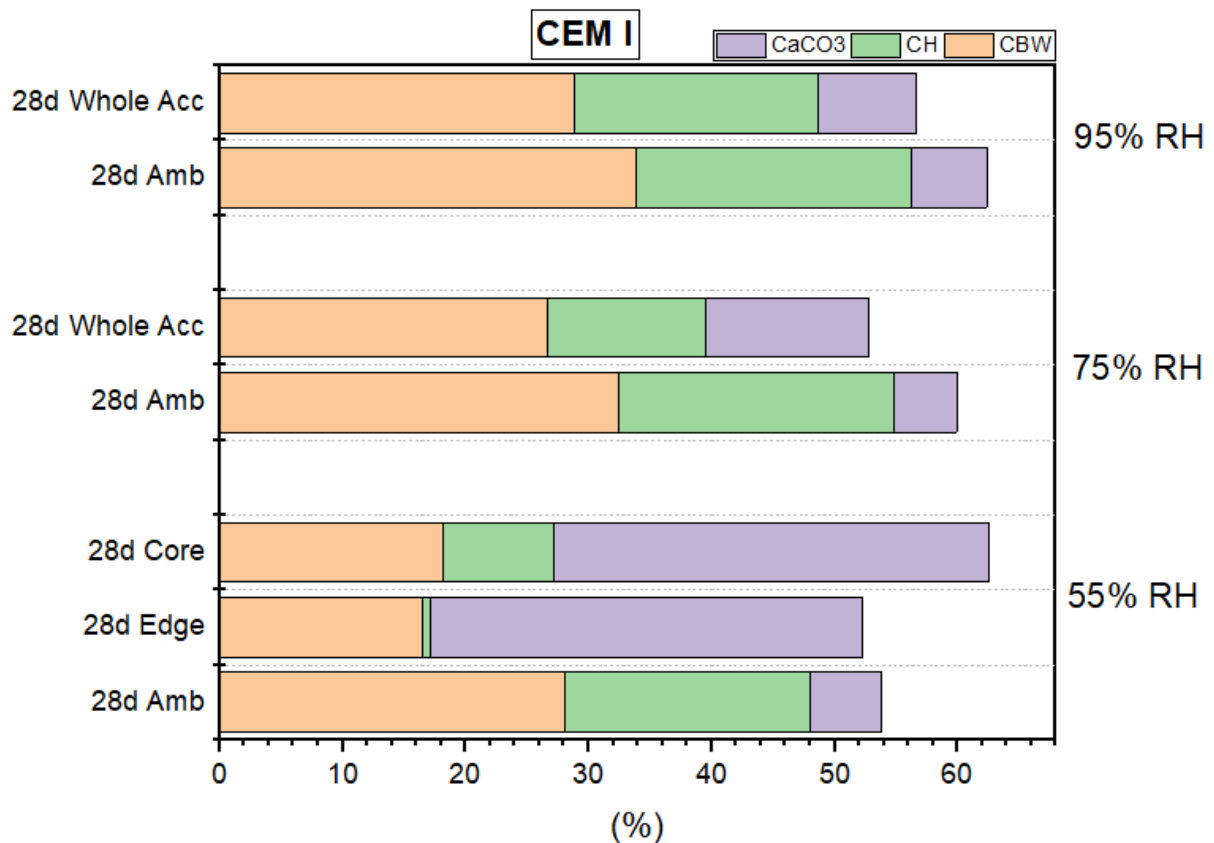


Figure 6.1: Measured chemically bound water (CBW), CH & CaCO<sub>3</sub> from TGA during ambient and accelerated carbonation for CEM I at all relative humidities.

Generally, the available amount of (CH) decreases upon production of CaCO<sub>3</sub>, both in cases of ambient and accelerated carbonation. Notably, the edge area showed a lower CH presence compared to other exposure conditions. This implies a reduced capacity to buffer against CO<sub>2</sub> [140] and consequently results in higher levels of CaCO<sub>3</sub> produced which validate CH as a key component of carbonation reaction.

It's evident that all samples, whether subjected to ambient or accelerated carbonation, produce CaCO<sub>3</sub>. However, there is a difference in the quantity of CaCO<sub>3</sub> produced. Samples exposed to ambient conditions yield nearly the same amount, confirming the earlier observation of minor carbonation from exposure as well during sample preparation in all RH.

At 95% RH for CEM I, despite a higher degree of saturation in the pore structure of the binder system, CH in accelerated carbonation experiences a slight decrease compared to ambient condition suggesting ongoing carbonation despite RH. Also,

subsequent higher  $\text{CaCO}_3$  formed with accelerated carbonation when compared to ambient carbonation at the same RH was observed.

When comparing these findings with earlier results discussed in chapter five, which showed that CH measured at 28 days was higher than at 7 days during accelerated carbonation for 95% RH, it is reasonable to conclude that both hydration and carbonation are occurring concurrently at 95% RH during both ambient and accelerated carbonation.

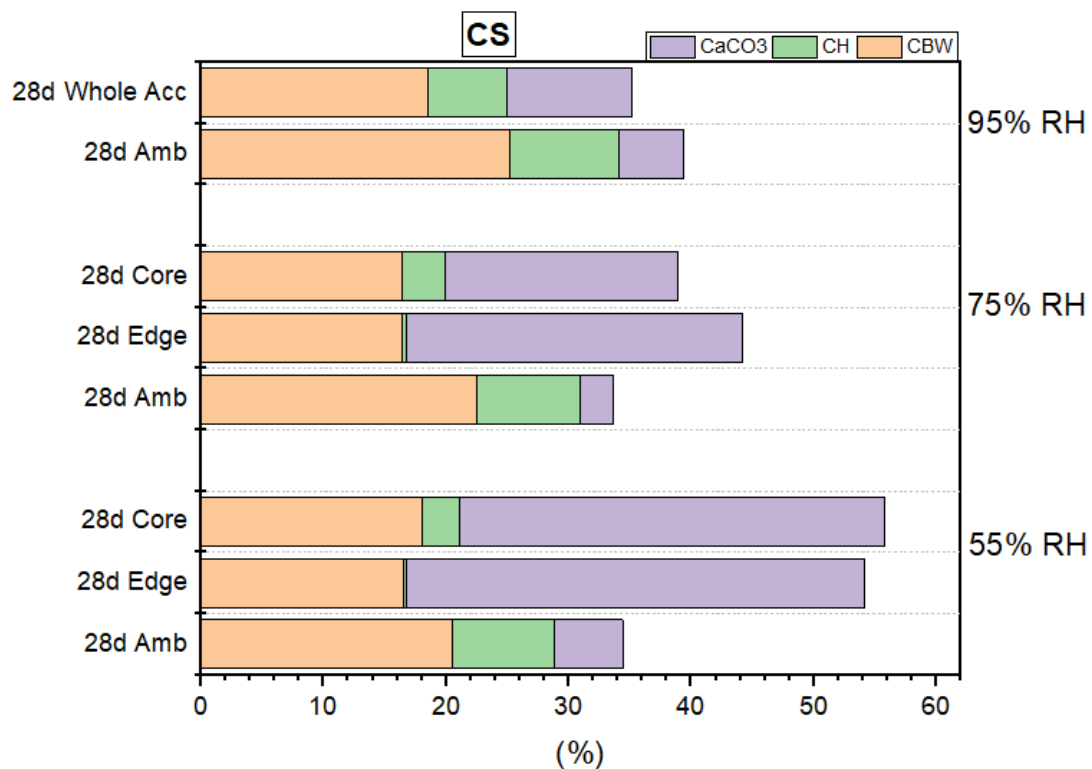


Figure 6.2: Measured chemically bound water (CBW), CH &  $\text{CaCO}_3$  from TGA during ambient and accelerated carbonation for CS (Binary blend) at all relative humidities.

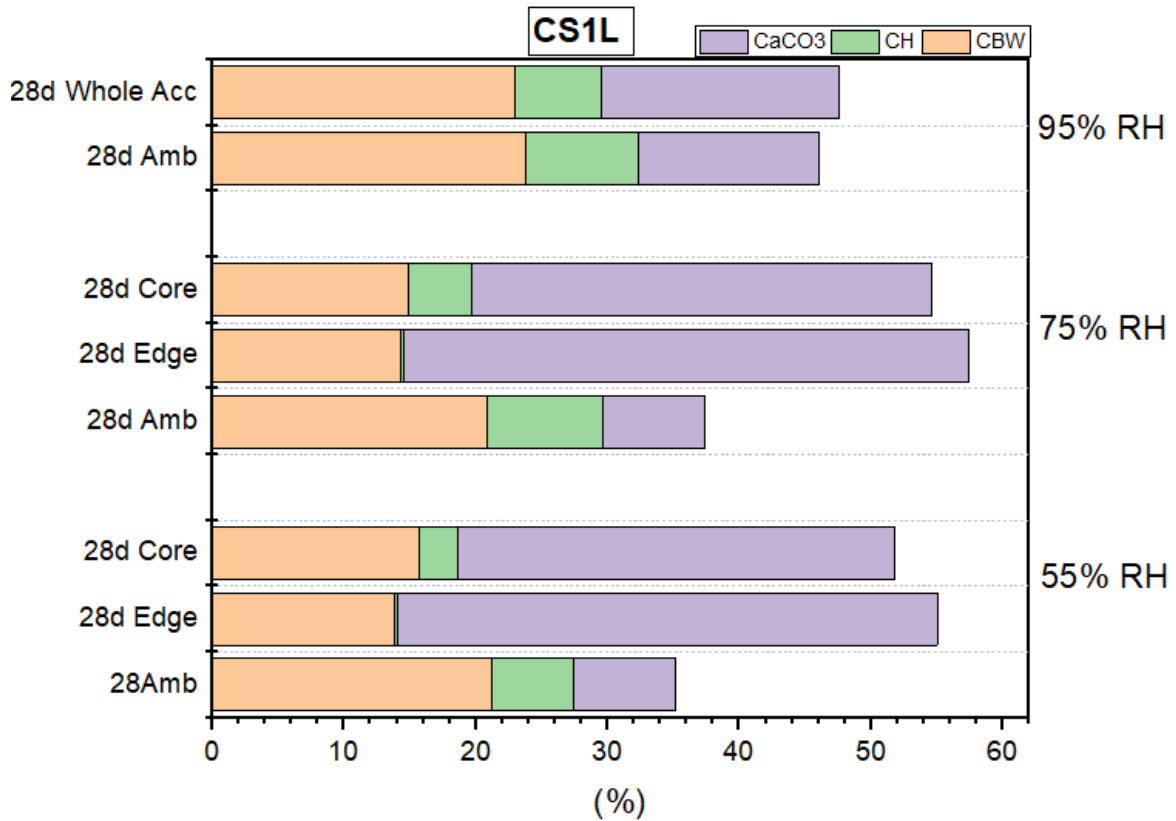


Figure 6.3: Measured chemically bound water (CBW), CH & CaCO<sub>3</sub> from TGA during ambient and accelerated carbonation for CS1L (Ternary blend) at all relative humidities.

Both composite binders exposed at both 75% and 95% relative humidity, as presented in Figure 6.2 and 6.3 above, followed similar trends as observed for CEM I. As anticipated, the CBW during ambient carbonation at 95% RH was the highest for both composite binders when compared to the two RH levels studied. This outcome aligns with expectations, as the hydration process remained undisturbed during both preconditioning and ambient exposure for this particular condition. Generally, comparing CBW measured in both ambient and accelerated (whole, edge, or core) where applicable, there was no indication that accelerated carbonation led to water release from hydrates from the edge areas and so leading to further hydration in the core.

#### 6.1.2 Portlandite measured by both TGA & QXRD

Portlandite serves as the primary alkalinity buffer for binders and tends to carbonate quickly upon exposure to CO<sub>2</sub> [135] hence its importance in hydration and carbonation studies. Table 6-1 below shows the CH measured by both TGA and XRD upon both

ambient and accelerated carbonation. There was a significant decrease in measured portlandite contents within the carbonation front (edge) compared to both core and ambient exposure, as determined by both TGA & XRD in all samples at all RH values. This is due to the depletion of CH through accelerated exposure; however, pastes from the core of the samples where applicable also show reduced CH contents compared to ambient exposure due to accuracy of the pH indicator, not the total representation of the carbonation fronts as reported elsewhere [178, 179, 213]. Therefore, it is likely that partial carbonation is occurring within the core area of the samples. CEM I retained the highest amount of CH after accelerated carbonation in all RH and the difference are significant with exposure at 55% RH compared to other RH conditions and this is due to the amount of clinker available to produce CH compared to the composite binder at 50% for CS and 40% CS1L, respectively and also due to pozzolanic reaction that consume CH. The changes observed in measured CH content with both TGA and XRD-Rietveld refinement are due to TGA measuring both crystalline and non- crystalline CH content while XRD only detect crystalline CH. TGA measurement are usually higher than values observed with XRD [107], with typical agreement at +/-2.5%.The data presented in Table 6-1 agrees generally with the error allowance which validates the CH data presented in Figure 6.1-6.3 except few data with CEM I at 75% RH and 95% RH at accelerated exposure (-2.65%) higher than TGA value for XRD and 3.52% difference between the two techniques which are likely due to experimental error.

Table 6-1: CH content measured with both TGA & XRD after 28 days ambient and accelerated carbonation.

RH	Mix		CH (/100g binder)		
			TGA	XRD	Diff. (+/-)
55%	CEM I	Amb	19.94	19.50	0.44
		Core	9.01	7.40	1.61
		Edge	0.70	0.50	0.2
	CS	Amb	8.26	6.40	1.86
		Whole Acc	0.00	0.30	-0.30
	CS1L	Amb	6.24	5.60	0.64
Whole Acc		0.00	0.00	0	
75%	CEM I	Amb	22.44	20.70	1.74
		Whole	12.85	15.50	-2.65
	CS	Amb	8.46	8.20	0.26
		Core	3.43	2.50	0.93
		Edge	0.00	0.50	-0.50
	CS1L	Amb	8.80	8.00	0.80
		Core	4.82	3.10	1.72
		Edge	0.00	0.40	-0.4
	95%	CEM I	Amb	22.34	20.50
Whole Acc			19.82	16.30	3.52
CS		Amb	8.90	7.20	1.7
		Whole Acc	6.49	5.00	1.49
CS1L		Amb	8.60	8.21	0.41
		Whole Acc	6.56	6.70	-0.14

### 6.1.3 Degree of reaction of clinker/slag by SEM-IA

Following the TGA results presented in Figure 6.1-6.3, SEM-IA were also used to examine paste samples after exposure for 28 days under accelerated and ambient conditions at all relative humidities as presented in Table 6-2 below, to further explore whether there are changes in the degree of reaction of both clinker and slag in the selected mix during exposure. From Table 6-2 presented below, there is seemed to be no notable change in degree of hydration of clinker and slag during both accelerated and ambient carbonation at 55% & 75% RH as both showed only slight differences in the degree of reaction under all conditions over the period of the test. This observation is corroborated with the result obtained from CBW measured by TGA. Samples exposed at 55% RH showed slightly lesser reaction with both the clinker and slag species and due to drying conditions. At 75% RH, for composite binder, there was insufficient difference in reaction of ambient exposed edge and core regions to conclude whether water released during the carbonation reaction from the carbonating

front influenced further hydration of the core. Although changes observed upon ambient and accelerated carbonation seems to suggest hydration is ongoing within samples albeit slower at 75% RH and this clearly explained the comparable degree of hydration of both clinker & slag for both core and ambient sample at 75% RH, as was similarly reported previously [214] where continuous hydration of both clinker and slag occurs further down the depth from the surface of carbonation.

With exposure at 95% relative humidity, samples showed progressive hydration in all blends, despite the pH indicator not showing any significant colour change to distinguish between the carbonation front and the core. However, there was an increase in clinker hydration and slag reaction compared to other relative humidity as obtained in Table 6-2 below which further supported results presented from TGA in chapter four and five of this thesis.

Table 6-2: Degree of clinker hydration/slag reaction measured by SEM-IA.

Mixes	55% RH		75% RH		95% RH	
	Clinker (%)	Slag (%)	Clinker (%)	Slag (%)	Clinker (%)	Slag (%)
<b>CEM I</b>						
Core	89.1	-	93.5	-	96.8	-
Edge	88.7	-	-	-	-	-
Amb.	93.6	-	95.7	-	97.6	-
<b>CS</b>						
Core	86.1	46.3	91.1	52.2	94.1	55.2
Edge	-	-	92.7	51.8	-	-
Amb.	91.9	59.5	94.6	53.3	94.1	55.8
<b>CS1L</b>						
Core	89.9	48.2	90.9	51.2	93.1	56.2
Edge	-	-	89.7	47.9	-	-
Amb.	90.5	49.5	91.3	54.4	92.3	57.1

## 6.2 Phase evolution due to carbonation

The various mixes were characterised by TGA, FTIR and XRD following both accelerated and ambient carbonation at 55%, 75% and 95% relative humidity. This gave an understanding of the transformation of various hydrates under all exposure conditions.

### 6.2.1 Differential Thermogravimetry Analysis

The DTG curves of the 3 blends carbonated under ambient and accelerated conditions can be seen in Figure 6.4-6.6. The broad temperature ranges from 450°C to 900°C is of specific interest due to transformation of portlandite to calcium carbonates. The carbonated samples show three modes of calcium carbonate decomposition, as

reported in the literature [77]. The temperature ranges of the three modes are 780-990°C, 610-780°C and 450-610°C, for mode I, II & III respectively.

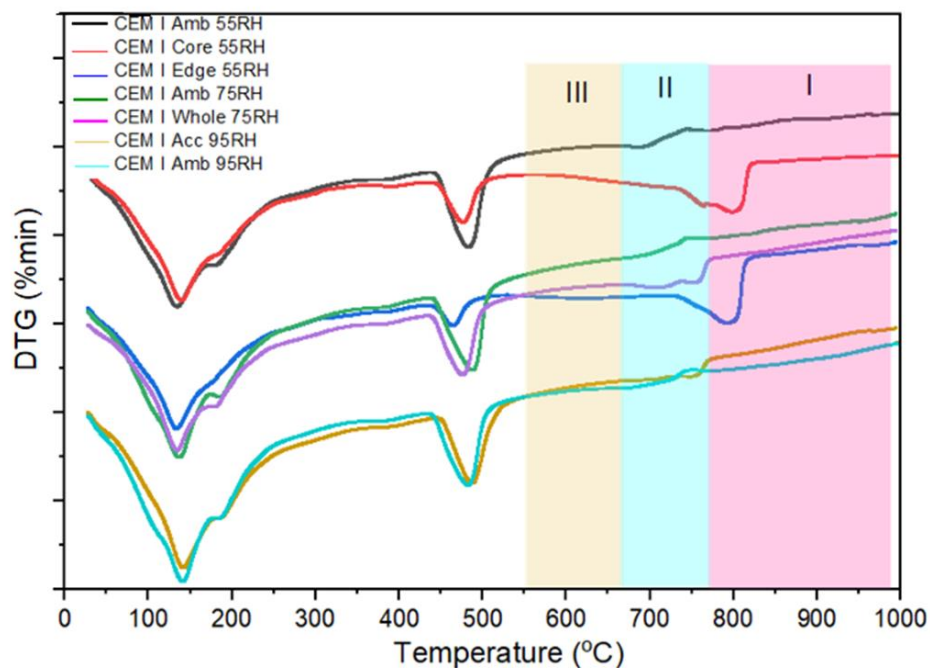


Figure 6.4: DTG plot comparison of CEM I at 55, 75 & 95% relative humidity for both ambient (Amb) and accelerated carbonation (Acc).

Ambient carbonation seems to mainly promote the formation of amorphous calcium carbonates (mode II) for CEM I system as confirmed in Figure 6.4 above for 55 RH, 75% RH and 95% RH. Mode II & I decomposition ranges were promoted during accelerated carbonation as evident with samples in both core and edge for 55% RH and 75% RH respectively suggesting both this form and well-ordered calcite are present, consistent with the XRD pattern in Figure 6.10. These shifts in calcium carbonate decomposition temperatures correspond to decrease or continuous depletion of the CH as evident with mass loss at 450<sup>o</sup>-550<sup>o</sup>C and near or complete disappearance of other AFm peak shoulder at 150-170<sup>o</sup>C and is consistent with [107] that AFm will either transform to monosulfoaluminate or to hemi- and monocarboaluminate before complete decalcification.

Comparing core and edge for the CEM I sample exposed to 55% RH shows clear consumption of CH at the sample edge. Calcite is the most dominant decomposition mode as evident from Figure 6.4 above i.e. carbonation of portlandite led to formation of calcite and is consistent with previous studies [13, 140]. However all CaCO<sub>3</sub>

decomposition modes were present, consistent with Dubina et al. [215] that found all three  $\text{CaCO}_3$  polymorphs formed upon free lime when exposed over the 20-60% RH range. CEM I samples exposed at both 75% & 95% RH under both ambient and accelerated carbonation conditions showed all modes of calcium carbonate present, with [162, 216] suggesting vaterite and calcite are likely polymorph at ambient or near ambient conditions and agrees with XRD results in Figure 6.10.

Figures 6.5 & 6.6 below present the DTG plots for the binary (CS) and ternary blends carbonated for 28 days under ambient or accelerated conditions, at 55, 75 and 95% RH. There was evidence of carbonation in all of the specimens exposed to accelerated carbonation conditions, but to a far lesser extent following exposure at 95% RH. The calcium carbonates decomposition starts immediate after CH peak with both 55% and 75% RH for edge and core areas of the sample. It's evident from Figure 6.5 & 6.6 that mode I II & II decomposition occurs for the binary blend. This suggests decalcification of the C-S-H coupled with CH carbonation. At 95% RH, both mode I & II decomposition were found however, CH peak decreases with accelerated carbonation compared to ambient exposure suggesting both CH & C-S-H carbonate simultaneously and consistent with findings of [122, 162, 217].

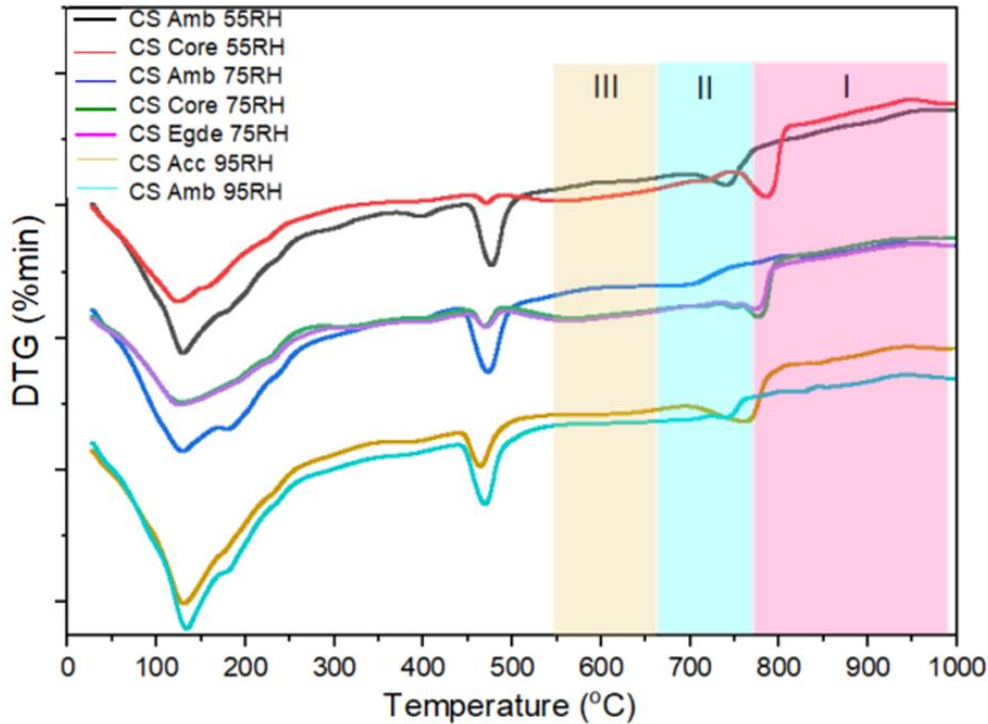


Figure 6.5: DTG plot comparison of CS (Clinker/Slag binary mix) at 55, 75 & 95% relative humidity.

The main difference was observed upon accelerated carbonation, where all temperature range modes of calcium carbonate decomposition were observed, regardless of the degree of carbonation and relative humidity. This suggests that a higher amount of C-S-H and other phases were carbonated under accelerated exposure. This was exacerbated for composite blends where there were lower CH and high C-S-H contents. This supports the susceptibility of SCM binders to carbonation compared to CEM I as observed in many studies [218, 219]. Both amorphous and well-crystalline calcium carbonate were observed and was further discussed with results obtained with FTIR in section 6.2.2 and as shown in the Figure 6.6 below.

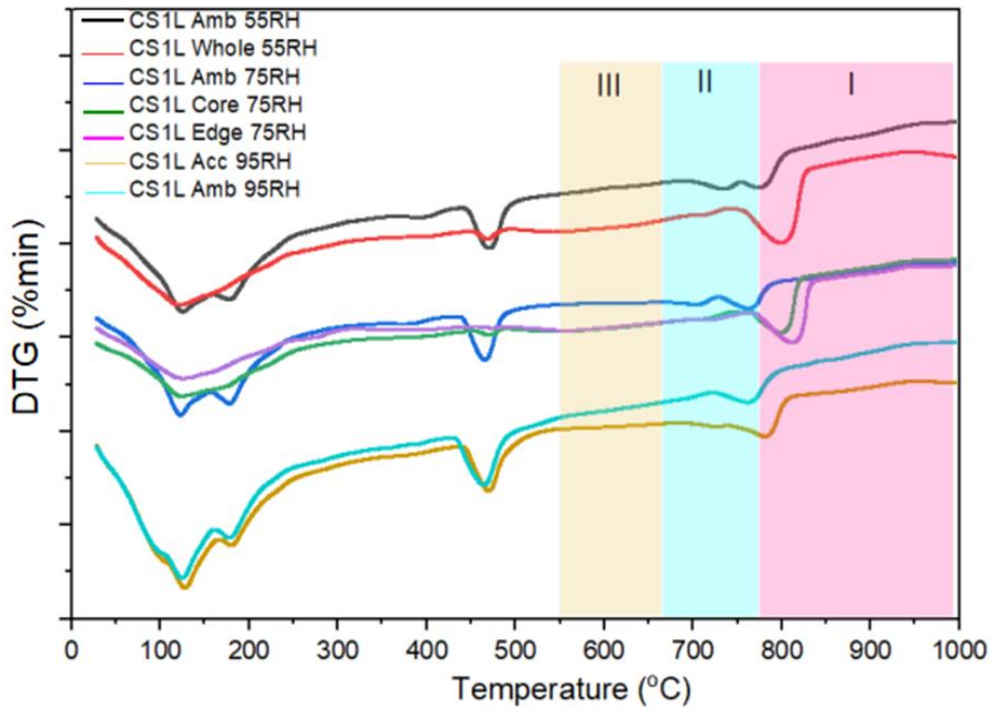


Figure 6.6: DTG plot comparison of CS1L (Clinker/Slag/Limestone ternary mix) at 55, 75 & 95% relative humidity

In general, as carbonation progressed, the mass loss associated with  $\text{CaCO}_3$  decomposition occurred at a lower temperature than represented as III on Figure 6.4-6.6 and thus presented in Table 6-3 below and plot presented in the appendices section of the thesis.

Table 6-3: Mass loss temperatures for CaCO<sub>3</sub> decomposition.

Mixes	RH	Start of decomposition temperature for CaCO <sub>3</sub> (°C)			
		Ambient	Edge	Core	Whole
<b>CEM I</b>	55%	550	520	520	-
	75%	550	-	-	550
	95%	550	-	-	550
<b>CS</b>	55%	550	-	-	500
	75%	550	500	500	-
	95%	550	-	-	500
<b>CS1L</b>	55%	550	-	-	500
	75%	550	495	480	-
	95%	550	-	-	540

Samples subjected to accelerated carbonation were shown to have lower decomposition temperatures than equivalent samples exposed to ambient carbonation as reported in the literature for mode III [98, 161] and this is due to the carbonation of C-S-H with amorphous calcium carbonate species formed as a result. Villian et al. [98] reported similar result with 3-month old cured mortar samples, with unstable form of vaterite and aragonite found at 530-650°C. Also the result obtained from this study are consistent with Herterich's [140] findings with composite cements.

#### 6.2.2 Phases Changes by FTIR

The FTIR spectra of binder pastes after 28 days of exposure to both accelerated and ambient carbonation are depicted in Figures 6.7, 6.8, and 6.9 for CEM I, binary, and ternary blends, respectively. The overall appearance is similar but there are changes in peak intensities and importantly changes in peak position and shape, indicating changes in some of the hydration and carbonation products.

For CEM I samples in Figure 6.7, the hydrates and carbonation products are consistent with those identified by XRD in Figure 6.11. The O-H stretching vibration at 3640 cm<sup>-1</sup>, assigned to portlandite, is weak or not visible after carbonation at 55% and 75% RH under both carbonation conditions, suggesting ongoing carbonation or

depletion of CH, and confirmed by the peak intensity of calcium carbonates and polymorphs observed at different assigned bands. The asymmetric C-O stretching mode ( $\nu_3$ ) around 1400-1500  $\text{cm}^{-1}$ , assigned to calcium carbonate, shows a sharp peak for both edge and core samples, indicating the formation of well-crystalline calcium carbonate, likely calcite and similar results obtained elsewhere [140] and consistent with TGA result explained above.

Portlandite carbonation is the major driver of calcium-bearing phases during accelerated carbonation of the CEM I system due to its abundance in the hydrated cement paste. In contrast, ambient carbonation shows a broader peak except 55% RH, suggesting the formation of amorphous calcium carbonate as evident from both TGA and XRD results presented. Also, there was no evidence of C-S-H decalcification in both accelerated and ambient carbonation as there was no shift in the absorption band assigned to C-S-H at 971  $\text{cm}^{-1}$  for CEM I sample. Carbonation at 55% RH led to the most intense carbonation peaks and this consistent with both XRD and TGA results.

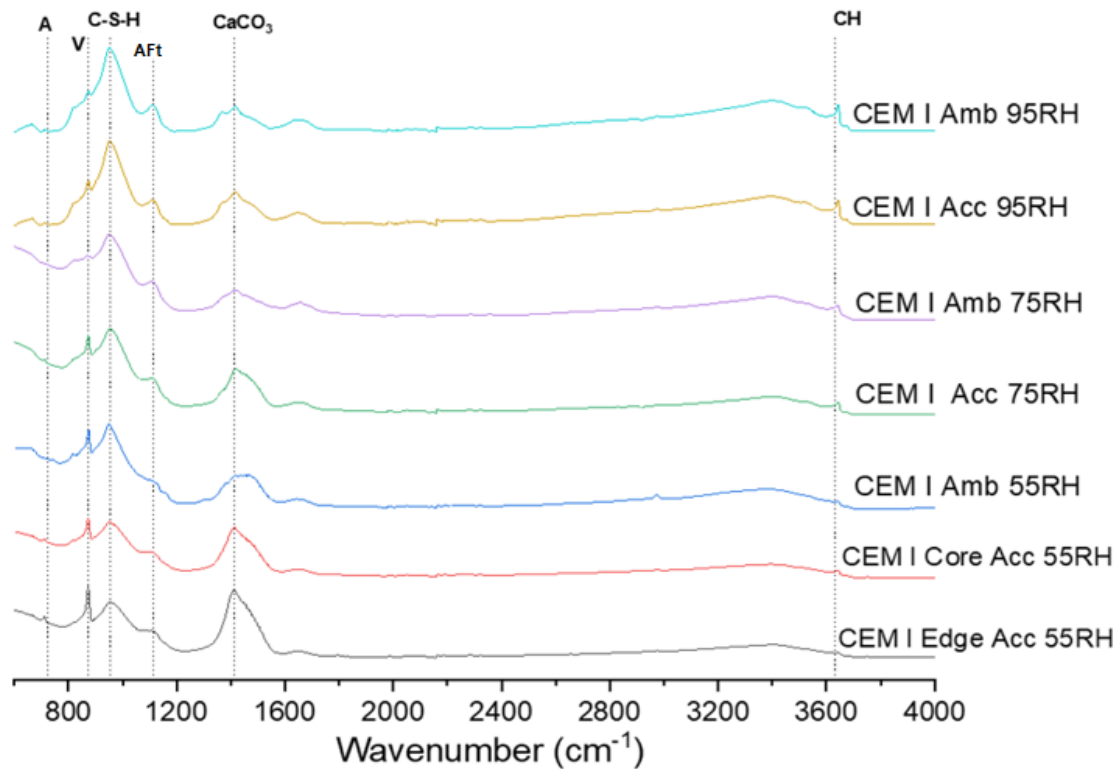


Figure 6.7: FTIR spectra plot comparing CEM I at both ambient & accelerated carbonation at different humidity.

For both binary (CS) and ternary blended samples FTIR plots are shown in Figures 6.7 & 6.8. FTIR revealed significant phase changes in the spectra of CS and CS1L samples upon ambient and accelerated carbonation. Portlandite was evident in the ambient carbonated specimens and all specimens carbonated at 95% RH, albeit at trace levels. Carbonation at 95% RH led to the growth of asymmetric carbonate bands, indicative of calcite formation. In these samples, there was no evidence of silicate polymerisation, i.e., the silicate stretching band remained at  $940\text{cm}^{-1}$ . Clinker dilution, coupled with slag hydration, led to lower CH contents observed for the composite cements than in CEM I. Carbonation of the samples therefore consumed portlandite more readily. Once portlandite was consumed, further carbonation led to significant changes in phase composition. It is the presence of portlandite that defines carbonation behaviour, and this is subsequently reflected in the silicate stretching band. A shift in the silicate stretching band of C-S-H from  $975\text{cm}^{-1}$  to higher wavelength ( $1150\text{cm}^{-1}$ ) was observed and at both 55% and 75% RH under accelerated carbonation conditions in both composite binders (CS and CS1L). The shift was

particularly pronounced following accelerated carbonation at 55% RH. This observation suggests decomposition of C-S-H seem to have occurred in either one or both steps identified in [12] i.e. (i) gradual decalcification of C-S-H by removing calcium from the interlayer space and defect sites in the silicate chains (ii) final decomposition and formation of amorphous silicate phase due to consumption of calcium from the principal layers.

The combination of different crystalline  $\text{CaCO}_3$  polymorphs were identified, with a combination of out-of-plane mode ( $\nu_2$ ) at  $711\text{cm}^{-1}$  assigned to aragonite and O-C-O in plane bending mode ( $\nu_4$ ) at  $873\text{cm}^{-1}$  assigned to both vaterite and calcite [164]. These polymorphs appeared at different relative humidities. Vaterite/calcite peak intensities were higher upon accelerated carbonation, especially at 55% RH, as shown in Figure 6.7 & 6.8. Given its concurrence with the earlier mentioned shift in the silicate stretching band of C-S-H at  $971\text{cm}^{-1}$ , this suggests intense carbonation of the C-S-H phase. Only trace levels of aragonite were observed in both binary and ternary samples, upon both carbonation conditions, and all relative humidities. However, a slight peak suspected to be due to aragonite was observed for CS1L samples at 95% relative humidity for both accelerated and ambient condition. Black et al. [167] found similar trace levels of aragonite following ambient carbonation of mechano-chemical activated C-S-H at various C/S levels and attributed it to formation  $\text{SiO}_2$  gel in the system which is present in the mixes studied.

The asymmetric C–O-stretching mode ( $\nu_3$ ) around  $1400\text{-}1500\text{cm}^{-1}$  assigned to calcium carbonate shows a broadening peak with both carbonation front (edge) and core samples suggesting the formation of both amorphous and well-crystalline calcium carbonate. A more intense carbonate peak was always evident in the accelerated carbonation samples, but the key observation was the change in peak symmetry once portlandite was no longer present. Samples exposed at 55 and 75% RH showed more of a symmetrical hump attributed to a mixture of carbonates including amorphous calcium carbonate, losing the characteristic asymmetric sharp peak associated with calcite. This broad hump was also associated with decalcification of the C-S-H.

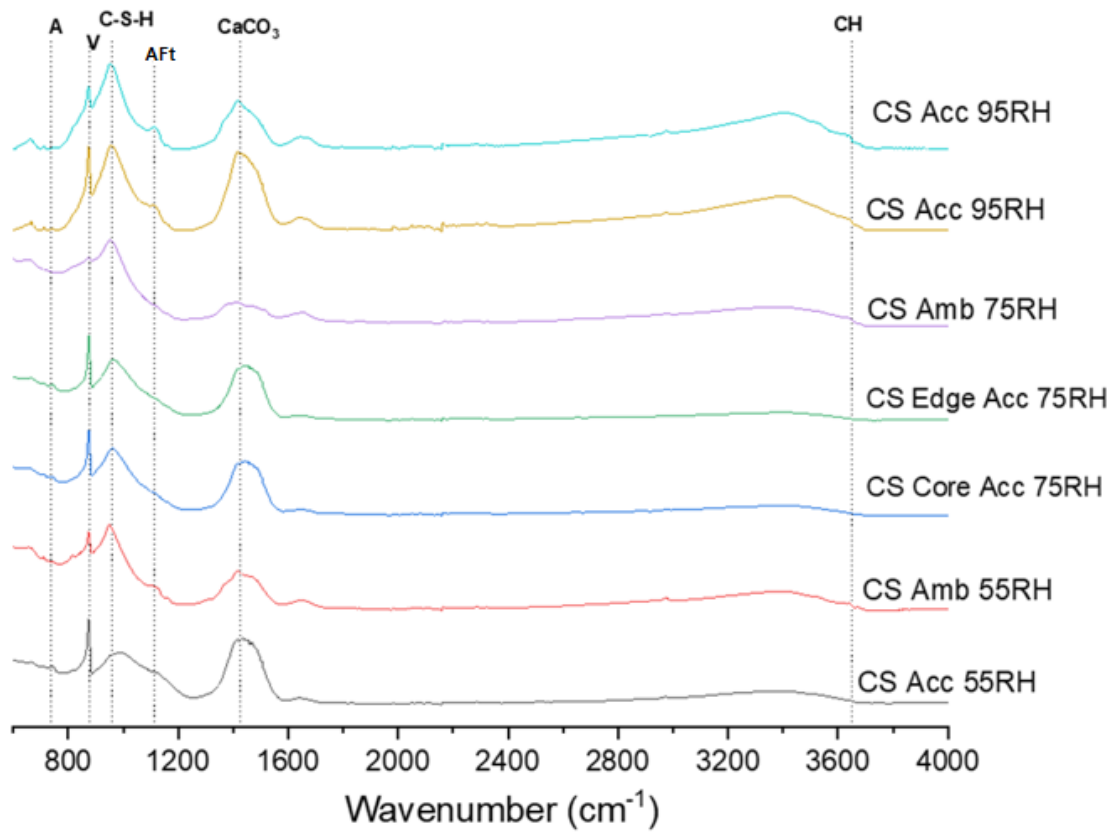


Figure 6.8: FTIR spectra plot comparing CS (binary blends) at both ambient & accelerated carbonation at different humidity.

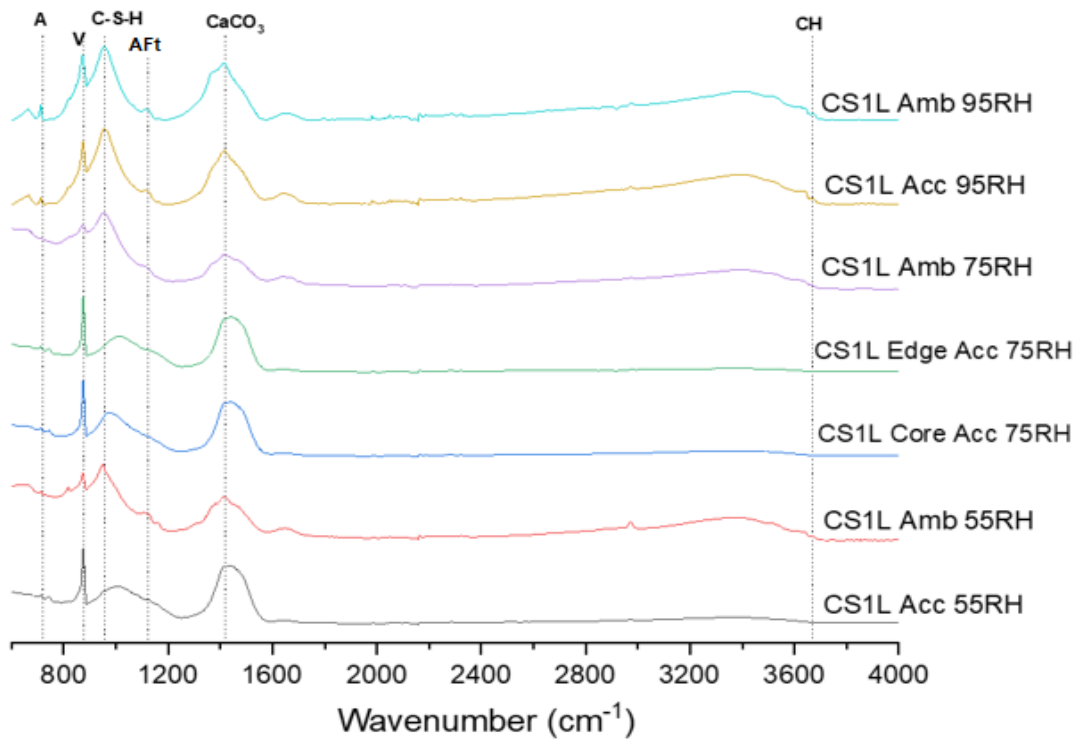


Figure 6.9: FTIR spectra plot comparing CS1L (Ternary blends) at both ambient & accelerated carbonation at different humidity.

### 6.2.3 Phases changes by XRD

To identify various phases that formed and transformed during carbonation, paste samples were investigated by XRD upon ambient and accelerated (edge & core) carbonation at 55%, 75% and 95% RH, as described in chapter three. Samples were analysed after 28 days and the diffractograms shown in Figures 6.10-6.12 for CEM I and CS and CS1L in all RH respectively.

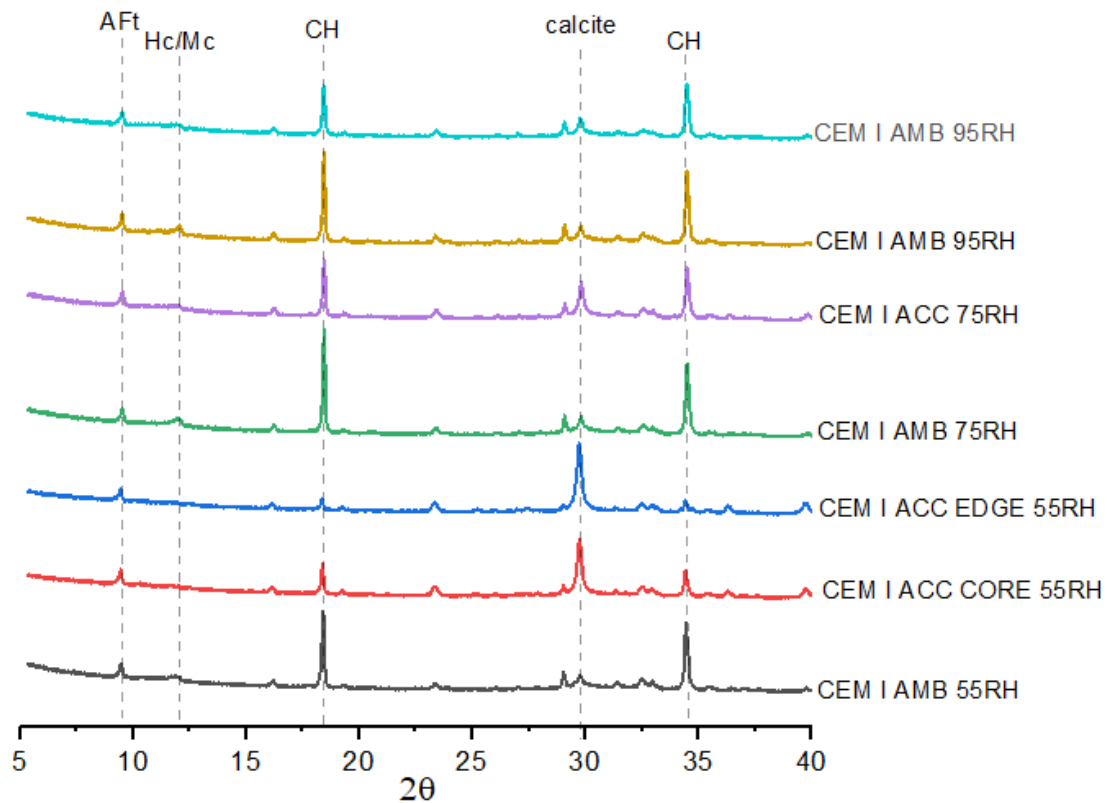


Figure 6.10: XRD pattern comparison for CEM I at both ambient & accelerated carbonation.

From Figure 6.10 above, CH transformed into calcite, with a significant decrease in peak intensity during accelerated carbonation exposure (edge) at both 55% & 75% relative humidity. The decrease in peak intensity of CH at  $18.2^\circ 2\theta$  corresponded with an increase in calcite peak intensity at  $29.5^\circ 2\theta$  as shown in Figure 6.9 with results obtained with both FTIR and TGA suggesting carbonation of CH transforms to calcite. Aragonite was not detected or visible at  $2\theta = 26^\circ$  and vaterite was not visible upon accelerated carbonation at both 55% and 75% RH. This suggests that calcite is the predominant calcium carbonate phase in PC systems [140] with very sharp intensity seen especially in accelerated (both edge & core). AFt was stable at all RH, consistent with FTIR results above.

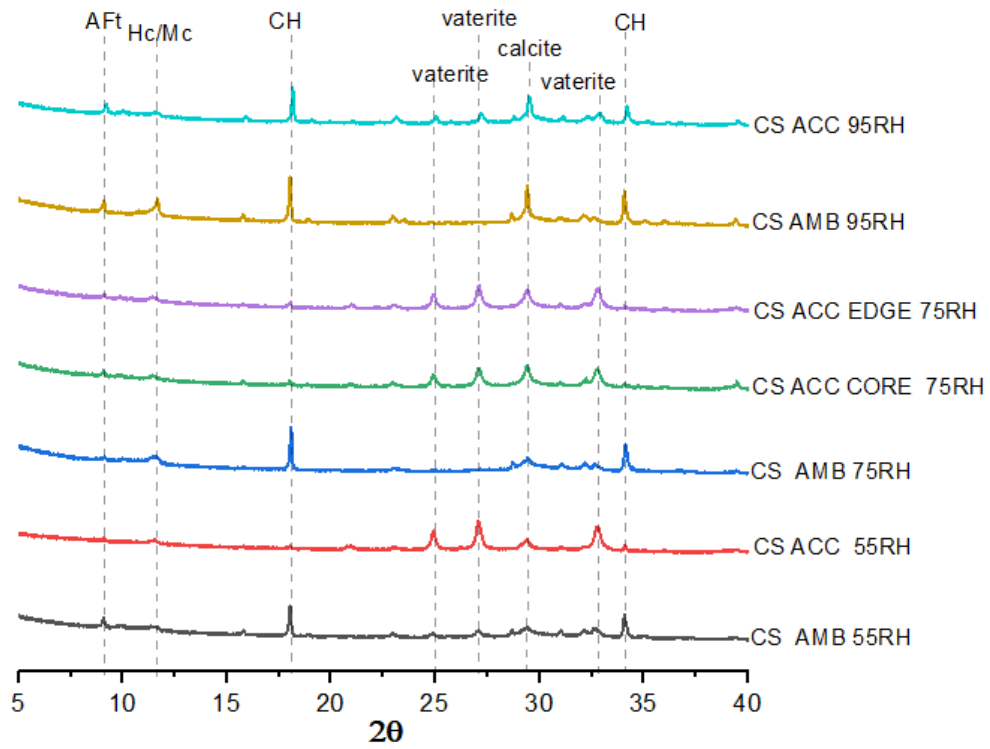


Figure 6.11: XRD pattern comparison for CS at both ambient & accelerated carbonation.

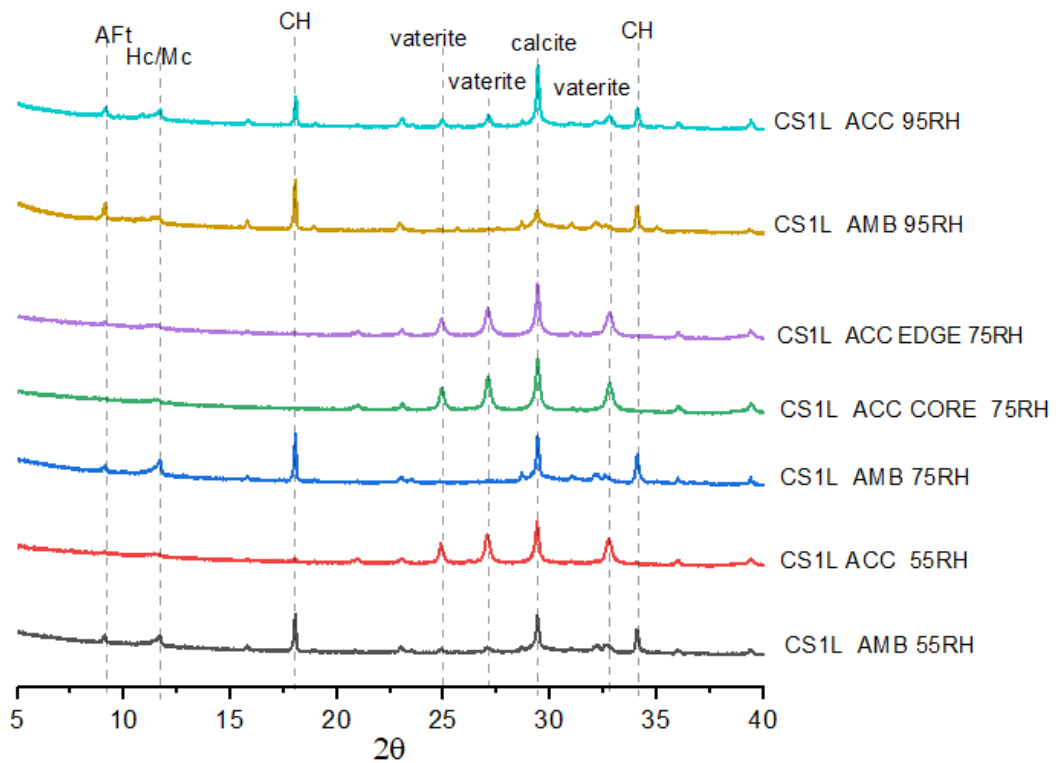


Figure 6.12: XRD pattern comparison for CS1L at both ambient & accelerated carbonation.

For binary and ternary binders in Figure 6.11 and 6.12 above, CH peaks were much weaker following accelerated carbonation at 55% RH and 75% RH, with a slightly visible peak following exposure at 95% RH. Following ambient carbonation, exposure at both 55% & 75% RH CH peak intensities decreased (much more than following exposure at 95% RH), suggesting slight CH carbonation or hydration are ongoing in the system.

Both vaterite and calcite are dominant polymorphs. However, whenever CH was no longer present, the vaterite peak increased. This suggests carbonation of C-S-H after depletion of CH, as evident by FTIR. C-S-H is poorly crystalline, so does not give rise to any distinct diffraction peaks but does give a diffuse hump around  $2\theta = 29-32^\circ$ . This peak cannot be totally distinguished from amorphous slag [220]. However, when vaterite was present, particularly in the carbonation front (edge), there was a flattening of the diffuse hump. This suggests breakdown of the C-S-H, as observed by FTIR, and seen elsewhere [221]. It is fair to assume that abstraction of calcium from the C-S-H led to vaterite formation. Carbonation of ettringite was observed after accelerated carbonation at both 55% and 75% but reduced in all relative humidities condition. Also, peaks due to Hc/Mc were clearly visible following ambient carbonation at 95% RH and either diminished or not present at all other RH levels and under accelerated carbonation conditions. This further reinforces earlier observations that other phases apart from CH and C-S-H are susceptible to carbonation under ambient conditions, as discussed in section 4.2.1 of chapter four above.

### 6.3 Microstructure changes due to carbonation.

#### 6.3.1 SEM-BSE

BSE-SEM images of selected exposed samples i.e., ambient, and accelerated carbonation (edge & core) after 28 days' exposure at different relative humidities (55%, 75% & 95%) were compared and shown in Figure 6.13-6.15. The most striking features observed in some samples were a network of micro-cracks developed during accelerated carbonation, as shown in Figure 6.12-6.15 and micrographs in Figure 6.16-6.18.

These were particularly prevalent in the carbonation fronts (edge) that experienced severe CO<sub>2</sub> attack. The micro-cracks appeared more where the pH indicator was colourless (pH < 9) corresponding to portlandite depletion and significant carbonation

of other phases i.e., C-S-H and AFt (as identified by TGA XRD & FTIR in the previous section). However, CEM I paste showed some CH depletion but not complete consumption and showed fewer micro-cracks (Figure 6.13 & 6.14). These specimens differed from both binary and ternary blends, where there was complete loss of portlandite and thus cracking may have resulted from the decalcification of C-S-H and further condensation of the silicates [127, 167]. Although ettringite is known to cause small cracks due to sample dehydration during vacuum preparation [222], cracking was seen here prior to any vacuum preparation for SEM analysis. With micro-cracks severe and more visible in both binary & ternary binders following accelerated carbonation at 55% RH than higher relative humidities as shown in Figure 6.13-6.15 namely the samples showing greatest decalcification when analysed by FTIR and XRD, micro-cracks may be linked with shrinkage of C-S-H during decalcification and further silicate condensation.

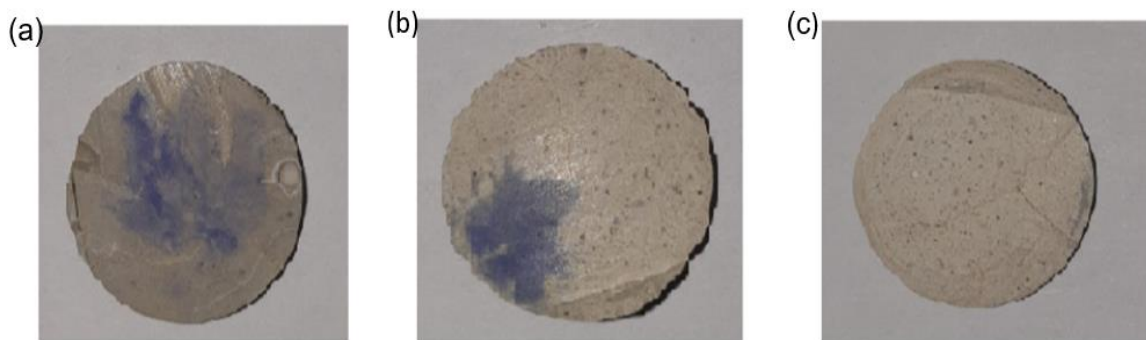


Figure 6.13: Micro-cracks developed during accelerated carbonation at 55% RH  
(a) CEM I (b) CS & (c) CS1L.

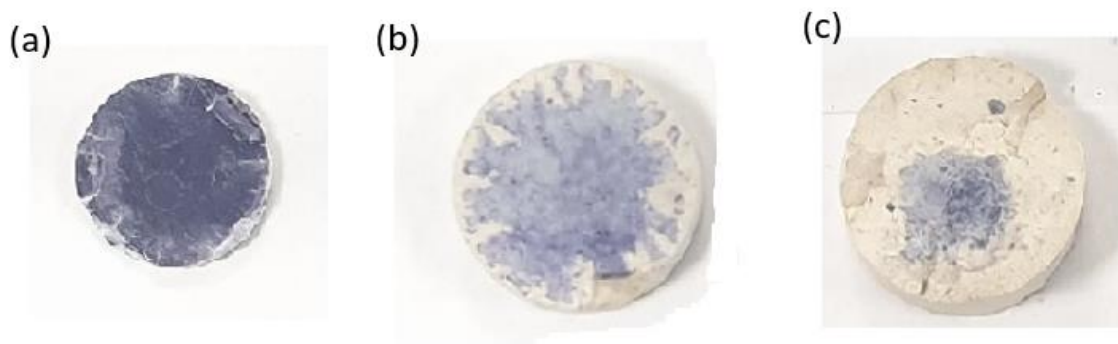


Figure 6.14: Micro-cracks developed during accelerated carbonation at 75% RH (a) CEM I (b) CS & (c) CS1L.

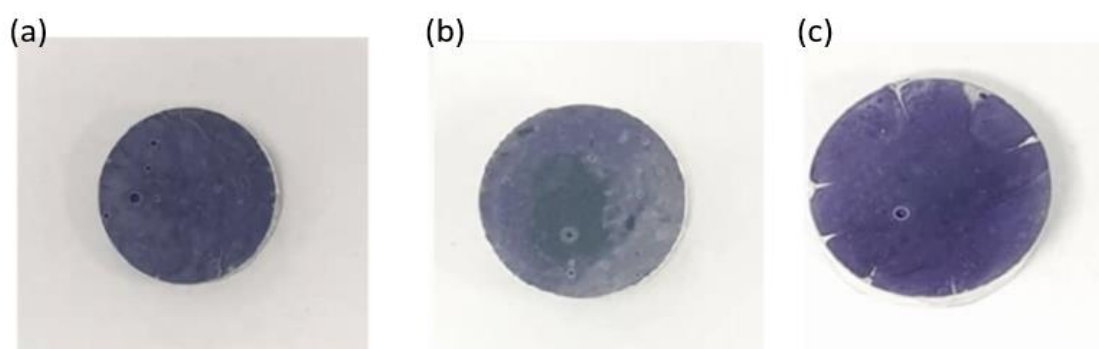


Figure 6.15: Micro-cracks developed during accelerated carbonation at 95% RH (a) CEM I (b) CS & (c) CS1L.

SEM-BSE micrographs showed a clear distinction between ambient and accelerated carbonated samples, as presented in Figure 6.16-6.18 below. This was also mentioned in [106, 185] and was attributed to changes in average atomic mass of the elements. In the case of CEM I, as shown in Figure 6.17a-g, following exposure at 95% relative humidity there was a significant reduction in anhydrous material comparable to other RH conditions, irrespective of the carbonation conditions, this suggest continuous hydration despite carbonation exposure due to reduced transport of  $\text{CO}_2$  through saturated pores and corroborated results from TGA & SEM-IA discussed earlier. Calcite was evident throughout the micrographs of samples exposed to accelerated carbonation at 55% but reduced after exposure at both 75% and 95% RH. This correlates with the MIP results presented in chapter five and reported in other studies [106, 223] due to carbonation of portlandite producing calcium carbonate, and with TGA and XRD results showing an increase in calcium carbonate contents after accelerated exposure. Both ambient and accelerated

exposure at 95% RH share similar features on the micrograph, which are due less ingress of CO<sub>2</sub>.

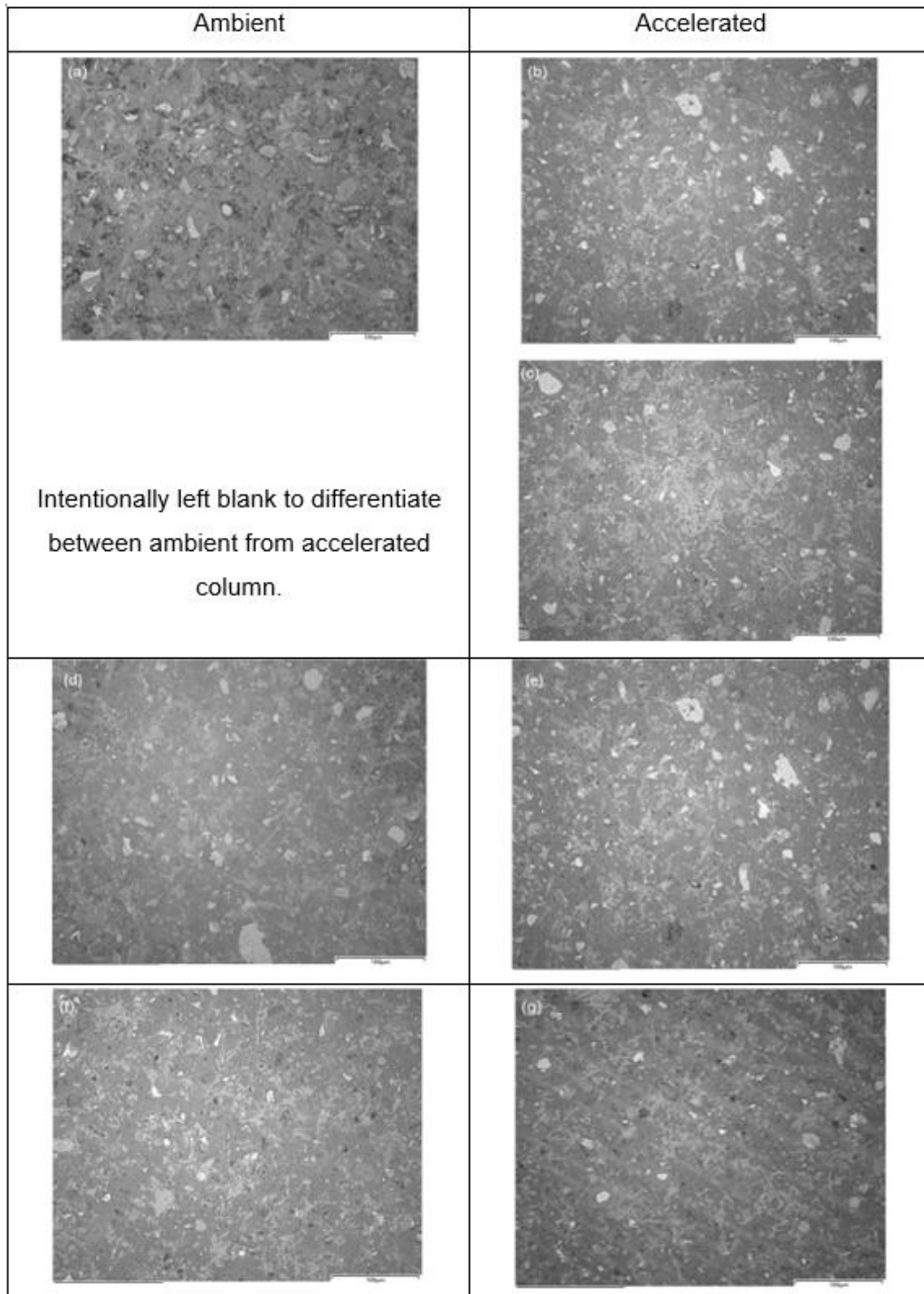


Figure 6.16: SEM-BSE Images of CEM I paste samples following (a) ambient carbonation at 55% RH (b) accelerated carbonation at 55% RH core (c) accelerated carbonation at 55% RH edge (d) ambient carbonation at 75% RH (e) accelerated carbonation at 75% RH (f) ambient carbonation at 95% RH (g) accelerated carbonation at 95% RH.

Figures 6.16a-g below, show micrographs from the binary blends, revealing relicts of clinker grains, portlandite and large grains of unreacted slag following both ambient carbonation and the core of the accelerated carbonation specimen. Accelerated carbonation appears to show increased porosity compared to ambient exposure at both 55% and 75% RH, especially with whole (b), core (d) and edge (e) in Figure 6.17. This is as a result of C-S-H carbonation precipitating metastable calcium carbonates as opposed to CH that form calcite and corroborates TGA, XRD and FTIR results in section 6.2 above.

Noticeable cracks visible in the micrographs following accelerated carbonation exposure at both 55% and 75% RH for both composite binders are known to occur due to shrinkage upon C-S-H carbonation [192] and confirmed C-S-H decalcification observed with reducing Ca/Si ratio from the EDS analysis below. In blended binders, C-S-H are abundant with less CH thus metastable calcium carbonate is expected to be a major product during sample carbonation [106] as opposed to CEM I with significant CH. This agrees with TGA & XRD data for both binary and ternary system. However, it is important to note that additional carbon carbonates found on the micrograph in Figure 6.18 in the ternary blend are due to limestone addition.

Portlandite was rarely found in the carbonation front (edge) following carbonation at 55% and 75% RH (Figure 6.17 and 6.18) as expected due significant carbonation however, relicts of CH were found in core especially following carbonation at 75% RH, consistent with TGA, FTIR & XRD results.

Visually, there were no significant changes in the microstructures of both the binary and ternary binders following both ambient and accelerated carbonation at 95% relative humidity. Carbonation of these specimens was minimal, since the high humidity will have left the pores saturated.

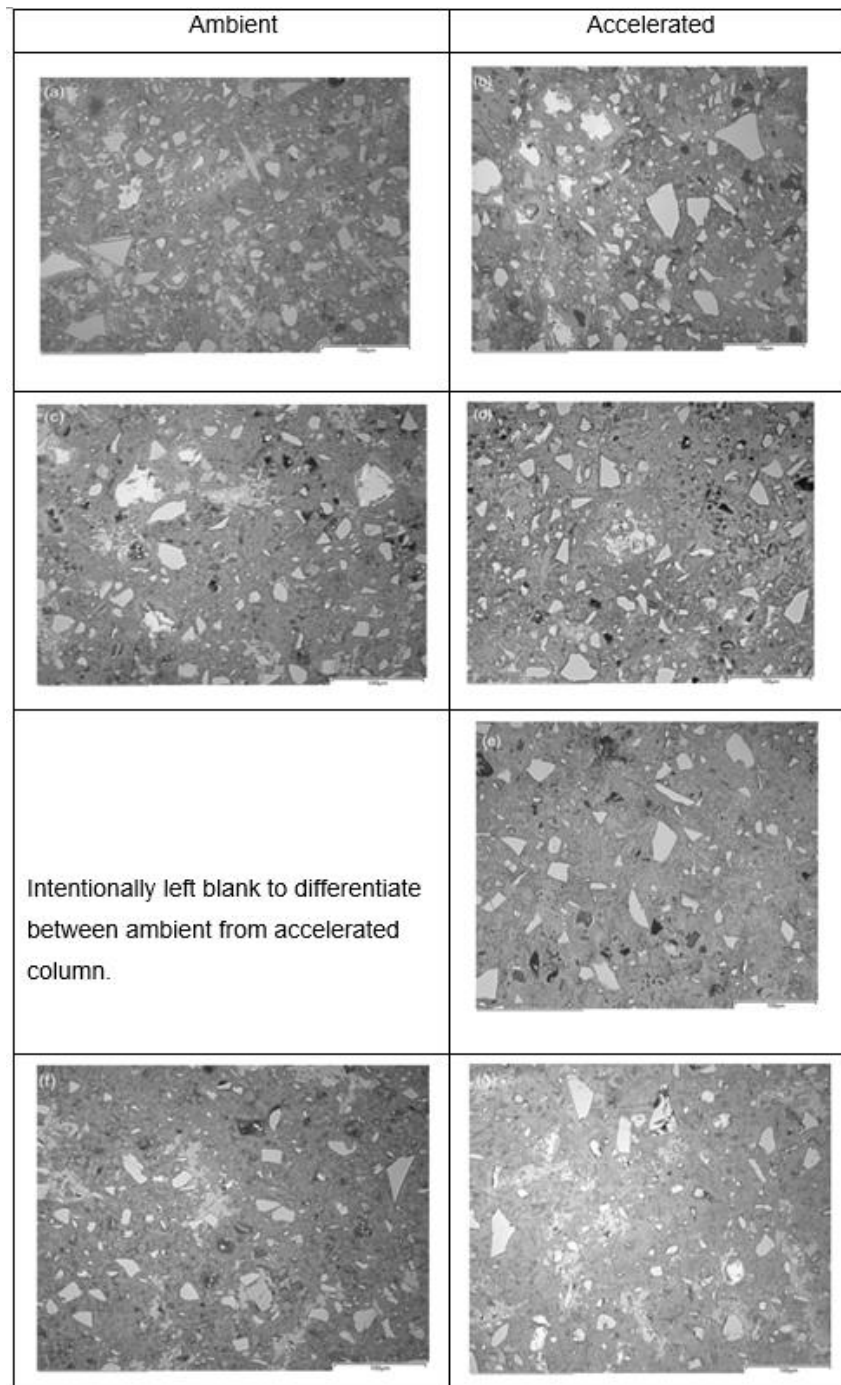


Figure 6.17: SEM-BSE Images of CS (binary) paste samples at (a) ambient carbonation at 55% RH (b) accelerated carbonation at 55% RH (c) ambient carbonation at 75% RH (d) accelerated carbonation at 75% RH core (e) accelerated carbonation at 75% RH edge (f) ambient carbonation at 95% RH (g) accelerated carbonation at 95% RH.

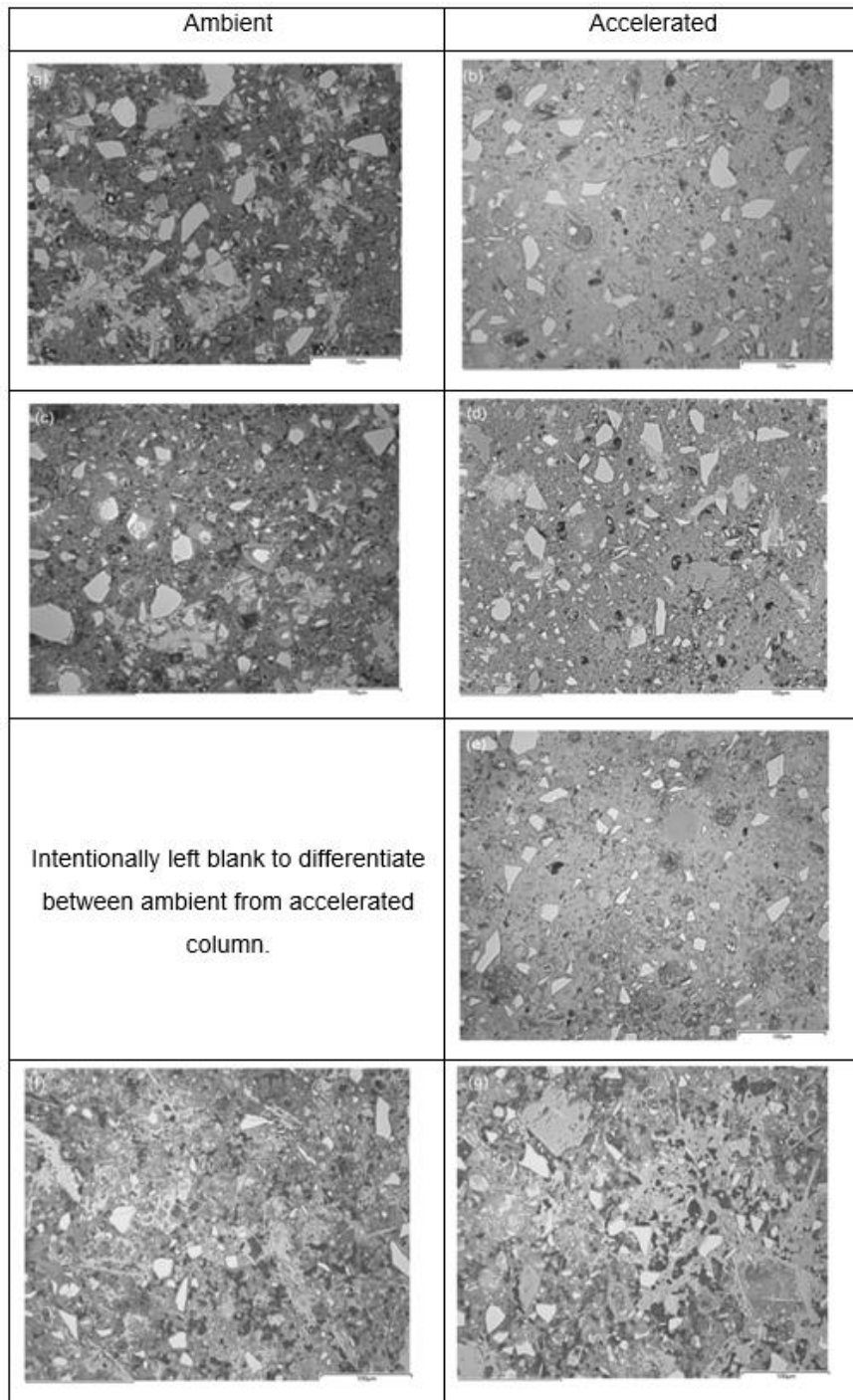


Figure 6.18: SEM-BSE Images of CS1L (Ternary paste) samples at (a) ambient carbonation at 55% RH (b) accelerated carbonation at 55% RH (c) ambient carbonation at 75% RH (d) accelerated carbonation at 75% RH core (e) accelerated carbonation at 75% RH edge (f) ambient carbonation at 95% RH (g) accelerated carbonation at 95%.

### 6.3.2 C-S-H composition by SEM-EDS

EDS point analysis was conducted to study C-S-H composition following both carbonation exposures. Inner product (Ip) C-S-H formed within the former boundaries of anhydrous grains and the outer product (Op) C-S-H formed in the space originally occupied by water in the paste [224, 225]. Both Ip and Op C-S-H have similar Ca/Si ratios for well-hydrated cements, at around 1.5-2.0 for CEM I [224]. Composite cements have lower Ca/Si ratios around 1.52 and 1.61 for slag cement and slag/limestone blend respectively [107, 131] and there can also be aluminium incorporation to give C-A-S-H, plus both ettringite and carboaluminates phases in the blend with Al/Si ratio of 0.13 and 0.11 reported for both slag cement and slag/limestone ternary blend [131]. The Ca/Si was expected to vary following accelerated carbonation due to heavy C-S-H decalcification, especially at the carbonation front (edge) considering the FTIR, TGA and XRD results. The scatter plots of both Ip and Op C-S-H are plotted in Figure 6.20-6.22 below.

Generally, the Al/Ca and Si/Ca ratios can be obtained by identifying the extremities of the scatter plot [121]. However, following accelerated carbonation, there was a large spread in the data points making it difficult to reported Ca/Si ratio correctly. This is likely due to significant carbonation of C-S-H for composite binders, especially at 55% RH as presented in Figure 6.20 below and carbonation fronts (edge) for all binder systems.

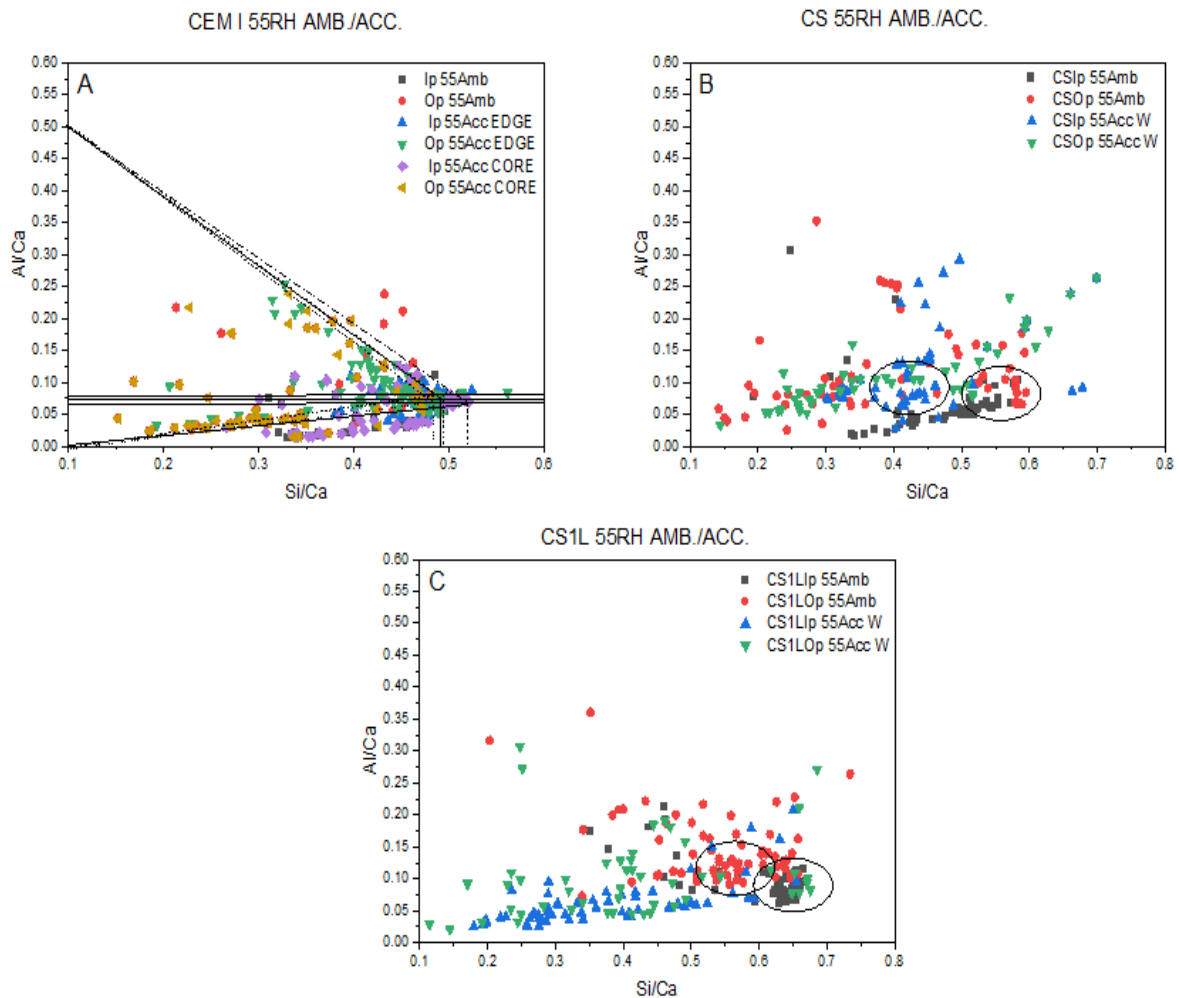


Figure 6.20: SEM-EDS point analysis of CEM I (A), CS (B) & CS1L(C) at 55% relative humidity.

This is consistent with observations obtained elsewhere with samples subjected to carbonation [185]. Despite this, there was not much significant difference between both Ip and Op C-S-H for all composite samples, as there was decalcification of both Ip and Op i.e., point slightly relocated toward higher Si/Ca ratio, and Ca/Si ranging from 1.36 to 2.0 for all the binders.

Following carbonation at 95% RH, samples following both accelerated and ambient carbonation showed no significant changes in Ca/Si ratio, as shown in Figure 6.22. This agrees with the results from other techniques showing minimal carbonation of these samples.

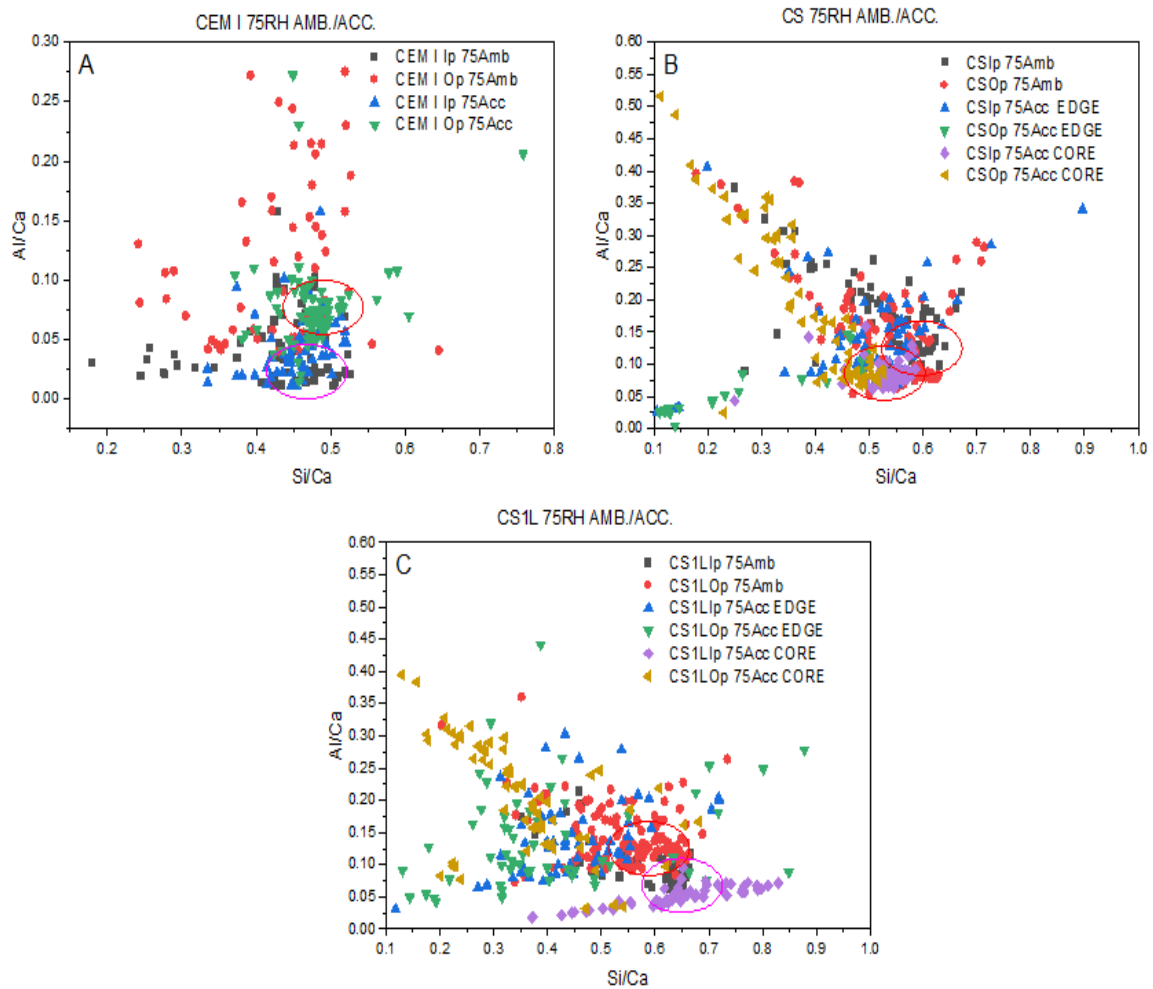


Figure 6.21: EDS point analysis of CEM I (A), CS (B) & CS1L(C) at 75% relative humidity.

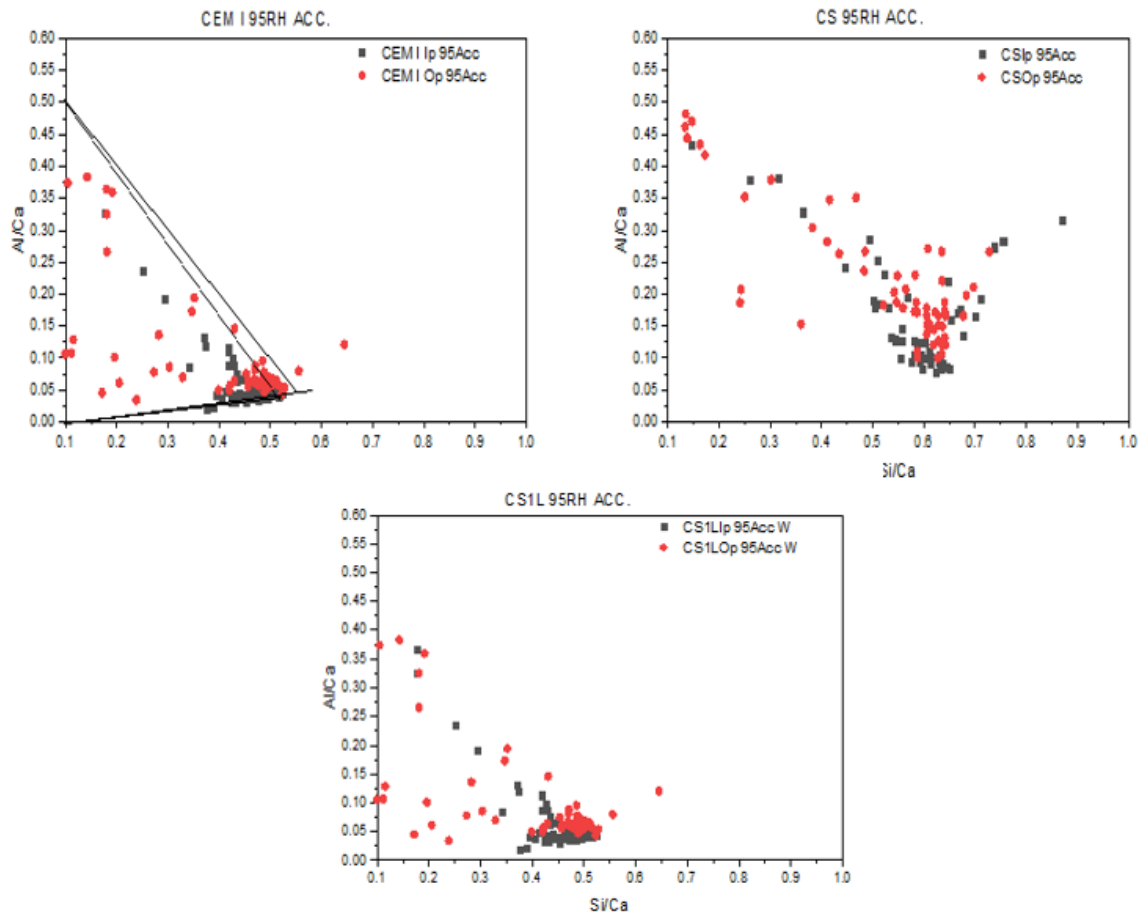
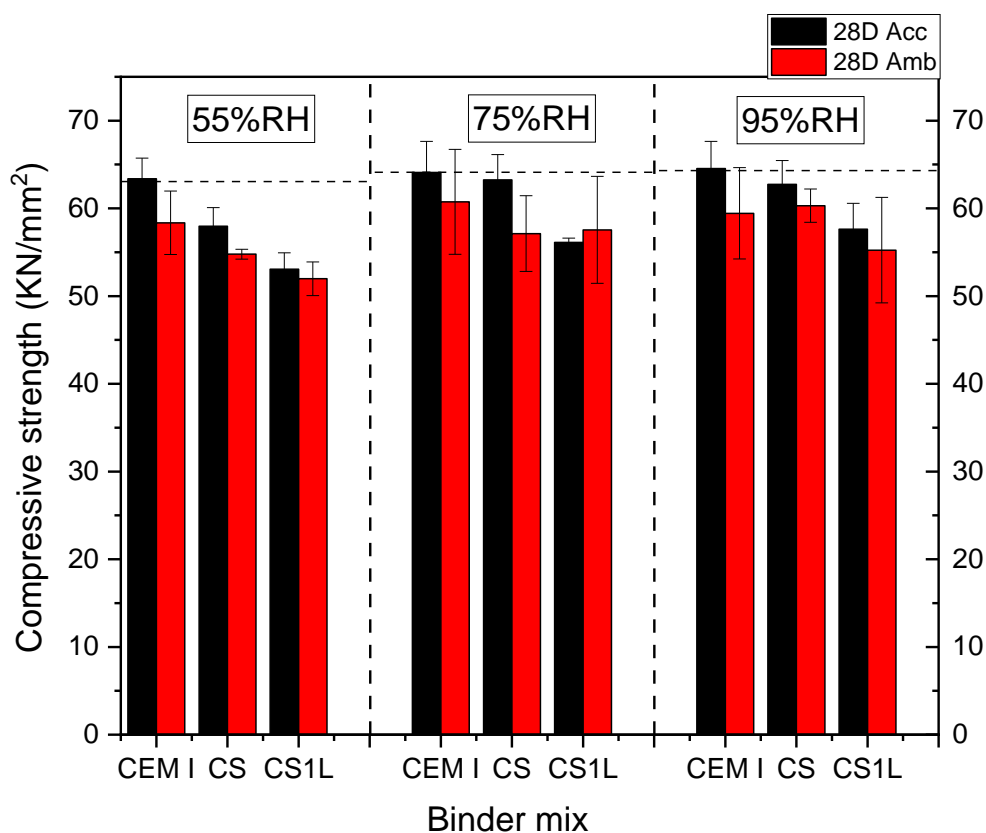


Figure 6.22: EDS point analysis of CEM I (A), CS (B) & CS1L(C) at 95% relative humidity.

#### 6.4 Compressive strength due to carbonation.

When comparing ambient and accelerated carbonation at same w/b, as presented in Figure 6.23 below, establishing reliable factors that cause changes in compressive strength may be challenging, especially when considering different testing parameters such RH, binder types and CO<sub>2</sub> exposure. Leemann et al. [108] have previously concluded that compressive strength during carbonation is influenced significantly by cement-specific effects and exposure conditions. These factors can be attributed to characteristics such as pore structure, hydration conditions, relative humidity, and CO<sub>2</sub> concentration. Generally, mortar samples subjected to accelerated carbonation exhibit slightly higher compressive strength compared to those exposed to ambient carbonation at all relative humidities across different mortar compositions, as presented in Figure 6.23 below. This is consistent with Chi et al. [226] findings showing similar results after 28-day carbonation and attributed to the CaCO<sub>3</sub> formed after accelerated carbonation occupying a greater volume than CH thereby reducing the

surface porosity of carbonated concrete. Drawing a connection to the earlier discussion in section 6.3.1, where SEM-BSE analysis was explored, it's worth noting that even though the CEM I sample exposed at 55% RH produces more calcium carbonate during accelerated carbonation, it does not achieve the highest compressive strength. However, the differences in compressive strength compared to RH levels of 75% and 95% are marginal, suggesting that accelerated carbonation might not have a significant impact on CEM I mortar at the various RH levels investigated in this study. This trend is also applicable to CEM I samples subjected to ambient carbonation, as depicted in Figure 6.23 below.

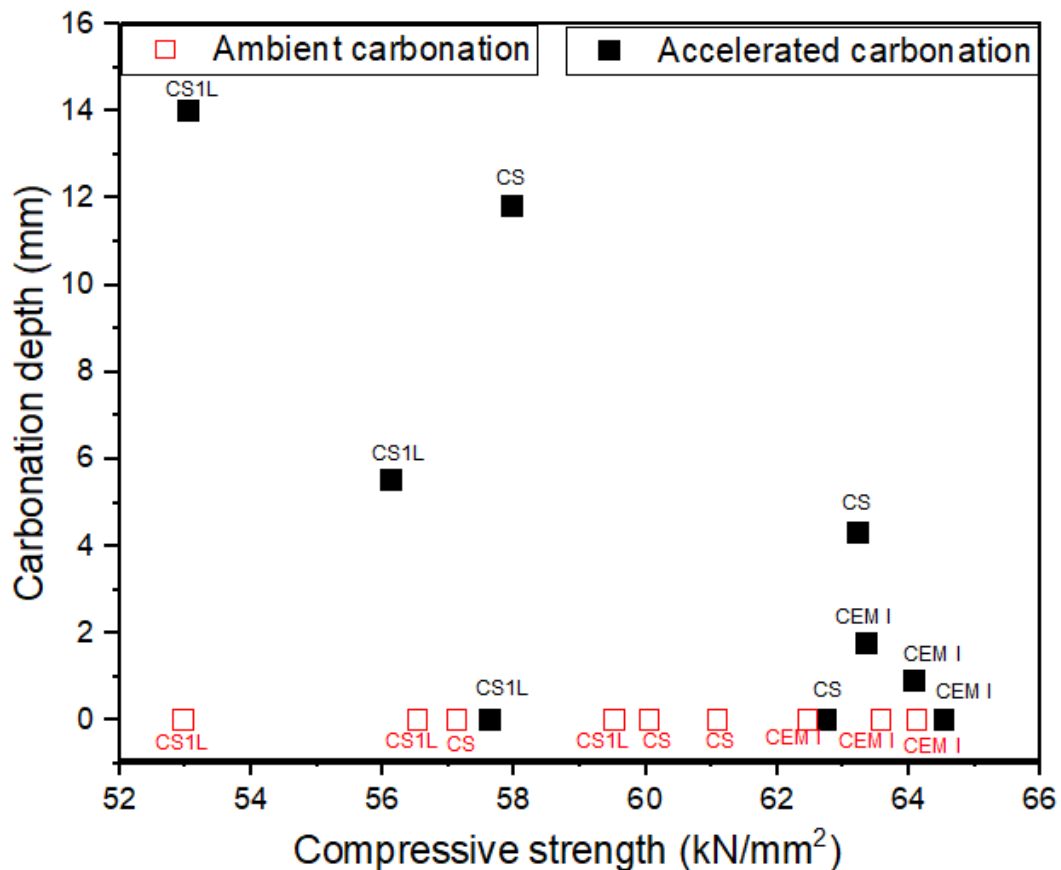


6.23: Compressive strength comparison for mortars at 55%, 75% and 95% relative humidities in both accelerated and ambient carbonation.

When considering both composite mortars (CS and CS1L), they had lower compressive strengths compared to CEM I at all RH conditions, either when subjected to accelerated or ambient carbonation. However, the differences were minimal for CS mortars at both 75% and 95% RH, suggesting that factors such as hydration, RH, porosity, and CO<sub>2</sub> ingress play a significant role in controlling the compressive strength

of composite mortars during accelerated carbonation. Analysing the hydration characteristics discussed in section 4.1 and 5.1, it becomes evident that hydration was continuous at both 75% and 95% relative humidity (RH) conditions. This continuous hydration likely contributed to enhanced compressive strength, irrespective of the ingress of CO<sub>2</sub> into the mortar's pores. Notably, the ingress of CO<sub>2</sub> was considerably lower for these RH conditions when compared to the 55% RH condition. This observation is further supported by the results from the MIP analysis presented in section 5.4, where it is apparent that the coarsening of the pores due to CSH carbonation is less pronounced at 75% RH compared to 55% RH. In the case of ambient exposure, the compressive strength values were slightly lower than those obtained in accelerated carbonation. However, this difference was minimal, with all composite mortar samples showing a decrease of less than 5 kN/mm<sup>2</sup>. This suggests that the influence of accelerated carbonation on the composite binders studied may not be significant.

Furthermore there appears to be an inverse relationship between carbonation depth and compressive strength, as evidenced with the scattered plot of carbonation depth measurements against compressive strengths presented in Figure 6.24 below and consistent with the findings of [96] that higher compressive strength led to decrease in carbonation depth. This also holds true for ambient exposure as both samples at higher RH shows higher compressive strength than lower RH i.e., 55% RH despite the pH indicator not showing any colour change. This observation is substantiated by both TGA and FTIR analyses, which confirmed carbonation during ambient exposures.



6.24: Carbonation depth against ambient & accelerated carbonation scatter diagram.

### 6.5 Summary

- Both CEM I and composite binders showed no increase in chemically bound water measurements during accelerated carbonation at 55% and 75% RH, however CBW remained consistent at 75% and 95% relative humidity during ambient carbonation but decreased at 55% RH, indicating reduced hydration at lower humidity levels.
- Concurrent hydration and carbonation were observed at 95% RH during accelerated and ambient carbonation, with a slight increase in clinker/slag reaction degree for all binders.
- Portlandite is vital for buffering alkalinity in binders and undergoes rapid carbonation when exposed to CO<sub>2</sub>, especially at 55% relative humidity and this led to a significant reduction in CH content in all binders except when exposed to

ambient carbonation. However, CEM I binders retained more CH due to higher clinker content in comparison to composite binders.

- Portlandite data obtained from both TGA and XRD was generally validated at +/- 2.5% with a few discrepancies attributed to experimental error.
- There are no significant changes in degree of hydration and slag reaction in composite binders during both accelerated and ambient carbonation especially relative humidity below saturation equilibrium > 80%; however, hydration is halted at lower relative humidities, and water released during carbonation does not seem to further hydration in non-carbonated areas.
- Carbonation initially led to the conversion of portlandite to calcium carbonate and once portlandite has been carbonated, then carbonation of other hydrated phases commences. Primarily, this involves decalcification of the C-S-H and typically led to metastable calcium carbonate (vaterite) formation as evident with XRD and FTIR.
- Despite, carbonation CH being the predominate with CEM I, CSH carbonation were also occurring simultaneous with CH as with lower  $\text{CaCO}_3$  decomposition temperatures observed with the composite binders at both the core and edge (carbonation front) suggesting amorphous calcium carbonates formed at lower temperature than Mode III at  $550^\circ\text{C}$  suggested in the literature.
- SEM-IA analysis indicated the presence of micro-cracks in samples exposed to accelerated carbonation, particularly in regions with severe  $\text{CO}_2$  exposure, signifying portlandite depletion and carbonation of C-S-H. This effect was more pronounced in binary and ternary binders at 55% RH.
- SEM-BSE micrographs revealed noticeable differences between samples exposed to ambient and accelerated carbonation. CEM I at 95% RH exhibited less anhydrous material, suggesting continuous hydration. However, calcite content decreased in samples at 75% and 95% RH during ambient carbonation due to limited portlandite carbonation.
- Accelerated carbonation increased porosity in composite binders due to C-S-H carbonation, leading to the precipitation of metastable calcium carbonates and crack formation. Portlandite was seldom detected at 55% and 75% RH in the carbonation front. EDS point analysis of C-S-H composition showed consistent Ca/Si ratios for well-hydrated cements but lower ratios for composite cements.

Carbonation led to significant data point variability, especially in composite binders, making Ca/Si ratio determination challenging. However, at 95% RH, no significant changes in Ca/Si ratios were observed following accelerated and ambient carbonation.

- In general, mortar samples subjected to accelerated carbonation exhibit higher compressive strength compared to those exposed to ambient carbonation, irrespective of relative humidity and mortar compositions. However, CEM I produced the highest compressive strength.
- Differences in relative humidity during accelerated carbonation (55%, 75% and 95% RH) for CEM I mortar show minimal impact on compressive strength, suggesting factors like hydration and CO<sub>2</sub> concentration may be the most important contributor to compressive strength and similar trend was observed in ambient carbonation, with CEM I mortars at 75% RH showing higher strength compared to others, with differences within the range of <5 kN/mm<sup>2</sup>.
- Composite mortars (CS and CS1L) consistently exhibited lower compressive strength compared to CEM I, with minimal differences at 75% and 95% RH, indicating the role of exposure RH, porosity, and CO<sub>2</sub> concentration in controlling strength. Pore structure coarsening in composite mortars due to decalcification of C-S-H and limited CH production contributes to lower strength, contrasting with CEM I under accelerated carbonation.
- An inverse relationship exists between carbonation depth and compressive strength as increase compressive strength led to decrease in carbonation depth.

## Chapter 7 Conclusions and further research.

### 7.1 Conclusions

The carbonation process is complex and controlled by several factors, including binder composition, relative humidity, and CO<sub>2</sub> concentration. Understanding these factors and their interplay is essential for correctly predicting carbonation's effects on the microstructure and durability of binders, especially composite cement. Comparing composite binders to Portland cement without considering its chemical composition and microstructure makes them more susceptible and under-performed during an accelerated aging test. This might have downplayed their potential and most importantly rank them according to the results obtained from accelerated test. However, it is essential to understand the underlying mechanisms of their carbonation behaviour to harness their vast potential in construction. Based on the objectives set out to achieve in the study, the key findings are summarised below:

The chemically bound water (CBW) being one of the key indicators to measure the continuous hydration in cement chemistry shows the levels in all samples remained consistent following ambient carbonation at 75% and 95% relative humidity (RH). However, there was a notable decrease in CBW at 55% RH, regardless of the water-binder ratio used in this study. This decline suggests a cessation of hydration at lower RH levels, coupled with carbonation of portlandite to form calcium carbonate.

Furthermore, in both CEM I and composite binders, CBW measurements did not exhibit an increase during accelerated and ambient carbonation at 55% RH. This implies that the water released from the carbonation of portlandite (CH), which is known to release water during the process, did not lead to further hydration in the core of the samples. This includes samples displaying such behaviour at the edge areas, which were fully carbonated at 55% and 75% RH.

However, simultaneous hydration and carbonation appear likely at 95% RH during both accelerated and ambient carbonation, as evidenced by an increase in CBW over 28 days. But this was due to condensation of water within the pores of the hardened cement paste. This observation is further supported by a slight increase in the degree of clinker/slag reaction for all binders at 95% RH. Portlandite, a key element in buffering alkalinity, undergoes rapid carbonation when exposed to CO<sub>2</sub>, making it a crucial factor in hydration and carbonation studies.

Additionally, the study identified a significant reduction in portlandite content during accelerated carbonation, especially at 55% RH, across all binders. This reduction was observed to a partial extent at other relative humidities and was not attributed to GGBS hydration in composite cement. CEM I binders consistently exhibited higher portlandite content compared to composite cement due to the greater presence of clinker and continuous hydration, particularly at higher relative humidities.

Regarding the phase assemblages of the samples under accelerated and ambient carbonation, distinct modes of calcium carbonate decomposition characterised by different temperature ranges. Ambient carbonation primarily led to the formation of amorphous calcium carbonates at 55% RH, whereas accelerated carbonation induced shifts in decomposition temperatures, suggesting the presence of various calcium carbonate polymorphs. Notably, lower decomposition temperatures than those majorly reported in literature, possibly due to the carbonation of C-S-H and the formation of amorphous calcium carbonate species. AFm and AFt phases decomposed to calcium carbonate at 55% and 75% RH during accelerated carbonation but remained stable at these humidities under ambient carbonation. Additionally, carbo-aluminate peaks were only observed at both 75% and 95% RH during ambient exposure and decompose at accelerated carbonation except 95% RH indicating susceptibility of phases other than CH and C-S-H.

Accelerated carbonation resulted in increased porosity and coarsening of the pores within composite binders in samples with extensive carbonation of C-S-H, leading to the precipitation of metastable calcium carbonates and subsequent crack formation. In contrast, decreases in total porosity and densification of pores were observed with CEM I. This is due to portlandite carbonation.

Regarding binder types, there was no significant difference between binary binder (CS) and 10% limestone addition (CS1L) in carbonation resistance and compressive strength despite differences in the slag volume. However, there were significant changes in compressive strength and carbonation between CS, CS1L, and CS2L, with CS and CS1L outperforming CS2L in all relative humidity conditions. When comparing ambient and accelerated carbonation of CEM I and composite at the same w/b ratio adopted in this study, factors like pore structure, hydration, and exposure RH significantly influence mortar compressive strength in both exposure conditions.

Overall, elevated CO<sub>2</sub> at 4% concentrations promoted aggressive carbonation, resulting in the densification of the microstructure in CEM I systems and coarsening of the pore structure in composite cement. Carbonation of portlandite results in the formation of calcium carbonate, primarily calcite. Carbonation of other hydrated phases follows, which led to vaterite formation through decalcification of the C-S-H established at lower relative humidity, i.e., 55% RH, during accelerated carbonation of composite cement. Carbonation is limited at high relative humidity levels, while lower levels led to more rapid carbonation. However, the standard accelerated carbonation conditions favour CEM I systems. The refined pore structures of composite cement can saturate at lower relative humidity, and elevated CO<sub>2</sub> levels cause rapid C-S-H decalcification and pore coarsening, as presented in the thesis. This finding is significant, as C-S-H is an essential component of the cement paste and plays a crucial role in the mechanical properties of concrete. C-S-H decalcification can impact the long-term durability of the concrete. Therefore, developing strategies to mitigate C-S-H decalcification in concrete structures is crucial if standard accelerated aging test will be acceptable for composite cement.

## 7.2 Further research

This study focused on the carbonation of composite cement under different humidities with the initial aim better understanding the accelerated aging technique used to determine the carbonation resistance, which favour CEM I system, and disadvantages composite cement without recourse to its peculiarity regarding hydration, chemical composition, and microstructure; meanwhile, future research can focus on the following:

- Understanding the durability and performance of composite cement under cyclic drying and wetting conditions can cause significant changes in the microstructure, hydration, and mechanical properties of composite cement, particularly concerning changes in CO<sub>2</sub>, relative humidity, and temperature.
- Investigating the effects of different environmental conditions on carbonation in the shelter and unsheltered environment, such as understanding how variations in temperature, humidity, and atmospheric CO<sub>2</sub> concentration affect the

carbonation process in composite cement. This would help better understand the environmental factors that impact the rate and extent of carbonation.

- Combined deteriorating mechanisms such as chloride, sulphate & leaching are essential to study, as such can occur concurrently in field conditions. Understanding the combined process is crucial to determine how each combined mechanism contributes to changes in composite cement's hydration, microstructural, and durability.
- Computational models can be developed to predict deterioration mechanisms and simulate the physical and chemical processes involved in multiple deterioration mechanisms.

## References

1. Transport, J.R.C.I.f.E.a., *Technology Map of the European Strategic Energy Technology Plan*, in 2014, Publications office of the European Union: Luxembourg.
2. Jones, G.H.a.C., *INVENTORY OF CARBON & ENERGY (ICE)*. 2008, University of Bath UK: Bath.
3. Scrivener, K.L. and R.J. Kirkpatrick, *Innovation in use and research on cementitious material*. Cement and Concrete Research, 2008. **38**(2): p. 128-136.
4. (CEMBUREAU), T.E.C.A., *The role of cement in the 2050 low carbon economy*. Brussels.
5. Zhijun Tan, G.Y., Yun Gao, Lieven Machiels, Els Bruneel and Geert De Schutte. *Experimental investigation of hydration of ternary blended cement paste*. in *14th International congress on the Chemistry of Cement (ICCC-2015)*. 2015. Beijing, PR China.
6. S. Tsivilisa, G. Batisa, E. Chaniotakisb, Gr. Grigoriadis, and D. Theodossisa, *Properties and behavior of limestone cement concrete and mortar*. Cement and Concrete Research, 2000. **30** p. 1679-1683.
7. Ramezaniapour, A.A., et al., *Influence of various amounts of limestone powder on performance of Portland limestone cement concretes*. Cement and Concrete Composites, 2009. **31**(10): p. 715-720.
8. Clayton, E.S.a.M., *Beyond Portland cement: Low-carbon alternatives*. 2022, The Institution of Structural Engineers UK: London.
9. Adu-Amankwah, S., Black, L and Zajac, M *Effect of Limestone Addition on the Early Age Hydration and Microstructure Evolution of composite slags cement*, in *14th International Congress on the Chemistry of Cement*. 2015: Beijing, China.
10. Voglis, N., et al., *Portland-limestone cements. Their properties and hydration compared to those of other composite cements*. Cement & Concrete Composites, 2005. **27**(2): p. 191-196.
11. Kolani, B., et al., *Hydration of slag-blended cements*. Cement and Concrete Composites, 2012. **34**(9): p. 1009-1018.

12. Papadakis, V.G., *Effect of supplementary cementing materials on concrete resistance against carbonation and chloride ingress*. Cement and Concrete Research, 2000. **30**(2): p. 291-299.
13. Morandea, A., M. Thiéry, and P. Dangla, *Investigation of the carbonation mechanism of CH and C-S-H in terms of kinetics, microstructure changes and moisture properties*. Cement and Concrete Research, 2014. **56**: p. 153-170.
14. Neville, A.M., *Properties of Concrete*. 5th ed. 2011, England: Pearson Education Limited.
15. Herfort, D., et al., *The chemistry of Portland cement clinker*. Advances in Cement Research, 2010. **22**(4): p. 187-194.
16. Bogue, R.H., *The chemistry of Portland cement*. 1947: Reinhold publishing corporation.
17. Robledo-Gutiérrez, M., et al., *Mineralogical Composition of Clinker as an Indicator of Sulfate Resistance: A Rietveld XRD/Takashima Approach*. Journal of the American Ceramic Society, 2013. **96**(11): p. 3637-3642.
18. U. T. Bezerra , A.E.M., D. M. A. Melo , M. A. F. Melo, and F. M. Lima, *A correlation between Bogue's equations and Taylor's procedure for the evaluation of crystalline phases in special class of portland oilwell cement clinker*. Journal of Cerâmica, 2011. **57**: p. 122-128.
19. Kurdowski, W., *Cement and Concrete Chemistry*. 2014, Poland: Springer.
20. Liu, F., 2014, *Early-age hydration studies of Portland cement*, in *Department of Civil and Environmental Engineering*. University of Louisville Louisville, Kentucky.
21. BROWN, P.W., *Early-Age Cement Hydration Reactions*, in *TRANSPORTATION RESEARCH RECORD 1284*, P.S.U. Department of Materials Science and Materials Research Laboratory, University Park, Pa. 16802., Editor.: Pennsylvania State University.
22. Taylor, H.F.W., *Cement chemistry*. 1997: Thomas Telford Publishing. -1.
23. Bullard, J.W., G.W. Scherer, and J.J. Thomas, *Time dependent driving forces and the kinetics of tricalcium silicate hydration*. Cement and Concrete Research, 2015. **74**: p. 26-34.

24. Scrivener, K.L., P. Juilland, and P.J.M. Monteiro, *Advances in understanding hydration of Portland cement*. Cement and Concrete Research, 2015. **78**: p. 38-56.
25. Sharpley, I., *The Effect of Hydration on the Microstructural Properties of Individual Phases of Ordinary Portland Cement*, in *Dept. Physics and Astronomy 2015*, University College London: London.
26. Eijk, R.J.v., *Hydration of cement mixtures containing contaminants*. 2001, University of Twente, The Netherland: Twente.
27. H.M. Jennings, J.J.T., D. Rothstein, and J.J. Chen, *Cements as Porous Materials*, in *Handbook of Porous Solids* 2002, Wiley-VCH, Weinheim,: Germany. p. .
28. Mindess, S., *Developments in the Formulation and Reinforcement of Concrete*. 2019: Woodhead Publishing.
29. Taylor, H.F.W., *Cement Chemistry*. Second ed. 1997, London: Thomas Telford
30. K.L. Scrivener, H.H.P., P.L. Pratt, and L.J. Parrott. *Analysis of Phases in Cement Paste Using Backscattered Electron Images*. in *Materials Research Society Symposium Proceedings*. 1987.
31. Buss, K., *TERNARY COMBINATION CONCRETES USING GGBS, FLY ASH & LIMESTONE* in *Department of Civil Engineering 2012*, University of Dundee: University of Dundee.
32. Ogirigbo, O.R. and L. Black, *Influence of slag composition and temperature on the hydration and microstructure of slag blended cements*. Construction and Building Materials, 2016. **126**: p. 496-507.
33. Lewis, D.W., *PROPERTIES AND USES OF IRON AND STEEL SLAGS*, in *National Institute for Transport and Road Research Sysposium*. 1992: South Africa.
34. Hammond, G. and C. Jones, *Inventory of carbon & energy: ICE*. Vol. 5. 2008: Sustainable Energy Research Team, Department of Mechanical Engineering ....
35. Darquennes, A., B. Espion, and S. Staquet, *How to assess the hydration of slag cement concretes?* Construction and Building Materials, 2013. **40**: p. 1012-1020.

36. Winnefeld, F., et al., *Influence of slag composition on the hydration of alkali-activated slags*. Journal of Sustainable Cement-Based Materials, 2014. **4**(2): p. 85-100.
37. Chen, W., *HYDRATION OF SLAG CEMENT Theory, Modeling and Application*. 2007, University of Twente, The Netherlands: Enschede,.
38. ŞENGÜL, Ö., *EFFECTS OF POZZOLANIC MATERIALS ON MECHANICAL PROPERTIES AND CHLORIDE DIFFUSIVITY OF CONCRETE*, in *Civil Engineering*. 2006, ISTANBUL TECHNICAL UNIVERSITY INSTITUTE OF SCIENCE AND TECHNOLOGY: Istanbul.
39. Lee, H.S., et al., *Analysis of the Optimum Usage of Slag for the Compressive Strength of Concrete*. Materials (Basel), 2015. **8**(3): p. 1213-1229.
40. M. Shariq , J.P.a.A.K.A., *STRENGTH DEVELOPMENT OF CEMENT MORTAR AND CONCRETE INCORPORATING GGBS*. ASIAN JOURNAL OF CIVIL ENGINEERING (BUILDING AND HOUSING), (2008) **9**(1 ): p. 61-74.
41. Oner, A., S.J.C. Akyuz, and c. composites, *An experimental study on optimum usage of GGBS for the compressive strength of concrete*. 2007. **29**(6): p. 505-514.
42. Daugherty, K.D.I.K.E., *A Review of Limestone Additions to Portland Cement and Concrete*. Cement & Concrete Composites, 1991. **13**: p. 165-170.
43. Bonavetti, V., et al., *Limestone filler cement in low w/c concrete: A rational use of energy*. Cement and Concrete Research, 2003. **33**(6): p. 865-871.
44. Tennis, P.D.T., M. D. A.; and. Weiss, W. J., *State-of-the-Art Report on Use of Limestone in Cements at Levels of up to 15%*. 2014, Portland Cement Association, Skokie, Illinois, USA: Illinois, USA.
45. Mohammadi, J. and W. South, *Effects of Intergrinding 12% Limestone with Cement on Properties of Cement and Mortar*. Journal of Advanced Concrete Technology, 2016. **14**(5): p. 215-228.
46. De Weerd, K., et al., *Hydration mechanisms of ternary Portland cements containing limestone powder and fly ash*. Cement and Concrete Research, 2011. **41**(3): p. 279-291.
47. Ramezani-pour, A.M., *Sulfate Resistance and Properties of Portland-Limestone Cements*, in *Department of Civil Engineering 2012*, University of Toronto: Toronto.

48. Adu-Amankwah, S., Black, L and Zajac, M *Effect of Limestone Addition on the Early Age Hydration and Microstructure Evolution of Composite Slag Cements*, in *The 14th International Congress on the Chemistry of Cement*. 2015 Beijing, China.
49. Turker, P.a.E., K. , *Effects of Limestone Addition on Microstructure and Hydration of cements.*, in *Proceedings of the International Conference on Cement Microscopy Ed 1999*, Jany, L. and Nisperos. p. pp. 265-283.
50. Tsvilis, S., et al., *An analysis of the properties of Portland limestone cements and concrete*. *Cement & Concrete Composites*, 2002. **24**(3-4): p. 371-378.
51. Bentz, D.P., et al., *Fine limestone additions to regulate setting in high volume fly ash mixtures*. 2012. **34**(1): p. 11-17.
52. Pipilikaki, P. and M. Katsioti, *Study of the hydration process of quaternary blended cements and durability of the produced mortars and concretes*. *Construction and Building Materials*, 2009. **23**(6): p. 2246-2250.
53. De Weerd, K., et al., *Hydration mechanisms of ternary Portland cements containing limestone powder and fly ash*. *Cement and Concrete Research*, 2011. **41**(3): p. 279-291.
54. Kim, S.-J., K.-H. Yang, and G.-D. Moon, *Hydration Characteristics of Low-Heat Cement Substituted by Fly Ash and Limestone Powder*. *Materials* 2015. **8**(9): p. 5847-5861.
55. Adu-Amankwah, S., et al., *Influence of limestone on the hydration of ternary slag cements*. *Cement and Concrete Research*, 2017. **100**: p. 96-109.
56. Zajac, M., et al., *Impact of microstructure on the performance of composite cements: Why higher total porosity can result in higher strength*. *Cement and Concrete Composites*, 2018. **90**: p. 178-192.
57. Avet, F., E. Boehm-Courjault, and K. Scrivener, *Investigation of C-A-S-H composition, morphology and density in Limestone Calcined Clay Cement (LC3)*. *Cement and Concrete Research*, 2019. **115**: p. 70-79.
58. Adu-Amankwah, S., et al., *Effect of sulfate additions on hydration and performance of ternary slag-limestone composite cements*. *Construction and Building Materials*, 2018. **164**: p. 451-462.
59. Avet, F. and K. Scrivener, *Investigation of the calcined kaolinite content on the hydration of Limestone Calcined Clay Cement (LC3)*. *Cement and Concrete Research*, 2018. **107**: p. 124-135.

60. Ghirci, M., S. Kenai, and M. Said-Mansour, *Mechanical properties and durability of mortar and concrete containing natural pozzolana and limestone blended cements*. Cement and Concrete Composites, 2007. **29**(7): p. 542-549.
61. Celik, K., et al., *High-volume natural volcanic pozzolan and limestone powder as partial replacements for portland cement in self-compacting and sustainable concrete*. Cement & Concrete Composites, 2014. **45**: p. 136-147.
62. Elgalhud, A.A., R.K. Dhir, and G. Ghataora, *Limestone addition effects on concrete porosity*. Cement and Concrete Composites, 2016. **72**: p. 222-234.
63. D.P. Bentz, *Replacement of "coarse" cement particles by inert fillers in low W/C ratio concretes II Experimental validation*. Cem. Concr. Res. , 2005 **35 (1)**: p. 185-188.
64. <EFFECT OF PORTLAND CEMENT WITH LIMESTONE ON THE PERFORMANCE OF CONCRETE FOR PAVEMENT AND BRIDGE DECKS.pdf>.
65. Thongsanitgarn, P., et al., *Effect of Limestone Powders on Compressive Strength and Setting Time of portland-Limestone Cement Pastes*. Materials for Environmental Protection and Energy Application, Pts 1 and 2, 2012. **343-344**: p. 322-+.
66. Kamile TOSUN, B.F., Bülent BARADAN İ. and Akin ALTUN, *Portland Limestone Cement Part I - Preparation of Cements in Digest 2009, December 2009* 2009. p. 1337-1355.
67. Diab, A.M., M. Abd Elmoaty, and A.A.J.A.E.J. Aly, *Long term study of mechanical properties, durability and environmental impact of limestone cement concrete*. 2016. **55**(2): p. 1465-1482.
68. Carrasco, M., et al., *Strength optimization of "tailor-made cement" with limestone filler and blast furnace slag*. 2005. **35**(7): p. 1324-1331.
69. Menéndez, G., V. Bonavetti, and E.F. Irassar, *Strength development of ternary blended cement with limestone filler and blast-furnace slag*. Cement and Concrete Composites, 2003. **25**(1): p. 61-67.
70. Hooton, R., M. Nokken, and M.J.r.p.f.S.L.C. Thomas, *Portland-limestone cement: state-of-the-art report and gap analysis for CSA A 3000*. 2007.
71. Emmanuel Rozière, Ahmed Loukili, and F. Cussigh, <A performance based approach for durability of concrete exposed to carbonation.pdf>. Construction and Building Materials. **23 (1)**: p. pp.190-199.

72. Hussain, S., D. Bhunia, and S.B. Singh, *An Experimental Investigation of Accelerated Carbonation on Properties of Concrete*. Engineering Journal- Thailand, 2016. **20**(2): p. 29-38.
73. Šavija, B. and M. Luković, *Carbonation of cement paste: Understanding, challenges, and opportunities*. Construction and Building Materials, 2016. **117**: p. 285-301.
74. Ekolu, S.O., *A review on effects of curing, sheltering, and CO<sub>2</sub> concentration upon natural carbonation of concrete*. Construction and Building Materials, 2016. **127**: p. 306-320.
75. Ge RHardus Koch, J.V., Neil Thompson, Oliver Moghissi, Melissa Gould and Joe Payer, *NACE, International measures of prevention, application, and economics of corrosion technologies study (IMPACT)*, G. Jacobson, Editor. 2016. p. 216.
76. Visser, J.H.M., *Influence of the carbon dioxide concentration on the resistance to carbonation of concrete*. Construction and Building Materials, 2014. **67**: p. 8-13.
77. Auroy, M., et al., *Comparison between natural and accelerated carbonation (3% CO<sub>2</sub>): Impact on mineralogy, microstructure, water retention and cracking*. Cement and Concrete Research, 2018. **109**: p. 64-80.
78. Visser, J.H.J.H., *Accelerated carbonation testing of mortar with supplementary cementing materials-Limitation of the acceleration due to drying*. 2012. **57**(3): p. 231-246.
79. Harrison, T.A., et al., *Experience of using the prTS 12390-12 accelerated carbonation test to assess the relative performance of concrete*. Magazine of Concrete Research, 2012. **64**(8): p. 737-747.
80. Goñi, S., M.T. Gaztañaga, and A. Guerrero, *Role of Cement Type on Carbonation Attack*. Journal of Materials Research, 2011. **17**(07): p. 1834-1842.
81. Sanjuán, M.Á., et al., *Effect of curing time on granulated blast-furnace slag cement mortars carbonation*. Cement and Concrete Composites, 2018. **90**: p. 257-265.
82. Sanjuan, M.A., C. Andrade, and M. Cheyrezy, *Concrete carbonation tests in natural and accelerated conditions*. Advances in Cement Research, 2003. **15**(4): p. 171-180.

83. A.Younsi , P.T., E. Rozière, A. Aït-Mokhtar, A. Loukili *Performance-based design and carbonation of concrete with high fly ash content*. Cement and Concrete Composites, Elsevier. **33 (10)**: p. 993 - 1000.
84. Bernal, S.A., et al., *Accelerated carbonation testing of alkali-activated slag/metakaolin blended concretes: effect of exposure conditions*. Materials and Structures, 2014. **48(3)**: p. 653-669.
85. Wang, X.Y., *Modeling of Hydration, Compressive Strength, and Carbonation of Portland-Limestone Cement (PLC) Concrete*. Materials (Basel), 2017. **10(2)**.
86. Czarnecki, L. and P. Woyciechowski, *Modelling of concrete carbonation; is it a process unlimited in time and restricted in space?* Bulletin of the Polish Academy of Sciences Technical Sciences, 2015. **63(1)**: p. 43-54.
87. Pacheco Torgal, F., et al., *An overview on concrete carbonation in the context of eco-efficient construction: Evaluation, use of SCMs and/or RAC*. Construction and Building Materials, 2012. **36**: p. 141-150.
88. YAO YAN, T.G., WANG LING, CUI SUPING, CAO YIN, *DIFFERENCE BETWEEN NATURAL AND ACCELERATED CARBONATION OF CONCRETE AT 2 % CO<sub>2</sub> AND 20 % CO<sub>2</sub>*. Romanian Journal of Materials, 2018. **48(1)**: p. 70-75.
89. Castellote, M., et al., *Chemical changes and phase analysis of OPC pastes carbonated at different CO<sub>2</sub> concentrations*. Materials and Structures/Materiaux et Constructions, 2009. **42(4)**: p. 515-525.
90. Dhir, R.K., et al., *Evaluation of Portland limestone cements for use in concrete construction*. Materials and Structures, 2007. **40(5)**: p. 459-473.
91. Russell, D., et al., *Effect of relative humidity and air permeability on prediction of the rate of carbonation of concrete*. Proceedings of the Institution of Civil Engineers-Structures and Buildings, 2001. **146(3)**: p. 319-326.
92. Chen, Y., P. Liu, and Z. Yu, *Effects of Environmental Factors on Concrete Carbonation Depth and Compressive Strength*. Materials (Basel), 2018. **11(11)**.
93. Leemann, A., et al., *Relation between carbonation resistance, mix design and exposure of mortar and concrete*. Cement & Concrete Composites, 2015. **62**: p. 33-43.
94. Osborne, G.J., *Durability of Portland blast-furnace slag cement concrete*. Cement and Concrete Composites 1991. **21**: p. 11-21.

95. Paweł Woliński<sup>1</sup>, P.W., Beata Jaworska, Grzegorz Adamczewski, Daniel Tokarski, Tomasz Grudniewski, Marta Chodyka, and Jerzy Antoni Nitychoruk, *The influence of the mineral additives on the carbonation of cement composites*, in *MATEC Web of Conferences 196, 04062 XXVII R-S-P Seminar 2018, Theoretical Foundation of Civil Engineering*. 2018.
96. Sulapha, P., et al., *Carbonation of concrete containing mineral admixtures*. *Journal of Materials in Civil Engineering*, 2003. **15**(2): p. 134-143.
97. Chang, C.F. and J.W. Chen, *The experimental investigation of concrete carbonation depth*. *Cement and Concrete Research*, 2006. **36**(9): p. 1760-1767.
98. Villain, G., M. Thiery, and G. Platret, *Measurement methods of carbonation profiles in concrete: Thermogravimetry, chemical analysis and gammadensimetry*. *Cement and Concrete Research*, 2007. **37**(8): p. 1182-1192.
99. Dong, B., et al., *Study on the Carbonation Behavior of Cement Mortar by Electrochemical Impedance Spectroscopy*. *Materials (Basel)*, 2014. **7**(1): p. 218-231.
100. Vagenas, N., A. Gatsouli, and C.J.T. Kontoyannis, *Quantitative analysis of synthetic calcium carbonate polymorphs using FT-IR spectroscopy*. 2003. **59**(4): p. 831-836.
101. Villarreal, A., et al., *Ultrasonic phase velocity of carbonated cement paste probes*. 2019. **154**: p. 129-134.
102. Galan, I., et al. *Neutron diffraction for studying the influence of the relative humidity on the carbonation process of cement pastes*. in *Journal of Physics: Conference Series*. 2011. IOP Publishing.
103. Castellote, M., et al., *Accelerated carbonation of cement pastes in situ monitored by neutron diffraction*. 2008. **38**(12): p. 1365-1373.
104. Dunster, A.J.A.i.C.R., *An investigation of the carbonation of cement paste using trimethylsilylation*. 1989. **2**(7): p. 99-106.
105. Morandeau, A., M. Thiéry, and P. Dangla, *Impact of accelerated carbonation on OPC cement paste blended with fly ash*. *Cement and Concrete Research*, 2015. **67**: p. 226-236.
106. Shah, V., et al., *Changes in in microstructure characteristics of cement paste on carbonation*. *Cement and Concrete Research*, 2018. **109**: p. 184-197.

107. Julia Herterich, B., L. and Richardson, I. *Microstructure and Phase Assemblage of Low-Clinker Cements during Early Stages of Carbonation*. in *The 14th International Congress on the Chemistry of Cement (ICCC 2015)*. 2015. Beijing, China.
108. Leemann, A. and F. Moro, *Carbonation of concrete: the role of CO<sub>2</sub> concentration, relative humidity and CO<sub>2</sub> buffer capacity*. *Materials and Structures*, 2016. **50**(1).
109. Shi, Z.G., et al., *Experimental studies and thermodynamic modeling of the carbonation of Portland cement, metakaolin and limestone mortars*. *Cement and Concrete Research*, 2016. **88**: p. 60-72.
110. Lauch, K.-S., V. Dieryck, and V. Pollet, *The use of ternary cements to reduce the environmental impact of concrete*. *RILEM Technical Letters*, 2016. **1**.
111. Khan, M.S.H., Q.D. Nguyen, and A. Castel, *Performance of limestone calcined clay blended cement-based concrete against carbonation*. *Advances in Cement Research*, 2020. **32**(11): p. 481-491.
112. Lothenbach, B. and M. Zajac, *Application of thermodynamic modelling to hydrated cements*. *Cement and Concrete Research*, 2019. **123**.
113. Bostancı, Ş.C., M. Limbachiya, and H. Kew, *Portland slag and composites cement concretes: engineering and durability properties*. *Journal of Cleaner Production*, 2016. **112**: p. 542-552.
114. Lin, R.-S., et al., *Experimental studies on hydration–strength–durability of limestone-cement-calcined Hwangtoh clay ternary composite*. *Construction and Building Materials*, 2021. **269**.
115. Adu-Amankwah, S., S. Rahmon, and L. Black, *From composition to the microstructure and durability of limestone ternary blended cements: A systematic review*. 2022. **34**(5): p. 206-224.
116. C.L.Page, V.T.N.a., *EFFECTS OF CARBONATION ON PORE STRUCTURE AND DIFFUSIONAL PROPERTIES OF HYDRATED CEMENT PASTES*. *Cement and Concrete Research*, 1997. **27**(7): p. 995-1007.
117. Paulo H.R. Borges, J.O.C., Neil B. Milestone, Cyril J. Lynsdale, Roger E. Streatfield, *Carbonation of CH and C–S–H in composite cement pastes containing high amounts of BFS*. *Cement and Concrete Research* 2010. **40** p. 284–292.

118. Adu-Amankwah, S., S. Rahmon, and L. Black, *From composition to the microstructure and durability of limestone ternary blended cements: A systematic review*. *Advances in Cement Research*, 2022: p. 1-19.
119. Medjigbodo, G., et al., *Hydration, shrinkage, and durability of ternary binders containing Portland cement, limestone filler and metakaolin*. *Construction and Building Materials*, 2018. **183**: p. 114-126.
120. Gruyaert, E., P. Van den Heede, and N. De Belie, *Carbonation of slag concrete: Effect of the cement replacement level and curing on the carbonation coefficient – Effect of carbonation on the pore structure*. *Cement and Concrete Composites*, 2013. **35**(1): p. 39-48.
121. Scrivener, K., R. Snellings, and B. Lothenbach, *A practical guide to microstructural analysis of cementitious materials*. Vol. 540. 2016: Crc Press Boca Raton, FL, USA:.
122. Shah, V., et al., *Changes in microstructure characteristics of cement paste on carbonation*. 2018. **109**: p. 184-197.
123. Shamaki, M.Y., *The use of a UK Alum Water Treatment Sludge as a Supplementary Cementitious Material—Characteristics, Hydration and Performance*. 2021, University of Leeds.
124. Dhandapani, Y., et al., *Mechanical properties and durability performance of concretes with Limestone Calcined Clay Cement (LC3)*. *Cement and Concrete Research*, 2018. **107**: p. 136-151.
125. Githachuri, K.u. and M.G. Alexander, *Durability performance potential and strength of blended Portland limestone cement concrete*. *Cement and Concrete Composites*, 2013. **39**: p. 115-121.
126. Garbev, K., et al., *Structural Features of C<sub>2</sub>S/H(I) and Its Carbonation in Air? A Raman Spectroscopic Study. Part I: Fresh Phases*. *Journal of the American Ceramic Society*, 2007. **90**(3): p. 900-907.
127. Justnes, H., et al., *Microstructural changes of hydrated cement blended with fly ash upon carbonation*. 2020. **137**: p. 106192.
128. Hren, M., V. Bokan Bosiljkov, and A. Legat, *Effects of blended cements and carbonation on chloride-induced corrosion propagation*. *Cement and Concrete Research*, 2021. **145**.
129. Leemann, A., et al., *Carbonation resistance of mortar produced with alternative cements*. *Materials and Structures*, 2018. **51**(5).

130. Marques, P.F., C. Chastre, and Â. Nunes, *Carbonation service life modelling of RC structures for concrete with Portland and blended cements*. Cement and Concrete Composites, 2013. **37**: p. 171-184.
131. Amankwah, S.A., *Relationship between Microstructure, Durability and Performance of CEMX Composite Cements*, in *School of Civil Engineering*. 2016, University of Leeds: Leeds.
132. Knop, Y., A. Peled, and R. Cohen, *Influences of limestone particle size distributions and contents on blended cement properties*. Construction and Building Materials, 2014. **71**: p. 26-34.
133. Mo, L., et al., *Accelerated carbonation and performance of concrete made with steel slag as binding materials and aggregates*. Cement and Concrete Composites, 2017. **83**: p. 138-145.
134. Branch, J., R. Epps, and D. Kosson, *The impact of carbonation on bulk and ITZ porosity in microconcrete materials with fly ash replacement*. Cement and Concrete Research, 2018. **103**: p. 170-178.
135. von Greve-Dierfeld, S., et al., *Understanding the carbonation of concrete with supplementary cementitious materials: a critical review by RILEM TC 281-CCC*. 2020. **53**(6): p. 1-34.
136. Zhang, J. and G.W. Scherer, *Comparison of methods for arresting hydration of cement*. Cement Concr Res, 2011. **41**.
137. Winnefeld, F., A. Schöler, and B. Lothenbach, *Sample preparation*, in *A practical guide to microstructural analysis of cementitious materials*, K.L. Scrivener, R. Snellings, and B. Lothenbach, Editors. 2016, CRC Press: Boca Raton.
138. Snellings, R., et al., *Report of TC 238-SCM: Hydration stoppage methods for phase assemblage studies of blended cements—results of a round robin test*. Mater Struct, 2018. **51**.
139. Jung, S.H., M.K. Lee, and B.H.J.A.M.J. Oh, *Measurement Device and Characteristics of Diffusion Coefficient of Carbon Dioxide in Concrete*. 2011. **108**(6).
140. Herterich, J., *Microstructure and phase assemblage of low-clinker cements during early stages of carbonation*. 2017, University of Leeds.
141. DURDZIŃSKI, P.T., *Hydration of multi-component cements containing cement clinker, slag, calcareous fly ash and limestone*, in *À LA FACULTÉ DES*

SCIENCES ET TECHNIQUES DE L'INGÉNIEUR. 2016, ÉCOLE POLYTECHNIQUE FÉDÉRALE DE LAUSANNE: Lausanne Switzerland.

142. Lo, Y. and H.M. Lee, *Curing effects on carbonation of concrete using a phenolphthalein indicator and Fourier-transform infrared spectroscopy*. Building and Environment, 2002. **37**(5): p. 507-514.
143. Kocaba, V., et al., *Methods for determination of degree of reaction of slag in blended cement pastes*. 2012. **42**(3): p. 511-525.
144. Zajac, M., et al., *Effect of carbonated cement paste on composite cement hydration and performance*. 2020. **134**: p. 106090.
145. Bougara, A., et al., *Reactivity and performance of blastfurnace slags of differing origin*. 2010. **32**(4): p. 319-324.
146. Shafiq, N.J.K.J.o.c.e., *Degree of hydration and compressive strength of conditioned samples made of normal and blended cement system*. 2011. **15**: p. 1253-1257.
147. Patel, R.G., et al., *Influence of curing at different relative humidities upon compound reactions and porosity in Portland cement paste*. Materials and Structures, 1988. **21**(3): p. 192-197.
148. Wyrzykowski, M., P.J.C. Lura, and C. Research, *Effect of relative humidity decrease due to self-desiccation on the hydration kinetics of cement*. 2016. **85**: p. 75-81.
149. Snyder, K.A., D.P.J.C. Bentz, and c. research, *Suspended hydration and loss of freezable water in cement pastes exposed to 90% relative humidity*. 2004. **34**(11): p. 2045-2056.
150. <*Influence of initial curing on the properties of concrete containing limestone blended cement.pdf*>.
151. Suraneni, P., et al., *New insights into the hydration of slag in alkaline media using a micro-reactor approach*. 2016. **79**: p. 209-216.
152. Kumar, A., et al., *A comparison of intergrinding and blending limestone on reaction and strength evolution in cementitious materials*. 2013. **43**: p. 428-435.
153. Adu-Amankwah, S., et al., *Influence of limestone on the hydration of ternary slag cements*. 2017. **100**: p. 96-109.
154. Scrivener, K.L., et al., *TC 238-SCM: hydration and microstructure of concrete with SCMs: State of the art on methods to determine degree of reaction of SCMs*. 2015. **48**: p. 835-862.

155. Shah, V., et al., *Influence of cement replacement by limestone calcined clay pozzolan on the engineering properties of mortar and concrete*. 2020. **32**(3): p. 101-111.
156. Yu, Q., B. Guo, and C.J.M. Li, *Effects of CO<sub>2</sub> Concentration and the Uptake on Carbonation of Cement-Based Materials*. 2022. **15**(18): p. 6445.
157. Zhang, Y., O.J.C. Çopuroğlu, and C. Composites, *The role of hydrotalcite-like phase and monosulfate in slag cement paste during atmospheric and accelerated carbonation*. 2022. **132**: p. 104642.
158. Damidot, D., et al., *Thermodynamics and cement science*. Cement and Concrete Research, 2011. **41**(7): p. 679-695.
159. Steiner, S., et al., *Effect of relative humidity on the carbonation rate of portlandite, calcium silicate hydrates and ettringite*. 2020. **135**: p. 106116.
160. Liu, X., et al., *Carbonation behavior of calcium silicate hydrate (CSH): Its potential for CO<sub>2</sub> capture*. 2022. **431**: p. 134243.
161. Thiery, M., et al., *Investigation of the carbonation front shape on cementitious materials: Effects of the chemical kinetics*. 2007. **37**(7): p. 1047-1058.
162. Groves, G.W., et al., *Progressive changes in the structure of hardened C3S cement pastes due to carbonation*. 1991. **74**(11): p. 2891-2896.
163. Zhang, Z., et al., *Transformation of amorphous calcium carbonate into aragonite*. Journal of Crystal Growth, 2012. **343**(1): p. 62-67.
164. Andersen, F.A. and L.J.A.C.S. Brecevic, *Infrared spectra of amorphous and crystalline calcium carbonate*. 1991. **45**(10): p. 1018-1024.
165. Vanoutrive, H., et al., *Carbonation of cement paste with GGBFS: Effect of curing duration, replacement level and CO<sub>2</sub> concentration on the reaction products and CO<sub>2</sub> buffer capacity*. 2022. **129**: p. 104449.
166. Slegers, P.A., P.G.J.C. Rouxhet, and C. Research, *Carbonation of the hydration products of tricalcium silicate*. 1976. **6**(3): p. 381-388.
167. Black, L., et al., *Structural features of C–S–H (I) and its carbonation in air—a Raman spectroscopic study. Part II: carbonated phases*. 2007. **90**(3): p. 908-917.
168. Li, J., et al., *Effects of Ca/Si ratio, aluminum and magnesium on the carbonation behavior of calcium silicate hydrate*. 2019. **12**(8): p. 1268.
169. Fernández-Carrasco, L., et al., *Infrared spectroscopy in the analysis of building and construction materials*. 2012. **510**.

170. Ylmen, R., U.J.I.J.o.C.S. Jäglid, and Materials, *Carbonation of Portland cement studied by diffuse reflection Fourier transform infrared spectroscopy*. 2013. **7**(2): p. 119-125.
171. Idowu, O.I., *Effect of improper curing on concrete properties that may affect concrete durability*. 2017, University of Leeds.
172. Shubbar, A.A., et al. *Investigating the influence of cement replacement by high volume of GGBS and PFA on the mechanical performance of cement mortar*. in *IOP Conference Series: Materials Science and Engineering*. 2019. IOP Publishing.
173. Mohamed, O.A., R. Al Khattab, and W.J.S.R. Al Hawat, *Effect of relative GGBS/fly contents and alkaline solution concentration on compressive strength development of geopolymer mortars subjected to sulfuric acid*. 2022. **12**(1): p. 5634.
174. Ekolu, S.J.C. and B. Materials, *A review on effects of curing, sheltering, and CO<sub>2</sub> concentration upon natural carbonation of concrete*. 2016. **127**: p. 306-320.
175. Van Gerven, T., et al., *Influence of carbonation and carbonation methods on leaching of metals from mortars*. 2004. **34**(1): p. 149-156.
176. Divsholi, B.S., T.Y.D. Lim, and S. Teng, *Durability Properties and Microstructure of Ground Granulated Blast Furnace Slag Cement Concrete*. *International Journal of Concrete Structures and Materials*, 2014. **8**(2): p. 157-164.
177. Zhang, D., Z. Ghoulah, and Y.J.J.o.C.U. Shao, *Review on carbonation curing of cement-based materials*. 2017. **21**: p. 119-131.
178. Vogler, N., et al., *Alternative pH-indicators for determination of carbonation depth on cement-based concretes*. 2020. **109**: p. 103565.
179. Cui, D., et al., *Use of a novel pH indicator extracted from petals to investigate the carbonation behavior in cementitious materials*. 2022. **134**: p. 104804.
180. Nilsson, P.G. and B.J.T.J.o.P.C. Lindman, *Water self-diffusion in nonionic surfactant solutions. Hydration and obstruction effects*. 1983. **87**(23): p. 4756-4761.
181. Shah, V., J. Mackechnie, and A.J.J.o.B.E. Scott, *Determination of carbonation resistance of concrete through a combination of cement content and tortuosity*. 2022. **60**: p. 105176.

182. Pinheiro, D.G.L., et al., *Physical and Chemical Effects in Blended Cement Pastes Elaborated with Calcined Clay and Nanosilica*. 2023. **16**(5): p. 1837.
183. Boualleg, S., et al., *The combined effect of the initial cure and the type of cement on the natural carbonation, the portlandite content, and nonevaporable water in blended cement*. 2017. **2017**.
184. Lo, Y., H.J.B. Lee, and environment, *Curing effects on carbonation of concrete using a phenolphthalein indicator and Fourier-transform infrared spectroscopy*. 2002. **37**(5): p. 507-514.
185. Soja, W., *Carbonation of low carbon binders*. 2019, EPFL.
186. Borges, P.H., et al., *Carbonation of CH and C–S–H in composite cement pastes containing high amounts of BFS*. 2010. **40**(2): p. 284-292.
187. Wu, B. and G. Ye, *Development of porosity of cement paste blended with supplementary cementitious materials after carbonation*. *Construction and Building Materials*, 2017. **145**: p. 52-61.
188. !!! INVALID CITATION !!! (111).
189. Frías, M. and S. Goñi, *Accelerated carbonation effect on behaviour of ternary Portland cements*. *Composites Part B: Engineering*, 2013. **48**: p. 122-128.
190. Leemann, A., et al., *Steady-state O<sub>2</sub> and CO<sub>2</sub> diffusion in carbonated mortars produced with blended cements*. 2017. **50**: p. 1-7.
191. Bier, T.A.J.M.O.P.L., *Influence of type of cement and curing on carbonation progress and pore structure of hydrated cement pastes*. 1986. **85**: p. 123.
192. Kangni-Foli, E., et al., *Carbonation of model cement pastes: The mineralogical origin of microstructural changes and shrinkage*. 2021. **144**: p. 106446.
193. Ba, M., et al., *Carbonation of magnesium oxysulfate cement and its influence on mechanical performance*. 2019. **223**: p. 1030-1037.
194. Leemann, A., et al., *Steady-state O<sub>2</sub> and CO<sub>2</sub> diffusion in carbonated mortars produced with blended cements*. 2017. **50**(6): p. 1-7.
195. Rao, N.V. and T. Meena. *A review on carbonation study in concrete*. in *IOP Conference Series: Materials Science and Engineering*. 2017. IOP Publishing.
196. Papadakis, V.G., C.G. Vayenas, and M.N.J.M.J. Fardis, *Fundamental modeling and experimental investigation of concrete carbonation*. 1991. **88**(4): p. 363-373.

197. Elsalamawy, M., A.R. Mohamed, and E.M.J.A.E.J. Kamal, *The role of relative humidity and cement type on carbonation resistance of concrete*. 2019. **58**(4): p. 1257-1264.
198. Silva, A., et al., *Statistical modelling of carbonation in reinforced concrete*. 2014. **50**: p. 73-81.
199. Parrott, L.J., *A review of carbonation in reinforced concrete*. 1987.
200. Hobbs, D.J.M.o.c.r., *Carbonation of concrete containing pfa*. 1988. **40**(143): p. 69-78.
201. Basheer, P., D. Russell, and G. Rankin, *40 Designs of Concrete to Resist Carbonation*. Vol. 1. 1999: NRC Research Press Ottawa, Canada.
202. Rivera, R.A., M.Á. Sanjuán, and D.A.J.S. Martín, *Granulated blast-furnace slag and coal fly ash ternary portland cements optimization*. 2020. **12**(14): p. 5783.
203. Scrivener, K., et al., *Impacting factors and properties of limestone calcined clay cements (LC3)*. 2018. **7**(1): p. 3-14.
204. Bucher, R., et al., *Service life of metakaolin-based concrete exposed to carbonation: Comparison with blended cement containing fly ash, blast furnace slag and limestone filler*. 2017. **99**: p. 18-29.
205. Wierig, H. *Longtime studies on the carbonation on concrete under normal outdoor exposure*. in *RILEM SEMINAR DURABILITY OF CONCRETE STRUCTURES UNDER NORMAL OUTDOOR EXPOSURE, 1984*. 1984.
206. Han-Seung, L., X.-Y.J.C. Wang, and B. Materials, *Evaluation of compressive strength development and carbonation depth of high volume slag-blended concrete*. 2016. **124**: p. 45-54.
207. Ye, X., et al., *Carbonation of cement paste under different pressures*. 2023. **370**: p. 130511.
208. Mo, L., et al., *Mechanical performance and microstructure of the calcium carbonate binders produced by carbonating steel slag paste under CO<sub>2</sub> curing*. 2016. **88**: p. 217-226.
209. Prem, P.R., B. Bharatkumar, and N.R.J.S. Iyer, *Influence of curing regimes on compressive strength of ultra high performance concrete*. 2013. **38**: p. 1421-1431.
210. Torgal, F.P., et al., *An overview on concrete carbonation in the context of eco-efficient construction: Evaluation, use of SCMs and/or RAC*. 2012. **36**: p. 141-150.

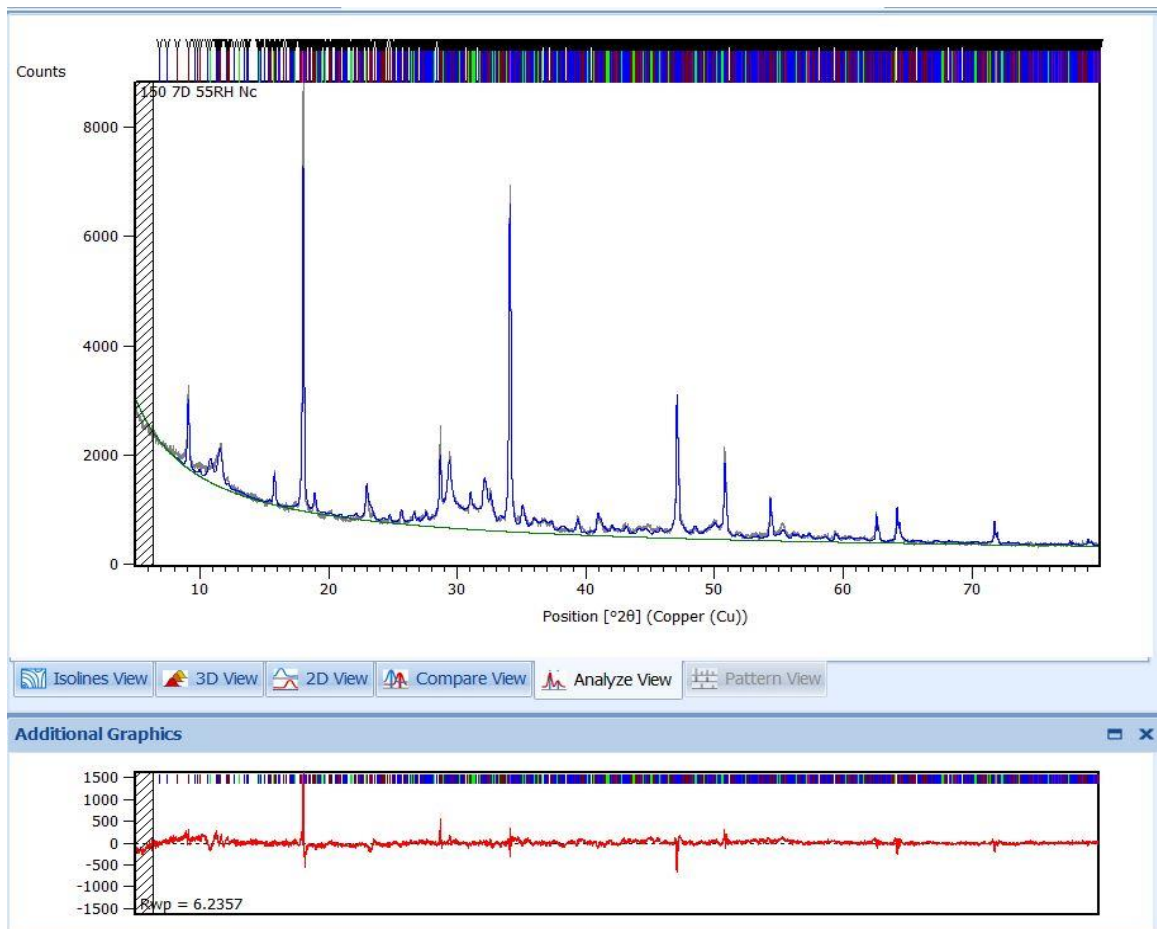
211. Tapas, M.J., et al. *Effect of Carbonation on Compressive Strength Development of High-Slag Mortars*. in *76th RILEM Annual Week 2022 and International Conference on Regeneration and Conservation of Structures*. 2022.
212. Lollini, F., et al., *Effects of portland cement replacement with limestone on the properties of hardened concrete*. 2014. **46**: p. 32-40.
213. Jia, Y., B. Aruhan, and P.J.M.o.C.R. Yan, *Natural and accelerated carbonation of concrete containing fly ash and GGBS after different initial curing period*. 2012. **64**(2): p. 143-150.
214. Bertin, M., et al. *Changes in microstructure and pore structure of low-clinker cementitious materials during early stages of carbonation*. in *Second International Conference on Concrete Sustainability (ICCS 16)*. 2016.
215. Dubina, E., et al., *Influence of water vapour and carbon dioxide on free lime during storage at 80 C, studied by Raman spectroscopy*. 2013. **111**: p. 299-303.
216. Lagerblad, B., *Carbon dioxide uptake during concrete life cycle: State of the art*. 2005: Swedish Cement and Concrete Research Institute Stockholm.
217. Morandea, A., et al., *Investigation of the carbonation mechanism of CH and CSH in terms of kinetics, microstructure changes and moisture properties*. 2014. **56**: p. 153-170.
218. Ashraf, W.J.C. and B. Materials, *Carbonation of cement-based materials: Challenges and opportunities*. 2016. **120**: p. 558-570.
219. Wang, X.-Y., H.-S.J.C. Lee, and B. Materials, *A model for predicting the carbonation depth of concrete containing low-calcium fly ash*. 2009. **23**(2): p. 725-733.
220. Bergold, S., et al., *Quantitative analysis of C–S–H in hydrating alite pastes by in-situ XRD*. 2013. **53**: p. 119-126.
221. Suda, Y., et al., *Phase Assemblage, Microstructure and Shrinkage of Cement Paste during Carbonation at Different Relative Humidities*. 2021. **19**(6): p. 687-699.
222. Cyr, M., et al., *Efficiency of mineral admixtures in mortars: Quantification of the physical and chemical effects of fine admixtures in relation with compressive strength*. 2006. **36**(2): p. 264-277.

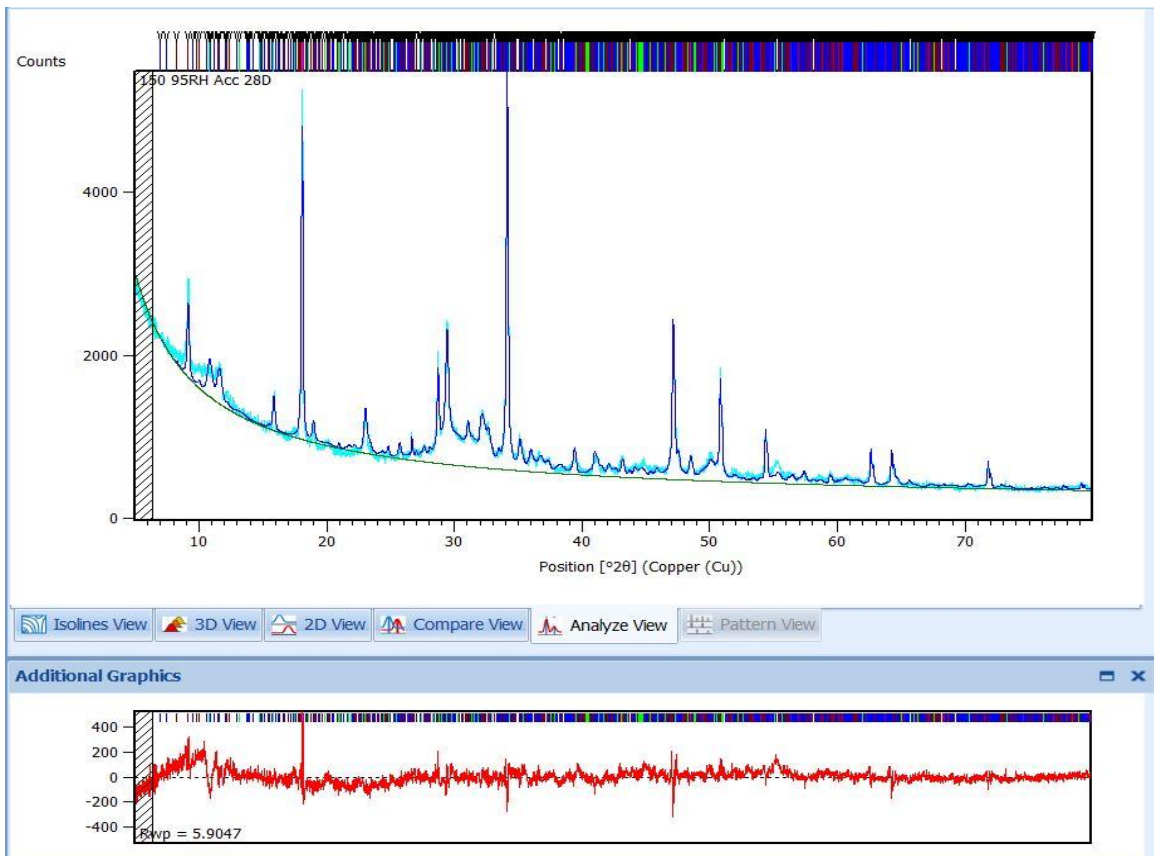
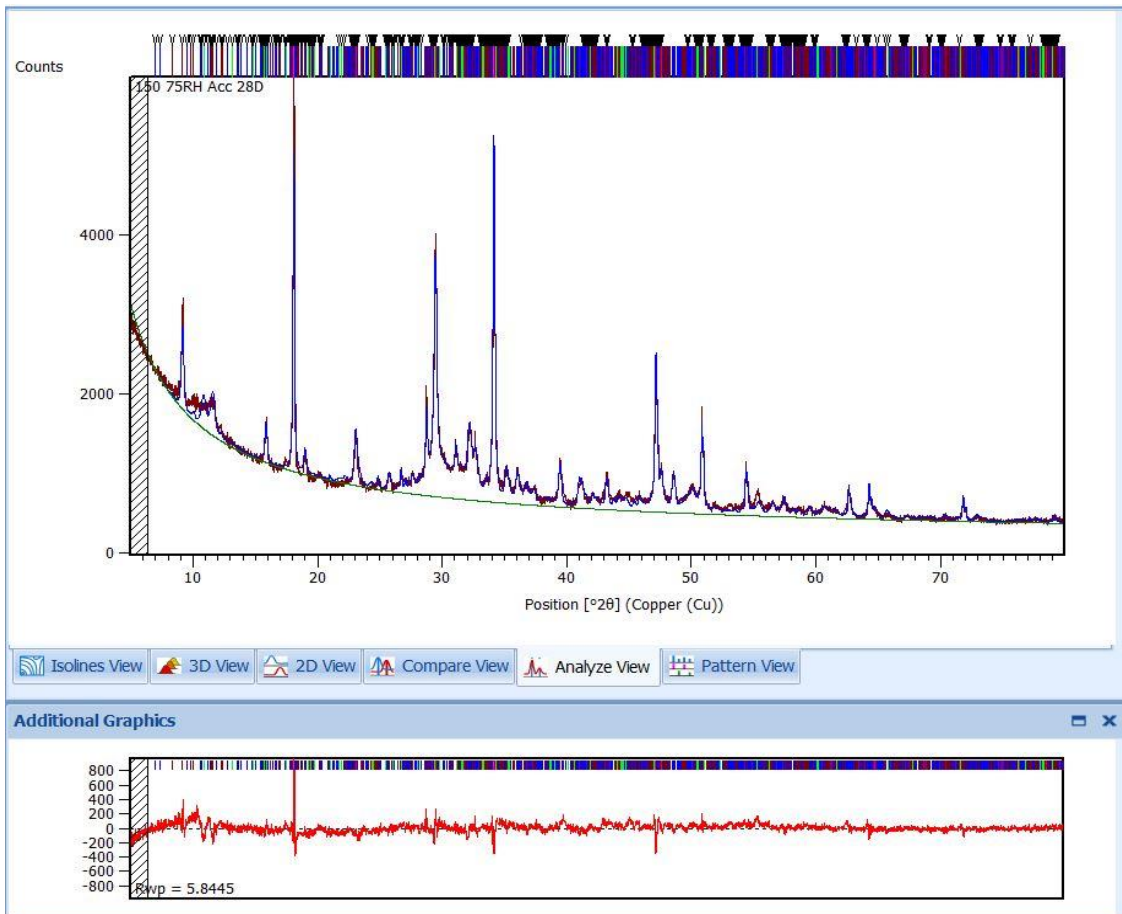
223. Li, R. and H.J.S. Ye, *Influence of Alkalis on Natural Carbonation of Limestone Calcined Clay Cement Pastes*. 2021. **13**(22): p. 12833.
224. Rossen, J. and K.J.M.C. Scrivener, *Optimization of SEM-EDS to determine the C–A–S–H composition in matured cement paste samples*. 2017. **123**: p. 294-306.
225. Richardson, I., G.J.C. Groves, and C. Research, *The incorporation of minor and trace elements into calcium silicate hydrate (C–S–H) gel in hardened cement pastes*. 1993. **23**(1): p. 131-138.
226. Chi, J.M., R. Huang, and C. Yang, *Effects of carbonation on mechanical properties and durability of concrete using accelerated testing method*. Journal of marine science and technology, 2002. **10**(1): p. 3.

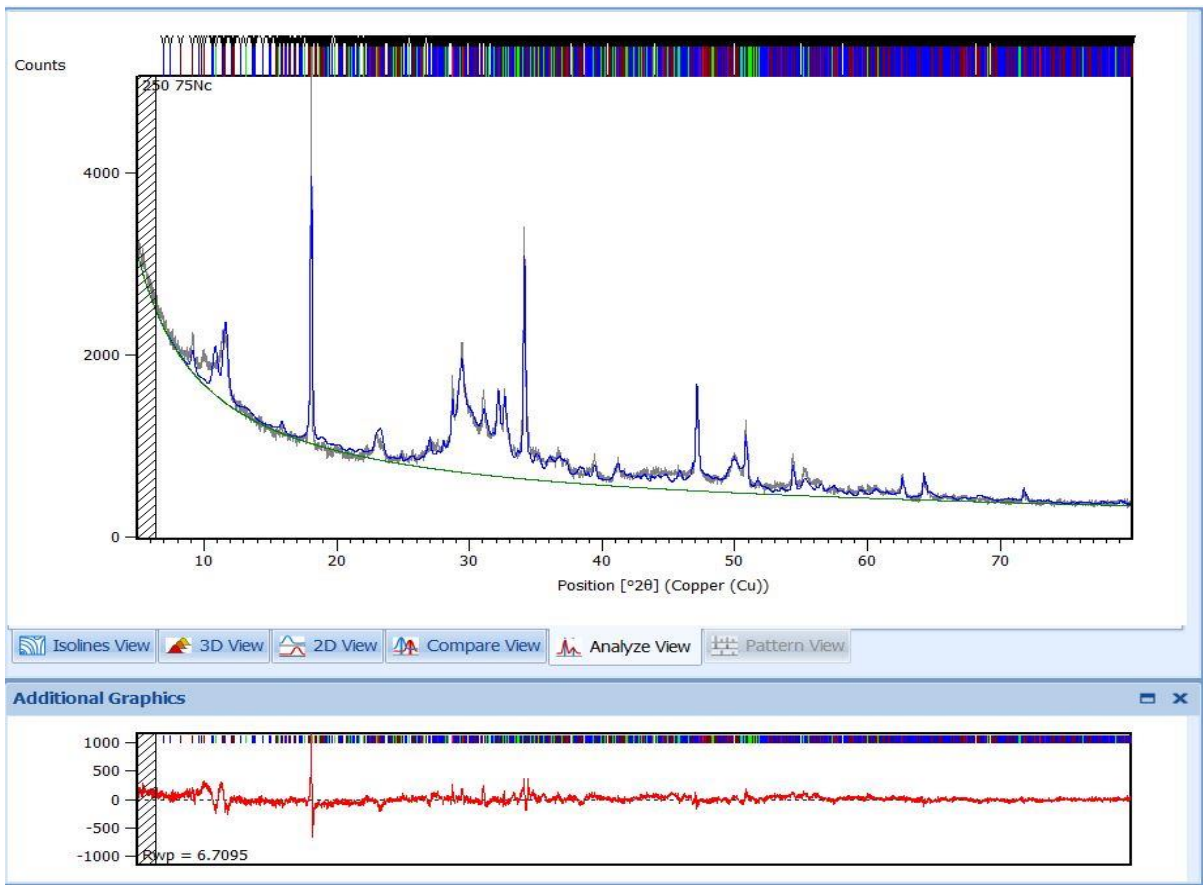
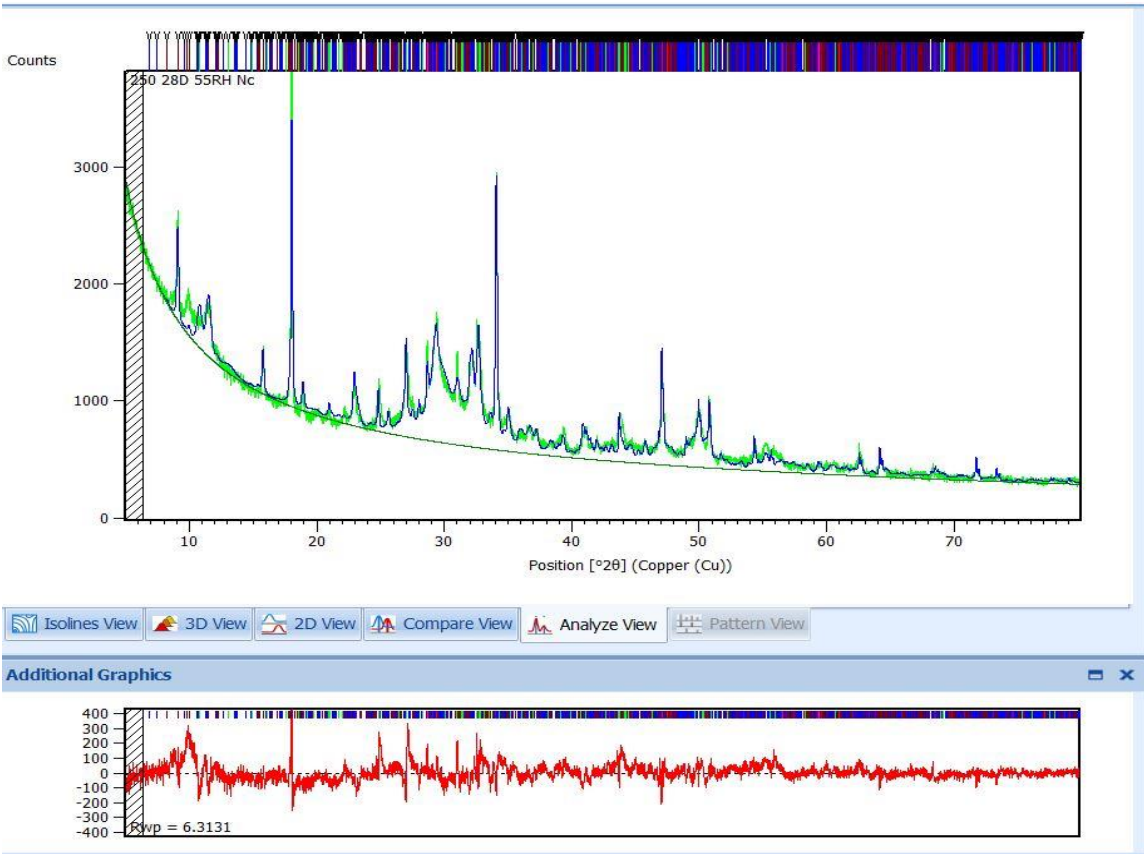
# Appendices

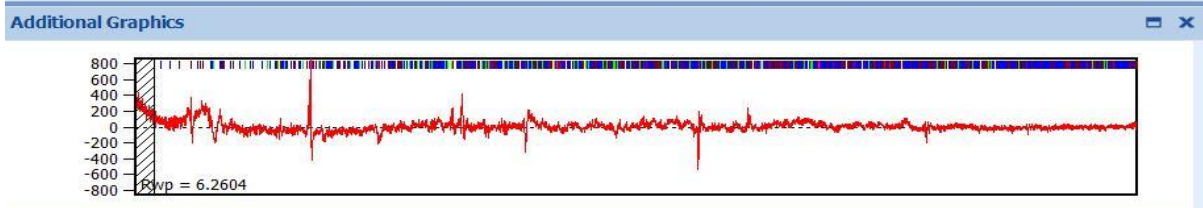
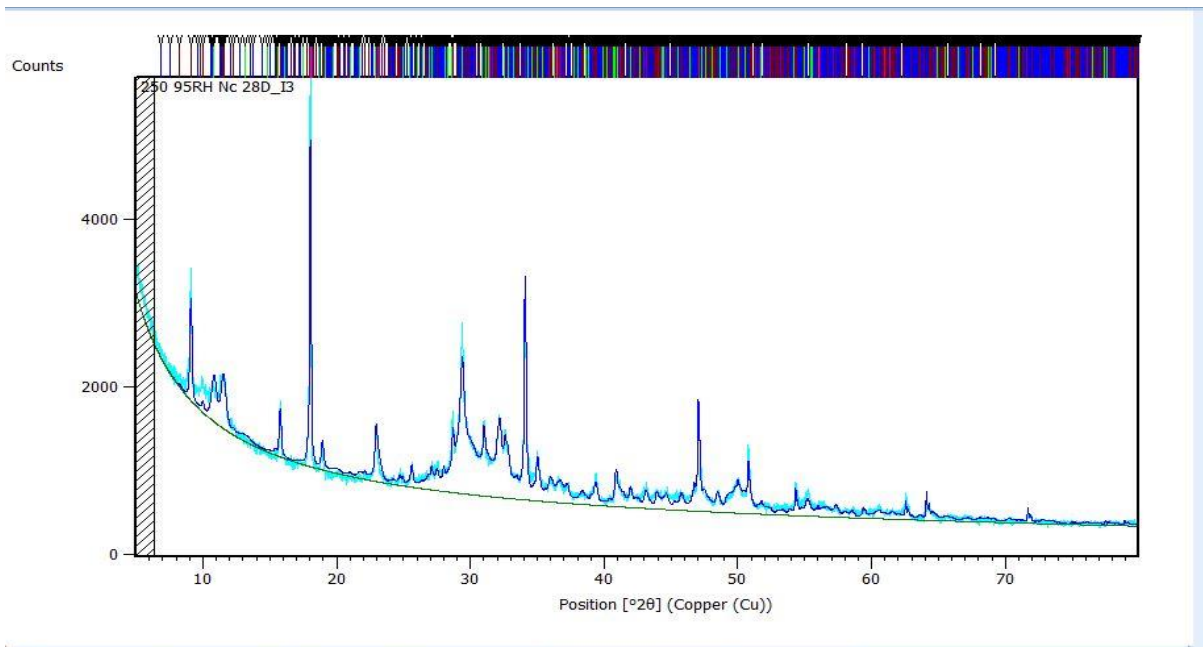
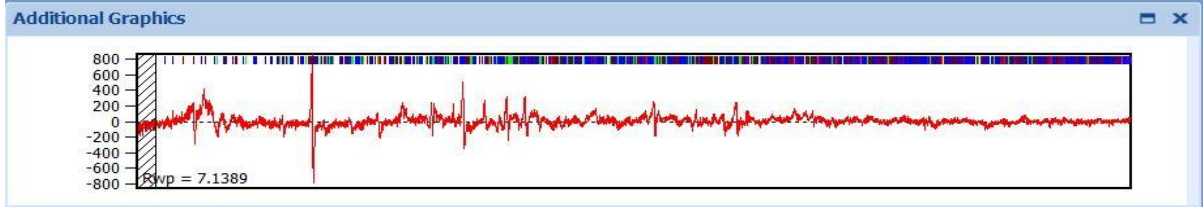
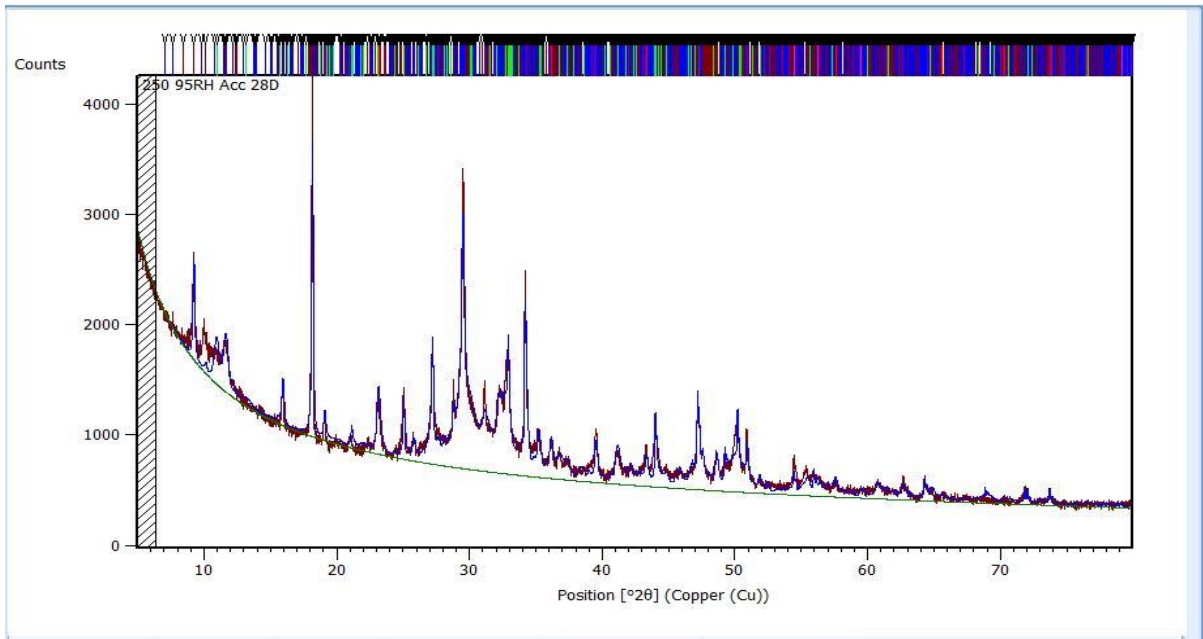
## A. Rietveld Refinement

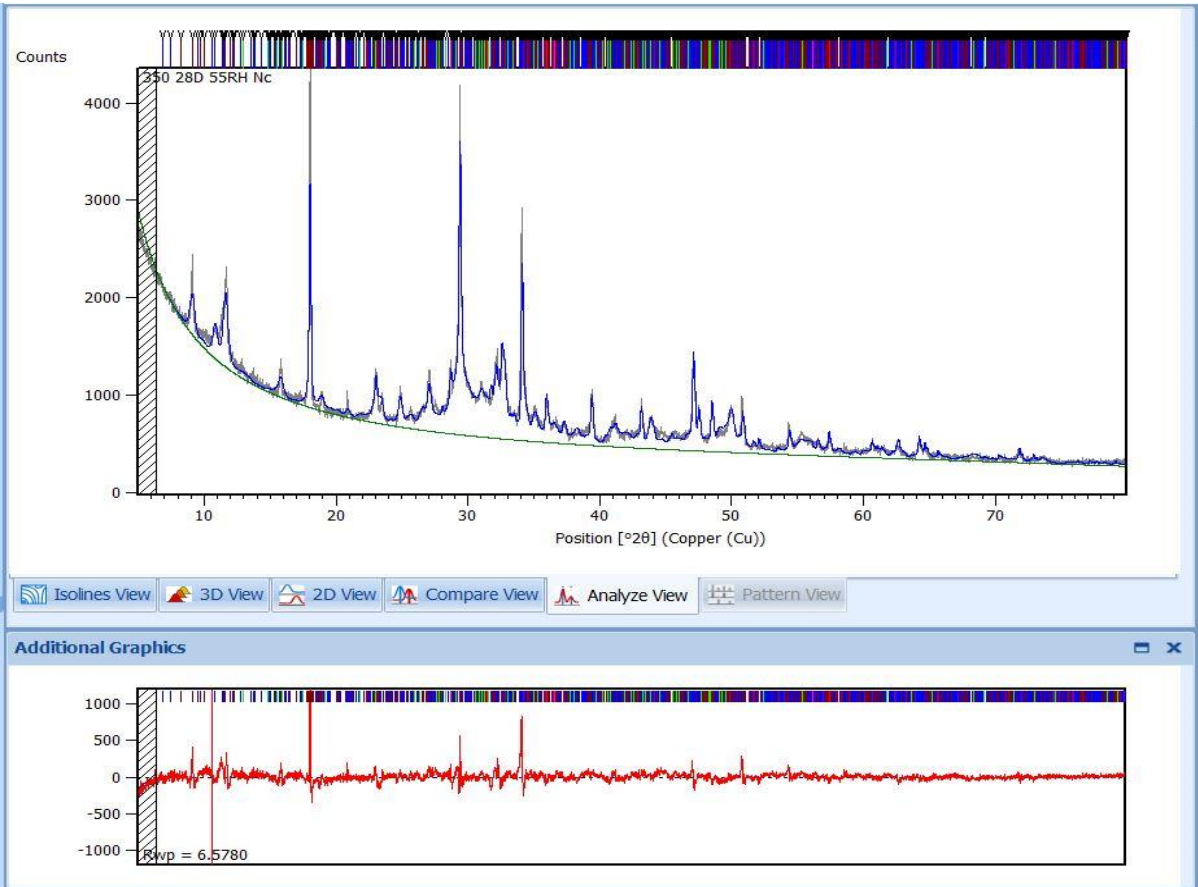
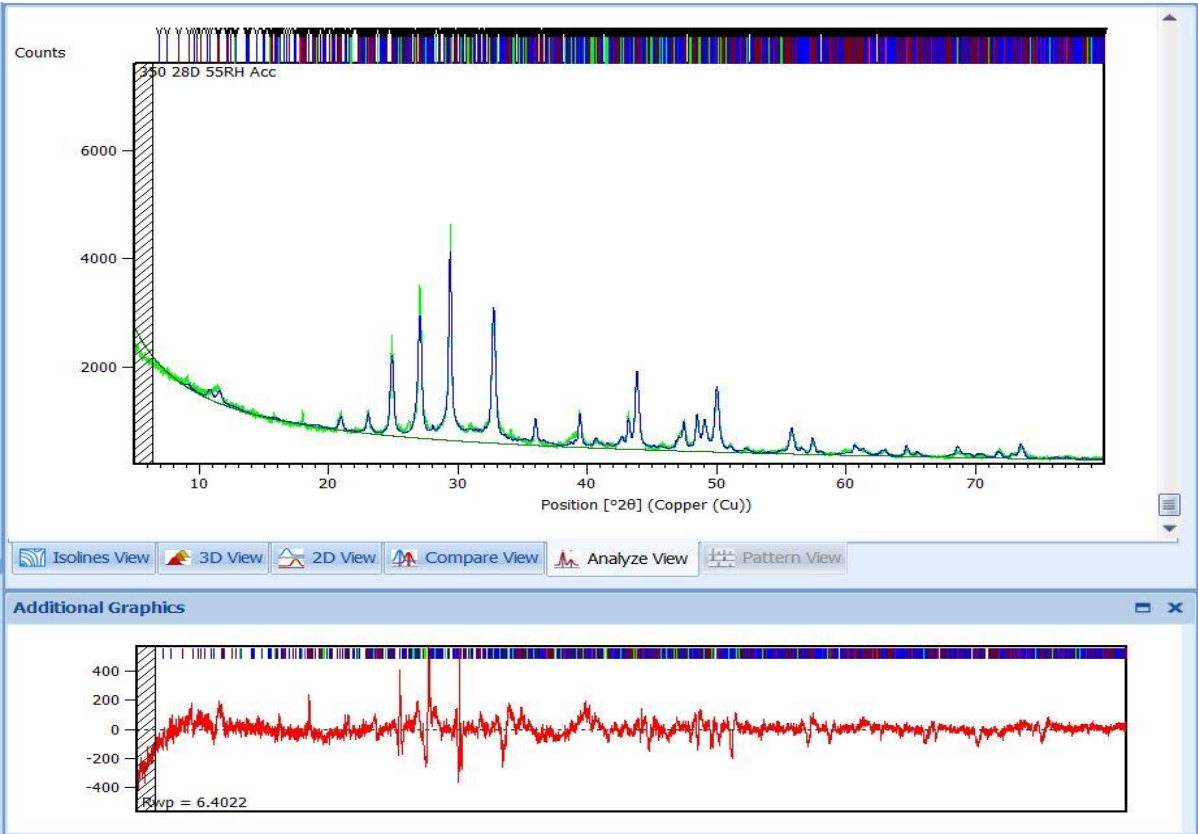
The outputs from Rietveld refinement of the various hydrated pastes are presented here. Various binders paste was analysed and the calculated patterns superimposed on the observed patterns. The background and difference plots are also shown for selected samples at 28 days of hydration. The agreement index Rwp is also provided for reference.

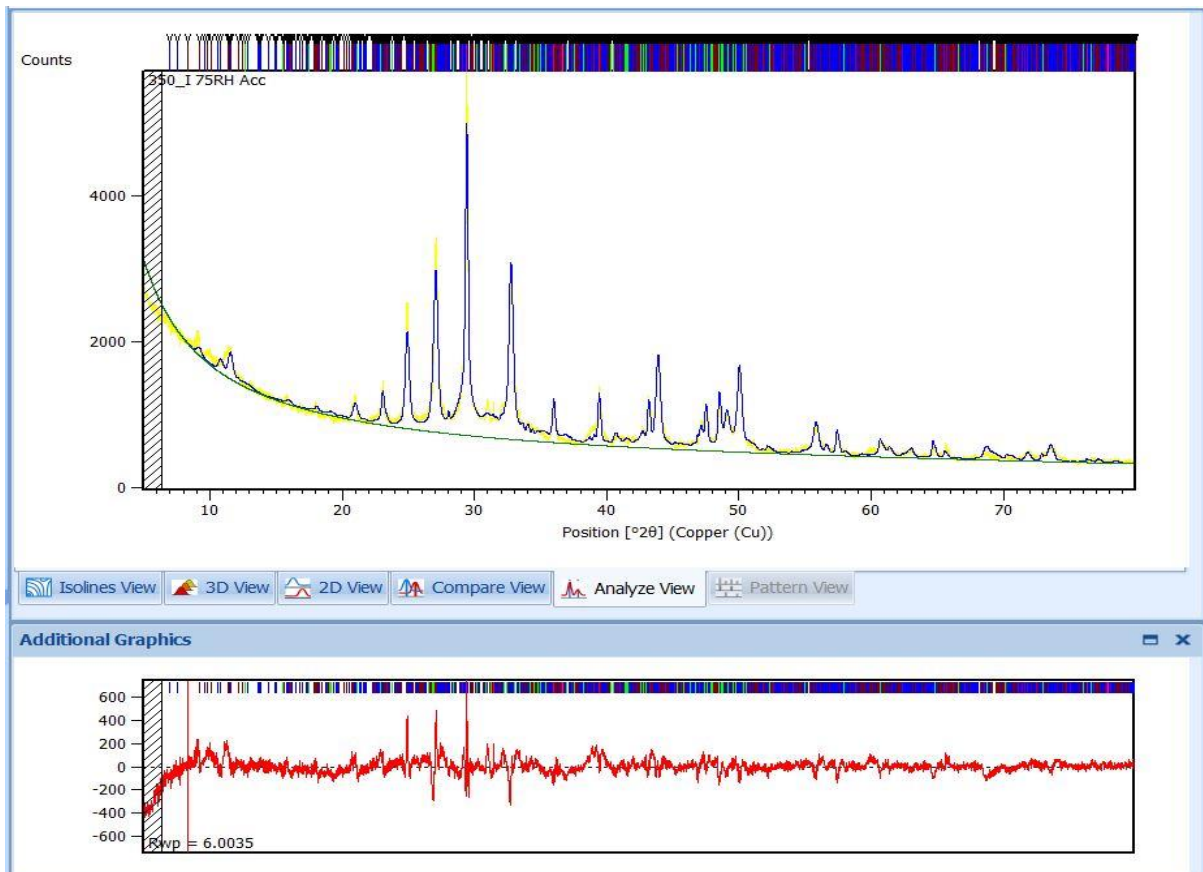
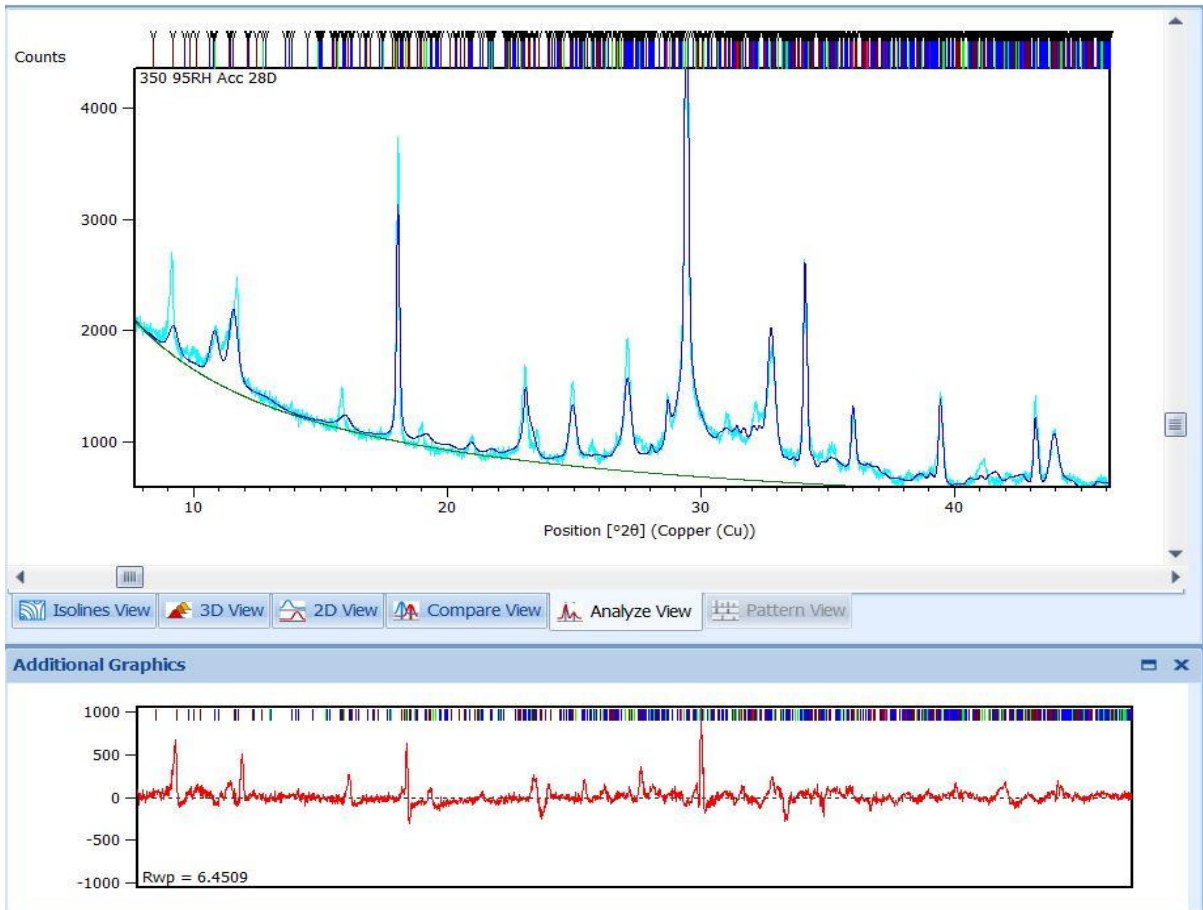




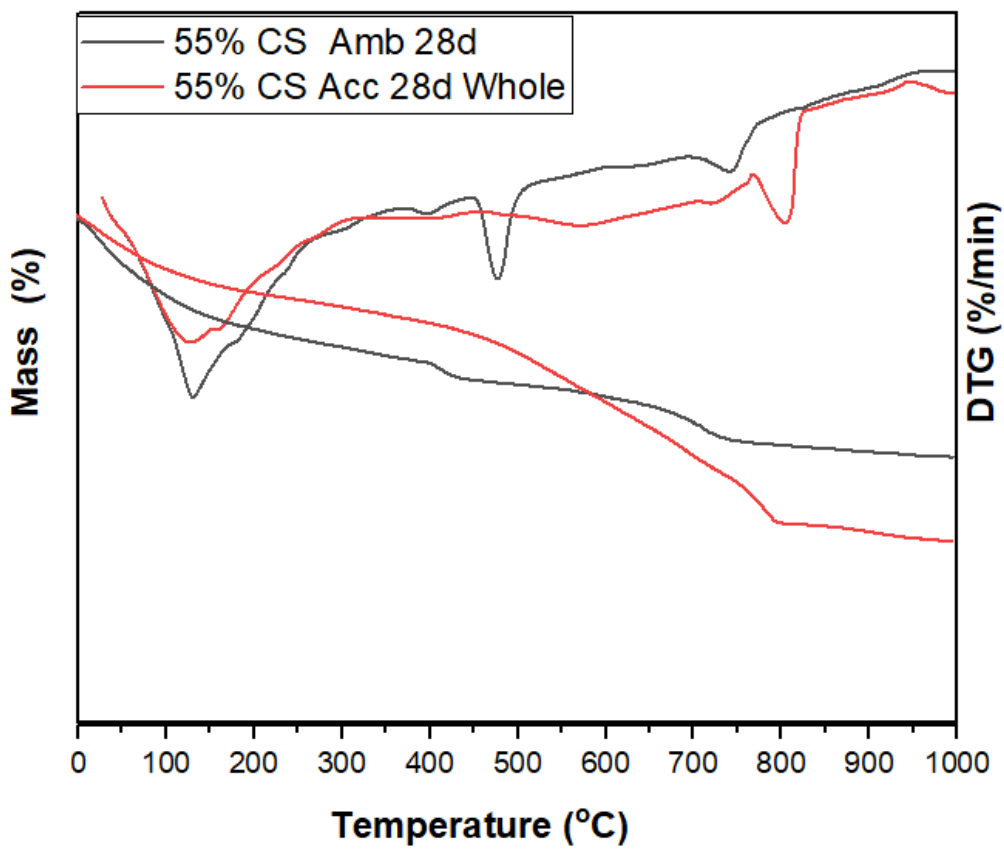
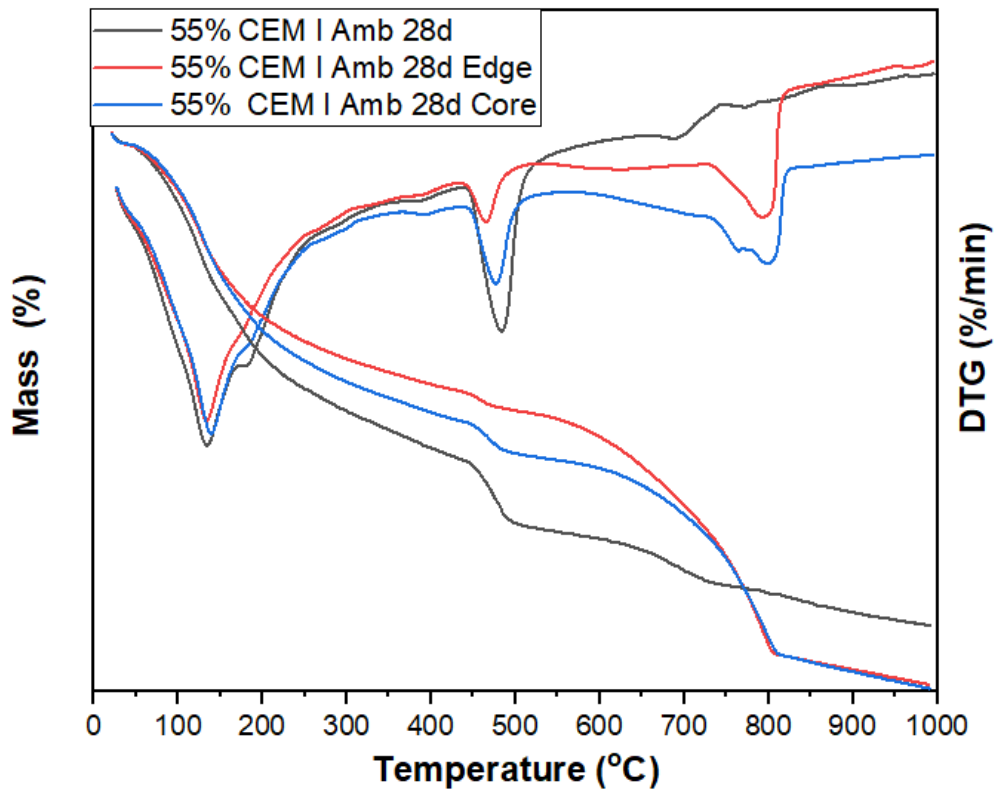


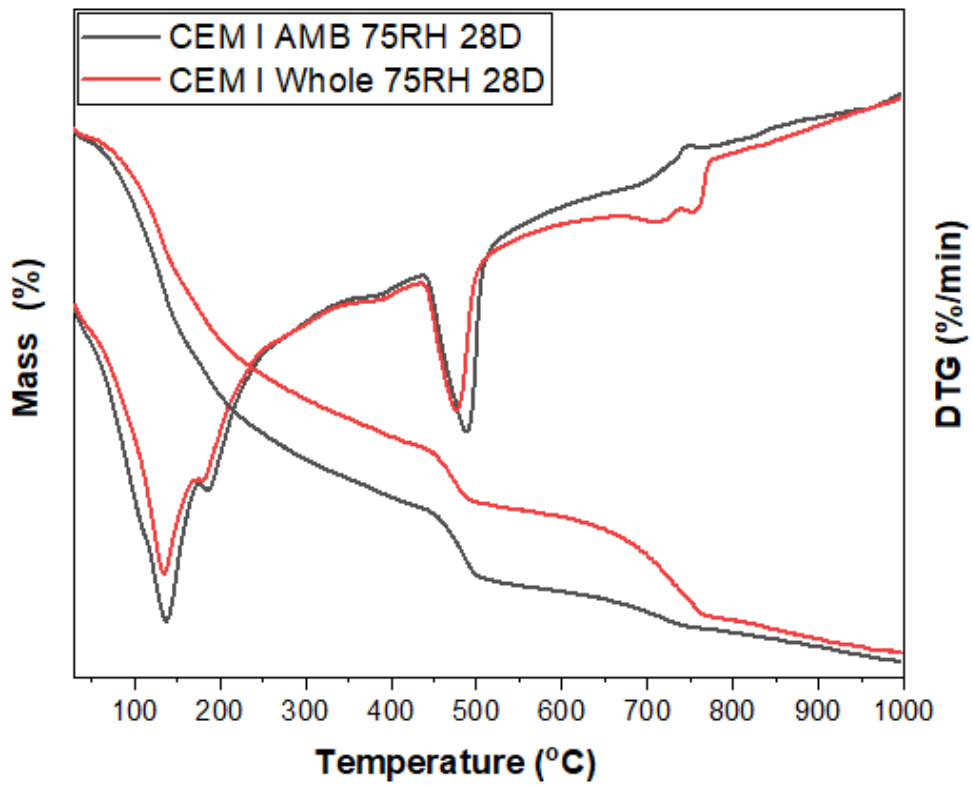
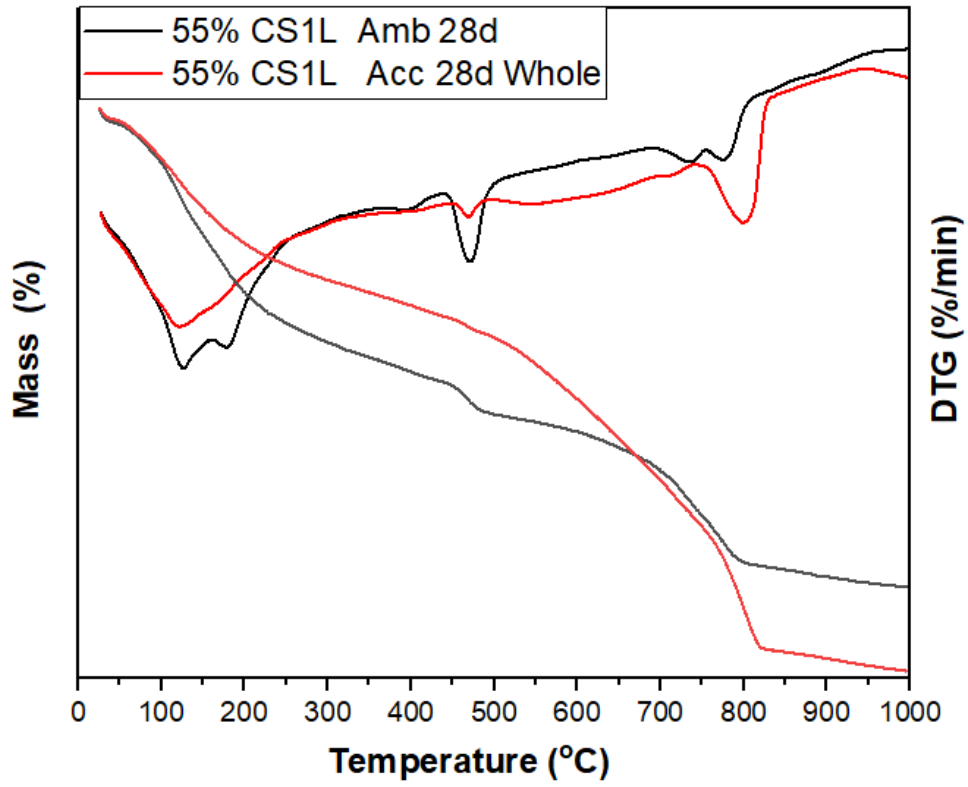


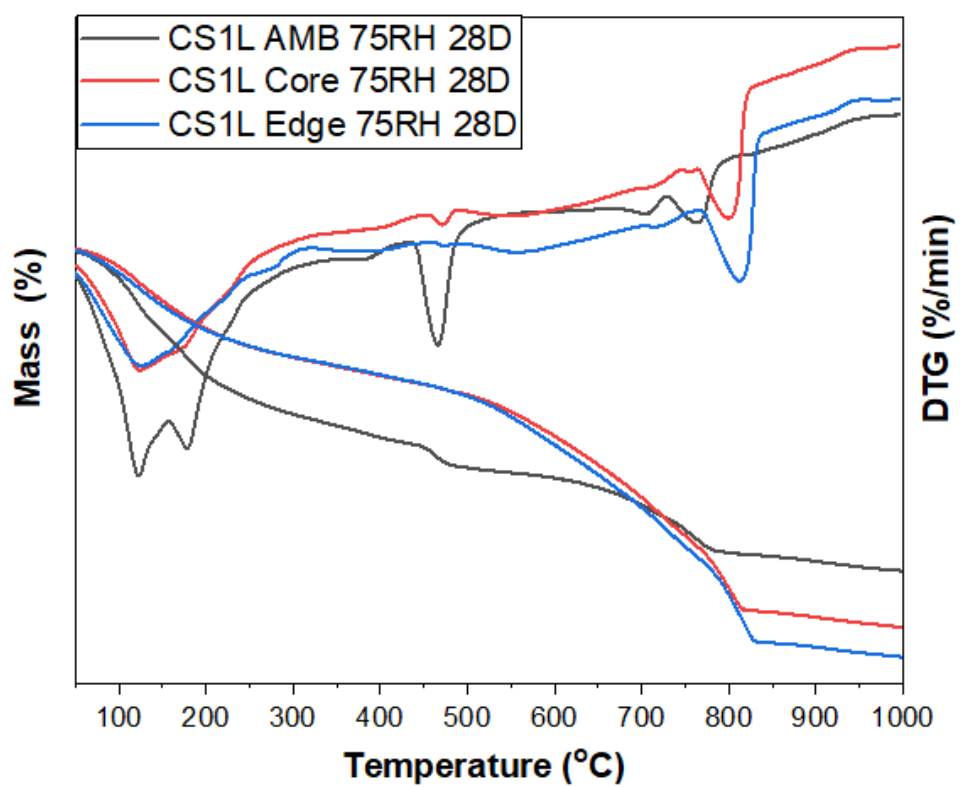
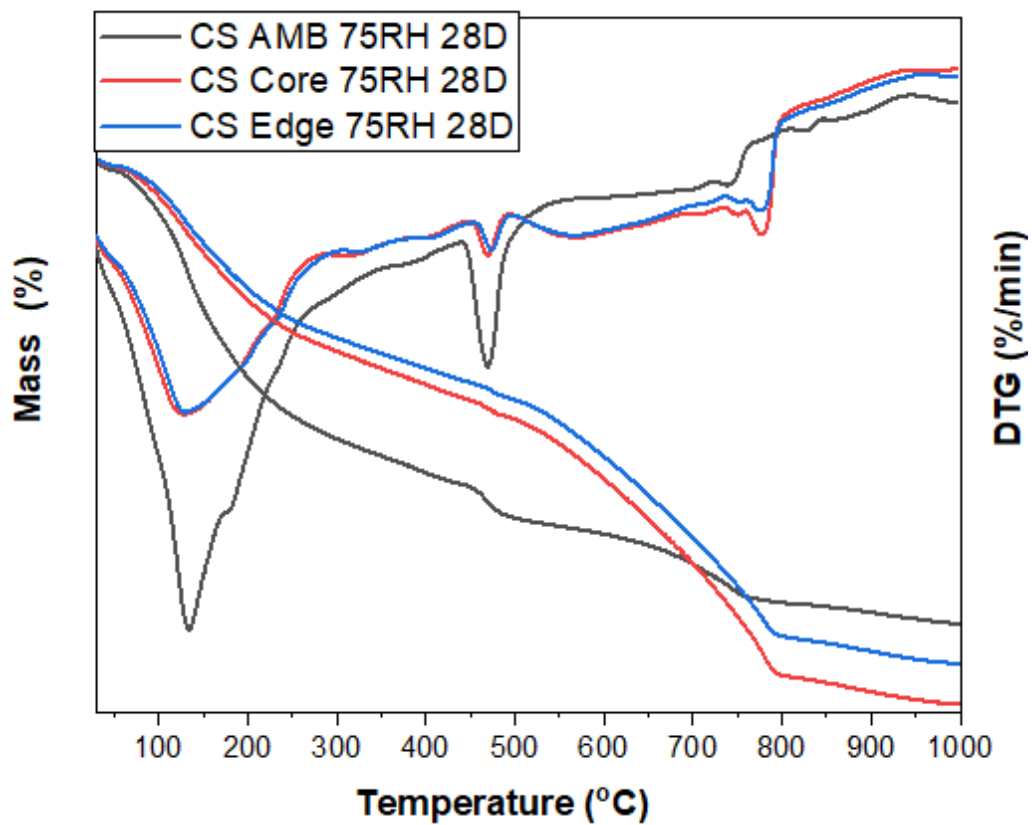




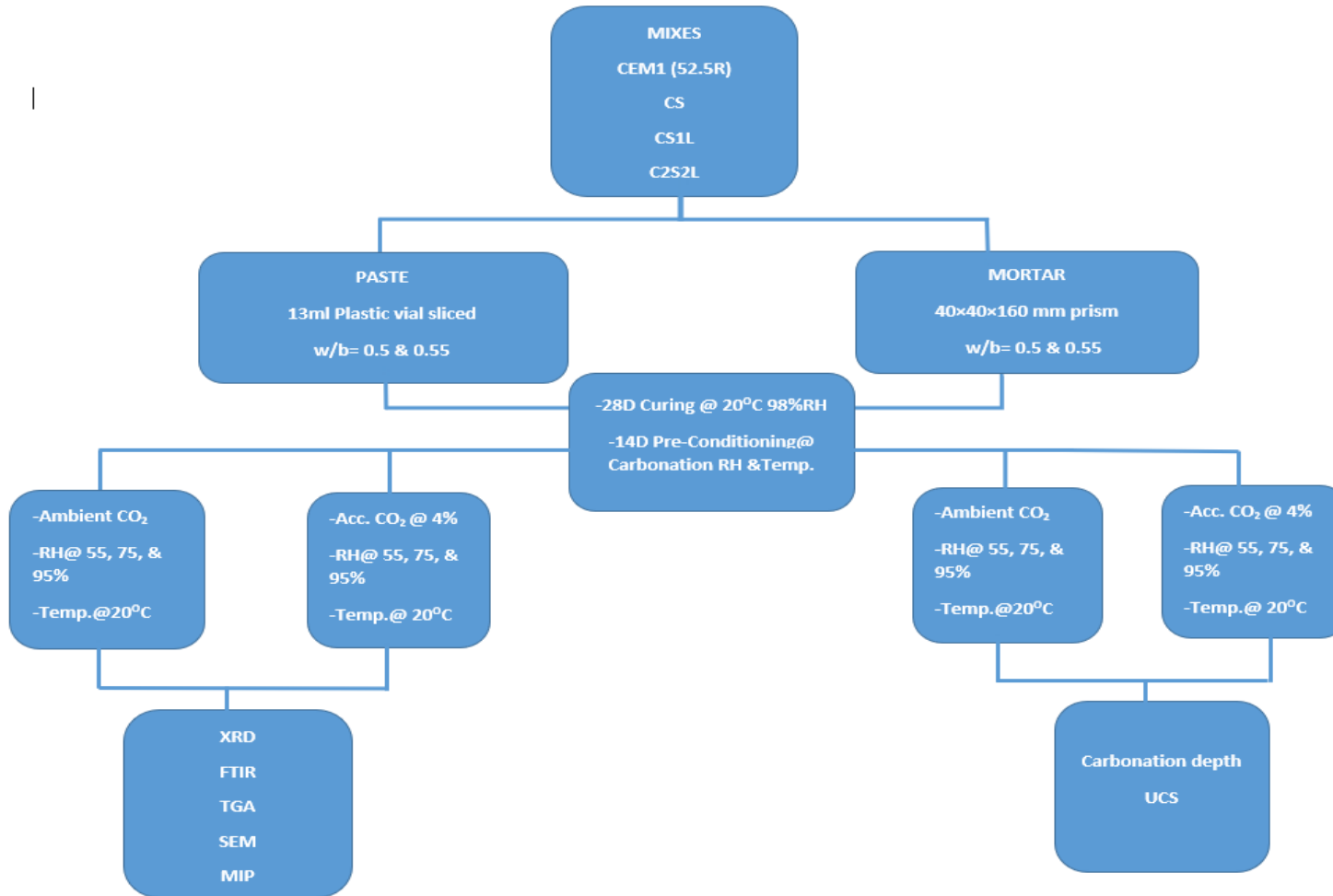
B. Mass against DTG plots (CaCO<sub>3</sub> decomposition temperature)







### C. Post-Covid Experimental Chart





E. Raw TGA and QXRD data.

Chemically bound water, portlandite content, and calcium carbonates of paste samples under both accelerated and ambient carbonation at 55%, 75% and 95% relative humidity.

RH	Mix	CH (/100g binder)				CBW (%)		CaCO <sub>3</sub> (%) (TGA)	
		TGA		XRD		Measured	Normalised		
		Mea.	Norm.	Mea.	Norm.				
55%	CEM I	Amb	19.94	21.18	19.50	20.71	28.02	29.76	5.86
		Core	9.01	13.96	7.40	11.47	18.10	28.05	35.48
		Edge	0.70	1.10	0.50	0.78	16.47	25.79	36.14
	CS	Amb	8.26	8.75	6.40	6.78	20.56	21.78	5.60
		Whole	0.00	0.00	0.30	0.49	16.87	20.51	38.68
	CS1L	Amb	6.24	6.76	5.60	6.07	21.19	22.97	7.76
Whole		0.00	0.00	0.00	0.00	14.80	21.12	38.63	
75%	CEM I	Amb	22.44	23.64	20.70	21.81	32.40	34.13	5.08
		Whole	12.85	14.82	15.50	17.88	26.63	30.72	13.30
	CS	Amb	8.46	8.70	8.20	8.43	22.47	23.10	2.72
		Core	3.43	4.24	2.50	3.32	16.44	20.30	19.01
		Edge	0.00	0.00	0.50	0.69	16.42	22.63	27.43
	CS1L	Amb	8.80	9.54	8.00	8.67	20.83	22.57	7.72
Core		4.82	7.41	3.10	4.15	14.87	22.85	34.93	
Edge		0.00	0.00	0.40	0.70	14.25	24.93	42.85	
95%	CEM I	Amb	22.34	23.79	20.50	21.83	33.92	36.12	6.10
		Acc	19.82	21.54	16.30	17.71	22.86	24.84	7.98
	CS	Amb	8.90	9.40	7.20	7.60	25.21	26.62	5.28
		Acc	6.49	7.22	5.00	5.57	18.47	20.56	10.17
	CS1L	Amb	8.60	9.96	8.21	9.51	23.75	27.50	13.65
		Acc	6.56	8.01	6.70	8.18	22.96	28.03	18.08